Clusters of Transition-Metal Atoms

MICHAEL D. MORSE

Department of Chemistry, University of Utah, Salt Lake City, Utah 84112

Received June 23, 1986 (Revised Manuscript Received August 28, 1986)

Contents

I. Introduction

In the past 10 years or so, a new type of chemical entity has come under both experimental and theoretical examination: clusters of transition-metal atoms, without benefit of stabilizing ligands. Numerous experimental and theoretical techniques have been developed, and these formerly unexamined species have now been characterized to a surprising degree. A considerable amount is now known concerning the spectroscopy, structure, and reactivity of bare transition-metal clusters; this forms the basis of the current review. Nevertheless, the knowledge we have gained raises more questions than it answers, and much is yet to be learned. The rate of progress in the field is staggering, however, and this makes the time ripe for a comprehensive review. A review such as this would have been impossible 10 years ago for lack of data; it will be impossible 10 years from now due to a superabundance of relevant work.

In this review I have attempted to provide a critical

0009-2665/86/0786-1049$06.50/0

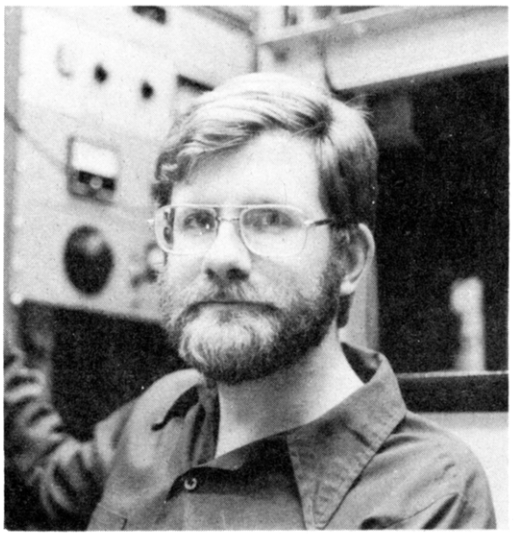

Michael D. Morse is an Assistant Professor of Chemistry at the University of Utah. He received his B.S. degree in 1974 from Haverford College and his Ph.D. degree in 1980 from the University of Chicago, where he worked under the direction of K. F. Freed and S. A. Rice. After postdoctoral research with S. A. Rice at the University of Chicago and with R. E. Smalley at Rice University, he joined the faculty of the University of Utah in 1985. Although he maintains an active interest in theoretical chemistry, Dr. Morse's research interests are now centered on the structure, spectroscopy, and dynamics of metal and semiconductor clusters, atom–ligand complexes, ions, and radicals.

and comprehensive account of what is currently known about the transition-metal clusters. Throughout the review I have suggested alternative interpretations of experimental data when the interpretations of the original authors are at odds with subsequent experiments. In many cases the definitive experiment has not been done and legitimate controversies exist. In such cases I have chosen to present alternative interpretations in order that the review be critical and comprehensive.

In the interest of writing a comprehensive review, I have limited the subject matter to clusters of transition-metal atoms, without ligands or atoms of nontransition-metal elements. I have also omitted discussion of molecular clusters and clusters of other elements, except when they are particularly relevant to transition-metal clusters. In making this choice I have unfortunately left out many exciting investigations of clusters containing ligands and of clusters of other elements. In addition I have omitted the vast field of chemical reactions of transition-metal atoms and clusters in matrices, in solution, and on supports. These studies lie outside the scope of this review.

Section II of this review covers the detailed spectroscopic, thermochemical, and theoretical studies of small transition-metal clusters of definite size, beginning with the dimers. In section III I examine the broader questions of physical and chemical properties as functions of cluster size and the approach to bulk properties. Section IV then provides a summary and an outlook for the future.

II. Experimental and Theoretical Results for Small Transition-Metal Clusters

In this section experimental results and theoretical calculations are summarized for small transition-metal clusters of definite size, with emphasis on their electronic structure, chemical bonding, and electronic spectroscopy. In the past 5 years or so, the literature on this subject has grown explosively, due to the concurrent and synergistic development of novel experimental techniques, new theoretical methods, and ultrahigh speed computers at reasonable cost. As a result, considerable progress has been made, even since the 1984 review of the subject by Weltner and Van Zee.[1]

Due to this work, we now understand the competing forces which determine the electronic structure of these molecules to a considerable degree. For example, we know that the tendency of the transition metals to form multiple *n*d bonds is governed by the relative sizes of the atomic $(n + 1)$s and *n*d orbitals, given in Table 1 as calculated by numerical Hartree–Fock methods.[2] This table demonstrates what is clearly a major determinant of bonding in the transition-metal molecules: the 3d and 4d orbitals contract considerably as the nuclear charge increases. In the extreme limit of d-orbital contraction, the orbitals will be too contracted to overlap significantly, thereby eliminating the possibility of d-electron bonds. The contribution of d-electron bonding is therefore reduced as one moves to the right in the periodic table. As Table 1 demonstrates, the *n*d contraction is much more severe for the 3d transition series than for the 4d and 5d transition series, indicating that d-electron participation in the chemical bonding will be more significant for the second and third transition series than for the first.

TABLE 1. Relative Orbital Sizes (Numerical Hartree–Fock)[a] and Excitation Energies (Experiment)[b] for Transition-Metal Atoms

atom	$\langle r_{(n+1)s}\rangle / \langle r_{nd}\rangle$ s^2d^m	$\langle r_{(n+1)s}\rangle / \langle r_{nd}\rangle$ sd^{m+1}	$(n+1)s^2nd^m \rightarrow (n+1)snd^{m+1}$, eV	$(n+1)s^2nd^m \rightarrow nd^{m+2}$, eV
Sc	2.36	2.03	1.43	4.19
Ti	2.59	2.32	0.81	3.35
V	2.74	2.51	0.25	2.47
Cr	2.87	2.69	−1.00	3.40
Mn	2.99	2.81	2.14	5.59
Fe	3.04	2.95	0.87	4.07
Co	3.10	3.08	0.42	3.36
Ni	3.17	3.22	−0.03	1.71
Cu	3.24	3.36	−1.49	...
Zn	3.31	...	...	...
Y	1.77	1.61	1.36	3.63
Zr	1.94	1.79	0.59	2.66
Nb	2.07	1.92	−0.18	1.14
Mo	2.17	2.05	−1.47	1.71
Tc	2.27	2.16	0.41	unknown
Ru	2.33	2.29	−0.87	0.22
Rh	2.39	2.42	−1.63	−1.29
Pd	2.45	2.54	−2.43	−3.38
Ag	2.52	2.67	−3.97	...
Cd	2.59	...	...	...
La			0.36	unknown
Hf	1.86		1.69	unknown
Ta	1.95		1.04	unknown
W	2.03		−0.19	unknown
Re	2.11		1.76	unknown
Os	2.14		0.75	unknown
Ir	2.18		0.40	2.90
Pt	2.23		−0.64	−0.16
Au	2.27		−1.74	...
Hg	2.32		...	...

[a] Numerical Hartree–Fock results for $(n + 1)s^2nd^m$ configuration are from ref 214; results for $(n + 1)snd^{m+2}$ are from ref 2. Relativistic effects are not included in these calculations; these would decrease the $\langle r_{(n+1)s}\rangle / \langle r_{nd}\rangle$ ratio, especially in the 5d transition series. [b] Experimental energies are from ref 3.

Table 1 also lists the energies required to promote an electron from the filled $(n + 1)s^2$ shell to the nd shell in the transition-metal atoms, determined by taking an average over the spin–orbit components of the lowest atomic term of each electronic configuration.[3] In elements in which this quantity is negative, no electronic promotion is required to form sσ bonds, since the half-filled $(n + 1)$s shell is already suitable for bonding. (An exception is Pd, in which the ground-state configuration $4d^{10}5s^0$ must be promoted to $4d^95s^1$ before bonding can occur.) In contrast, elements with ground-state configurations of $(n + 1)s^2nd^m$ must first promote an s electron to a d orbital before significant chemical bonding can occur. In these elements a significant energetic price must be paid before chemical bonding is possible: the promotion energy required to prepare the atoms for bonding substantially reduces the strength of the chemical bonds that are gained. This effect is particularly severe in Mn_2, which requires a promotion energy of 4.28 eV to prepare the atoms for a $(4s\sigma_g)^2$ bond.

In addition to these relatively straightforward determinants of bonding in transition-metal molecules, we now know that electron correlation and exchange effects are critically important to the proper description of the transition-metal molecules. Unfortunately, it is proving to be extremely difficult to estimate these two effects to the same degree of accuracy. In many calculations one effect may be well-estimated while the other is seriously in error. Since it is the balance of the two which often determines the electronic and geometrical structure, reliable theories must estimate both correlation and exchange to the same degree of accuracy. A similar possibility for error arises in basis set choices. Since the ground atomic configuration of the separated atoms may not correspond to the atomic configurations leading to chemical bonding, the basis set must be capable of accurately representing both the ground atomic configuration and the configurations responsible for chemical bonding in the transition-metal molecules. This is a difficult problem for theory, yet one which must be solved if reliable bond strengths are to be calculated. Coupled with these difficulties is the fact that relativistic effects become quite important in the latter half of the 4d transition series and remain important throughout the 5d transition series.[2] Together these factors make the transition-metal molecules a particularly difficult challenge for theoretical chemistry.

Experimental studies of the bare transition-metal clusters are also far from straightforward. In the earliest spectroscopic studies, furnaces were used to generate high vapor pressures of the coinage metals (Cu, Ag, and Au). Under these conditions some diatomic species were present, and ultraviolet and visible spectra of the dimers were obtained.[4-21] Although these methods provided the first spectroscopic data on the transition-metal molecules, they were not readily extended to more refractory metals, and for many years little was learned of the more refractory transition-metal molecules.

In other work employing high-temperature furnaces, Knudsen effusion has been combined with mass spectrometry to permit a determination of dimer (and, in some cases, higher cluster) binding energies.[22-28] In essence, these methods rely on Knudsen effusion mass spectrometry to sample the chemical composition of the vapor phase in equilibrium with a solid or liquid phase at a given temperature. The heat of vaporization for the reaction

$$n\mathrm{M}(\text{condensed phase}) \rightarrow \mathrm{M}_n(\mathrm{g}) \qquad (2.1)$$

may then be determined by the second-law method from the Clausius–Clapeyron relationship

$$\frac{\mathrm{d}\ln \mathrm{P}(\mathrm{M}_n)}{\mathrm{d}(1/T)} = -\frac{\Delta H^\circ_{\mathrm{T}}}{R} \qquad (2.2)$$

A comparison of the heat of vaporization to form atoms with the corresponding heat of vaporization for formation of clusters then gives $\Delta H^\circ_{\mathrm{T}}$ for the process

$$n\mathrm{M}(\mathrm{g}) \rightarrow \mathrm{M}_n(\mathrm{g}) \qquad (2.3)$$

An extrapolation of ΔH°_T to zero temperature then provides the binding energy, $D_0^\circ(\mathrm{M}_n)$. The second-law method, as described here, yields results of limited accuracy and requires that data be taken over a sufficient temperature range that the derivative (2.2) be well-determined. Nevertheless, the second-law method requires no assumptions about the nature of the vaporized molecules (apart from an estimate of $C_p(T)$, which is needed to extrapolate ΔH°_T to zero temperature). In light of our lack of knowledge of these species, this is a particularly valuable aspect of the method.

An alternative is provided by the third-law method, which is based on the statistical thermodynamics of dimerization. This method uses the statistical thermodynamic expression for the equilibrium constant of reaction 2.3 to directly calculate $D_0^\circ(\mathrm{M}_n)$. The third-law expression, therefore, is applicable to measurements made at only a single temperature but requires estimates of molecular parameters such as the bond length, vibrational frequency, ground-state electronic degeneracy, and the parameters of low-lying, thermally populated excited electronic states. Although the method gives results which are potentially more accurate than the second-law method, the necessity of estimating the molecular parameters of the relatively poorly understood transition-metal molecules limits its usefulness. Drowart and Honig[22] have provided a more detailed description of these two methods, and a number of critical reviews of the metal dimer and metal cluster binding energies $D_0^\circ(\mathrm{M}_n)$ have been published.[23-28]

I have attempted to critically review the published binding energies $D_0^\circ(\mathrm{M}_n)$. Where this has not been possible I have relied on the compilation by Gingerich in the most recent review.[27] One should note, however, that results based on the third-law method may be in error by much more than the published error bounds suggest, primarily due to poor estimates of the number of low-lying electronic states which are populated at elevated temperatures. Thus, for example, the binding energy of Co_2 was recently recalculated from the original mass spectrometric data of Kant and Strauss[29] by using an electronic partition function based on a careful all-electron ab initio Hartree–Fock CI calculation.[30] This resulted in a lowering of the accepted dissociation energy of Co_2 from 1.69 ± 0.26 to 0.96 ± 0.26 eV.[30] Since the number of low-lying excited electronic states is probably more often underestimated than overesti-

mated, most corrections due to this error will tend to decrease the accepted bond strengths of the diatomic transition-metal molecules.

More recently, a number of investigators have employed matrix-isolation techniques to investigate the UV/visible, Raman, IR, ESR, Mössbauer, magnetic circular dichroism, and EXAFS spectra of a variety of transition-metal dimers and clusters. A common difficulty of the matrix isolation technique is the unambiguous identification of the carrier of an observed spectroscopic transition. In favorable cases, the isotopic shift of the vibrational frequency may be used to identify the carrier of a transition in matrix IR and Raman work. In many instances the vibration frequencies of matrix-isolated species are within a few percent of the values for gas-phase molecules,[31] although weakly bound molecules may be strongly perturbed. In the van der Waals dimer, Cd_2, for example, the value of ω_e deduced from matrix isolation experiments (58 ± 1 cm^{-1}),[32] is 2.5 times as large as the gas-phase result (22 cm^{-1}).[33] This sort of disagreement is to be expected in cases where the vibrational frequency of the isolated molecule is comparable to the vibrational frequencies of the matrix itself. Apart from these cases of low-frequency vibrations, the most common cause of serious disagreements between gas-phase and matrix-isolated vibrational frequencies is the incorrect assignment of the carrier of the transition, either in the matrix or in the gas phase.

In ESR investigations of matrix-isolated species, hyperfine interactions associated with the various isotopic forms of the clusters under study may be used to provide a definitive assignment of the carrier of a transition. In many cases it is then possible to determine a large number of spectroscopic parameters, including **g** tensors, hyperfine splittings, and zero-field splittings. As a result, this method has enabled the symmetry designations and spectroscopic parameters of the ground states of a number of interesting transition-metal molecules to be unambiguously determined. A point of caution should be raised, however. Given that many of the transition-metal molecules may have very dense manifolds of low-lying electronic states, it is conceivable that in some cases the matrix ground state may differ from the ground state in the gas phase. The observation[34-36] that nickel atoms shift from a $3d^84s^2$ $^3F_4$ ground state in the gas phase to a $3d^94s^1$ ^3D ground state in argon, krypton, and xenon matrices certainly introduces a note of caution in this respect. These states of nickel are separated by 205 cm^{-1} in the gas phase, suggesting that molecular states separated by comparable amounts of energy may be inverted when the molecule is inserted into an inert matrix. Such an effect has not yet been observed in molecules, however.

In other recent work, investigators have produced gas-phase dimers of refractory transition-metal clusters by flash photolysis of the volatile metal carbonyls. This method, coupled with transient absorption spectroscopy, has provided valuable data on the spectroscopy of Cr_2,[37] CrMo,[38] and Mo_2.[39] In other work employing the transition-metal carbonyls, Lineberger and co-workers have produced Re_2^-,[40] Fe_2^-,[41] and Co_2^-[41] by passing the parent carbonyls $Re_2(CO)_{10}$, $Fe_2(CO)_9$, and $Co_2(CO)_8$ through a flowing afterglow ion source. Following mass separation of the resulting anions, photoelectron spectra of the dimer anions were obtained. Such spectra yield valuable data on the low-lying electronic states of the neutral dimers and will probably be extended to other transition-metal dimers and higher clusters in the near future.

Finally, one other experimental technique has enjoyed considerable success in providing detailed spectroscopic information about the transition-metal molecules: pulsed laser vaporization in a pulsed supersonic jet. This technique, introduced by Smalley and coworkers in 1981,[42] has been coupled with laser-induced fluorescence spectroscopy and resonant two-photon ionization spectroscopy to provide a great deal of detailed information about the electronic spectra and structure of V_2,[43] Cr_2,[44-46] Ni_2,[47] Cu_2,[48-50] Mo_2,[51] and Cu_3.[52] Future applications to other transition-metal dimers and clusters will certainly extend our knowledge of these interesting species.

The results obtained by using these various experimental methods, along with the predictions of quantum chemistry, are presented in the following subsections. In section II.A I summarize the present state of knowledge of the homonuclear transition-metal dimers. Section II.B is devoted to the heteronuclear transition-metal dimers, and section II.C summarizes current knowledge of the larger transition-metal clusters. A more complete discussion of the experimental and theoretical methods and their results is provided as appropriate in the following sections, where results on individual molecules are given.

A. Homonuclear Transition-Metal Diatomics

The known properties of the ground states of the homonuclear transition-metal dimers are summarized in Table 2. The individual molecules are discussed more completely below.

1. Scandium, Sc_2

The only gas-phase experimental data available for Sc_2 are mass spectrometric estimates of the dissociation energy, $D_0°$. Although initially reported by Verhaegen et al.[53] as $D_0° = 1.12 \pm 0.22$ eV, subsequent reviewers[23-27] have reported $D_0° = 1.65 \pm 0.22$ eV. These values, obtained by using the absolute entropy or third-law method,[22] require estimates of molecular parameters such as the electronic partition function and may be in error by more than the published error bounds suggest.

Investigators studying the visible and ultraviolet absorption spectra of matrix-isolated Sc_2 have assigned transitions at 15 100, 21 050, and 29 850 cm^{-1} to the Sc_2 dimer.[54] Using extended Hückel theory the same authors assign these transitions to $1\sigma_g \rightarrow 1\sigma_u$, $1\sigma_g \rightarrow 2\sigma_u$, and $1\sigma_g \rightarrow 2\pi_u$ excitations from a $(1\sigma_g)^2(2\sigma_g)^1(1\pi_u)^2(1\delta_g)^1$ ground configuration in which the $1\sigma_g$ orbital is primarily of 4s percentage with the remaining orbitals primarily 3d in origin.

More recent matrix-isolation work by Knight, Van Zee, and Weltner[55] on the ESR spectrum of Sc_2 isolated in argon or neon matrices establishes that the ground state of Sc_2 is $^5\Sigma$. This contradicts the assignment of previous investigators based on the extended Hückel theory.[54] Moreover, the hyperfine splitting parameters observed in the ESR spectrum are in agreement with an electronic configuration of $(4s\sigma_g)^2(4s\sigma_u^*)^1(3d\pi_u)^2$-

TABLE 2. Ground States of Homonuclear Transition-Metal Diatomic Molecules[a-c]

molecule	Sc_2	Ti_2	V_2	Cr_2	Mn_2	Fe_2	Co_2	Ni_2	Cu_2	Zn_2
term symbol	$^5\Sigma_u^-$	$(^1\Sigma_g^+)$	$^3\Sigma_g^-$	$^1\Sigma_g^+$	$^1\Sigma_g^+$	$(^7\Delta_u)$	$(^5\Sigma_g^+)$	$^3\Gamma_u$ or $^3\Gamma_g$	$^1\Sigma_g^+$	$^1\Sigma_g^+$
r_e, Å	(2.79)	(1.97)	1.77	1.68	3.4	2.02	(2.56)	2.20	2.2195	2.35
ω_e, cm^{-1}	238.9	407.9	537.5	$\Delta G_{1/2}$ = 452.34	[124.69]	300.26	290		265.1	[80 ± 1]
$\omega_e x_e$, cm^{-1}	0.93	1.08	4.2		[0.24]	1.45			1.0234	
D_0, eV	[1.65 ± 0.22]	1.23 ± 0.17	2.49 ± 0.13	1.78 ± 0.35	≤0.80	0.90 ± 0.10	[0.95 ± 0.26]	2.068 ± 0.01	2.01 ± 0.08	0.056
molecule	Y_2	Zr_2	Nb_2	Mo_2	Tc_2	Ru_2	Rh_2	Pd_2	Ag_2	Cd_2
term symbol	$(^1\Sigma_g^+)$		$(^3\Sigma_g^-$ or $^3\Delta_g)$	$^1\Sigma_g^+$		$(^7\Sigma)$			O_g^+ $^1\Sigma_g^+$	O_g^+ $^1\Sigma_g^+$
r_e, Å	(2.74)		(2.10 or 2.01)	1.938		2.42			(2.47)	[4.82]
ω_e, cm^{-1}	(206)		(488 or 501)	477.1		(330)			192.4	22
$\omega_e x_e$, cm^{-1}				1.51					0.643	0.4
D_0, eV	[1.62 ± 0.22]	(3.20 ± 0.24)	5.0 ± 0.4	4.38 ± 0.10	(3.17)	(3.29)	[2.92 ± 0.22]	1.03 ± 0.16	1.65 ± 0.03	0.0378
molecule	La_2	Hf_2	Ta_2	W_2	Re_2	Os_2	Ir_2	Pt_2	Au_2	Hg_2
term symbol									O_g^+ $^1\Sigma_g^+$	O_g^+ $^1\Sigma_g^+$
r_e, Å									2.4719	[3.35]
ω_e, cm^{-1}					340 ± 20				190.9	
$\omega_e x_e$, cm^{-1}									0.420	
D_0, eV	[2.50 ± 0.22]	(3.4 ± 0.6)	(4 ± 1)	(5 ± 1)	(4 ± 1)	(4.3 ± 0.8)	(3.7 ± 0.7)	3.71 ± 0.61	2.29 ± 0.02	0.074 ± 0.020

[a] Parentheses indicate theoretical results. [b] Square brackets indicate experimental results which are questionable. [c] For details and discussion see the text.

$(3d\sigma_g)^1(^5\Sigma_u^-)$, which has been calculated to be the ground state in several ab initio studies.[2,56-58] Other quantum chemical calculations have not obtained this result, because in some cases they have restricted consideration to closed-shell configurations[59] or fill molecular orbitals in order of increasing orbital energy without regard to the possibility of a high-spin ground state.[60] The $^5\Sigma$ state now established as the ground state correlates to one ground-state atom ($4s^23d^1$, ^2D) and one excited atom ($4s^13d^2$, ^4F); certain previous calculations have predicted other ground states because they have either failed to consider this atomic asymptote, have omitted quintet states from consideration,[59-61] or have failed to examine states arising from this limit over the full range of internuclear distances.[62]

Matrix isolation resonance Raman spectroscopy by Moskovits et al.[63] have provided a measurement of the vibrational constants of Sc_2 in argon matrices: ω_e = 238.9 cm^{-1}; $\omega_e x_e$ = 0.93 cm^{-1}. Although no experimental estimate of the bond length of discandium exists, calculations giving $^5\Sigma_u^-$ as the ground state predict bond lengths of 2.6,[57] 2.70,[56] and 2.79 Å.[58] The vibrational frequencies obtained in these calculations are in reasonable agreement with experiment: ω_e is calculated to be 200[56] or 184 cm^{-1},[58] in comparison to the experimental 239.9 cm^{-1}.[63] Finally, the bond energy calculated for the $^5\Sigma_u^-$ ground state of Sc_2 is 0.44,[58] 0.55,[57] or 1.80 eV[56] (obtained by using a density functional formalism which the authors acknowledge overestimates the binding energy). It has been estimated[58] that proper evaluation of the electronic partition function of Sc_2 will lower the experimental estimate of the binding energy by at least 0.43 eV, giving $D_0° \simeq 1.22 \pm 0.22$ eV, providing reasonable agreement between theory and experiment.

The $^5\Sigma_u^-(4s\sigma_g)^2(4s\sigma_u^*)^1(3d\pi_u)^2(3d\sigma_g)^1$ electronic configuration of Sc_2 places the two $3d\pi_u$ electrons in separate orbitals ($3d\pi_{ux}$ and $3d\pi_{uy}$), resulting in three one-electron 3d bonds ($(3d\sigma_g)^1$, $(3d\pi_{ux})^1$, and $(3d\pi_{uy})^1$). As has been extensively discussed by Walch and Bauschlicher,[2,58] this situation is optimal for chemical bonds formed from weakly overlapping atomic orbitals, since the chemical bonding in one-electron bonds is proportional to the overlap integral, S. In contrast, two-electron bonds formed from weakly interacting atomic orbitals are stabilized by an amount proportional to S^2, which is extremely small for small values of S. This factor, along with the loss of atomic exchange interactions which would result from spin-pairing the electrons, apparently accounts for the high-spin multiplicity of Sc_2 in its ground state.

2. Titanium, Ti_2

As in the case of discandium, the only gas-phase experimental data for Ti_2 are mass spectrometric estimates of the dissociation energy, $D_0°$. In an initial study by Kant and Strauss,[29] no titanium dimers were observed, and an upper limit to $D_0°$ of 2.52 eV was deduced. In subsequent work, dititanium was observed in equilibrium with liquid titanium, and $D_0°$ of Ti_2 was estimated as 1.23 ± 0.17 eV (by the second-law method) and as 1.42 ± 0.22 eV (by the third-law method).[64] The third-law estimate required an assumed electronic degeneracy of Ti_2 of 14, corresponding to a $^7\Delta$ ground state. The fact that the third-law estimate is still

considerably higher than the second-law value indicates that the electronic contribution to the partition function for Ti_2 is higher than 14 and that low-lying excited states of Ti_2 are thermally populated to a significant degree. Although other reviewers have cited 1.39 ± 0.22 eV for the dissociation energy of Ti_2,[25,26] and this has subsequently been revised to 1.31 ± 0.18 eV,[27] the original second-law value of 1.23 ± 0.17 eV is probably a more accurate estimate.

Ozin and co-workers[54] have investigated the visible and ultraviolet absorption spectra of argon matrices containing titanium and report absorption bands at 16 020, 18 310, and 23 250 cm^{-1}, which are assigned to Ti_2. As in the case of Sc_2,[54] these authors use extended Hückel theory to assign the transitions to $1\sigma_g \rightarrow 1\sigma_u$, $1\sigma_g \rightarrow 2\sigma_u$, and $1\sigma_g \rightarrow 2\pi_u$ excitations from a $(1\sigma_g)^2(2\sigma_g)^1(1\pi_u)^2(1\delta_u)^2(1\delta_g)^1$ ground electronic configuration, respectively.

In other matrix-isolation work, resonance Raman spectra were obtained of Ti_2 in argon matrices.[65] In this work a lengthy resonance Raman progression was excited, isotopic fine structure was resolved, and the spectroscopic constants ω_e = 407.9 cm^{-1} and $\omega_e x_e$ = 1.08 cm^{-1} were deduced, presumably for the $^{48}Ti_2$ isotopic modification. Recently Moskovits has performed a LeRoy–Bernstein extrapolation of the resonance Raman data to obtain $D_0(Ti_2)$ = 1.15 ± 0.20 eV, in close agreement with Knudsen effusion measurements.

A number of theoretical calculations have been undertaken for the titanium dimer. In several of these investigations a $^1\Sigma_g^+$ ground state with a formal bond order of 4 was obtained.[2,59,60] This state arises from the molecular configuration $(4s\sigma_g)^2(3d\sigma_g)^2(3d\pi_u)^4$ and correlates to two excited-state atoms in the $4s^13d^3$ electronic configuration. Although both a $(3d\sigma_g)^2(3d\pi_u)^4(3d\delta_g)^2\ ^3\Sigma_g^-$ molecular term and a high-spin nonet state with all eight electron spins parallel (giving a total electronic spin of $S = 4$) have been suggested for the ground state,[66] the most plausible alternative to the quadruply bonded $^1\Sigma_g^+$ term is a $^7\Sigma_u^+$ molecular term arising from the $(4s\sigma_g)^2(3d\sigma_g)^1(4s\sigma_u^*)^1(3d\pi_u)^2(3d\delta_g)^2$ electronic configuration. This configuration correlates to one excited- $(4s^13d^3)$ and one ground-state $(4s^23d^2)$ titanium atom and has a high-spin multiplicity which optimizes exchange interactions. Although the $^7\Sigma_u^+$ term lacks the favorable bonding afforded by the quadruply bonded $^1\Sigma_g^+$ term, only one atom has been promoted to an excited state, and the exchange interactions are quite favorable for high-spin coupling. The density functional method, which ends to overestimate the binding of high-spin states, predicts $^7\Sigma_u^+$ as the ground state.[56] A complete-active-space, self-consistent-field, configuration–interaction (CASSCF-CI) calculation also places $^7\Sigma_u^+$ as the ground state of Ti_2, although the quadruply bonded $^1\Sigma_g^+$ is calculated as lying only 0.40 eV above the $^7\Sigma_u^+$.[2] The calculated vibrational frequency for the high-spin $^7\Sigma_u^+$ is 205 cm^{-1} [2] (220 cm^{-1} [56]), however, while 438 cm^{-1} is obtained for the quadruply bonded $^1\Sigma_g^+$ term.[2] On the basis of the vibrational frequency observed in resonance Raman experiments[65] (ω_e = 407.9 cm^{-1}), it appears that the ground state of Ti_2 is $^1\Sigma_g^+(4s\sigma_g)^2(3d\sigma_g)^2(3d\pi_u)^4$. The CASSCF-CI calculation of this state gives a bond length of 1.97 Å[2] but underestimates the binding energy with respect to ground-state atoms as $D_0°$ = 0.32 eV.[2]

3. Vanadium, V_2

Divanadium was first investigated by Kant and Lin,[64] who utilized Knudsen effusion mass spectrometry to determine the dissociation energy, $D_0°$. A second-law value of $D_0°$ of 2.49 ± 0.13 eV was obtained, which compares well with the third-law value of 2.47 ± 0.22 eV which was obtained for a nondegenerate ground electronic state. Because of the agreement of these two methods, this value has been reported without change in more recent compilations of diatomic bond energies.[25-27] Some recent studies suggest that predissociation may set in above 1.85 eV, however.[43] This is based on the absence of an expected vibronic band in the resonant two-photon ionization spectrum and is not definitive. The missing band could be anomalously weak and shifted due to extensive perturbations. Nevertheless, if predissociation does set in at 1.85 eV, this would represent an upper limit to the binding energy of V_2.

As in the cases of Sc_2 and Ti_2, matrix-isolation studies of V_2 have been quite informative. Ozin and co-workers have again contributed significantly by providing ultraviolet, visible, and near-infrared spectra of V_2 isolated at low temperatures in argon and alkane matrices.[67-69] By following the concentration dependence of the observed bands these investigators have assigned transitions at approximately 12 500, 17 000, and 20 250 cm^{-1} to diatomic vanadium. In initial work, the extended Hückel model was used to rationalize the observed transitions.[67] In more recent studies, Andrews and Ozin have used SCF-Xα-SW MO calculations to assign the lowest energy transition to a $3d\delta_g \rightarrow 3d\delta_u^*$ excitation from the $(4s\sigma_g)^2(3d\sigma_g)^2(3d\pi_u)^4(3d\delta_g)^2$ ground configuration of V_2.[69]

In other matrix-isolation work the resonance Raman spectra of V_2 were extensively investigated.[65] A complicated set of resonance Raman bands were observed, some of which clearly involved transitions from radiatively and nonradiatively populated excited vibrational and electronic states. In addition, unstructured fluorescence was observed at about 17 200 and 14 400 cm^{-1}, and structured emission was observed near 13 400 cm^{-1}. Despite this complexity, a ground-state resonance Raman progression was identified, with ω_e'' = 537.5 cm^{-1} and $\omega_e x_e''$ = 4.2 cm^{-1}. Both the $0 \rightarrow n$ and $1 \rightarrow n$ members of this progression were observed, with the latter growing in at higher laser powers.

Resonance Raman processes within a slowly relaxing excited electronic state were also observed, particularly at high laser powers.[65] Again, members of both the $0 \rightarrow n$ and $1 \rightarrow n$ progressions were identified, allowing ω_e' = 508.0 cm^{-1} and $\omega_e x_e'$ = 3.3 cm^{-1} to be determined. In addition to resonance Raman processes within this excited electronic state, Raman transitions connecting the ground and excited electronic states were observed. On the basis of these observations, the excited state with the vibrational constants listed above is thought to lie 1860 cm^{-1} above the ground state. Further complicating the analysis is the observation of yet another resonance Raman progression corresponding to excitations from the ground state to a second excited electronic state. This excited state exhibits approximate vibrational constants of ω_e' = 510 cm^{-1} and $\omega_e x_e'$ = 2.5 cm^{-1}. Unfortunately, insufficient data quality prevented the determination of its energy relative to the ground

state.

In the case of divanadium a great deal of the uncertainty concerning the nature of the chemical bonding has been cleared up by detailed gas-phase electronic spectroscopy by Langridge-Smith et al.[43] In this work a pulsed Nd:YAG laser was used to vaporize metallic vanadium in a pulsed supersonic nozzle. Dimers and higher clusters were produced and were cooled to a few degrees Kelvin by supersonic expansion with helium carrier gas. Downstream, a scanning dye laser was used to excite V_2 molecules to an excited electronic state, which could then be photoionized by a KrF excimer laser operating at 248 nm. This photoionization laser was capable of ionizing the excited V_2 molecules with a single photon, but two photons were required at this wavelength to ionize ground-state V_2 molecules. Thus, as the dye laser was scanned, large enhancements of the V_2^+ signal observed in a time-of-flight mass spectrometer were obtained whenever the scanning dye laser was tuned to an absorption peak.

With use of this technique a number of weak bands were observed in the range 15 000–18 000 cm^{-1}.[43] Strong, relatively simple bands, however, were observed between 13 000 and 15 000 cm^{-1}. Under high resolution the rotational structure to these bands could be assigned, and the ground state of V_2 was determined to be $^3\Sigma_g^-$, with a bond length of 1.77 Å. This ground term was split into a $^3\Sigma_{0^+g}^-$ and $^3\Sigma_{1g}^-$ level, which were separated by 75 cm^{-1}. One quantum of vibrational excitation within the $^3\Sigma_{0^+g}^-$ ground level corresponds to 529.5 cm^{-1}, as compared with 529.1 cm^{-1} calculated from the vibrational constants obtained in matrix-isolated resonance Raman experiments.[65]

The excited electronic state accessed in these resonant two-photon ionization experiments is of $^3\Pi_u$ symmetry, split into $^3\Pi_{0u}$, $^3\Pi_{1u}$, and $^3\Pi_{2u}$ levels.[43] It possesses a bond length of 1.70 Å, and one vibrational quantum within the $^3\Pi_{0u}$ level corresponds to 639.7 cm^{-1}. Thus the excited electronic state is even more tightly bound than the ground state.

The large splitting between the $^3\Sigma_{0^+g}^-$ and $^3\Sigma_{1g}^-$ components of the ground state is indicative of a particularly large second-order spin–orbit coupling, such as would occur if a $^1\Sigma_g^+$ state were nearby. This occurs in S_2[70] and Se_2[71] and is characteristic of a half-filled π or δ molecular orbital. This observation suggests a molecular electronic configuration of $(4s\sigma_g)^2(3d\sigma_g)^2(3d\pi_u)^4(3d\delta_g)^2$ which gives $^3\Sigma_g^-$, $^1\Sigma_g^+$, and $^1\Gamma_g$ as molecular terms. The chemical bonding in the $^1\Sigma_g^+$ and $^1\Gamma_g$ terms should be similar to that of the $^3\Sigma_g^-$ ground term. These terms possibly account for the two long-lived excited electronic states observed in resonance Raman studies of matrix-isolated V_2.[65] Transitions from both $^1\Sigma_g^+$ and $^1\Gamma_g$ to the $^3\Sigma_g^-$ ground state are spin *and* Laporte forbidden, so these excited states would be expected to decay very slowly and could build up a sizable population in the matrix. Electronic Raman transitions from the $^3\Sigma_g^-$ ground state to either $^1\Sigma_g^+$ or $^1\Gamma_g$, however, are spin-forbidden and should not be observed unless there is gross spin–orbit contamination of one of the electronic states. In the case of V_2 the large splitting of the $^3\Sigma_{0^+g}^-$ and $^3\Sigma_{1g}^-$ levels of the ground state, and the observation of the $^3\Pi_{0^+u} \leftarrow {}^3\Sigma_{0^+g}^-$ subband (which is formally forbidden according to Hund's case (a) selection rules) imply that gross spin–orbit contamination of the ground state is indeed present.[43] Thus, it is plausible that the excited states observed in resonance Raman spectroscopy[65] may be the $^1\Sigma_g^+$ and $^1\Gamma_g$ predicted for the ground molecular configuration $(4s\sigma_g)^2(3d\sigma_g)^2(3d\pi_u)^4(3d\delta_g)^2$. This interpretation is far from certain, however.

In recent unpublished work using the laser-vaporization, resonant two-photon ionization technique, a number of bands of V_2 have been observed in the 11 250–12 500 cm^{-1} spectral region.[72] These bands are presumably the gas-phase equivalent of the infrared bands observed by Andrews and Ozin,[69] which were assigned to the $3d\delta_g \rightarrow 3d\delta_u^*$ electronic transition. Rotational analysis of these bands has not yet been performed.

In view of this amount of experimental work it is not surprising that a great deal of theoretical work has been done on V_2 as well. In the earliest work,[60] employing the extended Hückel method, a ground electronic state of $(3d\sigma_g)^2(3d\pi_u)^4(3d\delta_g)^4\ ^1\Sigma_g^+$ was obtained, contrary to later experiments. Subsequent extended Hückel calculations also failed to obtain the correct molecular orbital description of the ground state.[68] On the basis of the failure of extended Hückel methods for Sc_2, V_2, and Cr_2, it now appears that this theory is too oversimplified to properly treat the open d-shell transition-metal clusters.

Divanadium was poorly described in an early restricted Hartree–Fock calculation as well, primarily because only closed-shell configurations were considered.[59] In subsequent complete-active-space self-consistent-field (CASSCF) calculations V_2 was accurately calculated to exist as a $(4s\sigma_g)^2(3d\sigma_g)^2(3d\pi_u)^4(3d\delta_g)^2\ ^3\Sigma_g^-$ ground-state molecule, with $r_e = 1.77$ Å, $\omega_e = 593.6$ cm^{-1}, and $D_e = 0.33$ eV.[73] Upon inclusion of configuration interaction, D_e is expected to increase to approximately 2.3 eV, in close agreement with experiment.[73] The low-lying $^1\Gamma_g$ and $^1\Sigma_g^+$ states of V_2, which arise from the same $(3d\delta_g)^2$ configuration as $^3\Sigma_g^-$ have also been calculated at the CASSCF level. These states are very low-lying indeed, with $^1\Gamma_g$ calculated only 0.02 eV above the $^3\Sigma_g^-$ ground state and with $^1\Sigma_g^+$ only slightly higher.[2] The calculated vibrational frequency of V_2 in the $^1\Gamma_g$ state (486 cm^{-1}) is somewhat reduced over that calculated for $^3\Sigma_g^-$ (564 cm^{-1}).[2] This, along with the relative energies calculated for the two states, is consistent with the interpretation that the excited electronic states observed in resonance Raman studies may be the $^1\Gamma_g$ and $^1\Sigma_g^+$ states.

Initial application of local spin density (LSD) methods to V_2 resulted in predictions grossly in error.[56] Owing to a marked propensity to overestimate exchange effects, V_2 was predicted to exist as a high-spin $^9\Sigma_u^-$ or $^9\Delta_u$ ground state.[56] In subsequent applications of local spin density methods, these errors have been corrected. Using spin-polarized, broken-symmetry LCAO local spin density methods, Salahub and Baykara[74] calculate the V_2 ground state to be $^3\Sigma_g^-$, along with $r_e = 1.75$ Å and $\omega_e = 594$ cm^{-1}, in close agreement with experiment. Using the SCF-Xα-SW MO method, Andrews and Ozin also predict $^3\Sigma_g^-$ as the ground state of V_2.[69] Detailed discussions of the advantages and drawbacks of local spin density methods, especially as applied to the transition-metal molecules have been recently presented by Salahub.[75,76]

TABLE 3. Electronic States of $^{51}V_2$[a]

state	T_e, cm^{-1}	ω_e, cm^{-1}	$\omega_e x_e$, cm^{-1}	B_e, cm^{-1}	α_e, cm^{-1}	r_e, Å	obsd transitns: designatn	obsd transitns: ν_{00}	ref
A $^3\Pi_2$	~14 331			B_0 = 0.2313		r_0 = 1.692	A ← X	14 386	43
A $^3\Pi_1$	~14 286			B_0 = 0.2294		r_0 = 1.699	A ← X	14 341	43
A $^3\Pi_0$	~14 251	$\Delta G_{1/2}$ = 639.7		0.2284	0.0011	1.703	A ← X	14 306	43
A′	≤11 200						A′ ← X		69, 72
X″ ($^1\Sigma_g^+$?)	x	510	2.5				resonance Raman		65
X′ ($^1\Gamma_g$?)	1874	508.0	3.3				X′ ← X	1860	65
X $^3\Sigma_{1_g}^-$	~69.5	$\Delta G_{1/2}$ = 540.5		0.2142	0.0014	1.758		75	43
X $^3\Sigma_{0_g}^-$	0	537.1	4.2	0.2104	0.0013	1.774	resonance Raman		43, 65

[a] Uncertain assignments are given in parentheses. See text for details. $D_0°(V_2)$ = 2.49 ± 0.13 eV.

Table 3 provides a summary of our current experimental knowledge of the ground and excited electronic states of V_2. Potential curves of the X, X′, and A states of V_2, calculated from experimental data, are given in Figure 1.

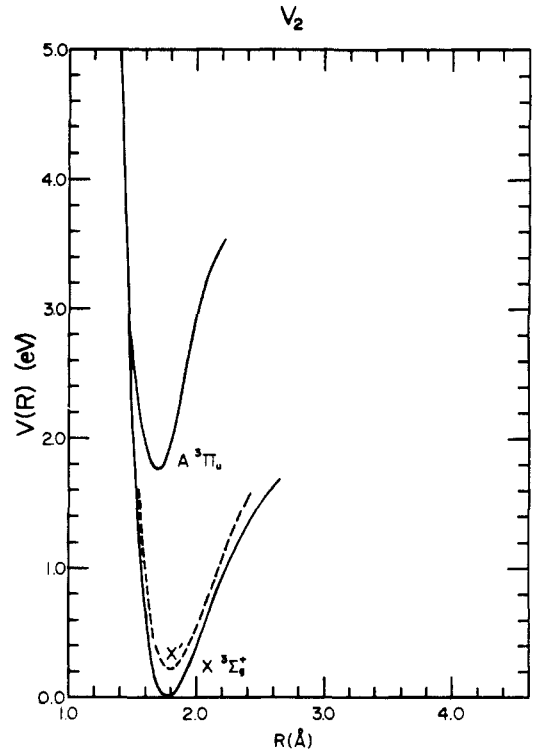

Figure 1. Potential energy curves for V_2, calculated from the experimental data of Table 3. The X′ state is designated by the dashed curve to indicate that its equilibrium position is unknown. This curve must therefore be translated along the R axis by an unknown amount to bring it into coincidence with the true X′ potential curve.

4. Chromium, Cr_2

The first studies of dichromium were Knudsen effusion mass spectrometric measurements of the binding energy. In the initial attempts no Cr_2 was observed, and an upper limit of 1.91 eV was set for $D_0°$.[29,77] At higher temperatures Cr_2 was observed, and the dissociation energy was estimated as 1.56 ± 0.30 eV (as determined by the third-law method) or 1.78 ± 0.35 eV (using the second-law method).[78] Critical reviews have consistently listed the former value,[23-27] although the latter may be more reliable in view of the uncertainty of the parameters necessary for a third-law determination.

Subsequent work has greatly extended our understanding of Cr_2. In 1974 Efremov, Samoilova, and Gurvich observed a rotationally resolved band at 4597.4 Å in a transient absorption experiment following flash photolysis of $Cr(CO)_6$.[37] Although the carrier of the band system was thought to be Cr_2 with a ground-state bond length of 1.71 Å, and the spectrum was assigned as $^1\Sigma_u^+ \leftarrow {}^1\Sigma_g^+$, other possibilities were CrO_2 and CrC_2, which could be formed through fragmentation of CO. Because of this ambiguity, this report was ignored for many years.

Matrix-isolation spectra of Cr_2 were reported in 1975 by Kündig, Moskovits, and Ozin.[79] A broad, unsaturated absorption at 260 nm was tentatively assigned to Cr_2, and an intense, sharp band at 455 nm was definitely assigned to Cr on the basis of its concentration dependence. The rotationally resolved band observed by Efremov et al. at 4597.4 Å clearly corresponded to the matrix band at 455 nm; unfortunately, neither group appears to have been aware of the others' efforts at the time.

Following this work, a number of matrix isolation studies have contributed to our knowledge of Cr_2. Irradiation into the chromium atomic bands at 335[80] and 390 nm[81] has been demonstrated to lead to Cr_2 formation in matrices initially lacking the dimer. In addition, new absorption bands at 332 (30 100) and 340 nm (29 400 cm^{-1}) have been identified following excitation of a chromium-containing matrix at 390 nm.[81] These bands have been assigned to Cr_2, since their irradiation leads to depletion of the Cr_2 absorption near 460 nm.[81] They have been unobserved in other matrix-isolation studies because of severe overlap with the very intense a $^7S \rightarrow$ y $^7P^0$ transition of atomic chromium. Pellin and Gruen[81] tentatively assign them to a $^1\Pi_u \leftarrow {}^1\Sigma_g^+$ transition analogous to the $^1\Pi_u \leftarrow {}^1\Sigma_g^+$ transition of Mo_2, which occurs near 390 nm.[39] These transitions are thought to derive from the intense 4p ← 4s (5p ← 5s in molybdenum) transition of atomic chromium,[81] which has also been suggested[45,46] as the parent transition for the intense $^1\Sigma_u^+ \leftarrow {}^1\Sigma_g^+$ transition of Cr_2, which occurs at 4597.4 Å.

Pellin and Gruen also report a banded emission system which is obtained following excitation of Cr_2 at 351.1 nm, in the wing of the 340-nm absorption system.[81] The banded emission system which they observe has an origin band near 460 nm, and a vibrational frequency of approximately 235 cm^{-1} in the lower state. In addition, a peculiar negative anharmonicity is observed. From other work (see below) the ground-state vibrational frequency of Cr_2 is known to be near 450 cm^{-1}, so these transitions cannot terminate on the ground state. In all probability, these emissions arise from a state of different multiplicity than the ground state and occur as a result of intersystem crossing following 351.1-nm excitation. Pellin and Gruen suggest $^3\Sigma_g^+ \rightarrow {}^3\Sigma_u^+$ as a possibility.[81]

TABLE 4. Electronic States of $^{52}Cr_2$[a]

state	T_e, cm^{-1}	ω_e, cm^{-1}	B_e, cm^{-1}	α_e, cm^{-1}	r_e, Å	obsd transitns: designatn	obsd transitns: ν_{00}	ref
C ($^1\Lambda$)	~38 500					C ← X	38 500	79
B ($^1\Lambda$)	~29 400					B ← X	29 400	81
b ($^3\Sigma_g^+$)	~x + 21 700					b → a	~21 700	81
A $^1\Sigma_u^+$	~21 780	$\Delta G_{1/2}$ = 396.8	0.2313	0.0077	1.6751	A ← X	21 751.42	37, 44, 45, 46, 79
A′ $^1\Sigma_u^+$	~19 430	$\Delta G_{3/2}$ = 468.2	B_1 = 0.2165		r_1 = 1.730	A′ ← X	ν_{10} = 19 907.6	86
A″ $^1\Sigma_u^+$	~19 335	$\Delta G_{1/2}$ = 575.2	B_0 = 0.2417		r_0 = 1.635	A″ ← X	19 396.1	86
A‴($^1\Lambda$)	~14 100					A‴ ← X	14 100	69
a ($^3\Sigma_u^+$)	x	235				b → a	~21 700	81
X $^1\Sigma_g^+$	0	$\Delta G_{1/2}$ = 452.34	0.2303	0.0038	1.6788			

[a] Uncertain assignments are given in parentheses. See text for details. $D_0°(Cr_2)$ = 1.78 ± 0.35 eV.

In other matrix-isolation work, extended into the near-infrared, Andrews and Ozin have recently reported weak transitions in Cr_2 isolated in an argon matrix at 688 (14 500) and 710 nm (14 100 cm^{-1}).[69] On the basis of a comparison with the low energy transitions of V_2 (740–840 nm) these have been assigned to the $3d\delta_u^* \leftarrow 3d\delta_g$ transition in Cr_2.[69]

Matrix-isolation resonance Raman studies have also been undertaken on dichromium.[82-84] In the earliest report a resonance Raman progression with ω_e'' = 427.5 cm^{-1} and $\omega_e''x_e''$ = 15.75 cm^{-1} were obtained for Cr_2 isolated in argon matrices.[82] The identity of the carrier of the spectrum was established by comparison of the calculated and experimental isotopic fine structure. Subsequent gas-phase work[45] determined $\Delta G_{1/2}''$ = 452.34 cm^{-1}, in substantial disagreement with that obtained from ω_e'' and $\omega_e''x_e''$ given above (which give $\Delta G_{1/2}''$ = 396 cm^{-1}). Moskovits et al. suggest that this discrepancy arises due to an anomalously large matrix shift.[83] Resonance Raman studies in xenon matrices support this hypothesis: in xenon ω_e'' = 438.0 and $\omega_e''x_e''$ = 14.5 cm^{-1} are found.[83] The shift of ω_e'' by 10.5 cm^{-1} is unusually large and is indicative of a surprising sensitivity of molecular vibration to the matrix environment.

In addition to the strongly bonded ground electronic state of Cr_2, Moskovits et al.[84] have recently found evidence of a very weakly bonded metastable state. By irradiating into the absorption system near 460 nm while simultaneously taking an absorption spectrum of the chromium-containing matrix, a new absorption system was found. In argon matrices this broad, unstructured absorption was centered at 588 nm (17 000 cm^{-1}). In xenon matrices the absorption induced by irradiating into the 460 nm system occurred at either 629 (15 900) or 704 nm (14 200 cm^{-1}), dependent upon the precise wavelength of irradiation within the 460-nm band. These induced absorption systems are quite persistent, with lifetimes of 0.2–0.9 s. Clearly a metastable state of Cr_2 is being nonradiatively populated in these experiments.[84]

Resonance Raman spectra have been obtained of the metastable species produced in these experiments by simultaneously irradiating the 460-nm band while using a second laser to excite the resonance Raman progression by tuning it near the induced absorption system. In argon matrices ω_e'' = 78.6 cm^{-1} and $\omega_e'x_e'$ = 0.4 cm^{-1} were obtained for this metastable state.[84] In xenon matrices a weak fundamental was observed at approximately 100 cm^{-1} under similar conditions.[84] For such low-frequency vibrations, matrix-dependent shifts of this magnitude are not unexpected. Moskovits et al. suggest two possible explanations for this weakly bonded metastable state. One possibility is that a long-lived state of high multiplicity is formed, and spin selection rules prevent its rapid decay to the singlet ground state. Alternatively, the true ground state of Cr_2 may be a double-minimum potential (see the discussion of this possibility later in this subsection) with an outer well dominated by the $4s\sigma$ bond and an inner well dominated by 3d bonds. The metastable state produced in these experiments could be due to ground-state chromium dimers trapped at low temperatures in the outer well. Such a double-minimum well has been calculated for the dimolybdenum molecule[85] and is not unreasonable for the ground state of Cr_2.

The work of Efremov et al.[37] demonstrating that Cr_2 has a remarkably short bond length was finally confirmed in 1982 when Michalopoulos et al. performed a resonant two-photon ionization study.[44] With use of laser vaporization to produce chromium clusters and a mass spectrometric detection scheme, transitions in the various naturally occurring isotopic species could be separated and identified, leaving no doubt as to the validity of the assignment. Subsequent laser-induced fluorescence spectroscopy at higher rotational temperatures,[45] again using pulsed laser vaporization as the source of Cr_2, permitted accurate determination of the spectroscopic constants. These are given in Table 4, along with a listing of the known electronic states of Cr_2.

In these studies of the 4597.4-Å band of Cr_2, an unusual predissociation pattern was observed.[45,46] This pattern shows a strong dependence on the isotopic species as well as a strong dependence on upper state rotational quantum number, J. Riley et al. have provided a beautiful analysis of the predissociation of Cr_2 in its excited $^1\Sigma_u^+$ state at 21 751 cm^{-1}.[46] The predissociation rate appears to be a periodic function of the rotational energy of the excited state. Riley et al. have analyzed this observation and have deduced the presence of a bound perturber state.[46] They have also suggested a potential energy curve for this perturber state which accounts for the observed J-dependent predissociation. In addition to the perturber state, a dissociative state must also be present to account for the irreversible nonradiative decay of the excited Cr_2 molecule. From these studies it is clear that the photophysical and photochemical pathways in even *diatomic* molecules can be complicated indeed.

Finally, two more excited electronic states have been observed in unpublished resonant two-photon ionization studies by Geusic et al.[86] Both band systems lie to the red of the previously studied 4597 Å $^1\Sigma_u^+ \leftarrow {}^1\Sigma_g^+$ band

TABLE 5. Band Positions of Cr_2[a]

system	band	$^{50}Cr^{52}Cr$	$^{52}Cr_2$	$^{52}Cr^{54}Cr$	ref
A-X	0-0	21751.20 ± 0.05	21751.42 ± 0.02	21751.58 ± 0.05	44, 45
	1-1		21695.9 ± 1		46
	0-1		21299.08 ± 0.02		45
A′-X	2-0		20375.60[b]		86
	2-1		19923.51[b]		86
	1-0	19912.53[b]	19907.64[b]		86
	2-2	19477.81[b]	19477.91[b]		86
	1-1		19455.05[b]		86
A″-X	1-0	19976.21[b]	19970.66[b]		86
	1-1		19519.91[b]		86
	0-0	19395.77[b]	19396.12[b]		86
	0-1	18947.69[b]	18944.02[b]		86
perturbing state			19904.71[b]		86

[a] Gas-phase data only are reported. See text for details. [b] Uncertainty in band positions estimated to be ±2 cm^{-1}; however, the relative uncertainty between band positions for different isotopic species is ±0.1 cm^{-1}.

system, in the 5000–5100 Å region. Although the analysis is not yet complete, both band systems are also $^1\Sigma_u^+ \leftarrow {}^1\Sigma_g^+$ transitions. In fact, one of these excited $^1\Sigma_u^+$ states may be the perturber state which was deduced by Riley et al.[46]

System I is characterized by a 0–0 band at 19396.1 ± 2 cm^{-1} which has been rotationally analyzed to give $B_0' = 0.2417 \pm 0.003$ cm^{-1}, from which $r_0' = 1.635 \pm 0.01$ Å.[86] The decrease in bond length which is observed upon electronic excitation in this band system is consistent with the high observed value of the excited-state vibrational frequency: $\Delta G_{1/2}' = 575.2 \pm 2$ cm^{-1}.[86] The observed rotational constant of the lower state is $B_0'' = 0.2289 \pm 0.003$ cm^{-1}. This is identical (within experimental error) with the accepted value for the ground state of Cr_2, so this band system is unlikely to arise from metastable states of Cr_2 which might be present in the molecular beam. This possibility is further reduced by the observation of hot bands 452 ± 2 cm^{-1} to the red of the parent 0–0 and 1–0 transitions. This is in close agreement to Bondybey's measured $\Delta G_{1/2}'' = 452.34$ cm^{-1} for the lower state of the 4597-Å band system.[45]

System II is not so well-characterized, primarily because the 0–0 band is not present in the spectrum. This could be due to poor Franck–Condon factors or to rapid predissociation, but the remaining bands do form a clear picture. A band at 19907.6 ± 2 cm^{-1} has been assigned as the 1–0 band on the basis of the isotopic shift between the $^{52}Cr_2$ and $^{50}Cr^{52}Cr$ isotopic species. Rotational analysis again indicates a $^1\Sigma_u^+ \leftarrow {}^1\Sigma_g^+$ transition, with $B_1' = 0.2165 \pm 0.003$ cm^{-1} (giving $r_1' = 1.730 \pm 0.01$ Å). The observed rotational constant for the lower state and observed hot bands are again consistent with the accepted values for the Cr_2 ground state. The observed vibrational interval for the excited state is $\Delta G_{3/2} = 468.2$ ± 2 cm^{-1}, again somewhat more strongly bonded than in the ground state. The observed positions for these two band systems are given in Table 5, and the spectroscopic constants of these and other band systems for Cr_2 are summarized in Table 4. Potential energy curves for the X, A, A′, and A″ states of Cr_2 are given in Figure 2.

Since the gas-phase work on chromium dimer has been accomplished, a new matrix-isolation study has appeared, confirming the short bond length of Cr_2.[87] In this work Montano et al. have used EXAFS to determine the distance between chromium atoms in a dilute (0.1 at %) neon matrix. A value of 1.70 ± 0.02 Å was

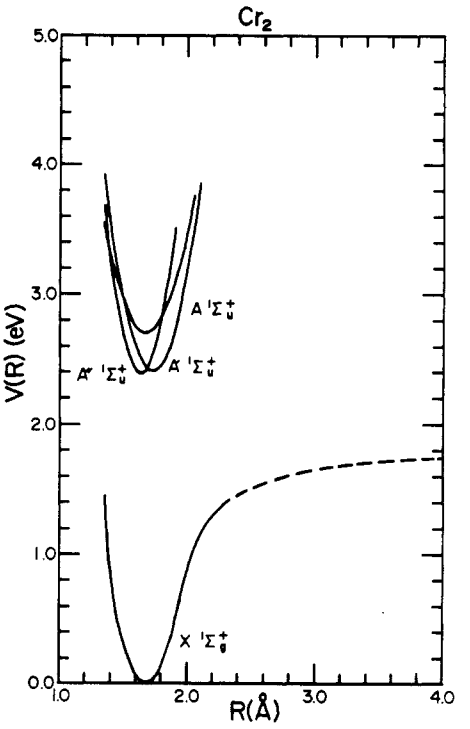

Figure 2. Potential energy curves for the $X\ ^1\Sigma_g^+$, $A\ ^1\Sigma_u^+$, $A'\ ^1\Sigma_u^+$, and $A''\ ^1\Sigma_u^+$, states of Cr_2, calculated from the experimental data of Table 4.

obtained, in agreement with the gas-phase value of r_e'' = 1.6788 Å.[45]

In view of the considerable interest aroused by the observation of metal–metal multiple bonds,[88-92] it is not surprising that considerable theoretical work has been done on Cr_2. Early studies employing extended Hückel methods predicted bond lengths in the range of 1.6–1.9 Å, indicative of multiple bonding involving 3d electrons.[60,93,94] Anderson, using a modified Hückel method, obtains a bond length of 2.5 Å, however.[66] In the earliest self-consistent-field calculations, Wolf and Schmidtke used nonempirical restricted Hartree–Fock methods to obtain $r_e'' = 1.56$ Å and $\omega_e'' = 750$ cm^{-1} for the ground state of Cr_2.[59] At about the same time Hillier and co-workers used a multiconfiguration self-consistent-field method[57] along with configuration interaction[95] to investigate the bonding in Cr_2 and Mo_2. Assuming a molecular term of $(4s\sigma_g)^2(3d\sigma_g)^2(3d\pi_u)^4(3d\delta_g)^4\ ^1\Sigma_g^+$, these authors found a bond length of 1.91 Å and a binding energy of 1.48 eV by using a limited MCSCF procedure.[57] When a more extensive MCSCF

calculation was performed, however, r_e'' = 3.14 Å, ω_e'' = 92 cm^{-1}, and D_0 = 0.14 eV were obtained.[95] The dominant electron configuration possessed a coefficient of only 0.106, contributing only 1.1% to the total wave function, indicating a remarkable degree of electron correlation necessary for the correct description of Cr_2.[95] This observation is especially appalling when one considers that this CI calculation, involving 3196 configurations, utterly failed to reproduce the experimental data for Cr_2.

In an ambitious and well-designed MCSCF calculation based on the generalized valence bond (GVB) method Goodgame and Goddard calculate Cr_2 to be weakly bound, with r_e'' = 3.06 Å, ω_e'' = 110 cm^{-1}, and D_0 = 0.34 eV.[96] The failure of this 6000—configuratioin MCSCF calculation to accurately describe Cr_2 is sobering indeed. Some insight into the reasons for its failure may be found in Goodgame and Goddard's calculation of the analogous dimolybdenum molecule.[85] In this work a full MCSCF optimization involving some 6000 configurations was used to investigate the bonding in Mo_2, in a manner quite analogous to that used for Cr_2. The resulting ground-state potential energy surface for Mo_2 exhibited a double-minimum potential, with the outer minimium occurring at 3.09 Å, with $D_0°$ = 0.49 eV and ω_e'' = 80 cm^{-1}.[85] This well corresponds to a molybdenum dimer bonded primarily by a $(5s\sigma)^2$ bond, with relatively weakly interacting $4d^5$ cores on each atom. The $4d^5$ cores are high-spin coupled on each center, forming ^6S cores on each atom. These are then antiferromagnetically coupled to give a $^1\Sigma_g^+$ ground state.[85]

At small internuclear distances spin recoupling occurs in the Goodgame–Goddard calculation of Mo_2, leading to a second, deeper potential minimum with r_e'' = 1.97 Å, ω_e'' = 455 cm^{-1}, and $D_0°$ = 1.38 eV.[85] Excepting the calculated value of $D_0°$, these values are in good agreement with experiment (see below). Why then is the corresponding calculation so drastically in error in the case of Cr_2? McLean and Liu point out the general problem: to successfully describe Cr_2 an ab initio calculation must place the interaction potentials for the long-bonded, $4s\sigma$-dominated well and the short-bonded, 3d-dominated well correctly on a relative energy scale.[97] This is a very difficult task because the correlation energy of the 3d-dominated bonding arrangement is enormously greater than in the antiferromagnetic, $4s\sigma$-dominated well. This complexity explains why increasing the degree of configuration interaction worsened the agreement with experiment in the studies by Hillier et al.[57,95] Inclusion of a limited number of configurations preferentially lowers the energy of the $4s\sigma$-bonded well, to the point that the 3d-bonded well actually disappears in Cr_2. This effect is present in Mo_2 but is far less severe, owing to the much greater bond strength of the 4d-bonded dimolybdenum molecule.

McLean and Liu also indicate two further difficulties in the accurate treatment of Cr_2.[97] First, in chromium atoms the position of the maximum of the outermost lobe of the 3p orbitals is essentially identical with that of the 3d orbitals. By this measure the 4d orbital in atomic molybdenum is 0.16 Å larger in radius than is the 4p orbital. In the region of significant d bonding, dichromium suffers from repulsions of the filled 3p shells to a much greater extent than its congener, dimolybdenum, suffers from 4p repulsions. As a result the 3p orbitals in Cr_2 must be included as valence orbitals to allow them to move out of the way, thereby permitting the formation of 3d bonds. Of course, the molecule pays an energetic price for this electronic rearrangement. In addition to this effect, McLean and Liu find that the inclusion of 4f basis functions contributes substantially to the strength of the chemical bond in Cr_2 and Mo_2.[97] In these molecules the inclusion of f and g functions increases the calculated bond strength by 0.93 eV for Cr_2 and 1.4 eV for Mo_2.[97] In both cases (but especially Cr_2) this is a very significant fraction of the bond strength (see Table 2).

Walch et al. have used the complete active space self-consistent-field (CASSCF) method to investigate the bonding in Cr_2 by using a large basis set including 4f functions.[73] With 4f functions included and by using a number of configurations equivalent to the Goodgame–goddard calculation, a shoulder is finally observed at the experimental bond length.[73] As a measure of the degree of correlation required, these authors estimate that a reasonable CASSCF-CI calculations would require the inclusion of 57 million configurations![73] More recently, Das and Jaffe have demonstrated that this number can be reduced by the introduction of partially localized orbitals which are of neither g nor u symmetry.[98] With this method a weak potential minimum is obtained for the 3d-bonded form of Cr_2, located at the experimental bond distance; it still lies above the dissociation limit however.[98] In view of the importance of an accurate treatment of the correlation energy as found by these Herculean calculations it now appears that earlier calculations[57,59,60,93,94,99] successfully predicted the tight, 3d-bonded form the Cr_2 due to fortuitous cancellation of errors and in some cases to a failure of the calculated wave function to dissociate properly.

Alternatives to these cumbersome ab initio approaches are the various density functional methods. In these methods the exchange and correlation energies are approximated by functionals of the electron density, ρ, thereby eliminating the need to perform extensive configuration interaction calculations. In the earliest application of these methods to Cr_2, Harris and Jones predicted a $^{13}\Sigma_g^+$ ground state with r_e'' = 3.66 Å.[56] In this calculation the exchange energy was systematically overestimated, leading to the prediction of high spin states for all of the transition-metal dimers. Subsequent local spin density calculations have been more successful. Dunlap, for example, obtains a double-minimum potential for Cr_2 using an $X\alpha$ method and one-electron orbitals without inversion symmetry.[100] Despite the fact that the $X\alpha$ potential fails to reasonably treat correlation in the homogeneous electron gas model on which it is based,[74] this calculation is quite encouraging. Local spin density calculations based on more accurate exchange-correlation potentials, such as those of von Barth and Hedin,[101] Janak, Moruzzi, and Williams,[102] Gunnarsson and Lundqvist,[103] or Vosko, Wilk, and Nusair,[104] provide excellent agreement with experiment,[105–107] although dissociation energies tend to be somewhat overestimated. In all cases where these potentials have been successfully used for dichromium,[105–107] the symmetry requirement placed on the molecular orbitals has been lifted from $D_{\infty h}$ to $C_{\infty v}$. At present it appears that this reduction in orbital

symmetry is without formal justification but is a pragmatic necessity for agreement with experiment.[75] In any case, in view of the extreme difficulty in treating open d-shell transition-metal dimers by conventional ab initio methods, it appears that local spin density methods are preferable candidates for the extension to larger transition-metal cluster systems.

5. Manganese, Mn_2

The initial experimental attempt to observe Mn_2 was a Knudsen mass spectrometric investigation by Kant and Strauss.[29] In this study no Mn_2 was observed, placing an upper limit on $D_0°(Mn_2)$ of 0.91 eV. Following improvements to the mass spectrometer, however, Kant et al. were able to observe Mn_2 at temperatures between 1350 and 1500 K.[108] On the basis of this data, Kant et al. calculate a second-law dissociation energy $D_0°(Mn_2) = 0.1 \pm 0.1$ eV.[108] Applying the third-law method to their data, these authors obtain $D_0°(Mn_2) = 0.33 \pm 0.26$ eV (assuming a van der Waals bond in Mn_2) or $D_0°(Mn_2) = 0.56 \pm 0.26$ eV (assuming covalent bonding). Reviews of dimer bond energies[25-28] typically report an average of the third-law values, $D_0°(Mn_2) = 0.44 \pm 0.30$ eV; to be safe $D_0°(Mn_2) \leq 0.8$ eV is suggested.

Visible and ultraviolet absorption spectra of Mn_2 isolated in rare gas matrices have been reported.[109,110] A banded absorption system with its origin at 14 430 cm^{-1} has been attributed to Mn_2 isolated in argon.[109] This system displays an extended progression, peaking in intensity at the 10–0 transition. The average separation between vibrational bands is 111 cm^{-1}, indicative of a weakly bonded excited state.[109] Klotzbücher and Ozin observe this same system, as well as features at 410, 317, and 254 nm.[110] In this context it should be noted that the identification of the carrier of a spectroscopic transition is a particularly vexing problem in matrix-isolation work, and these bands do not unambiguously correspond to Mn_2. Nevertheless, in an elegant study utilizing magnetic circular dichroism Rivoal et al. have identified bands at 331.5, 347, and 375–386 nm as belonging to the manganese dimer without any ambiguity (see below).[111]

By far the greatest information on the Mn_2 molecule has been obtained by ESR spectroscopy of matrix-isolated dimanganese. In 1981 Van Zee, Baumann, and Weltner observed a number of ESR transitions in samples of manganese matrix-isolated in krypton or xenon.[112] On the basis of the 11-line hyperfine pattern which was observed, these transitions could be definitely assigned to a molecule with two symmetrically equivalent Mn ($I = {}^5/_2$) nuclei. The temperature dependence of the bands demonstrated that the ground state of Mn_2 is a singlet ($S = 0$), with no ESR spectrum. In subsequent work ESR lines corresponding to $S = 1$, 2, and 3 were observed to grow in at successively higher temperatures.[113] Analysis of the temperature dependence of the $S = 2$ transitions clearly indicated antiferromagnetic coupling of the 3d electrons on each atomic center, with a Heisenberg exchange integral, J, of -9 ± 3 cm^{-1}.[113] A fit of the observed transitions to the appropriate spin Hamiltonian provided the axial anisotropic exchange parameter, D_e, which in this case arises solely from magnetic dipolar interactions. From this parameter an internuclear distance of 3.4 Å is calculated for Mn_2.[113] The internuclear distance for a weakly bound, van der Waals molecule such as Mn_2 may be significantly perturbed by matrix interactions. Nevertheless, it appears that the parameters entering the spin Hamiltonian are essentially the same for Mn_2 isolated in Ar, Kr, or Xe matrices. This indicates that the Mn–Mn interaction is considerably stronger than the interaction of manganese with rare gas atoms, including xenon.[113]

Following the initial study which demonstrated temperature-dependent ESR bands,[112] Rivoal et al. used temperature variation and magnetic circular dichroism to identify several ultraviolet bands as belonging to Mn_2.[111] A transition occurring at 347 nm was shown to belong to the excited $S = 2$ state of Mn_2, and from its temperature dependence the Heisenberg exchange integral, J, was determined to be $J = -10.3 \pm 0.6$ cm^{-1},[111] in agreement with ESR results.[112,113] A weaker band at 331.5 nm exhibited a similar temperature dependence and probably also derives from the $S = 2$ state.[111] Transitions at 375, 380, and 386 nm exhibit a different temperature dependence and may originate from the lower energy $S = 1$ state.[111]

More recently, Moskovits, DiLella, and Limm have investigated the resonance Raman spectrum of manganese isolated in argon matrices.[63] The most intense spectra were obtained with 676.5-nm irradiation, which is undoubtedly due to excitation into the 650-nm band reported by DeVore et al.[109] Three resonance Raman progressions were observed, at frequencies given by $\Delta\nu = \delta + n\omega_e - (n^2 + n)\omega_e x_e$, with δ, ω_e, and $\omega_e x_e$ given by (0, 124.69, 0.24 cm^{-1}), (135.7, 124.6, 0.20 cm^{-1}), and (196.69, 123.97, 0.275 cm^{-1}), respectively. The latter two resonance Raman progressions decrease in intensity relative to the first progression as the concentration of manganese in the matrix is decreased. All of these are true resonance Raman, rather than fluorescence, because they occur at the same spectral positions relative to the exciting line with more than one exciting frequency.[63]

Moskovits et al. attribute the first progression to resonance Raman transitions within the ${}^1\Sigma_g^+$ ground state of Mn_2 and assign the latter two progressions to electronic resonance Raman processes involving ${}^9\Sigma_g^+ \leftarrow {}^1\Sigma_g^+$ and ${}^{11}\Sigma_u^+ \leftarrow {}^3\Sigma_u^+$ transitions, respectively.[63] This assignment appears extremely dubious considering that transitions involving $\Delta S = 4$ are invoked. An alternative interpretation is that a polyatomic resonance Raman spectrum is excited in these experiments and that the molecule has Raman-active vibrations with frequencies of approximately 124, 136, and 197 cm^{-1}. If the 124 cm^{-1} vibration were a totally symmetric vibration which undergoes a large change in equilibrium position in the resonant, excited electronic state, a long progression in this mode would be observed. If this were the case, it would not be surprising to find long progressions in this mode built upon other Raman-active vibrations as well. In this context one may note that the 650-nm band system which is responsible for these resonance Raman progressions is observed only with relatively high manganese concentrations.[110,111] It also exhibits a long vibration progression in visible absorption, indicative of a large change in equilibrium geometry upon electronic excitation, as required for this explanation.[109] It is also known that a manganese

cluster of high nuclearity (Mn_5 or larger) is readily formed under matrix conditions and has been observed by ESR.[113,114] Armed with the knowledge of the ESR spectra of Mn_2 and Mn_5, the entire question could probably be resolved by an optical ESR double-resonance experiment, but this has yet to be performed.

In other work on dimanganese, Ervin, Loh, Aristov, and Armentrout have measured the bond energy of Mn_2^+ by using an ion beam apparatus.[115] Electron-impact ionization/fragmentation was used to produce Mn_2^+ from volatile $Mn_2(CO)_{10}$, and cross-sections for collision-induced dissociation with argon were measured as a function of Mn_2^+ kinetic energy. Analysis of the data identified the bond energy of Mn_2^+ as 0.85 ± 0.20 eV. Although the bond strengths of Cr_2 and Mn_2 are poorly known, it appears that the bond energy of Mn_2^+ is intermediate, falling between the values for Cr_2 and Mn_2. This is not surprising since Cr_2 exhibits multiple 3d bonds, while Mn_2 appears to be a van der Waals molecule. The detailed electronic and geometrical structure of Mn_2^+ would be fascinating, since it lies on the border between these two extremes of chemical bonding.

Theoretical work on dimanganese began in 1964 when Nesbet used Hartree–Fock theory and a Heisenberg treatment.[116] He predicted that the ground state of Mn_2 would have $r_e'' = 2.88$ Å and $D_e'' = 0.79$ eV. The ground term, calculated as $^1\Sigma_g^+$, would possess a single σ-bond and antiferromagnetically coupled π and δ electrons, with $J = -4.13$ cm^{-1}.[116] This is in remarkably good agreement with the experimentally derived values $J = -10.3 \pm 0.6$ cm^{-1} and $r_e = 3.4$ Å.[111,113]

Less rigorous theories resulted in a wide range of predictions for Mn_2 in the ensuing 20 years. Extended Hückel methods predicted a bond length of 1.90 Å with $\omega_e'' = 325$ cm^{-1},[60] while Hartree–Fock methods restricted to closed-shell configurations predicted $r_e'' = 1.52$ Å and $\omega_e'' = 680$ cm^{-1}.[59] As in its other applications, local spin density calculations by Harris and Jones predicted an extremely high multiplicity ground state, either $^{11}\Pi_u$ or $^{11}\Sigma_u^+$.[56]

More recently, Salahub and Baykara have applied the same version of local spin density theory which succeeded so well for Cr_2 to the manganese dimer.[74] This version of LSD theory uses broken-symmetry ($C_{\infty v}$) molecular orbitals and the Janak–Moruzzi–Williams correlation-exchange potential,[102] as discussed in the previous subsection. Various electronic configurations were investigated, and three were found to lie within 0.3 eV of one another.[74] Considering only the 4s and 3d electrons, the lowest energy state calculated corresponded to a $(4s\sigma_g)^2(3d\pi_u)^4(3d\sigma_g)^2(3d\delta_g)^4(3d\delta_u^*)^2\ ^3\Sigma_g^-$ state with $r_e = 1.67$ Å and $D_e = 0.98$ eV and with full symmetry-adapted orbitals, as designated by the u and g subscripts.[74] Calculated only 0.12 eV above this is a $1\sigma^2 1\delta^4 1\pi^4 2\sigma^2 3\sigma^2$ configuration in which the symmetry remains broken, resulting in an antiferromagnetically coupled state.[74] This state, with $r_e = 2.52$ Å, $D_e = 0.86$ eV, and $\omega_e = 144$ cm^{-1}, is the local spin density equivalent of the ground state found by Nesbet.[116] Finally, a broken-symmetry, antiferromagnetically coupled state arising from the $1\sigma^2 1\delta^4 1\pi^4 2\sigma^2 2\pi^2$ configuration is calculated with $r_e = 2.15$ Å and $D_e = 0.72$ eV.[74] The possibility of three completely different states, with r_e ranging from 1.67 to 2.52 Å, lying within 0.3 eV of the true ground state underscores with complexity of the transition-metal dimers and points out the need for further experiments on these molecules.

6. Iron, Fe_2

In the first experimental investigations of the iron dimer, Lin and Kant measured the dimerization equilibrium of $2Fe(g) \rightleftarrows Fe_2(g)$ over molten iron in the temperature range 1900–2100 K.[117] The second-law method of analysis yielded a dissociation energy, $D_0°(Fe_2) = 0.82 \pm 0.30$ eV. Agreement between this second-law value and the result based on the third-law or absolute-entropy method requires both a high electronic degeneracy in Fe_2 and a large number of low-lying energy levels.[117] A subsequent study by Shim and Gingerich[118] essentially confirmed the measurements of Lin and Kant.[117] In this more recent investigation, however, ab initio Hartree–Fock plus configuration interaction calculations were used to evaluate the electronic contribution in the third-law method.[118] With use of the experimental value of ω_e'' obtained from resonance Raman studies (see below), a third-law value of $D_0°$ was obtained as $D_0°(Fe_2) = 0.78 \pm 0.17$ eV,[118] in close agreement with the second-law value reported by Lin and Kant.[117]

In an argon-matrix-containing iron, DeVore et al. have attributed three band systems to Fe_2.[109] Two are characterized by band origins and vibrational frequencies of (18 355, 194 cm^{-1}) and (21 095, 218 cm^{-1}), respectively. The third system is a continuum, with a maximum at 24 100 cm^{-1}.[109] These absorption systems have also been observed by Moskovits et al. and assigned to Fe_2.[119–121]

Moskovits and DiLella have investigated the resonance Raman spectra obtained from argon and krypton matrices containing iron and have assigned overtones up to $v = 16$ to Fe_2.[121,122] Both the predominant $^{56}Fe_2$ (84.40%) and the less common $^{54}Fe^{56}Fe$ (10.7%) isotopic modifications were identified, and the observed isotopic shift and relative intensities confirmed the assignment as diatomic iron.[121] Resonance Raman spectra were observed with excitation in the wavelength range 457–514 nm but were *not* observed in the range 575–615 nm.[121] This is consistent with the matrix-isolation spectra attributed to Fe_2, which show absorption in the range 540–450 nm, but not at 575–615 nm.[109,119–121] Analysis of the observed resonance Raman progressions yields $\omega_e'' = 300.26$ cm^{-1} and $\omega_e''x_e'' = 1.45$ cm^{-1} for $^{56}Fe_2$.[122] Fitting a Morse oscillator to these parameters implies $D_e = 1.9$ eV, while a LeRoy–Bernstein analysis[123] yields $D_e = 1.20$ eV.[122] More recently, Moskovits has reported a revised LeRoy–Bernstein value of $D_0 = 0.90 \pm 0.10$ eV. This is in agreement with the work of Shim and Gingerich,[118] and is given as the selected value in Table 2.

Mössbauer spectroscopy has also been applied to Fe_2 isolated in rare gas matrices.[124–126] In matrices which were composed of 1–2 at. % Fe, the dimer Mössbauer spectrum is dominated by two sharp lines which result from the quadrupole splitting of the ^{57}Fe nucleus in the axially symmetric field gradient of the molecule.[124] In addition, a dimer isomer shift of $\delta = -0.14 \pm 0.02$ mm/s is obtained, which is indicative of an effective atomic configuration between $3d^64s^2$ and $3d^64s$.[126] From an analysis of the magnetic hyperfine interaction observed,

Montano concludes that Fe_2 possesses a high electronic angular momentum.[125,126] This is in agreement with the conclusions of Lin and Kant[117] and Shim and Gingerich,[118] who find that a high electronic degeneracy is necessary to bring the second-law and third-law dissociation energies into agreement.

EXAFS and XANES spectra of Fe_2 isolated in rare gas matrices have also been obtained by Montano and co-workers.[127,128] Analysis of these spectra yielded $r_0'' = 1.87 \pm 0.13$ Å for Fe_2 isolated in argon[127] and $r_0'' = 2.02 \pm 0.02$ Å for Fe_2 isolated in neon.[128] Attempts to observe Fe_2 by ESR methods by Baumann, Van Zee, and Weltner have been unsuccessful.[129]

A few studies of gas-phase iron dimers have been recently reported. Measurements of the photoionization threshold place the ionization potential of Fe_2 at 6.30 ± 0.01 eV,[130,131] in good agreement with the value of 5.9 ± 0.2 eV obtained by Lin and Kant using high-temperature mass spectrometry.[117] The observed ionization potential of Fe_2 compared to the ionization potential of atomic iron indicates that Fe_2^+ is bound by 1.6 eV more than Fe_2.[131] Rohlfing et al. have rationalized this observation by noting that in order to form a $(4s\sigma_g)^2$ bond in Fe_2 both atoms must be promoted from $3d^64s^2$ to $3d^74s$.[131] In Fe_2^+, however, only one atom need be promoted, since the atomic Fe^+ ion already has a $3d^64s$ configuration. From Table 1 we see that formation of a $(4s\sigma_g)^2$ bond in Fe_2 will require 0.87 eV of additional promotion energy compared to Fe_2^+. The remaining 0.73 eV of additional bond energy in Fe_2^+ as compared to Fe_2 may arise because the 4s orbital is more contracted in Fe_2^+, allowing the atoms to approach each other more closely, thereby permitting significant bonding interactions of the 3d orbitals.

Recent photoelectron spectroscopic investigations on Fe_2^- demonstrate that this anion is also more strongly bound than Fe_2.[41] The observed electron affinities (0.902 ± 0.008 eV for Fe_2; 0.151 ± 0.003 eV for Fe) indicate that Fe_2^- is bound 0.75 ± 0.01 eV more strongly than Fe_2.[41] Although it is not clear how to explain this observation in terms of simple molecular orbital theory, the general phenomenon is readily explained by classical electrostatics. By treating a metallic cluster as a conducting sphere of radius R, one may calculate the difference in the amount of energy required to remove an electron from a sphere of radius R and from a sphere of infinite radius.[132-134] This may be rearranged to give the ionization potential and electron affinity of a sphere of radius R in terms of the bulk work function, W:

$$\mathrm{IP}(R) = W + \tfrac{3}{8}\, e/R \qquad (2.4)$$

$$\mathrm{EA}(R) = W - \tfrac{5}{8}\, e/R \qquad (2.5)$$

From these formulae one notes that in general, the ionization potential will *decrease* with increasing R (corresponding to increasing cluster size) while the electron affinity will *increase* with increasing R. Thus it is easier to stabilize a charge of either sign on a larger cluster than on a smaller one. This classical, electrostatic effect contributes to the increased binding energy of both anionic *and* cationic clusters compared to neutral clusters, as is observed in Fe_2. Recent work has demonstrated a second $1/R$ term also contributes to the ionization potential and electron affinity of clusters.[135,136] It involves the surface tension of a cluster, and causes a small deviation of the measured coefficient of $1/R$ from the values given above.[135,136] Nevertheless, the above formula for ionization potential has been strikingly confirmed by Schumacher and co-workers in studies with alkali clusters; it is remarkably well-obeyed for alkali clusters of more than three atoms.[134,135] No doubt this electrostatic effect contributes to the increased electron affinity of Fe_2 compared to Fe as well.

Only a few high-quality calculations have been made on Fe_2. In an early effective Hückel calculation bond energies of 3–5 eV were obtained, depending on basis set, in gross disagreement with experiment.[60] A subsequent restricted Hartree–Fock calculation predicted $r_e'' = 1.58$ Å and $\omega_e'' = 660$ cm^{-1}, again differing substantially from experiment.[59] In the first application of local spin density theory, Harris and Jones predicted a $^7\Delta_u$ ground state with $r_e'' = 2.10$ Å, $\omega_e'' = 390$ cm^{-1}, and $D_e = 3.45$ eV to arise from a $(4s\sigma_g)^2(3d\sigma_g)^2(3d\pi_u)^4(3d\delta_g)^3(3d\delta_u{}^*)^2(3d\pi_g{}^*)^2(3d\sigma_u{}^*)^1$ configuration.[56] A similar result is obtained by Salahub and co-workers using improved, broken-symmetry local spin density methods; $r_e'' = 2.01$ Å, $\omega_e'' = 402$ cm^{-1}, and $D_e = 4.0$ eV are obtained.[138] Apart from the gross overestimate of the binding energy these local spin density results are not too unreasonable.

Finally, an all-electron Hartree–Fock configuration interaction calculation has been performed on Fe_2.[118] In this work all 112 states resulting from the interactions of two excited ^{5}F $3d^74s^1$ iron atoms were calculated, and configuration interaction allowing full reorganization of the electrons within the 3d shells was included.[118] The ground state was again calculated to be $^7\Delta_u$, with $r_e'' = 2.40$ Å and $\omega_e'' = 204$ cm^{-1}, with an electronic configuration of $(3d\sigma_g)^{1.57}(3d\pi_u)^{3.06}(3d\delta_g)^{2.53}(3d\delta_u)^{2.47}(3d\pi_g)^{2.89}(3d\sigma_u)^{1.49}(4s\sigma_g)^{2.00}$. An important result of this calculation was that all 112 electronic states were calculated to lie within 0.54 eV of the ground state. The energies of these electronic states, calculated for an internuclear separation of 2.482 Å, are given in Figure 3. According to this calculation Fe_2 is properly described as bonded by a $(4s\sigma)^2$ bond, with two relatively weakly interacting $3d^7$ cores.

The theoretical model of Fe_2 described above is expected to gain applicability as one moves further to the right in the transition series. As one traverses the transition series from left to right, the 3d orbitals contract relative to the 4s orbital (see Table 1), until eventually they are too contracted to actively take part in chemical bonding. At this point the transition-metal dimers are best described as consisting of a $(4s\sigma)^2$ bond, with weakly interacting $3d^n$ cores. As a result of weak interactions between th $3d^n$ cores there will be a large number of low-lying electronic states corresponding to the various angular momentum couplings of the $3d^n$ cores. This is essentially the picture which emerges from recent calculations on Fe_2,[118] Co_2,[30] Ni_2,[139-141] NiFe,[142] and NiCu.[143] Recent experimental work has confirmed this picture for Ni_2,[47] and photofragmentation studies confirm it for Fe_2^+ and Ni_2^+ as well.[137]

The photoelectron spectra obtained for Fe_2, however, cast considerable doubt on this model for the neutral iron dimer.[41] Two vibronic band systems are observed in the photoelectron spectrum, both characterized by an anion vibrational frequency of 250 ± 20 cm^{-1} and a neutral vibrational frequency of 300 ± 15 cm^{-1}.[41] The

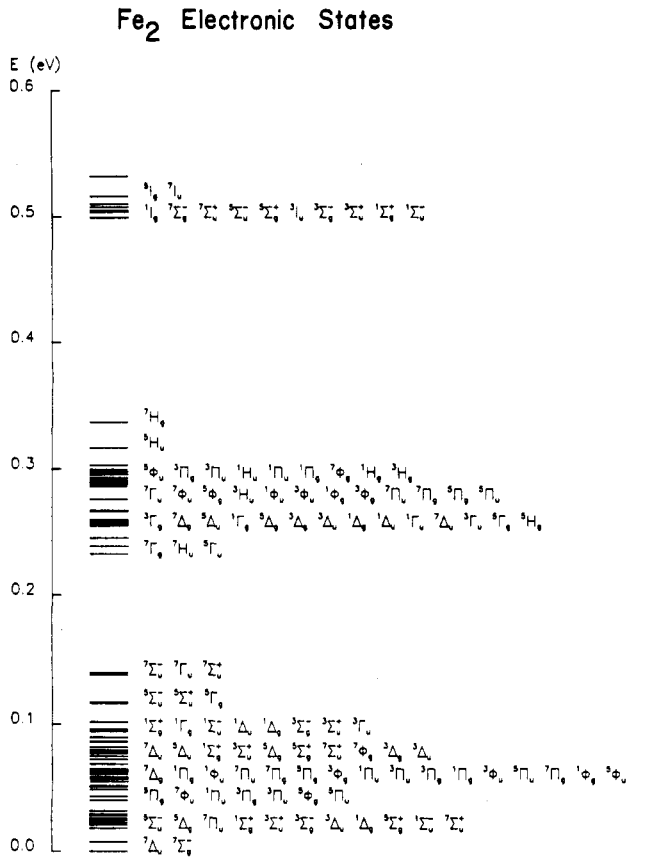

Figure 3. Electronic states of Fe_2, neglecting spin–orbit coupling, calculated for an internuclear separation of 2.48 Å. Reprinted with permission from ref 118. Copyright 1982 American Institute of Physics.

neutral vibrational frequency is in agreement with the resonance Raman results $\omega_e'' = 300.26$ cm^{-1} and $\omega_e''x_e'' = 1.45$ cm^{-1}.[121,122] On the basis of the observed vibronic intensities, a harmonic Franck–Condon analysis yields a bond length change of 0.08 ± 0.02 Å upon electron attachment, giving 2.10 ± 0.04 Å for the Fe_2^- bond length.[41] The only excited state of Fe_2 populated by photodetachment of Fe_2^- is observed 4310 ± 30 cm^{-1} above the ground state, with the same vibrational frequency and bond length as ground-state Fe_2.[41]

The sparse photoelectron spectrum of Fe_2^-, in which only one excited electronic state of Fe_2 is observed within 1 eV of the ground state, is in marked contrast to the 112 electronic states calculated to lie within 0.54 eV of the ground state by Shim and Gingerich.[118] In the Shim–Gingerich model, the chemical bonding of Fe_2 is essentially due to a $(4s\sigma_g)^2$ bond, with the 112 electronic states arising from the couplings of the weakly interacting $3d^7$ cores. In the Fe_2^- anion, then, one expects the additional electron to enter either a $4s\sigma_u$ antibonding orbital or the 3d core. In the former case, the two prominent photoelectron band systems are likely due to detachment of $4s\sigma_g$ and $4s\sigma_u$ electrons, respectively, since detachment of 3d electrons is observed with only weak intensity in the atomic anions.[41] Thus the ground and excited states of Fe_2 observed by photoelectron spectroscopy are expected to arise from $(4s\sigma_g)^2$ and $(4s\sigma_g)(4s\sigma_u)$ configurations, respectively. The observation of identical equilibrium internuclear separations and vibrational frequencies in these states of Fe_2 then implies that the $4s\sigma_g$ and $4s\sigma_u$ orbitals are of nonbonding or weak antibonding character,[41] contrary to the calculations of Shim and Gingerich.[118]

The second possibility places the additional electron of Fe_2^- in a 3d core orbital.[41] The two prominent band systems of Fe_2^- then cannot arise from detachments of 4s electrons, since the Fe_2 neutral would remain in a $(4s\sigma_g)$ configuration, and this would lead to only one band. Other bands, arising from detachment of 3d electrons, would be expected to be much weaker in intensity and would lead to many different electronic states of Fe_2 corresponding to the various couplings of the 3d electrons left behind in the molecule. In the Shim–Gingerich model these would form a near continuum of electronic states,[118] which is again inconsistent with the observed spectrum.[41]

On the basis of the photoelectron spectrum, it thus appears that the 3d electrons are more intimately involved in the chemical bonding of Fe_2 than predicted by careful ab initio calculations. In addition, the fact that no excited electronic states of Fe_2^- are populated in the 300 K ion source used in these experiments suggests that 3d bonding is important in Fe_2^- as well. More surprising still is the fact that very similar results are obtained in the photoelectron spectrum of Co_2^-,[41] a dimer in which the model sketched above is expected to be more appropriate still (see below).

Finally, a photofragmentation study has been recently reported for jet-cooled Fe_2^+. In this work, Fe_2^+ was separated from other Fe_n^+ ions in the first leg of a tandem mass spectrometer. The mass-separated, jet-cooled Fe_2^+ was then irradiated with a pulse of visible laser light, and the product atomic ions were observed in the second leg of the mass spectrometer. On the basis of the observed fluence dependences it was concluded that the Fe_2^+ dissociation threshold lies between 2.43 and 2.92 eV.[137] In combination with the ionization potential of 6.30 ± 0.01 eV,[131] this places the dissociation threshold of Fe_2 between 0.83 and 1.32 eV.[137] In contrast to Ni_2^+ and Nb_2^+, no sharp, resonance-enhanced two-photon dissociation spectra were observed.[137] Only a broad continuum was observed, indicating that Fe_2^+ possesses a very high density of optically accessible states in the 2-eV region.[137] This is in marked contrast to the results for Fe_2^- and Fe_2 observed by photoelectron spectroscopy. Clearly much more work is required on the Fe_2 system before a complete understanding will be attained.

7. *Cobalt, Co_2*

The dissociation energy of dicobalt was determined by monitoring the equilibrium $2Co(g) \rightleftarrows Co_2(g)$ over molten cobalt by Kant and Strauss in 1964.[29] Insufficient data were obtained for a second-law determination of $D_0°(Co_2)$. A third-law determination gave $D_0°(Co_2) = 1.69 \pm 0.26$ eV,[29] which has remained the value cited in critical reviews for many years.[23–26] Recently, however, Shim and Gingerich have performed an all-electron Hartree–Fock configuration interaction calculation on Co_2 and have used their results to recalculate $D_0°(Co_2)$, finding $D_0°(Co_2) = 0.95 \pm 0.26$ eV.[30] The considerable difference between these values illustrates the problems of third-law determinations of $D_0°$ for molecules which are poorly known.

Ozin and Hanlan have reported UV–visible absorption spectra of cobalt isolated in argon.[144] On the basis of the observed concentration dependence and cryo-

photochemical behavior, bands at 442, 418, 340, 320, 280, and 270 nm were assigned to Co_2. In other matrix-isolation work, DiLella, Loewenschuss, and Moskovits have obtained a resonance Raman spectrum of Co_2.[145] On the basis of this spectrum the vibrational frequency of Co_2 is assigned to be $\omega_e'' = 290$ cm^{-1}.[82] In another study, an attempt to observe an ESR spectrum for Co_2 isolated in rare gas matrices failed to produce detectable Co_2 signals.[129]

The only other experimental data on Co_2 were obtained by photoelectron spectroscopy on Co_2^- produced from $Co_2(CO)_8$ in a flowing afterglow ion source.[41] In this work the electron affinities of Co and Co_2 were determined to be 0.662 ± 0.003 and 1.110 ± 0.008 eV, respectively. From these data we may conclude that Co_2^- is bound 0.448 ± 0.011 eV more strongly than Co_2, in keeping with the general behavior expected for metal clusters as discussed in the previous subsection. Two intense band systems of Co_2 were observed in the photoelectron spectrum reported by Leopold and Lineberger.[41] The lower energy system produces Co_2 in its ground electronic state. A vibrational progression is observed with $\omega_e'' = 280 \pm 20$ cm^{-1}, which is consistent with the reported matrix-isolation value.[82] Hot bands arising from $v = 1$ and $v = 2$ levels of Co_2^- determine the vibrational frequency of the anion to be $\omega_e'' = 240 \pm 15$ cm^{-1}. On the basis of the Franck–Condon intensity pattern observed, it is suggested that the bond length of Co_2^- exceeds the value for Co_2 by 0.08 ± 0.02 Å.[41]

The second intense band system observed in Co_2 produces dicobalt with 600 ± 20 cm^{-1} of electronic energy. The vibrational frequency of Co_2 in this excited electronic state is identical (within experimental error) with the value of ground-state Co_2. At higher energies, at least two weak band systems are observed, producing Co_2 with approximately 5000 cm^{-1} of electronic energy.[41]

As discussed in the previous subsection, these results are in conflict with the expected model of chemical bonding in the heavier homonuclear dimers of the 3d transition series. Apart from early extended Hückel,[60] restricted Hartree–Fock,[59] and preliminary local spin density calculations[56] which are generally unreliable, the only calculation on Co_2 is an all-electron, ab initio Hartree–Fock configuration calculation by Shim and Gingerich.[30] In this calculation, orbitals were optimized for the lowest energy configuration and used without further change in a configuration interaction calculation which allowed full reorganization within the 3d shells. All 84 states arising from the interaction of two ^{4}F ($3d^84s^1$) cobalt atoms were found to lie in an energy range within 0.42 eV of the ground state. The energies of these 84 electronic states, calculated for an internuclear separation of 2.50 Å, are given in Figure 4. The ground state itself was calculated to be $^5\Sigma_g^+$, arising from a $(3d\sigma_g)^{2.00}(3d\pi_u)^{3.09}(3d\delta_g)^{3.02}(3d\delta_u)^{2.98}(3d\pi_g)^{2.91}(3d\sigma_u)^{2.00}(4s\sigma_g)^{1.94}(4s\sigma_u)^{0.06}$ natural orbital occupation. The near equality of occupation number for the 3d bonding and antibonding orbitals indicates that these orbitals are essentially localized on the individual atoms, which are held together by a $(4s\sigma_g)^2$ bond. The values $r_e'' = 2.56$ Å and $\omega_e'' = 162$ cm^{-1} are obtained for the $^5\Sigma_g^+$ ground state of Co_2.[30] This value for ω_e'' is considerably less than the value obtained in resonance Raman[82,145] and photoelectron spectroscopic[41] experiments. In addition, the dense manifold of low-lying electronic states is in conflict with the observed photoelectron spectra.[41] At this point it appears that 3d contributions to the chemical bonding in dicobalt are underestimated in current ab initio theories, as is apparently true for diiron as well. Further work is necessary to clearly establish the relative importance of 3d and 4s contributions to the chemical bond in dicobalt, however.

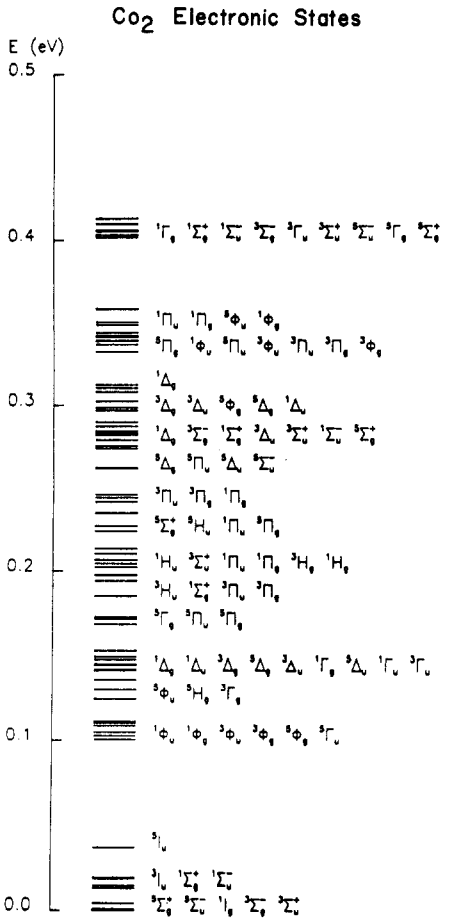

Figure 4. Electronic states of Co_2, neglecting spin–orbit coupling, calculated for an internuclear separation of 2.50 Å. Reprinted with permission from ref 30. Copyright 1983 American Institute of Physics.

8. Nickel, Ni_2

Kant first confirmed the existence of Ni_2 by observing it mass spectrometrically in the vapor phase over liquid nickel at 2000–2200 K.[146] A second-law calculation from his data gave $D_0°(Ni_2) = 2.03 \pm 0.30$ eV, while the absolute entropy method gave $D_0°(Ni_2) = 2.36 \pm 0.22$ eV. Kant also determined the appearance potential of Ni_2^+ to be 6.4 ± 0.2 eV, from which one may derive $D_0°(Ni_2^+) = 3.26 \pm 0.5$ eV using the second-law value of $D_0°(Ni_2)$.[146] Subsequent experiments on jet-cooled Ni_2 establish $D_0°(Ni_2) = 2.068 \pm 0.01$ eV (see below),[47] in good agreement with the second-law value. This value then places $D_0°(Ni_2^+) = 3.30 \pm 0.2$ eV, indicating significantly stronger chemical bonding in Ni_2^+ than in Ni_2.

A number of optical transitions have been observed in absorption spectroscopy of rare gas matrices containing nickel. In the earliest reported study, DeVore et al. observed a series of sharp absorptions with $\nu_{00} = 21\,786$ cm^{-1} and $\omega_e = 192$ cm^{-1} in an argon matrix containing nickel.[109] Although this band system was at-

TABLE 6. Electronic States of $^{58}Ni_2$[a]

state[b]	T_e, cm^{-1}	ω_e, cm^{-1}	$\omega_e x_e$, cm^{-1}	B_e, cm^{-1}	r_e, Å	obsd transitns: designatn	obsd transitns: ν_{00}	ref
D						D ← X	43 300	35
C		$\Delta\bar{G} \approx 329$				C ← X	26 500	147-149
B						B ← X	ν_{max} = 24 400	148, 149
A						(A → X)	22 246	150
(A′)		($\Delta\bar{G} \approx 192$)				(A′ ← X)	(21 786)	(109)
A″		$\Delta\bar{G} \approx 328$				A″ ← X	18 920	148, 149
A (Ω = 5)				B_v = 0.1042 ± 0.0006	r_v = 2.364	A ← X		47
X $^1\Gamma_g$ or $^3\Gamma_u$ (Ω = 4)	0	(380.9)	(1.08)	B_0 = 0.1203 ± 0.0007	r_0 = 2.200			47, 150

[a] Uncertain values or assignments are given in parentheses. When the entire system could pertain to another molecule, the reference is given in parentheses. See text for details. $D_0°(Ni_2)$ = 2.068 ± 0.01 eV. [b] State designations are almost meaningless due to the high density of electronic states in this molecule. They are provided simply to permit designations of the observed transitions.

tributed to Ni_2, subsequent investigators have not succeeded in reproducing it. A banded system with ν_{00} = 26 500 cm^{-1} and ω_e' = 329 cm^{-1} has been observed and attributed to dinickel,[145-147] along with a continuous band centered at 410 nm,[148,149] and a second banded system with ν_{00} = 18 920 cm^{-1} and ω_e' = 328 cm^{-1}.[148,149] Finally, Ahmed and Nixon have observed an emission band system with ν_{00} = 22 246 cm^{-1}, ω_e = 380.95 cm^{-1}, and $\omega_e x_e$ = 1.08 cm^{-1} when a matrix containing nickel is irradiated in the absorption band system near 360 nm.[150] Recent work by Bondybey, however, suggests that this band system is due to Se_2, presumably left over in the source from a previous experiment.

Morse et al. reported investigations of the jet-cooled nickel dimer using the resonant two-photon ionization technique.[47] Despite numerous attempts, no spectra could be obtained corresponding to the band systems observed in rare gas matrices. Further to the red, however, a complicated, congested spectral pattern was obtained, extending from 6000 to beyond 9000 Å. At the blue end of this range vibronic transitions were very dense indeed, with vibronic bands separated by only 10 cm^{-1} on average. By using time-delayed resonant two-photon ionization methods Morse et al. measured the excited-state lifetimes for several transitions in the 16 400–16 900 cm^{-1} range. A sharp transition from long (~10 μs) to short (~10 ns) lifetimes was observed to occur at 16 680 ± 10 cm^{-1}. This sudden drop in lifetime signaled the opening of a new decay channel and was identified as a predissociation limit. The high density of observed vibronic bands in Ni_2 is evidence of strong perturbations between Born–Oppenheimer states, leading to a sharing of oscillator strength among many states. Such strong perturbations ensure that any state above the dissociation limit is coupled to the dissociative continuum, leading to predissociation on a short time scale. With this reasoning, Morse et al. assigned 16 680 ± 10 cm^{-1} as the true dissociation limit, from which $D_0°(Ni_2)$ = 2.068 ± 0.01 eV was obtained.[47]

Yet further to the red, isolated vibronic bands of Ni_2 were found.[47] A high-resolution study of the 8751 Å band of both $^{58}Ni_2$ and $^{58}Ni^{60}Ni$ then established a ground-state bond length r_0'' = 2.200 ± 0.007 Å and r' = 2.364 ± 0.007 Å. The transition was assigned as Ω' = 5 ← Ω'' = 4, from which the ground state of Ni_2 was determined as either $^3\Gamma_u$ or $^1\Gamma_g$ by comparison with the results of several careful ab initio calculations.[139-141]

The dense manifold of highly perturbed levels observed for Ni_2 is precisely what is expected for a Ni_2 molecule dominated by a $(4s\sigma)^2$ bond with weakly interacting $3d^9$ cores. This general picture is apparently true for Ni_2^+ as well, since the jet-cooled dinickel cation also exhibits a dense pattern of vibronic transitions in recently obtained resonant two-photon dissociation spectra.[137] It will be extremely interesting to learn what is revealed by photoelectron spectroscopy on Ni_2^-, since a comparison of gas-phase optical spectra of Ni_2 and photoelectron spectra of Ni_2^- may help to resolve the puzzle of the Co_2^- and Fe_2^- photoelectron spectra.[41]

A considerable number of theoretical calculations have focussed on the dinickel molecule. An early extended Hückel calculation predicted D_e = 2.45 eV, r_e'' = 2.21 Å, and ω_e'' = 370 cm^{-1}, in remarkable, yet fortuitous, agreement with experiment.[60] Subsequent extended Hückel calculations by Anderson predicted the dinickel ground state to be $^3\Sigma_g^-$, with r_e'' = 2.21 Å and D_e = 2.78 eV.[151] Apart from predicting an incorrect ground-state symmetry, this calculation is surprisingly accurate. In the first application of local spin density theory to Ni_2, Harris and Jones also predict a $^3\Sigma_g^-$ ground state with r_e'' = 2.18 Å, ω_e'' = 320 cm^{-1}, and D_e = 2.70 eV.[56] Again, aside from the incorrect ground-state symmetry, this calculation presents a fairly accurate view of the nickel dimer. A restricted Hartree–Fock calculation constrained to closed-shell configurations found r_e'' = 2.28 Å and ω_e'' = 240 cm^{-1}.[59]

Aside from the above-mentioned calculations, most theoretical work on Ni_2 has involved Hartree–Fock configuration interaction methods,[57,139-141,149,152-154] all of which agree on the basic structure of diatomic nickel. The bonding of dinickel is described as consisting of a $(4s\sigma)^2$ bond with weakly interacting $3d^9$ cores. In all calculations the 3d holes are preferentially placed in δ orbitals, which enables more favorable configuration interaction with states arising from the $3d^84s^2$ configuration of atomic nickel. The resulting $^3\Sigma_u^+$, $^3\Sigma_g^-$, $^1\Sigma_g^+$, $^1\Sigma_u^-$, $^3\Gamma_u$, and $^1\Gamma_g$ molecular terms are essentially degenerate in all calculations so long as spin–orbit interactions are neglected.[57,139-141,152,154] Lying above these molecular terms one finds the terms arising from the $\pi\delta$-hole configuration, followed by the $\sigma\delta$, $\pi\pi$, $\sigma\pi$, and $\sigma\sigma$ configurations, respectively.[139,141] The energies of these electronic states of Ni_2, calculated for an internuclear separation of 2.434 Å, are given in Figure 5.

The agreement between these various ab initio calculations is quite remarkable; nevertheless, considerable variation in the calculated properties of Ni_2 is found. The calculated values of r_e'' and D_e are (as follows): (2.04 Å, 2.92 eV),[139] (2.20 Å, 1.42 eV),[140] (2.26 Å, 1.88 eV),[141] (2.33 Å, 1.43 eV),[154] and (2.36 Å, 0.52 eV),[57] which may be compared to the experimental results of (2.20 Å, 2.068 eV).[47]

TABLE 7. Electronic States of $^{63}Cu_2$[a]

state	T_e, cm^{-1}	ω_e, cm^{-1}	$\omega_e x_e$, cm^{-1}	B_e, cm^{-1}	α_e, cm^{-1}	$10^{-8}D_e$, cm^{-1}	r_e, Å	obsd transitns designatn	obsd transitns ν_{00}	ref
J	37 440.1	288.4	0.64					J ← X	37451.1	50
I	~35 000	280	1					I ← X		50
H	~36 782	$\Delta G_{1/2}$ = 713						H ← X	36559.0	50
(c $^3\Lambda$)	~34 870	100	0.5					(c → a)	19435	166, 167
(b $^3\Lambda$)	~33 120	90	0.5					(b → a)	17679	166, 167
G	~30 753	116.0	0.046				2.73	G ↔ X		50, 161
F	~28 560	248.0	0.90					F ← X		50
E	~27 153	231.5	−4.25					E → X	27136	167
D ($^3\Lambda$)	~25 560	~160					2.38 ± 0.03	D → X	25508	171, 176
C	~21 870	221	2					C ↔ X	21848	48, 49, 165, 177
B $^1\Sigma_u^+$	21 758.35	245.8	2.0	0.098 89	0.000 606	6.30	2.3274	B ↔ X	21747.88	4, 5, 7, 8, 10, 164
A ($^1\Pi_u$)	20 433.2	191.9	0.348	0.081 85	0.000 62	3.81	2.559	A ↔ X	20396.0	4, 5, 9, 163
or ($^1\Sigma_u^+$)	20 433.2	192.47	0.353	0.102 76	0.000 917	11.34	2.2832	A ↔ X	20396.0	4, 5, 11, 163
a $^3\Sigma_u^+$	~15 420	125 ± 25					2.48 ± 0.03	a → X	15350	49, 175
X $^1\Sigma_g^+$	0	266.43	1.035	0.108 74	0.000 614	7.16	2.2197			

[a] Uncertain assignments are given in parentheses. See text for details. $D_0°(Cu_2)$ = 2.01 ± 0.08 eV. IP(Cu_2) = 7.894 ± 0.015 eV. $D_0°(Cu_2^+)$ = 1.84 ± 0.10 eV.

Finally, a careful calculation of Ni_2^+, which finds the ground state to be derived from the Ni_2 $\delta\delta$ ground state by removal of a 3dσ-electron should be noted.[139] The ground state either is then $^4\Gamma_g$, $^4\Sigma_g^+$, or $^4\Sigma_u^-$ and is calculated to be bound by 4.14 eV,[139] in comparison with an experimental value of 3.30 eV (see above). Another investigation demonstrates that nickel atoms interact through a simple Heisenberg exchange Hamiltonian at large internuclear separations.[155] The calculation for Ni_2, however, would predict antiferromagnetic behavior for bulk crystalline nickel at its known internuclear separation, demonstrating that many-body effects are important determinants of ferromagnetic behavior in bulk solids.[155]

9. Copper, Cu_2

Among the best-known and most-studied of the transition-metal dimers is dicopper, Cu_2. Accurate estimates of its binding energy have been available since 1956, when Drowart and Honig investigated it by Knudsen effusion mass spectrometry.[156] The measurements have been repeated by various workers[22,157-159] and are all in close agreement. Hilpert's measurements are the most precise[159] and are now generally quoted in current reviews.[27,160] Hilpert's second-law determination, $D_0°(Cu_2)$ = 1.98 ± 0.04 eV, and his third-law value, $D_0°(Cu_2)$ = 1.96 ± 0.06 eV, are in good agreement.[159] These numbers may be compared with the value obtained from a Birge–Sponer extrapolation, $D_0°(Cu_2)$ = 2.1 eV.[4] More recently Rohlfing and Valentini[161] have used a laser vaporization–supersonic expansion source combined with dispersed fluorescence studies to investigate the high vibrational levels of Cu_2 in its ground state. A LeRoy–Bernstein plot was then used to evaluate $D_0°(Cu_2)$ as 2.061 ± 0.025 eV.[161] On the basis of these results, the value $D_0°(Cu_2)$ = 2.01 ± 0.08 eV is adopted and listed in Table 2. In addition, Hilpert has determined the appearance potential of Cu_2^+ to be 7.8 ± 0.4 eV.[159]

The evaluation of third-law values of $D_0°(Cu_2)$ has been greatly facilitated by knowledge of the molecular constants, obtained from absorption and emission spectra of Cu_2 in King furnaces.[4-11] Two band systems were observed in these studies, A–X (5780–4850 Å) and B–X (4750–4400 Å). Vibrational[4,5,8] and rotational[7] analyses of the B–X system have unambiguously determined the transition to be B $^1\Sigma_u^+$ ↔ X $^1\Sigma_g^+$, and an

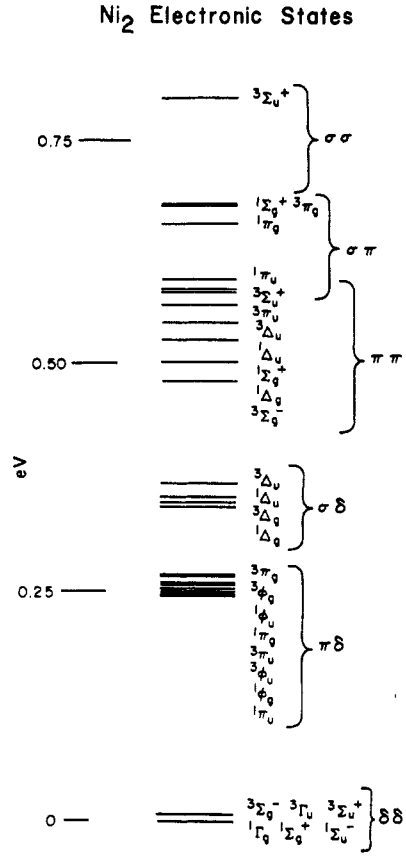

Figure 5. Electronic states of Ni_2, neglecting spin–orbit coupling, calculated for an internuclear separation of 2.43 Å. Reprinted with permission from ref 141. Copyright 1980 American Institute of Physics.

RKRV analysis of the data has permitted construction of the potential curves, giving r_e'' = 2.2195 Å and r_e' = 2.3274 Å.[10]

Vibrational[4,5] and rotational[9,11] analyses of the A–X system have also been performed, with some ambiguity, however. Pesič and Weniger assign the transition as A $^1\Pi_u$–X $^1\Sigma_g^+$ and identify many members of the R, Q, and P branches.[9] Lochet, however, observes only P and R branches in the fluorescence excited by the argon ion laser 5145 Å line,[11] casting considerable doubt on this assignment. As might be expected, the rotational constants obtained by Lochet[11] differ considerably from those of Pesič and Weniger.[9] Both are listed in Table

7 although the failure to observe Q-branch lines in fluorescence is a strong argument for an assignment of the A–X system as $A\ ^1\Sigma_u^+$–$X\ ^1\Sigma_g^+$, with the spectroscopic constants of Lochet.[11]

Lochet's analysis is further supported by Bondybey's vibronically resolved A → X and B → X systems in matrix-isolated Cu_2.[175,176] The intensities of the vibronic bands in these fluorescence systems clearly show a larger change in equilibrium internuclear distance for the B → X transition than the A → X transition.[175,176] This is obtained if Lochet's assignment[11] is adopted; the opposite case is found if the assignment of Pesič and Weniger[9] is used. An alternative possibility is that two absorption systems are present in this spectral region and both sets of investigators are correct. This possibility is unlikely, however.

Fluorescence lifetimes for both the A and B states have been measured at low pressures, yielding $\tau = 30 \pm 15$ ns for fluorescence from $v = 0$, 1, and 2 levels of the B state and $\tau = 70 \pm 15$ ns for the $v = 0$ level of the A state.[162] In more recent work Smirnov et al. have provided values for the Franck–Condon factors and r centroids for both the A–X[163] and B–X[164] band systems in Cu_2. Bondybey et al., however, find the values for the A–X system to be in error.[165]

In addition to the A–X and B–X band systems, Singh has observed two emission systems attributed to Cu_2 while studying the spectra of flames of copper salts.[166] These have also been observed as emissions from a copper arc, along with the A–X, B–X, and two additional band systems, all attributed to Cu_2.[167] Of these four new emission band systems,[166,167] only one terminates on a state with the vibrational constants of the Cu_2 $X\ ^1\Sigma_g^+$ ground state. It is listed in Table 7 as the E state of Cu_2. The remaining three band systems either involve species other than Cu_2 or involve otherwise unknown states of Cu_2 (the triplet manifold being a likely possibility). Finally, Ruamps has observed ultraviolet absorption systems, again attributed to Cu_2, in the regions 2700–2900, 2490–2560, and 2330–2460 Å.[6] Some of these have been investigated by subsequent workers using resonant two-photon ionization techniques applied to jet-cooled copper dimer.[50]

Dicopper has also received considerable attention from those employing matrix-isolation methods of study.[168-176] Absorption bands near 400,[168-171] 370,[169-172] 260,[170-172] 235,[168-172] and 220 nm[169-171] have been observed in rare gas matrices and have been assigned to Cu_2. In all cases these absorption bands are broad and difficult to interpret, however. A similar conclusion was reached by Grinter et al., who investigated copper clusters in argon and methane matrices by magnetic circular dichroism.[173] Subsequent efforts by Zeringue et al., also using magnetic circular dichroism, assigned a transition at 251 nm to dicopper.[174]

In contrast to matrix-isolation studies of the UV and visible absorptions of Cu_2, matrix-isolation *fluorescence* studies of dicopper have been most informative. By exciting Cu_2 in solid neon at 21 150 cm^{-1} (473-nm) Bondybey observed the vibrationally resolved A → X system in fluorescence along with a new emission system with a 27-ms lifetime.[175] Excitation at 22 700 cm^{-1} (440 nm) instead yielded vibrationally resolved B → X fluorescence along with the new, long-lived system.[175] The A–X and B–X systems were slightly blue-shifted (350 cm^{-1}) relative to the corresponding gas-phase systems. The long-lived emission system exhibited a 0–0 transition at 15 350 cm^{-1} and a long vibrational progression in the lower state vibration, with $\omega_e = 260$ cm^{-1}. On the basis of the long lifetime of the upper state and a comparison of the observed ω_e'' to the gas-phase value of ω_e'' for the ground state of Cu_2, Bondybey assigned the transition as phosphorescence from the lowest triplet state of Cu_2, designated as a $^3\Sigma_u^+$.[175] An analysis of the intensity pattern of the vibronic transitions of this band gives $r_e' = 2.48 \pm 0.03$ Å and $\omega_e' = 125 \pm 25$ cm^{-1} for the a $^3\Sigma_u^+$ state of Cu_2. Comparison with the binding energy of Cu_2 in its ground state shows a $^3\Sigma_u^+$ to be bound by 1000–1500 cm^{-1} relative to two ground-state ($^2S_{1/2}$) copper atoms.[175] With this vibrational frequency ($\omega_e' = 125 \pm 25$ cm^{-1}) in mind, two of the band systems observed in a copper arc[167] and in flames of copper halides[166] may be tentatively assigned as emissions terminating on Cu_2 a $^3\Sigma_u^+$. Both band systems observed have $\omega_e'' = 150$ cm^{-1},[167] in agreement with Bondybey's estimated value for the Cu_2 a $^3\Sigma_u^+$ state.[175] For completeness the upper states of both transitions are listed in Table 7, as the $b^3\Lambda$ and $c^3\Lambda$ states of Cu_2.

Ozin et al.[171] and Bondybey and English[176] report another band system observed in fluorescence when Cu_2 is excited at 35 700 or 26 000 cm^{-1}, respectively. In solid neon this system exhibits a 0–0 band near 25 508 cm^{-1} with a long, 260 cm^{-1}, vibrational progression extending to the red.[176] Although initially identified as the A → X fluorescence system,[171] Bondybey's observation of the A → X system with only a small matrix blue shift rules out this possibility.[175] Accordingly, this is assigned as a transition from a new excited state, designated D → X. The excited state lifetime is 6.5 μs, consistent with assignment of the D state to another excited triplet state of Cu_2.[176] On the basis of a Franck–Condon fit to the observed emission intensities, Bondybey and English estimate $r_e' = 2.38 \pm 0.03$ Å and $\omega_e' = 160$ cm^{-1} for the D state of copper dimer.[176]

Diatomic copper has also received considerable attention from laser spectroscopists employing laser vaporization of bulk solid copper, supersonic expansions, or both. With use of a supersonic expansion of pure copper vapor at 2500 K, Preuss, Pace, and Gole were able to observe laser-induced fluorescence from yet another band system, overlapping with the well-known $B\ ^1\Sigma_u^+$–$X\ ^1\Sigma_g^+$ system.[177] Subsequent work using Nb:YAG laser vaporization of metallic copper with laser-induced fluorescence[49] and resonant two-photon ionization spectroscopy[48] provided unambiguous identification that the new band system is due to diatomic copper, with $\nu_{00} = 21\,848$ cm^{-1}, $\omega_e' = 221$ cm^{-1}, and $\omega_e'x_e' = 2$ cm^{-1}. The upper state of this band system, designated as the C state of Cu_2, exhibits a lifetime of 800 ± 100 ns and is efficiently collisionally quenched.[48,49,165] Collisions have been shown to lead to efficient equilibration of Cu_2 between the B and C states, thereby quenching the long-lived C-state emission.[165] Bondybey et al. report collision-free lifetimes as follows: A state, $v = 0$, 115 ± 10 ns; A state, $v = 1$, 75 ± 10 ns; A state, $v = 2$, 40 ± 10 ns; B state, $v = 0$–2, 40 ± 5 ns; C state, $v = 0$, 800 ± 100 ns.[165]

Finally, Powers et al. observed five new band systems of diatomic copper in the region between 3200 and 2590

Å, using resonant two-photon ionization spectroscopy of jet-cooled copper dimer.[50] All bands are attributed to transitions from Cu_2 X $^1\Sigma_g^+$, and this assignment is supported by the observation of hot bands with the ground-state vibrational frequency previously known from studies of the A–X and B–X band systems. The lower two transitions observed by Powers et al. involve long progressions in the excited-state vibration. The upper states of these transitions, designated F and G in Table 7, perturb one another strongly. Powers, et al. have presented a crude, local deperturbation treatment from which the spectroscopic constants of Table 7 are derived.[50] Rohlfing and Valentini have dispersed the fluorescence from single vibronic levels of the G state of Cu_2.[161] The Franck–Condon envelopes observed in fluorescence indicate that the vibrational numbering of Powers et al.[50] should be shifted down by one quantum, a procedure which changes the value of T_e for the G state of Cu_2. The corrected value is given in Table 7. Rohlfing and Valentini have also analyzed the Franck–Condon envelopes to estimate r_e' for the G state as 2.73 Å.

At higher energies Powers et al. report the system designated H–X in Table 7.[50] The interpretation of this band system involves hot bands of v'' up to 10 and assigns $\Delta G'_{1/2}$ = 713 cm^{-1} for the $^{63}Cu_2$ H state. Both of these assignments are problematic: no hot bands beyond v'' = 1 are observed in any other band systems reported by these authors, and the value assigned to $\Delta G'_{1/2}$ is the highest vibrational frequency reported for any electronic state of any of the 3d-series transition-metal dimers. The former problem may be explained by assuming that the conditions of the supersonic expansion were not properly optimized when this spectral range was investigated. The drastic increase in vibrational frequency, however, requires considerable electronic rearrangement upon electronic excitation and appears somewhat dubious. An additional problem with the assignment is that the observation of the 0–1, 0–2, 0–3, ... vibrational hot bands implies a considerable change in bond length upon electronic excitation. One would therefore expect to observe a lengthy excited-state progression as well. Powers et al. report only the 0–0 and 1–0 members of this progression, however, despite the fact that the 2–0 band would have been expected in the spectral region scanned.[50] It is hoped that future investigations will resolve some of the difficulties with this band system.

Powers et al. finally report two additional band systems (I–X and J–X of Table 7) in the 37 000–38 600 cm^{-1} region. The J–X system is well-characterized, but the vibrational numbering of the I–X system is as yet unknown. Again, further work is needed to resolve this issue. Finally, Powers et al. have used resonant two-photon ionization methods to determine the adiabatic ionization potential of Cu_2 as 7.894 ± 0.015 eV,[50] in close agreement with Hilpert's value, 7.8 ± 0.4 eV.[159] Potential curves for the known states of dicopper are presented in Figure 6.

Copper atom possesses a $3d^{10}4s^1$, $^2S_{1/2}$ ground state and is in many respects analogous to an alkali atom. In light of the substantial 3d contraction occurring in atomic copper (see Table 1) we expect Cu_2 to have a ground state of $(3d^{10})(3d^{10})(4s\sigma_g)^2$, $^1\Sigma_g^+$, as is experimentally observed. This simple picture of the bonding

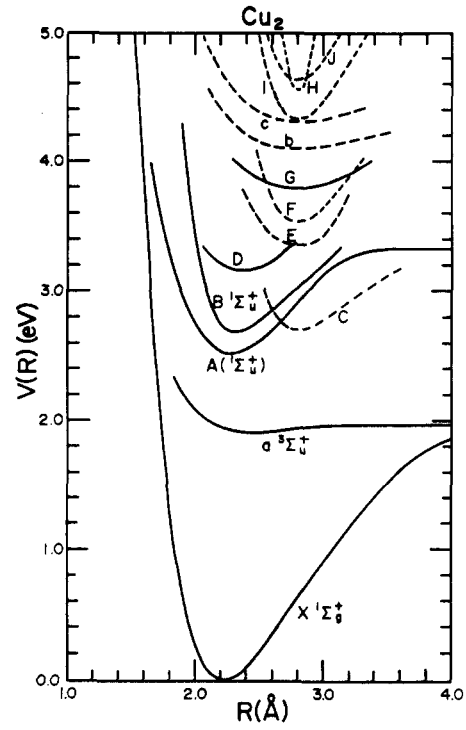

Figure 6. Potential energy curves of Cu_2, calculated from the experimental data of Table 7. States for which r_e is unknown are designated by dashed lines; these curves must be shifted along the R axis by an unknown amount to bring them into coincidence with the true potential energy curves.

in copper dimer is however, only a zeroth-order approximation and is insufficent to account for the observed properties (r_e, D_e, ω_e) of the dicopper ground state. As Cu_2 is the simplest of the 3d-series transition-metal dimers and since it is experimentally well-characterized, it has become an important test molecule for numerous theoretical approaches. Essentially all theoretical methods must be proven on Cu_2 before they may be credibly applied to the open d-shell dimers or larger clusters. As a result, a large number of calculations have been reported or Cu_2. In the following paragraphs a brief review of the various methods and their results for Cu_2 is presented.

The earliest calculations reported for diatomic copper used the extended Hückel[178–180] and CNDO[180] semiempirical methods. Although these methods can provide excellent agreement with experiment, the results are dramatically dependent on the parameters used. Since the parameters are not well-known from other sources, they are obtained by fits to the molecule under consideration, thereby robbing the methods of much predictive power.

An alternative method which retains some simplicity is to replace the core electrons with a pseudopotential. Beginning in 1977, a number of investigators have used this method to study diatomic copper.[181–190] In an early investigation, Dixon and Robertson demonstrated that copper dimer was not properly described by using a pseudopotential which incorporated the 3d electrons in a frozen core.[182] Such a procedure, which treats Cu_2 as a two-electron system, predicts r_e = 2.44 Å and D_e = 0.93 eV compared to the experimental values r_e = 2.22 Å and D_e = 2.01 ± 0.08 eV.[182] Much better results were obtained by treating the 3d orbitals as part of the valence space (r_e = 2.22 Å and D_e = 1.84 eV).[182] Unfortunately, this leaves Cu_2 as a 22-electron problem and

makes extension to higher copper clusters quite difficult. The necessity of permitting reorganization of the 3d electrons for an adequate description of Cu_2 has been emphasized by many practitioners of the pseudopotential approach.[182-190] Several recent calculations of Cu_2 as a two-electron system have provided excellent descriptions of the Cu_2 ground state, however, by including core-valence polarization and correlation energies by perturbation theory[185-190] and by including overlap corrections to the point-charge model of the core-core interactions.[186-190] Most recently, a pseudopotential method incorporating these improvements along with a configuration interaction treatment of valence correlation and quadrupole contributions to the core polarization has predicted $D_e(Cu_2)$ = 1.85 eV and $IP(Cu_2)$ = 7.84 eV,[187] in good agreement with the experimental values of 2.01 ± 0.08[159] and 7.894 ± 0.015 eV,[50] respectively. Moreover, this method may be readily extended to copper and silver clusters, since each atom contributes only a single valence electron.[189,190] In view of the successful description of copper dimer obtained with these methods, it is likely that the procedure will be successful for the calculation of larger clusters as well.[188-190]

The various density functional theories, including the Xα method[170,191-195] and methods based on other exchange-correlation potentials,[56,75,76,138,195] show promise for extension to larger clusters and have been applied to diatomic copper with considerable success. Painter and Averill, for example, present spectroscopic constants of Cu_2 X $^1\Sigma_g^+$ calculated in five versions of local spin density theory.[195] The results span the range D_e = 2.10–2.65 eV, r_e = 2.17–2.28 Å, and ω_e = 268–330 cm^{-1}, in reasonable agreement with the experimental values given in Table 7.

Ab initio calculations of dicopper have also been reported by using Hartree–Fock self-consistent-field, configuration interaction, and Möller–Plesset/many-body perturbation theory methods.[2,59,196-207] Calculations employing only the Hartree–Fock self-consistent-field, without configuration interaction, invariably underestimate the binding energy by approximately 1 eV, regardless of the basis set used.[197-202] Of course, the $(4s\sigma_g)^2 \rightarrow (4s\sigma_u)^2$ configuration must be included to ensure proper dissociation of the molecule; additional correlation of the 4sσ-electrons is obtained by inclusion of a significant contribution from the $(4s\sigma_g)^2 \rightarrow (4p\pi_u)^2$ excitation in a configuration interaction treatment.[204] This excitation provides angular correlation of the 4sσ-electrons and is particularly important because of the near degeneracy of the 4s and 4p orbitals in copper.[204] The same excitation is also found to be important in describing the outer $(4s\sigma_g)^2$-bonded well of Cr_2.[96]

Correlation of the 3d electrons is also important to the correct description of Cu_2. The correlation of these electrons increases the calculated binding energy of Cu_2 by 0.8 eV.[207] The major effect of such correlation appears to be the reduction of d–d repulsions between metal centers,[204] thereby allowing closer approach of the atoms, and formation of a stronger, more contracted $(4s\sigma_g)^2$ bond.[207]

Relativistic effects in copper dimer have been investigated and are found to be significant.[153,208-211] Although calculations vary, on average relativistic effects shorten the bond by about 0.03 Å, increase the binding energy by 0.06 eV and stiffen the vibrational frequency by approximately 10 cm^{-1}.[153,208-211]

Finally, Pauling has suggested that diatomic copper may be bound by a triple bond, formed from spd hybrid orbitals on each atom, correlating to the excited $3d^9 4s4p$ configuration of atomic copper.[212] Following this suggestion, more detailed calculations using the CASSCF-CI method resulted in a 3d population on each atom of 9.99, indicating very little contribution from the $3d^9 4s4p$ configuration.[213] Although the CASSCF-CI calculation has not converged to the experimental limit at this level of theory, it is suggested that the presence of a triple bond in Cu_2 is unlikely.[213] The bonding in dicopper is still thought to consist almost entirely of a $(4s\sigma_g)^2$ single bond.

10. Zinc, Zn_2

Atomic zinc possess the closed-shell configuration $3d^{10}4s^2$. As is the case with the other group IIB (12^{577}) (and all closed-shell) atoms, only weak, van der Waals binding is expected for the interaction of ground-state zinc atoms. Excited states of the Zn_2 molecule, on the other hand, may be bound by a substantial amount, at considerably smaller values of r_e than the ground state, which is denoted by $X^1\Sigma_g^+$.

As might be expected from the foregoing description, the electronic spectrum of Zn_2 is dominated by continuum absorptions with intensity maxima at the resonance lines of atomic zinc.[215-218] The binding energy of Zn_2 has been estimated from the energy difference of a resonance line and the short-wave limit of the associated continuum absorption of Zn_2 as $D_0°(Zn_2)$ = 0.246 eV by Winans[218] and as $D_0°(Zn_2)$ = 0.29 eV by Hamada.[215] An alternative approach, based on a fit of the vapor viscosity coefficient to an exp-6 interatomic potential function, has given $D_0°(Zn_2)$ = 0.168 ± 0.025 eV and r_0 = 2.35 ± 0.08 Å.[219] More recently Brebrick and co-workers have measured the temperature dependence of the Zn_2 absorption spectrum to obtain D_e = 0.056 eV.[302] As this method yields reasonable results for Cd_2 (see below), this value is selected for Table 2.

Ault and Andrews report an ultraviolet absorption system in an argon matrix containing zinc.[220] It is centered at 252 nm, corresponds to a banded absorption system observed by Mohler and Moore (2636–2551 Å) in the gas phase,[217] and is attributed to a $^1\Sigma_u^+ \leftarrow {}^1\Sigma_g^+$ transition in diatomic zinc.[220] A vibration progression with spacings of 120–140 cm^{-1} is observed, with ν_{00} = 38 289 cm^{-1}. The excited state is assumed to correlate with $Zn(^1S_0)$ + $Zn(^1P_1)$ in the separated atom limit. From these data the binding energy of the upper state may be approximated as $D_0'(Zn_2, {}^1\Sigma_u^+)$ = 1.5 eV.[220] In addition to this band system, numerous other continua and diffuse bands have been observed. The interested reader is referred to Finkelnburg's review for further details.[221] Finally, Givan and Loewenschuss report a Raman frequency of 80 ± 1 cm^{-1} for Zn_2 isolated in solid krypton.[32] Vibrational frequencies this low, however, are subject to considerable matrix shifts, and this value is unlikely to be representative of the gas-phase zinc dimer.

Ab initio calculations of the zinc dimer are all in agreement that the molecule is bound by a van der Waals interaction in its ground state.[222-226] On the other

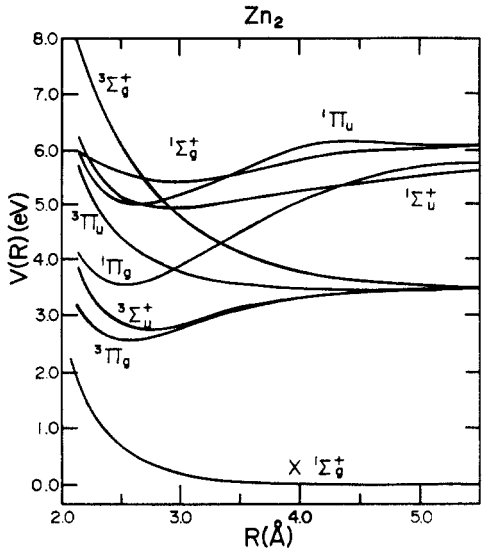

Figure 7. Potential energy curves for Zn_2, as calculated by ab initio methods. Reprinted with permission from ref 224. Copyright 1979 American Institute of Physics.

hand, the $^3\Pi_g$ and $^3\Sigma_u^+$ excited states arising from the $Zn(^1S) + Zn(^3P)$ asymptote are strongly bound, as are the $^1\Pi_g$, $^1\Sigma_u^+$, $^1\Pi_u$, and $^1\Sigma_g^+$ excited states arising from $Zn(^1S) + Zn(^1P)$.[222,224-226] The zinc dimer has attracted considerable attention as a candidate for possible excimer laser systems, since lasing is possible on a bound-continuum transition. The dissociative ground state then insures that population does not build up in the lower level, spoiling the population inversion. Potential energy curves calculated[224] for Zn_2 are given in Figure 7. For further details on the calculated potential curves of the zinc dimer, the interested reader is referred to ref 222 and 224–226.

11. Yttrium, Y_2

The only experimental datum for diyttrium is its binding energy, $D_0°(Y_2) = 1.62 \pm 0.22$ eV. This was determined by using the third-law or absolute entropy method by Verhaegan, Smoes, and Drowart[53] and suffers from the previously mentioned difficulties of this method.

Walch and Bauschlicher have recently provided a CASSCF-CI calculation of yttrium dimer.[2] A $^5\Sigma_u^-$ state, arising from a $(5s\sigma_g)^2(5s\sigma_u)^1(4d\sigma_g)^1(4d\pi_{xu})^1(4d\pi_{yu})^1$ configuration is calculated to be the ground state. Spectroscopic constants $r_e = 3.03$ Å, $\omega_e = 171$ cm^{-1}, and $D_e = 2.44$ eV are predicted. This state is completely analogous to the $^5\Sigma_u^-$ ground state calculated[2,56-58] and observed[55] for discandium. A possible contender for the ground state of diatomic yttrium is $(5s\sigma_g)^2(4d\pi_u)^4\ ^1\Sigma_g^+$, which correlates to two excited $5s^14d^2$ yttrium atoms. The promotion energy required to produce this atomic asymptote is roughly the same in yttrium as in scandium; in yttrium, however, the 4d and 5s orbitals are more nearly comparable in size, thereby facilitating 4d bonding. This illustrates the significantly greater possibilities of d bonding in the second transition series compared to the first. In this context it should be noted that Knight et al. have sought the ESR spectrum of Y_2 without success.[227] The discandium $^5\Sigma_u^-$ ground state was readily observed under similar conditions, suggesting that in Y_2 the strongly d-bonded $^1\Sigma_g^+$ state may lie lower in energy. Walch and Bauschlicher point out that extensive correlation of the 4d electrons will preferentially lower the energy of $(5s\sigma_g)^2(4d\pi_u)^4\ ^1\Sigma_g^+$ relative to the long bonded $^5\Sigma_u^-$ state.[2] Spectroscopic constants calculated for the $^1\Sigma_g^+$ state are $r_e = 2.74$ Å, $\omega_e = 206$ cm^{-1}, and $D_e = 2.93$ eV.[2]

12. Zirconium, Zr_2

The only experimental investigation of dizirconium has been an ultraviolet-visible spectral survey of matrix-isolated Zr_2.[228] Four bands were observed, at 390, 422, 585, and 615. From concentration studies it was demonstrated that these bands belong to a single cluster species, which has been assigned as Zr_2.[228] On the basis of extended Hückel calculations, Klotzbücher and Ozin assign the four bands listed above to $1\pi_u \rightarrow 3\sigma_g$, $1\sigma_g \rightarrow 2\pi_u$, and $1\sigma_g \rightarrow 2\sigma_u$ orbital transitions, respectively, with the latter assigned to both the 585 and 615 nm bands.[228]

Although no experimental measurement of $D_0°(Zr_2)$ exists, Miedema and Gingerich have provided a predicted value by using an empirical correlation between the heat of vaporization of zirconium metal, $\Delta H_{vap}°$, the surface energy of pure solid zirconium, γ_s^0, and the dimer dissociation energy.[229] The method is a generalization of previous work by Miedema on the heats of mixing and heats of formation of liquid and solid alloys of transition metals.[230-233] The predicted value is $D_0°(Zr_2) = 3.20 \pm 0.24$ eV.[229]

The only theoretical calculation of Zr_2 reported to date is the extended Hückel calculation of Klotzbücher and Ozin,[228] discussed above.

13. Niobium, Nb_2

Gupta and Gingerich have recently reported the dissociation energy of diniobium by monitoring the vapor pressure of Nb and Nb_2 over solid niobium near its melting point of 2741 K.[234] The second-law determination, based on the narrow temperature range investigated, gave $D_0°(Nb_2) = 5.57 \pm 0.41$ eV, while the third-law determination gave $D_0°(Nb_2) = 5.22 \pm 0.02$ eV. The third-law value is based on an assumed bond length of 2.20 Å, which is probably 5–10% too long, and on an assumed electronic contribution to the entropy of Nb_2 of zero (indicating a nondegenerate ground state and no low-lying excited states). Decreasing the bond length of Nb_2 to 2.0 Å increases the third-law value of $D_0°(Nb_2)$ by only 0.04 eV, while assuming an effective electronic degeneracy of 6 lowers $D_0°(Nb_2)$ by 0.40 eV, giving $D_0°(Nb_2) = 4.86 \pm 0.02$ eV for this choice of parameters. In the sample calculation given here, an electronic degeneracy of 6 has been considered, in analogy to the known V_2 molecule. When the ground $^3\Sigma_g^-$ and low-lying $^1\Sigma_g^+$ and $^1\Gamma_g$ electronic states of V_2 are considered, an effective electronic degeneracy of 6 is obtained. Calculations of Nb_2 suggest the possibility of a very low-lying $^3\Delta_g$ state,[2] so an effective electronic degeneracy of 12 may pertain for Nb_2. On the basis of these considerations $D_0°(Nb_2) = 5.0 \pm 0.4$ eV may be adopted as an acceptable compromise, given our lack of detailed knowledge of the diniobium molecule. The values 5.20,[235] 3.85 ± 0.35,[229] and 4.19 ± 0.46 eV[236] have been predicted by using various empirical and semiempirical methods.

Green and Gruen investigated the absorption spectra of niobium atoms isolated in rare gas matrices in

TABLE 8. Electronic States of Nb_2[a]

state	T_e, cm^{-1}	ω_e, cm^{-1}	r_e, Å	D_e, eV
$^3\Phi_g$	7742	340	2.19	2.24
$^3\Delta_g$	968	501	2.01	2.15
$^1\Gamma_g$	725	427	2.11	2.12
$^3\Sigma_g^-$	0	448	2.10	1.28

[a] As calculated by using the CASSCF method in ref 2.

1972.[237] A banded spectrum was observed to grow in as an argon matrix containing niobium was annealed. The spectrum consists of a progression of doublets separated by approximately 50 cm^{-1} and with ν_{00} = 18700 cm^{-1} and $\overline{\Delta G}$ = 275 cm^{-1}. It was assigned by Green and Gruen to Nb_2.[237] In subsequent work Kotzbücher and Ozin reported absorption spectra of Nb_2 at 660, 420, and 280 nm.[93] The band system observed by Green and Gruen was notably absent in this work, leading Klotzbücher and Ozin to assign it to an impurity present in the former investigation. With use of the extended Hückel theory the bands at 660, 420, and 280 nm were assigned to $1\sigma_g \rightarrow 2\sigma_u$, $1\sigma_g \rightarrow 2\pi_u$, and $1\pi_u \rightarrow 3\sigma_g$ orbital excitations, respectively.[93] In a subsequent publication Andrews and Ozin attribute the 660-nm absorption to the $1\delta_g \rightarrow 1\delta_u^*$ orbital excitation, however.[69]

Theoretical descriptions of diniobium have been presented by using semiempirical extended Hückel methods,[93,238] SW-Xα methods,[238,239] Hartree–Fock plus configuration interaction allowing full reorganization within the 4d shell,[240] and complete-active-space self-consistent-field methods (CASSCF).[2] Of these, the CASSCF method is certainly the most reliable. With the CASSCF method, Walch and Bauschlicher predict several low-lying states in Nb_2.[2] In analogy to V_2, $^3\Sigma_g^-$, $^1\Sigma_g^+$, and $^1\Gamma_g$ arising from a $(5s\sigma_g)^2(4d\sigma_g)^2(4d\pi_u)^4(4d\delta_g)^2$ electronic configuration are calculated to be lowest in energy, with $^3\Sigma_g^-$ as the ground state and $^1\Gamma_g$ lying 0.09 eV above. In addition to these states, however, a $^3\Delta_g$ molecular term, arising from a $(5s\sigma_g)^2(4d\sigma_g)^1(4d\pi_u)^4(4d\delta_g)^3$ electronic configuration is calculated to lie only 0.12 eV above the $^3\Sigma_g^-$ state. The increased stability obtained for Nb_2 $^3\Delta_g$ compared to the analogous V_2 $^3\Delta_g$ implies strong 4dδ bonding in Nb_2 as compared to the 3dδ bonding in V_2. This occurs because the 4d and 5s orbitals are more nearly comparable in size than are the 3d and 4s orbitals (see Table 1), enabling stronger d-bonding interactions in the second transition series as compared to the first. Finally, Walch and Bauschlicher calculate a low-lying $^3\Phi_g$ $(5s\sigma_g)^2(4d\sigma_g)^2(4d\pi_u)^3(4d\delta_g)^3$ state 0.96 eV above the calculated ground state.[2] In the absence of configuration interaction, it is difficult to predict whether the ground state of Nb_2 will be $^3\Sigma_g^-$, as in divanadium, or $^3\Delta_g$. The spectroscopic constants calculated at the CASSCF level for Nb_2 are given in Table 8.[2]

Cotton and Shim have employed a Hartree–Fock plus configuration interaction method which allows full reorganization of the 4d electrons within the 4d shell to investigate Nb_2.[240] In agreement with Walch and Bauschlicher,[2] Cotton and Shim find the ground state of Nb_2 to arise from a predominant molecular orbital configuration of $(5s\sigma_g)^2(4d\sigma_g)^2(4d\pi_u)^4(4d\delta_g)^2$.[240] The calculated bond length of approximately 2.9 Å, however, is much too long, indicating that the Cotton–Shim calculation omits some important physical effects.

14. Molybdenum, Mo_2

Gupta, Atkins, and Gingerich have recently reported the dissociation energy of dimolybdenum by monitoring the equilibrium $2Mo(g) \rightleftarrows Mo_2(g)$ in the temperature range 2772–2963 K using Knudsen effusion mass spectrometry.[241] A second-law determination of $D_0°(Mo_2)$ over this temperature range gives $D_0°(Mo_2)$ = 4.34 ± 0.35 eV, while the third-law value, recalculated by using r_e = 1.94 Å and ω_e = 477.1 cm^{-1} (see below), gives $D_0°(Mo_2)$ = 4.43 ± 0.02 eV, assuming no electronic contribution to the entropy of Mo_2.[241] On the basis of these results $D_0°(Mo_2)$ = 4.38 ± 0.10 eV may be selected as the dissociation energy of dimolybdenum.

Absorption features at 512, 308, and 232 nm were observed in a molybdenum-containing argon matrix in 1977 and were assigned to diatomic molybdenum.[93] Although Klotzbücher and Ozin[93] were the first to assign these transitions to Mo_2, previous investigators had observed the 512 and 308 nm features[242–244] and had suggested the possibility of a diatomic or polyatomic carrier of the spectrum.[243,244] The matrix-isolated dimolybdenum absorptions have since been observed in several studies,[80,94,245–248] and the assignment of at least the 512- and 308-nm features to Mo_2 may be considered definite.

Pellin, Foosnaes, and Gruen have collected and dispersed the fluorescence resulting from laser excitation of the 512-nm feature in argon- and krypton-isolated dimolybdenum.[247,248] The fluorescence observed consisted of a progression in the lower state vibration with a frequency of 476 ± 6 cm^{-1} and a 0–0 band near 13700 cm^{-1}. The emission possessed a lifetime of 2.1 ms or thereabouts, indicating that the transition is spin-forbidden.[247,248] Raman studies of Mo_2 isolated in argon indicated a ground-state vibrational frequency of 475 cm^{-1}, demonstrating that the lower state of this phosphorescence system is the Mo_2 ground state.[248]

Gas-phase spectra of dimolybdenum were actually obtained prior to matrix-isolated spectra through the work of Becker and Shurgers,[249] although this was not recognized by the matrix-isolation community until some time later. Becker and Schürgers produced a spectrum of Mo_2 in 1971 by reacting molybdenum hexacarbonyl with H, O, and N atoms and dispersing the resulting chemiluminescence.[249] A banded emission system was observed near 5180 Å, which was correctly identified by the lack of a Q-branch as a $\Sigma \rightarrow \Sigma$ transition.[249] At this time other molecules, such as MoO and MoC, were considered as possible emitters, so a definite assignment to Mo_2 could not be made. A few years later Efremov et al. observed the same transition in both absorption and emission, using isotopically enriched $^{98}Mo(CO)_6$ to unambiguously identify the carrier.[39,250] The 5180-Å band system observed in the gas phase corresponds to the 512-nm absorption band found in inert matrices. In addition, gas-phase band systems were observed at 3897 and 3140 Å, the latter corresponding to the 308-nm absorption system found for Mo_2 isolated in an argon matrix.

Efremov et al. have rotationally analyzed the B $^1\Pi_u$–X $^1\Sigma_g^+$ band system near 3897 Å for $^{98}Mo_2$, establishing the symmetry species of both states.[39] The rotational analysis provided r_e'' = 1.929 Å and r_e' = 1.912 Å, although it was acknowledged that the rotational numbering could have been off by several units, placing

TABLE 9. Electronic States of $^{98}Mo_2$[a]

state	T_e, cm^{-1}	ω_e, cm^{-1}	$\omega_e x_e$, cm^{-1}	B_e, cm^{-1}	α_e, cm^{-1}	$10^{-8}D_e$, cm^{-1}	r_e, Å	obsd transitns: designatn	obsd transitns: ν_{00}	ref
C	31 867	($\Delta G_{1/2}$ = 408)						C ↔ X	31 833	39, 51, 250
B $^1\Pi_u$	25 684	$\Delta G_{1/2}$ = 412		(0.094 17)	(0.000 78)	(1.9)	(1.912)	B ↔ X	25 651.9	39, 250
A $^1\Sigma_u^+$	19 318	449.0	2.3	0.0948	0.00045		1.937	A ← X	19 303.7	39, 51, 249, 250
a ($^3\Lambda$)	~13 700							a → X	13 700	247, 248
X $^1\Sigma_g^+$	0	477.1	1.51	0.0916	(0.00039)	(1.4)	1.938			

[a] Uncertain values are given in parentheses. See text for details. $D_0°(Mo_2)$ = 4.38 ± 0.10 eV.

an uncertainty of ±0.06 Å on both r_e'' and r_e'.[39] A subsequent study of the A–X band system in jet-cooled Mo_2 provided a more definite value for r_e'' of 1.938 ± 0.009 Å and identified this system as A $^1\Sigma_u^+$ ← X $^1\Sigma_g^+$.[51] The C–X transition, located near 3140 Å, has a complicated spectral structure in both conventional and jet-cooled spectroscopic studies and has not yet received a convincing assignment. A summary of the known electronic states of dimolybdenum is given in Table 9. Potential energy curves of the known electronic states are given in Figure 8.

Hopkins et al. have called attention to the short and nearly constant bond length of Mo_2 in its X $^1\Sigma_g^+$, A $^1\Sigma_u^+$, and B $^1\Pi_u$ states.[51] Constancy in bond length over several electronic states is common in molecules which possess nonbonding electrons, such as NH and AlH, but is quite rare in homonuclear diatomics. Hopkins et al. suggest that in Mo_2 the 5sσ_g electrons are essentially nonbonding and consider dimolybdenum to consist of a tightly bonded Mo_2^{2+} core surrounded by a nonbonding pair of 5sσ_g electrons. An excitation of the 5sσ_g electrons then leaves the quintuply bonded Mo_2^{2+} core unchanged, resulting in only minor changes in the Mo_2 bond length. In support of this model, it should be noted that the average distance of a 5s electron from the nucleus is 3.79 Å for a molybdenum atom in its $(4d)^4(5s)^2$ ^5D state (as calculated by numerical Hartree–Fock methods).[214] This may be compared to Mo_2 bond lengths of about 1.9 Å. Unless the 5s orbitals contract substantially upon dimerization, the 5sσ_g electrons will lie considerably outside the Mo_2^{2+} 4d-bonded core.

Numerous theoretical calculations have been reported for dimolybdenum.[2,57,75,85,90,93,95,97,105–107,251–256] The computational difficulties associated with diatomic molybdenum are similar to those discussed above for the chromium dimer. In dimolybdenum, however, d bonding is more favorable than it is in dichromium, leading to a much deeper well for the multiply d-bonded Mo_2 molecule than for Cr_2. As a result, all calculations have predicted the Mo_2 bond length in the 1.8–2.1 Å range, and all predict a multiply bonded $^1\Sigma_g^+$ ground state. Unless correlation of d electrons and contributions from 4f functions are included, however, predicted dissociation energies are seriously underestimated. It appears that local spin density methods offer a promising means of estimating correlation energy without extensive configuration interaction.[75,105–107,256] In this regard one should note that Salahub has recently combined local spin density methods with a model potential representation of the inner core electrons in a very successful manner.[256] In this calculation r_e = 1.98 Å, D_e = 4.8 eV, and ω_e = 479 cm^{-1} were obtained for Mo_2, in good agreement with experiment.[256] An advantage of this method is the ability to easily introduce an approximate treatment of the relativistic mass velocity and Darwin terms, although this was not done for Mo_2.[256]

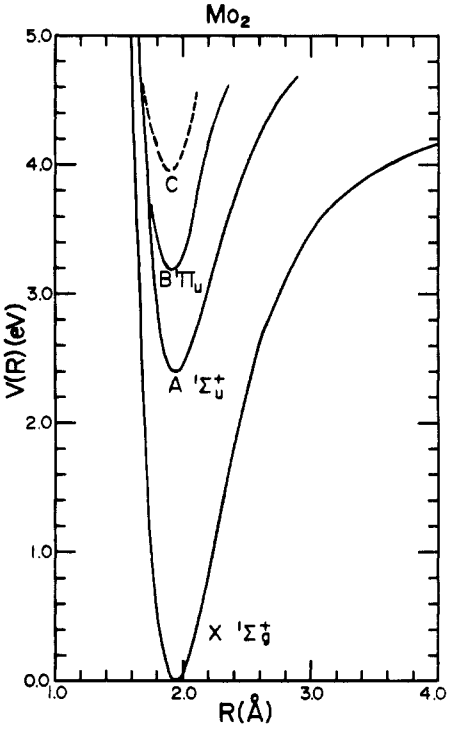

Figure 8. Potential energy curves for Mo_2, calculated from the experimental data of Table 9. The potential curve for the C state is dashed to indicate that the equilibrium internuclear separation in this state is unknown. The curve displayed for the C state must therefore be translated along the R axis by an unknown amount to bring it into coincidence with the true C state curve. This curve is also based on a value for ω' of 408 cm^{-1}, which is far from certain. It should be viewed with some caution, therefore.

15. Technetium, Tc_2

At present no experimental data on ditechnetium exist. Apparently no theoretical calculations on the technetium dimer have been performed either. Nevertheless, several ligated Tc_2 species have been synthesized which display multiple 4d bonding between the metal atoms.[91] Known chemical species are $Tc_2Cl_8^{3-}$ (Tc–Tc bond distance 2.117 ± 0.002 Å),[257] $Tc_2(O_2CC(CH_3)_3)_4Cl_2$ (Tc–Tc bond distance 2.192 ± 0.002 Å),[258] and Tc_2(2-hydroxypyridine)$_4$Cl (Tc–Tc bond distance 2.095 ± 0.001 Å).[259] These compounds are in marked contrast with what is found for manganese, which does not form multiply bonded dimeric compounds.[91] The more nearly comparable sizes of the 4d and 5s orbitals in technetium as compared to the 3d and 4s orbitals in manganese, probably contributes to the increased stability of the multiply bonded Tc_2 moiety as compared to Mn_2. This factor, along with the lower 5s → 4d promotion energy in Tc (0.41 eV) as compared to the 4s → 3d promotion energy in Mn (2.14 eV), suggests

that Tc_2 is likely to possess a multiply bonded ground state with a short internuclear distance. In agreement with this model, Miedema and Gingerich predict $D_0°(Tc_2) = 3.42 \pm 0.10$ eV, using an empirical correlation of bond strength with the heat of vaporization and surface energy of the bulk metal.[229,260] Brewer and Winn estimate the binding energy of Tc_2 as $D_0°(Tc_2) = 2.93$ eV.[261]

16. Ruthenium, Ru_2

At present it appears that no experimental information on diruthenium exists. On the basis of empirical correlations between the heat of vaporization, $\Delta H_{vap}°$, and the surface energy, γ_s^0, of pure solid metals and the dissociation energy of the corresponding metal dimer, Miedema and Gingerich predict $D_0°(Ru_2) = 3.39$ eV.[229,260] Brewer and Winn estimate $D_0°(Ru_2) = 3.19$ eV, using similar correlation methods.[261] Such a strong bond would indicate multiple 4d bonds; this is in agreement with the known propensity of ruthenium to form multiply bonded binuclear compounds, with Ru–Ru distances as small as 2.248 Å.[91]

Cotton and Shim have provided an all-electron ab initio self-consistent field calculation for diruthenium followed by configuration interaction calculations allowing full reorganization of the 4d shell.[262] The calculated ground state was found to be $^7\Delta_u$, with natural orbital populations of $(4d\sigma_g)^{1.67}(4d\pi_u)^{3.31}(4d\delta_g)^{2.73}(4d\delta_u)^{2.42}(4d\pi_g)^{2.60}(4d\sigma_u)^{1.27}(5s\sigma_g)^{1.94}(5s\sigma_u)^{0.06}$. This state corresponds to the $^7\Delta_u$ state calculated by Shim and Gingerich as the ground state of the analogous Fe_2 molecule.[118] Cotton and Shim report calculated values of $r_e = 2.71$ Å, $\omega_e = 116$ cm^{-1}, and $D_e = 0.64$ eV, although inadequacies in the calculation are acknowledged to underestimate D_e and overestimate r_e.[262] The actual bond distance is predicted to be 2.57 ± 0.03 Å.[262]

Andzelm, Radzio, and Salahub have combined the local spin density method with a model potential for the inner-shell electrons.[256] Judging from the calculated results for Mo_2 (see above) and Ag_2 (see below), the predictions for Ru_2 should be quite accurate. With use of the model potential method, Ru_2 is found to possess a $^7\Sigma$ ground state, with $r_e = 2.42$ Å, $D_e = 3.0$ eV, and $\omega_e = 330$ cm^{-1}.[256] This compares to an all-electron calculation by the same authors giving $^7\Sigma$ with $r_e = 2.41$ Å, $D_e = 2.7$ eV, and $\omega_e = 380$ cm^{-1}.[256] The large discrepancy between this result and the calculation of Cotton and Shim[262] must await further experimental studies for its resolution.

17. Rhodium, Rh_2

Dirhodium has been investigated by high-temperature mass spectrometry by Cocke and Gingerich.[263,264] A second-law determination of $D_0°(Rh_2)$ was not possible because of insufficient data. A third-law determination, based on assumed values of $r_e = 2.28$ Å, $\omega_e = 267$ cm^{-1}, and an electronic contribution to the free energy of 3 cal K^{-1} mol^{-1} for Rh_2, provides $D_0°(Rh_2) = 2.92 \pm 0.22$ eV.[264]

Matrix-isolation spectra of dirhodium have been obtained by Hanlan and Ozin.[144,265] Bands at 460, 400, 352, 344, 325, 317, 312, 297, 223, 217, 213, and 208 nm were assigned to Rh_2. Some of these, particularly the intense, sharp 344-nm band, were previously observed by Weltner and attributed to atomic rhodium.[266] The assignment of these features to Rh_2, especially the 344-nm band, now appears secure, however.

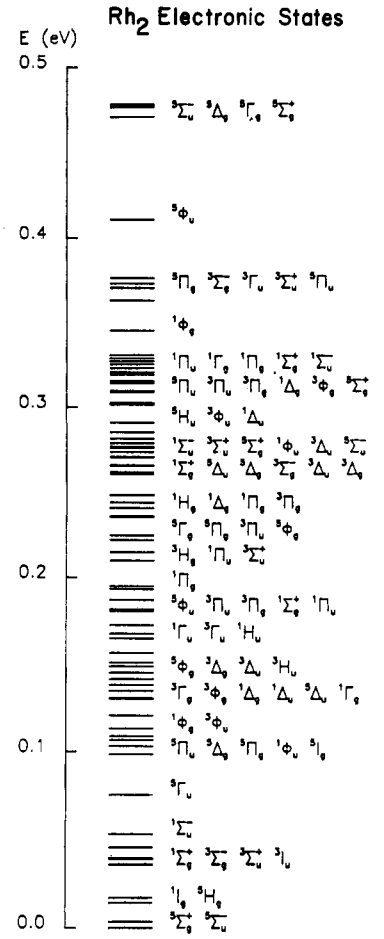

Figure 9. Electronic states of Rh_2, neglecting spin–orbit coupling, calculated for an internuclear separation of 2.69 Å. Reprinted with permission from ref 268. Copyright 1985 Munksgaard.

Two calculations for diatomic rhodium have been reported.[267,268] Using the SCF-Xα-SW method, at a fixed internuclear separation of 2.39 Å, Norman and Kolari calculate Rh_2 to possess a $^5\Delta_u$ ground state, arising from a $(4d\sigma_g)^2(4d\pi_u)^4(4d\delta_g)^4(4d\delta_u)^4(5s\sigma_g)^1(4d\pi_g)^2(4d\sigma_u)^1$ electronic configuration.[267] This gives a formal bond order of 2 for the dirhodium molecule.

In a substantially more ambitious study, carried out in a manner analogous to her study of dicobalt, Shim has investigated the electronic structure of Rh_2.[268] The ground state is calculated, in the CI approximation, as $^5\Sigma_g^+$, arising from an orbital occupation of $(4d\sigma_g)^{1.98}(4d\pi_u)^{3.20}(4d\delta_g)^{3.07}(4d\delta_u)^{2.97}(4d\pi_g)^{2.79}(4d\sigma_u)^{1.98}(5s\sigma_g)^{1.94}(5s\sigma_u)^{0.06}$. This ground state ($^5\Sigma_g^+$) and orbital occupancy bears a striking similarity to that found for the congeneric dicobalt molecule.[30] The calculated properties are $r_e = 2.86$ Å, $\omega_e = 118$ cm^{-1}, and $D_e = 0.85$ eV.[268] Shim estimates, however, that more complete configuration interaction studies will decrease r_e to 2.51 Å and will markedly increase D_e. Relative energies of the 84 low-lying electronic states of Rh_2, calculated allowing full CI within the 4d shell at an internuclear separation of 2.69 Å, are shown in Figure 9.

18. Palladium, Pd_2

Although an initial high-temperature mass spectrometric study was unsuccessful in producing Pd_2 in de-

tectable quantities,[77] a subsequent study by Lin, Strauss, and Kant did provide an experimental estimate of $D_0°(Pd_2)$.[269] The second-law value $D_0°(Pd_2) = 1.13 \pm 0.22$ eV, however, was not in agreement with the third-law value, $D_0°(Pd_2) = 0.73 \pm 0.26$ eV, which was derived assuming $r_e = 2.566$ Å and $\omega_e = 344$ cm^{-1} and assuming a nondegenerate ground electronic state.[269] This work has been criticized by Shim and Gingerich[270] for failing to monitor the absolute pressure in the system, instead assuming nearly unit activity of molten palladium in contact with either a ThO_2- or Al_2O_3-lined crucible. Shim and Gingerich have reinvestigated the $2Pd(g) \rightleftarrows Pd_2(g)$ equilibrium with proper pressure calibration and have derived a third-law value of $D_0°(Pd_2) = 1.03 \pm 0.16$ eV.[270] This value is based on $r_e = 2.65$ Å and $\omega_e = 133$ cm^{-1} and includes contributions from many low-lying electronic states, which were calculated by using an all-electron ab initio Hartree–Fock and configuration interaction procedure.[270] With use of the assumptions of Lin et al., Shim and Gingerich obtain $D_0°(Pd_2) = 1.69 \pm 0.16$ eV; the discrepancy of this value as compared to $D_0°(Pd_2) = 0.73 \pm 0.26$ eV as obtained by Lin et al. indicates that the assumption of unit activity of palladium in the condensed phase may have been invalid.[270]

Diatomic palladium was first investigated theoretically by using extended Hückel and CNDO methods by Baetzold in 1971.[180] The results obtained varied widely depending on the version of the theory being implemented and lack much predictive value, however. More recently, Basch, Cohen, and Topiol have investigated dipalladium by using relativistic core potentials in an ab initio MCSCF framework.[271] As in the congeneric dinickel molecule, chemical bonding is thought to arise from separated palladium atoms in their d^9s^1 ^3D states. Bringing the atoms together results in formation of a $(5s\sigma_g)^2$ bond and two weakly interacting $4d^9$ cores.[271] As calculated for Ni_2, holes in the otherwise filled 4d shell are preferentially placed in δ orbitals. Of the $^1\Gamma_g$, $^3\Gamma_u$, $^1\Sigma_g^+$, $^1\Sigma_u^-$, $^3\Sigma_g^-$, and $^3\Sigma_u^+$ states arising from the $\delta\delta$-hole configuration, Basch et al. have investigated only $^1\Gamma_g$ and $^3\Gamma_u$.[271] Spectroscopic constants calculated for these states were virtually identical, with $r_e = 2.808$ Å and $\omega_e = 215$ cm^{-1} for $^1\Gamma_g$ and $r_e = 2.811$ Å and $\omega_e = 216$ cm^{-1} for $^3\Gamma_u$. Basch et al. place the $^3\Sigma_u^+$ and $^1\Sigma_g^+$ $\sigma\sigma$ hole states at somewhat higher energies, with $r_e = 2.944$ Å and $\omega_e = 232$ cm^{-1} for $^3\Sigma_u^+$ and $r_e = 2.876$ Å and $\omega_e = 177$ cm^{-1} for $^1\Sigma_g^+$.[271] No evidence is found for significant 4d-orbital participation in the bonding of Pd_2.[153,271]

Theoretical results obtained by Shim and Gingerich using an all electron ab initio Hartree–Fock calculation with configuration interaction allowing full reorganization within the 4d and 5s shells provides a similar picture for Pd_2.[270] The six lowest energy states were calculated to be the $\delta\delta$ hole states $^1\Sigma_g^+$, $^1\Gamma_g$, $^1\Sigma_u^-$, $^3\Sigma_g^-$, $^3\Sigma_u^+$, and $^3\Gamma_u$, with $r_e = 2.84$ Å and $\omega_e = 126$ cm^{-1}. The other states, derived from $\pi\delta$, $\sigma\delta$, $\pi\pi$, $\sigma\pi$, and $\sigma\sigma$ hole configurations, appear at slightly higher energies.[270] Shim and Gingerich have also investigated the effects of spin–orbit coupling in Pd_2. With 30 molecular terms calculated to lie within an energy range of 0.37 eV ignoring spin–orbit coupling, it is not surprising that such coupling can dramatically effect the potential energy curves. When spin–orbit coupling is considered, the three lowest states are of 0_g^+, 5_u, and 0_u^- symmetry, and all derive primarily from the $\delta\delta$ configuration of 4d holes.[270] Figure 10 presents the energy levels calculated ignoring spin–orbit coupling, at an internuclear separation of 2.75 Å.

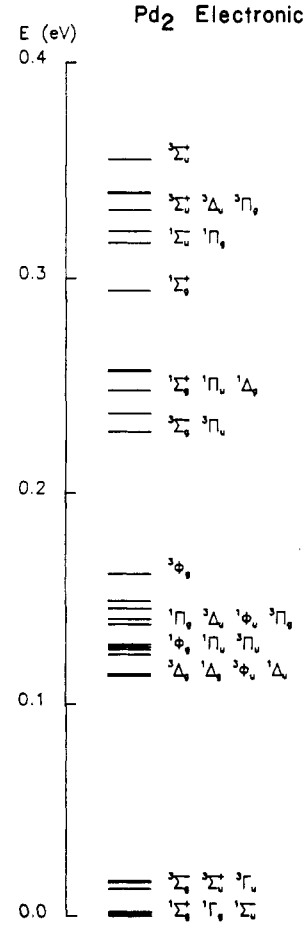

Figure 10. Electronic states of Pd_2, neglecting spin–orbit coupling, calculated for an internuclear separation of 2.75 Å. Reprinted with permission from ref 270. Copyright 1984 American Institute of Physics.

Finally Andzelm, Radzio, and Salahub have applied model-potential methods with relativistic corrections to Pd_2, using a local spin density framework.[75,137] With this method the values $r_e = 2.30$ Å, $\omega_e = 320$ cm^{-1}, and $D_e = 1.1$ eV were obtained.

The bond dissociation energy of Pd_2, as reported by Shim and Gingerich,[270] and as obtained in all reported calculations, is quite low. Dipalladium presents the interesting case of a molecule in which the atoms must be promoted from $4d^{10}$ to $4d^95s^1$ before significant bonding can occur. The energetic cost of promoting both atoms to this configuration is obtained from Table 1 as 1.90 eV, and this must be subtracted from the energy gained by bond formation to obtain the true $D_0°(Pd_2)$. Here again, as in the case of Mn_2, the necessity of promoting the atoms to configurations suitable for bonding dramatically reduces the strength of the bond which is formed. In light of this observation, a theoretical investigation of states correlating to the mixed $4d^{10}(^1S) + 4d^95s^1(^3D)$ asymptote might prove interesting. Although the chemical bonding from such a configuration would not be as favorable as that from the $4d^95s^1 + 4d^95s^1$ asymptote, the reduction in promotion energy required may compensate for the loss of chemical bonding.

TABLE 10. Electronic States of $^{107}Ag_2$[a]

state	T_e, cm^{-1}	ω_e, cm^{-1}	$\omega_e x_e$, cm^{-1}	B_e, cm^{-1}	α_e, cm^{-1}	r_e, Å	obsd transitns designatn	obsd transitns ν_{00}	ref
H (0_u^+?)	58273.1	166.7	2.48				H ← X	58259.8	15, 16
E (0_u^+?)	40159.4	146.2	1.55				E ↔ X	40136.7	6, 13–16
D 0_u^+	39014.5	169.0	1.21				D ↔ X	39002.7	6, 14–16
C 1_u $^1\Pi_u$	37631.3	171.4	0.91	(0.05098)	(0.00022)	(2.486)	C ↔ X	37620.8	6, 13–16
B (0_u^+?)	35838.6	152.5	0.88				B ↔ X	35818.6	6, 14–16
A 0_u^+ ($^1\Sigma_u^+$)	22996.4	155.3	0.59				A ↔ X	22977.9	5, 6, 12, 14–16
X 0_g^+ $^1\Sigma_g^+$	0	192.4	0.60	(0.05121)	(0.000136)	(2.480)			

[a] Uncertain values are given in parentheses. See text for details. $D_0°(Ag_2)$ = 1.65 ± 0.03 eV. IP(Ag_2) = 7.56 ± 0.02 eV. $D_0°(Ag_2^+)$ = 1.66 ± 0.05 eV.

19. Silver, Ag_2

The equilibrium between atomic and diatomic silver has been investigated by Knudsen effusion mass spectrometry by numerous authors.[22,156–158,272] Although most studies report only third-law values, the spectroscopic constants of Ag_2 are sufficiently well established that these values are preferable to second-law determinations. In addition, it now appears that the lowest excited electronic state of Ag_2 contributes negligibly to the overall entropy, even at temperatures of 1500–2000 K. The dissociation energy of disilver, $D_0°(Ag_2)$, may therefore be regarded as definitely established as 1.65 ± 0.03 eV.[25–27,272]

The absorption and emission spectra of gas-phase diatomic silver have been studied by various workers.[5,6,12–16] Selected values of the resulting spectroscopic constants are presented in Table 10. The spectroscopic transitions which have been observed are A ↔ X,[5,6,12,14–16] B ↔ X,[6,14–16] C ↔ X,[6,13–16] D ↔ X,[6,14–16] E ↔ X,[6,13–16] and H ↔ X[15,16] and a continuous emission spectrum joining onto the 3280.7 and 3382.9 Å lines of atomic silver.[14] The vibrational analysis of these band systems is fairly complete. In some cases the electronic symmetry species is known from the number of band heads observed, although this analysis is complicated by the isotopic modifications of disilver:[107] Ag_2 (26.85%); $^{107}Ag^{109}Ag$ (49.93%); $^{109}Ag_2$ (23.21%). None of the band systems have been rotationally analyzed, so no reliable values for the rotational constants and bond lengths exist. All observed bands are red-degraded, indicating an increase in bond length upon electronic excitation, however. Some attempts have been made to evaluate rotational constants and bond lengths of excited states on the basis of observed band origins and band head positions, but this procedure requires that a bond length for the ground state be assumed.[15,16] Table 10 lists rotational constants and bond lengths obtained by this procedure[16] in parentheses, although the reader is cautioned that these must be regarded only as estimates. The values obtained are based on an assumed r_e = 2.480 Å[16] for the Ag_2 ground state. Experimentally derived potential curves for Ag_2 are given in Figure 11.

Visible and ultraviolet spectra of silver dimers and polymers isolated in rare gas matrices have been extensively studied.[168,170,173,273–281] All investigators report Ag_2 absorptions near 390 and 263 nm; other absorptions are possible in the 290–330-nm range where atomic silver is strongly absorbing. A magnetic circular dichroism study indicates that the upper state of the 263-nm system is electronically degenerate but that the 390-nm system corresponds to a transition with non-

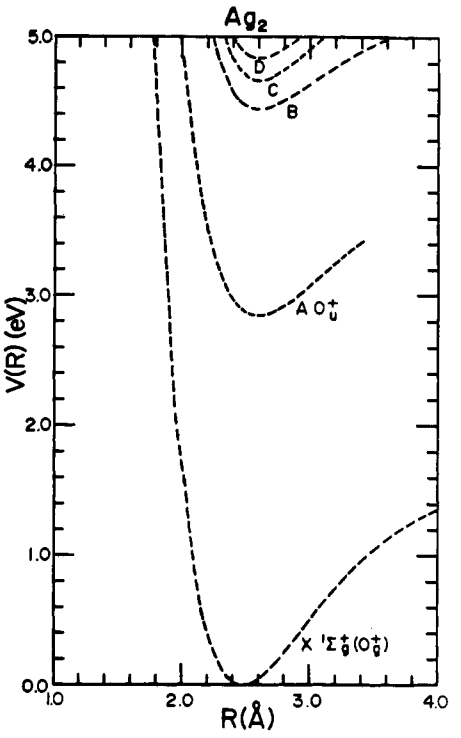

Figure 11. Potential energy curves for Ag_2, calculated from the experimental data of Table 10. Potential curves are dashed to indicate that the equilibrium positions are unknown and that a horizontal adjustment of unknown magnitude is required to bring these curves into correct position.

degenerate upper and lower states.[173] The 390-nm band system corresponds to the gas-phase A–X system, and on the basis of this observation the A state may be assigned as 0_u^+, probably originating from $^1\Sigma_u^+$. In very recent work, a study employing synchrotron radiation has extended the ultraviolet absorption spectrum of disilver into the vacuum ultraviolet.[280] Absorptions were identified by their excitation of the disilver fluorescence at 3.57 or 2.8 eV.[280] With this method, absorptions were located at 331, 265, 259, 244, 175, 167, and 159 nm for Ag_2 isolated in solid neon.[280] Finally, a Raman study of disilver isolated in solid krypton provides $\Delta G_{1/2}$ = 194 ± 0.5 cm^{-1},[279,284] in good agreement with the gas-phase value of 191 cm^{-1}. Resonance Raman studies have recently been used to unambiguously identify certain absorptions as arising from Ag_2 rather than higher polymers.[282,283] These studies have demonstrated the existence of more than one matrix site for Ag_2 as well.[283]

In unpublished work, Hopkins, Langridge–Smith, Morse, and Smalley have investigated disilver by resonant two-photon ionization methods in a supersonic cluster beam.[285] With a dye laser to excite Ag_2 and an

ArF excimer laser (193 nm; 6.4 eV) to ionize electronically excited disilver, the v–0 progression of the A–X band system was readily observed for $0 \leq v \leq 8$. When the fourth harmonic of a Nd:YAG laser (266 nm; 4.66 eV) was used as the ionizing laser, however, only members of the v–0 progression with $v \geq 3$ were observed. The 2–0 band would have been observed if it were a factor of 100 less intense than the 3–0 band, leading these investigators to conclude that poor Franck–Condon factors were not responsible for this drop in intensity. It is suggested instead that the adiabatic ionization potential of disilver is such that the A ($v = 3$) level lies within 4.66 eV of the ionization limit, but the A ($v = 2$) level does not. On this basis the ionization potential of Ag_2 is placed at 7.56 ± 0.02 eV. Within experimental error this is equal to the atomic ionization potential of silver, indicating that the binding energy of disilver cation is equal to that of the neutral molecule.[285]

Theoretical studies of disilver and silver clusters have been numerous, due in part to the importance of these molecules to the field of photography. A number of semiempirical calculations have been published based on extended Hückel and CNDO methods,[180,286-291] and Mitchell has used an empirical method based on van der Waals and ion–dipole forces to estimate the stability of various neutral and charged silver clusters.[292] Ozin et al. have applied the SCF-Xα-SW MO method to diatomic silver and have presented an assignment of the spectroscopic transitions to particular electronic excitations.[170]

Ab initio calculations of disilver have been presented by numerous investigators.[153,206,208,293-297] Some have explicitly included all electrons,[206,294] while others have employed relativistic or nonrelativistic effective core potentials.[153,293,295-297] Relativistic effects are shown to be important, shortening the bond by 0.06–0.15 Å, depending on calculational method. In addition, correlation of the 4d electrons is important, decreasing r_e about 0.1 Å from the relativistic Hartree–Fock value. The nonrelativistic Hartree–Fock limit for disilver produces $r_e = 2.79$ Å;[206,294] with substantial configuration interaction r_e is reduced to 2.72 Å. Relativistic calculations employing the model potential method obtain $r_e = 2.73$ Å without configuration interaction;[293] values as small as $r_e = 2.62$ Å are obtained for relativistic effective core potential studies with extensive CI.[153,295]

Attempts to treat disilver as a two-electron system using pseudopotentials were at first quite unsuccessful, predicting an absurdly short bond length of 1.64 Å.[181] More recently, however, a pseudopotential has been developed which explicitly allows polarization of the core electrons and treats the core at a level beyond the point charge approximation.[186-190] Correlation of the valence electrons is handled by either local spin density methods[186,188-190] or by a configuration interaction treatment.[187] Relativistic effects are also included. Predictions for the Ag_2 ground state are $r_e = 2.55$ Å, $D_e = 1.78$ eV, $\omega_e = 186$ cm^{-1}, and IP = 7.93 eV, in remarkably good agreement with the available experimental data.[186]

Local spin density methods have also been applied to Ag_2 by Martins and Andreoni[298] and by Salahub and co-workers.[75,256] Spectroscopic parameters for the various calculations are in reasonable agreement, with $r_e = 2.48$ Å, $D_e = 2.1$ eV, and $\omega_e = 186$ cm^{-1} obtained by Andzelm, Radzio, and Salahub[256] in the most extensive study.

Finally, a few theoretical calculations of electronically excited disilver should be noted. Basch has calculated bound excited states as follows: $^1\Sigma_u^+$ ($T_e = 2.59$ eV; $r_e = 2.997$ Å; $\omega_e = 165$ cm^{-1}); $^3\Pi_u$ ($T_e = 2.72$ eV; $r_e = 2.732$ Å; $\omega_e = 139$ cm^{-1}); $^1\Pi_u$ ($T_e = 3.83$ eV; $r_e = 2.942$ Å; $\omega_e = 96$ cm^{-1}).[296] All three excited states arise from the Ag(^{2}S) + Ag(^{2}P) separated atom limit and involve excitation of an electron from a $5s\sigma_g$ orbital to a π_u or σ_u orbital. Of these excited states, Basch assigns $^1\Sigma_u^+$ to the observed A state.[296] Grinter has recently provided a semiempirical analysis of the observed spectroscopic transitions in disilver, in which spin–orbit coupling is explicitly considered.[299] Grinter assigns the A state as $^1\Sigma_u^+$, derived from the promotion of a $5s\sigma_g$ electron to a $5s\sigma_u$* antibonding orbital.[299] This assignment has also been given on the basis of extended Hückel and Xα calculations for Ag_2.[170,290] Grinter then assigns the B and C states to $^1\Pi_{1u}$ and $^3\Sigma_{1u}^+$ electronic states deriving from $(5s\sigma_g)^1(5p\pi_u)^1$ and $(5s\sigma_g^1)(5p\sigma_u)^1$ configurations, which undergo extensive mixing by second-order spin–orbit coupling.[299] The D and E states are then assigned to $^3\Pi_{0u}^+$ $(5s\sigma_g)^1(5p\pi_u)^1$ and $^1\Sigma_{0u}^+$ $(5s\sigma_g)^1(5p\sigma_u)^1$, respectively.[299] Since electronic state symmetries for most of these states are not experimentally known at present, however, no experimental corroboration of these assignments is currently available.

Theoretical investigations of Ag_2^+ are in some disagreement. Basch finds Ag_2^+ to be more strongly bound than the neutral dimer, with $r_e(Ag_2^+) = 2.922$ Å.[296] Stoll et al., however, find Ag_2^+ to be more weakly bound than Ag_2, with $r_e(Ag_2^+) = 2.80$ Å and $\omega_e = 113$ cm^{-1}.[186] Experimental results, as discussed above, provide $D_0°(Ag_2) = 1.65 \pm 0.03$ eV and $D_0°(Ag_2^+) = 1.66 \pm 0.05$ eV, indicating very little change in the bond energy upon ionization. Finally, one should note a calculation by Benard investigating the $3d\sigma_u$ and $4d\sigma_u$ hole states of Ag_2^+.[300] The core hole state ($3d\sigma_u$) is best described by broken symmetry orbitals, while the valence hole state ($4d\sigma_u$) is best described by a CI expansion. Of course, no experimental information is available for these states.

20. Cadmium, Cd_2

As in the case of zinc, cadmium possesses a ground-state atomic configuration of $d^{10}s^2$, and only van der Waals forces bind Cd_2 in its ground state. Excited states of Cd_2 may be strongly bound, however, making dicadmium an interesting candidate for an excimer laser.

A large number of continuum absorptions and emissions have been observed in cadmium vapors.[215-218,221,301,308,310] Most of this work dates to the 1930s and has been reviewed by Finkelnburg,[221] to whom the interested reader is referred. The binding energy of dicadmium has been estimated by Winans as $D_0°(Cd_2) = 0.20$ eV from the energy difference between a cadmium atomic resonance line and the short-wavelength limit of the associated continuum absorption of Cd_2.[218] With use of similar methods Hamada estimates $D_0°(Cd_2) = 0.24$ eV.[215] Carlson and Kuschnir obtain $D_0°(Cd_2) = 0.095 \pm 0.009$ eV and $r_e = 3.02 \pm 0.08$ Å by fitting the measured viscosity coefficient of cadmium

TABLE 11. Electronic State of Cd_2[a]

state	T_e, cm^{-1}	ω_e, cm^{-1}	$\omega_e x_e$, cm^{-1}	separated atom limit	dissociatn energy to this limit	obsd transitns designatn	obsd transitns ν_{00}	ref
B 1_u $^1\Pi_u$				$^1S_0 + {}^1P_1$		B ← X	[45 000]	217, 310
A 0_u^+ $^1\Sigma_u^+$	35 500	$\Delta\bar{G} = 104$		$^1S_0 + {}^1P_1$		A ← X	35 543	220, 303-306
b 0_u^+ $^3\Pi_u$	30 728	17.8	0.34	$^1S_0 + {}^3P_1$	0.0291 eV	b ↔ X	30 726	33, 215, 217
a 1_u $^3\Sigma_u^+$				$^1S_0 + {}^3P_1$		a → X	[21 000]	307, 308
X 0_g^+ $^1\Sigma_g^+$	0	22	0.4	$^1S_0 + {}^1S_0$	0.0378 eV			33

[a] Wavenumbers in brackets provide the wavenumber of maximum absorption or emission intensity. $D_0°(Cd_2) = 0.0378$ eV.

vapor to the results calculated from an exponential-inverse sixth power interatomic potential function.[219] More recently, an investigation of the absorption coefficient of continuum absorption bands of Cd_2 as a function of temperature has provided $D_e(Cd_2) = 0.0475$ eV and $r_e = 4.82$ Å.[302] Finally, Kowalski et al. have performed a Birge–Sponer extrapolation of vibronic bands observed in the laser-induced fluorescence spectrum of jet-cooled dicadmium to obtain the reliable value $D_0°(Cd_2) = 0.0378$ eV, which is selected for Table 2.[33]

The ultraviolet absorption spectra of dicadmium isolated in rare gas matrices have been reported by various workers.[220,303-306] A diffuse band system, observed at 273 nm for Cd_2/Ar and 279 nm for Cd_2/Kr, has been observed by numerous authors.[220,303-306] Freedhoff has assigned this band as the A 0_u^+ ($^1\Sigma_u^+$) ← X 0_g^+ ($^1\Sigma_g^+$) transition of Cd_2, where A 0_u^+ ($^1\Sigma_u^+$) derives from the Cd($5s^2$ ^1S) + Cd(5s5p ^1P) separated atom limit.[304] A vibrational progression is observed within the excited electronic state with $\Delta\bar{G} = 104$ cm^{-1}.[220,305,306]

Fluorescence spectra of Cd_2 isolated in inert matrices have been obtained by excitation at 320 nm.[307] An intense green fluorescence, with maximum intensity at 545 nm for Cd_2/Ar was observed and attributed to the a 1_u ($^3\Sigma_u^+$) → X 0_g^+ ($^1\Sigma_g^+$) transition in dicadmium.[307] A gas-phase study of dicadmium demonstrated that an analogous long-lived green emission, with maximum intensity at 470 nm, could be excited by irradiation of cadmium vapor with either a He–Cd laser (325 nm) or a nitrogen laser (337.1 nm).[308] Decay times were shortened at higher temperatures and pressures, with the longest decay time reported as $\tau = 700$ μs (850 K, 5×10^{17} molecules/cm^3).[308] Such a long decay time is to be expected for decay occurring through a spin-forbidden radiative mechanism, made allowed by considerable spin–orbit coupling. The only plausible alternative to the assignment of the upper state as 1_u ($^3\Sigma_u^+$) is $^3\Pi_g$, arising from the same atomic limit, but calculated as lying below $^3\Sigma_u^+$.[224] This assignment is unlikely, however, since both the spin *and* Laporte selection rules are violated, leading one to expect a much longer phosphorescence lifetime than is observed.

Finally, Kowalski et al. report a laser-induced fluorescence study of the 324–326-nm band system of jet-cooled Cd_2.[33] This band system, built on the $^3P_1$ – $^1S_0$ transition of atomic cadmium at 326.1 nm, has been previously observed as long ago as 1927.[215,217] Under jet-cooled conditions, however, vibronic bands are readily assigned. Spectroscopic constants are reported in Table 11. Both ground and excited states are weakly bound, with $\omega_e'' = 22$ cm^{-1} and $\omega_e' = 17.8$ cm^{-1}, respectively.[33] As discussed in ref 309, two molecular states of *ungerade* symmetry arise from the $^3P_1 + {}^1S_0$ separated atom limit: 1_u ($^3\Sigma_u^+$) and 0_u^+ ($^3\Pi_u$). Bender et al. calculate the former to be bound by approximately 6000 cm^{-1}, while the latter exhibits only a van der Waals well.[224] Clearly Kowalski et al. have observed the b 0_u^+ ($^3\Pi_u$) ↔ X 0_g^+ ($^1\Sigma_g^+$) transition.[33] The deep well predicted by Bender et al.[224] for both the 1_u and 0_u^- components of the $^3\Sigma_u^+$ state is in qualitative agreement with the long wavelength emission assigned as a 1_u ($^3\Sigma_u^+$) → X 0_g^+ ($^1\Sigma_g^+$) (545 nm for Cd_2/Ar; 470 nm for gas-phase Cd_2).[307,308]

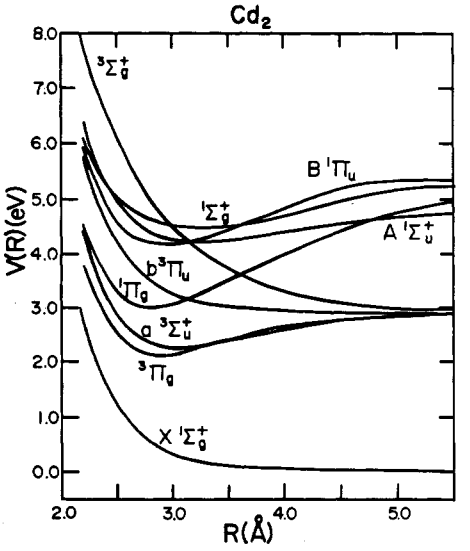

Figure 12. Potential energy curves for Cd_2, ignoring spin–orbit coupling, as calculated by ab initio methods. Reprinted with permission from ref 224. Copyright 1979 American Institute of Physics.

The electronic structure of dicadmium, as calculated by Bender et al., provides support for the assignments given here.[224] Potential energy curves for Cd_2, as calculated by Bender et al., are presented in Figure 12. Absorption or emission spectra involving three of the four *ungerade* states arising from the Cd($^1S_0$) + Cd($^1P_1$) and Cd($^1S_0$) + Cd(^3P) separated atom limits have been observed and identified. The B 1_u $^1\Pi_u$ ← X 0_g^+ ($^1\Sigma_g^+$) absorption is calculated to occur deeper in the ultraviolet than any transitions reported here[224] and has been suggested as the designation of the prominent absorption band of Cd_2 occurring at 2212 Å.[217,310] The occurrence of this band to the *blue* of the parent $^1P_1$ ← $^1S_0$ transition (2288 Å) in atomic cadmium is nicely predicted by the presence of a potential barrier in the excited B 1_u $^1\Pi_u$ state by the calculations of Bender et al.[224]

Finally a Raman study of dicadmium isolated in a krypton matrix at 20 K has been reported.[32] A vibrational fundamental of 58 ± 1 cm^{-1} is reported, in considerable disagreement with the gas-phase value of 22 cm^{-1}.[33] Obviously, vibrational motions of this frequency are strongly perturbed by the matrix and are not rep-

resentative of the isolated gas-phase molecule.

21. Lanthanum, La_2

The only experimental datum on dilanthanum was obtained by Verhaegen et al. by high-temperature Knudsen effusion mass spectrometry in 1963.[53] The absolute entropy method was used to determine $D_0°(La_2)$ = 2.50 ± 0.22 eV, assuming r_e = 2.80 Å, ω_e = 230 cm^{-1}, and a ground-state effective electronic degeneracy of 5. This value has been reported in many critical reviews,[23-26,229,259,260] although the validity of the assumptions is by no means obvious.

The only other piece of information available about La_2 is the failure of Knight et al. to observe an ESR spectrum attributable to La_2.[227] As is the case for the congeneric diyttrium, Y_2, this suggests a possible $^1\Sigma_g^+$ ground state for La_2. At present, no calculations are available for comparison on this point.

22. Hafnium, Hf_2

At present, neither experimental data nor theoretical calculations are available for dihafnium, Hf_2. The dissociation energy, $D_0°(Hf_2)$, has been estimated by using empirical correlation rules as 3.15 ± 0.28,[229] 3.86 ± 0.61,[236] 3.15,[260] and 3.45 ± 0.52 eV.[261] A selected value of 3.4 ± 0.6 eV is given in Table 2.

23. Tantalum, Ta_2

Experimental and theoretical results are also lacking for ditantalum, Ta_2. Empirical estimates of $D_0°(Ta_2)$ are 4.09 ± 0.06,[229] 5.09 ± 1.02,[236] 4.09,[260] and 3.62 ± 0.52 eV.[261] In a very recent study Gingerich et al. have failed to observe Ta_2 over solid tantalum at 3100 K, placing an upper limit on $D_0°(Ta_2)$ of 5.2 ± 0.2 eV.[160] On the basis of these results, a selected value of $D_0°(Ta_2)$ = 4 ± 1 eV is given in Table 2.

These estimates of bond energy in ditantalum suggests strong participation of the 5d electrons in the chemical bonding. In this regard several ligated Ta_2 molecules should be noted, which are considered to possess a doubly bonded Ta_2 moiety: Ta_2Cl_6(tetrahydrothiophene)$_3$, r_{Ta-Ta} = 2.681 Å; Ta_2Br_6(tetrahydrothiophene)$_3$, r_{Ta-Ta} = 2.710 Å; Ta_2Cl_6(di-*tert*-butylacetylene)(tetrahydrothiophene)$_2$, r_{Ta-Ta} = 2.677 Å; $Ta_2Cl_6(S(CH_3)_2)_3$, r_{Ta-Ta} = 2.691 Å; and $Ta_2Cl_6(P(CH_3)_3)_4$, r_{Ta-Ta} = 2.721 Å.[91] These bond lengths may be compared to the nearest-neighbor distance in bcc tantalum crystal of 2.87 Å.[311]

24. Tungsten, W_2

Experimental and theoretical studies of ditungsten are also nonexistent. Estimates of the binding energy, $D_0°(W_2)$ are 4.69 ± 0.89,[229] 5.62 ± 1.23,[236] 4.68,[260] and 5.00 ± 0.69 eV.[261] Accordingly, a selected value of $D_0°(W_2)$ = 5 ± 1 eV is adopted.

As expected from its congeners Cr_2 and Mo_2, W_2 is thought to form a strong, multiply d-bonded W–W bond, probably with a sextuply bonded 0_g^+ ($^1\Sigma_g^+$) ground state. This expectation is in accord with the dissociation energies estimated above and is supported by known binuclear complexes of tungsten with multiple W–W bonds. Quadruply-bonded ditungsten moieties are now well-established, with some representative examples: $W_2(O_2CCF_3)_4$(diglyme)$_{2/3}$, r_{W-W} = 2.211, 2.207 Å; $Li_4W_2(CH_3)_8 \cdot 4(C_2H_5)_2O$, r_{W-W} = 2.264 Å, and W_2(2,4-dimethyl-6-hydroxypyrimidine)$_4 \cdot {}^1/_2$(diglyme), r_{W-W} = 2.155 Å.[91]

25. Rhenium, Re_2

Very little experimental work and no theoretical work exist for dirhenium. At present, no experimental measurement of the Re_2 bond energy is available, but $D_0°(Re_2)$ has been empirically estimated as 3.89 ± 0.53,[229] 5.03 ± 1.04,[236] 3.90,[260] and 3.28 ± 0.86 eV.[261] A selected value of 4 ± 1 eV is cautiously listed in Table 2 on the basis of these estimates.

In the first gas-phase spectroscopic study of a third-row open d-shell transition-metal dimer, Leopold, Miller, and Lineberger have recently investigated Re_2.[40] The experiment produces diatomic rhenium *anions* by seeding $Re_2(CO)_{10}$ vapor into a flowing afterglow source. The resulting anions are extracted, mass-selected, and photodetached with 488.0-nm radiation from an argon ion laser. The ejected photoelectrons are then energy analyzed, yielding an electronic spectrum of the neutral dirhenium molecule, Re_2.[40] With this method the adiabatic electron affinity of Re_2 was measured to be 1.571 ± 0.008 eV, which is larger than the (estimated) electron affinity of atomic rhenium of 0.15 eV.[439] Vibronic structure in the observed photodetachment spectrum provides $\omega_e(Re_2^-)$ = 320 ± 15 cm^{-1}, while $\omega_e(Re_2)$ = 340 ± 20 cm^{-1} for the neutral dirhenium ground state. A harmonic Franck–Condon analysis indicated a change of 0.03 Å in the internuclear separation upon electron attachment to the neutral Re_2 molecule.[40]

An electronically excited state of dirhenium was located 890 ± 30 cm^{-1} above the ground state.[40] The vibrational frequency and equilibrium internuclear distance in this state are identical with that of the ground state. At least two additional excited states were observed, with intensity maxima approximately 5100 and 6200 cm^{-1} above the ground electronic state.

The vibrational frequencies observed imply large force constants of 6.4 ± 0.8 and 5.6 ± 0.5 mdyn $Å^{-1}$ in Re_2 and Re_2^-, respectively. These may be compared to the force constants of multiply bonded V_2 ($X\ ^3\Sigma_g^-$, k = 4.33 mdyn $Å^{-1}$) and Mo_2 ($X\ ^1\Sigma_g^+$, k = 6.57 mdyn $Å^{-1}$) and to singly bonded Cu_2 ($X\ ^1\Sigma_g^+$, k = 1.30 mdyn $Å^{-1}$), Ag_2 ($X\ ^1\Sigma_g^+$, k = 1.17 mdyn $Å^{-1}$), and Au_2 ($X\ 0_g^+\ ^1\Sigma_g^+$, k = 2.11 mdyn $Å^{-1}$). On the basis of these values there is little doubt that dirhenium exists as a multiply 5d-bonded dimer, in stark contrast to its congener, Mn_2 (see above). Although the 6s → 5d promotion energy in rhenium is nearly as large as the 4s → 3d promotion energy in manganese, the more nearly comparable sizes of the 6s and 5d orbitals apparently permits this energy to be recovered by effective 5d-bond formation in Re_2.

The possibility of a multiply bonded dirhenium molecule should not come as a surprise since multiply bonded dirhenium compounds have been well-known since 1964, when the structure of $[Re_2Cl_8]^{2-}$ (r_{Re-Re} = 2.24 Å) was explained in terms of a quadruple bond between rhenium atoms.[312] Since that time numerous examples of quadruply bonded Re_2 moieties have been discovered, with the rhenium–rhenium distance as small as 2.177 Å in certain cases.[91]

26. Osmium, Os_2

Neither experimental nor theoretical results are available for diosmium, Os_2. Empirical estimates of the

TABLE 12. Electronic States of $^{197}Au_2$[c]

state	T_e, cm^{-1}	ω_e, cm^{-1}	$\omega_e x_e$, cm^{-1}	B_e, cm^{-1}	α_e, cm^{-1}	$10^{-8}D_e$, cm^{-1}	r_e, Å	obsd transitns: designatn	obsd transitns: ν_{00}	ref
E	~50 500							E ← X		228
D	~48 000							D ← X		228
C	~31 500							C ← X		228
B 0_u^+	25 685.5	179.85	0.680	0.026 961[a]	0.000 096 3[b]	0.260[a]	2.5197[a]	B ↔ X	25 679.87	5, 6, 18
A 0_u^+	19 668.1	142.3	0.445	0.025 958	0.000 090 3	0.35	2.5678	A ↔ X	19 643.8	5, 6, 17, 18
X 0_g^+ $^1\Sigma_g^+$	0	190.9	0.420	0.028 013	0.000 072 3	0.250	2.4719			

[a] Data refers to the level $v = 0$ of B 0_u^+. [b] Estimated from the Pekeris relationship. [c] $D_0°(Au_2) = 2.29 \pm 0.02$ eV.

bond dissociation energy, $D_0°(Os_2)$, have been provided, however, as 4.20 ± 0.26,[229] 5.13 ± 1.07,[236] 4.20,[260] and 3.79 ± 0.52 eV.[261] On the basis of these values, an estimated $D_0°(Os_2)$ of 4.3 ± 0.8 eV is selected. Binuclear osmium compounds containing a triple bond, such as Os_2(2-hydroxypyridine)$_4Cl_2$·$(C_2H_5)_2O$ (r_{Os-Os} = 2.344 Å), are now well-known and demonstrate the potential of multiple 5d bonding between osmium atoms.[91]

27. Iridium, Ir_2

The dissociation energy of diatomic iridium has been empirically estimated as 3.46 ± 0.12,[229] 4.23 ± 0.76,[236] 3.45,[260] and 3.62 ± 0.52 eV.[261] A recent investigation by Gingerich et al. has failed to observe Ir_2 in equilibrium with molten iridium metal at 3100 K, thereby placing an upper limit on $D_0°(Ir_2)$ of 4.66 ± 0.21 eV.[160] In view of these estimates, $D_0°(Ir_2) = 3.7 \pm 0.7$ eV may be considered a reasonable estimate. In support of the ability of iridium to form multiple 5d bonds one may note the compound $[(C_5(CH_3)_5)Ir(\mu\text{-}H)_3Ir(C_5(CH_3)_5)]^+$-$BF_4^-$, in which the Ir–Ir triple bond (2.458 Å) is bridged by hydrogen atoms.[91]

28. Platinum, Pt_2

An early investigation of the equilibrium vapor over high-temperature platinum failed to detect Pt_2,[313] a result which has been attributed to insufficiently high activity of platinum in the condensed phase.[314] In subsequent work, Gupta, Nappi, and Gingerich have detected diplatinum in equilibrium with atomic platinum over the temperature range 2259–2736 K.[314] From a second-law evaluation $D_0°(Pt_2) = 3.71 \pm 0.61$ eV, while the third-law evaluation gives $D_0°(Pt_2) = 3.71 \pm 0.16$ eV, assuming r_e = 2.34 Å, ω_e = 259.4 cm^{-1}, a $^1\Sigma$ ground state, and a high-lying triplet excited state at 11 248.7 cm^{-1} [314] (see below). In view of the uncertainty of the third-law assumptions the second-law value is selected as more reliable. This may be compared to empirical estimates of $D_0°(Pt_2)$ of 2.88 ± 0.26,[229] 3.43 ± 0.48,[236] and 2.88 eV.[260]

Spectroscopic investigations of diatomic platinum in the gas phase have thus far been unsuccessful, presumably due to the low concentration of dimers formed.[315] An investigation using matrix-deposited platinum, however, has provided an electronic absorption system of Pt_2 with beautiful, sharp, well-resolved vibronic transitions.[316] In an annealed argon matrix ν_{00} = 11 248.7 cm^{-1}, ω_e' = 217.2 cm^{-1}, and ω_e' = 0.45 cm^{-1} are obtained, based on observation of the 0–0, 1–0, and 2–0 bands.[316] In krypton ν_{00} shifts to 11 204 cm^{-1} (average of two matrix sites), and $\Delta G_{1/2}$ is approximately 211.7 cm^{-1}.

Basch et al. have investigated Pt_2 by using relativistic core potentials in an ab initio self-consistent field framework.[153,271] As obtained in previous calculations on the congeneric Ni_2 and Pd_2 molecules (see above), diplatinum may be described as *primarily* bonded through a $(6s\sigma_g)^2$ single bond. The 5d shells then contain two holes, which may be configured in dσ, dπ, or dδ orbitals as $\delta\delta$, $\pi\delta$, $\sigma\delta$, $\pi\pi$, $\sigma\pi$, or $\sigma\sigma$. Of these, Basch has investigated the $^1\Gamma_g(\delta\delta)$, $^3\Gamma_u(\delta\delta)$, $^3\Sigma_u^+(\sigma\sigma)$, and $^1\Sigma_g^+(\sigma\sigma)$ molecular terms. As found for Ni_2 and Pd_2, the lowest states of Pt_2 derive from the $\delta\delta$ hole configuration. Basch calculates (r_e, ω_e, D_e) of the various states as follows: $^1\Gamma_g(\delta\delta)$, (2.574 Å, 267 cm^{-1}, 0.93 eV); $^3\Gamma_u(\delta\delta)$, (2.581 Å, 271 cm^{-1}, 0.92 eV); $^1\Sigma_g^+(\sigma\sigma)$, (2.506 Å, 247 cm^{-1}, 0.43 eV); $^3\Sigma_u^+(\sigma\sigma)$, (2.634 Å, 225 cm^{-1}, 0.18 eV).[271] The shorter bond length of the $^1\Sigma_g^+(\sigma\sigma)$ state arises because significant 5d overlap on adjacent metal centers begins to occur in Pt_2, lending some doubly bonded character to the $^1\Sigma_g^+(\sigma\sigma)$ state. This state possesses a $(6s\sigma_g)^2$ bond and a component of $(5d\sigma_g)^2$ bonding as well. In view of simplicity of the matrix-isolation spectra of Pt_2 and the high dissociation energy recently measured it appears likely that the 5d orbitals will be found to play a larger role in the bonding of platinum dimer at a higher level of theory. Diplatinum appears to be an excellent candidate for more detailed experimental and theoretical investigations of the role of the 5d electrons in the chemical bonding of third-row transition metals.

29. Gold, Au_2

High-temperature Knudsen effusion mass spectrometric studies of digold have been reported by numerous authors.[22,156–158,272,317,318] Second- and third-law determinations are in superb agreement, with $D_0°(Au_2)$ = 2.29 ± 0.02 eV.[318]

Accurate third-law determinations of $D_0°(Au_2)$ have been possible because the values of r_e and ω_e are accurately known from optical spectroscopy. Two gas-phase band systems are known: A–X (4800–6500 Å) and B–X (3800–4100 Å).[5,6,17,18] Vibrational[6,17] and rotational[18] analyses have been provided, and both systems are now known to be 0_u^+–0_g^+ $^1\Sigma_g^+$ transitions.[18] Spectroscopic constants are given in Table 12, and potential energy curves are given in Figure 13.

An extrapolation of the ground-state vibrational levels gives a binding energy of 21 060 cm^{-1} (2.61 eV), in fair agreement with the mass spectrometric value.[18] The extrapolated dissociation energy of A 0_u^+ is 9230 cm^{-1}, corresponding to a dissociation limit 10 405 cm^{-1} above Au($^2S_{1/2}$) + Au($^2S_{1/2}$), using the $D_0°(Au_2)$ determined from high-temperature mass spectrometry. The only asymptote in this vicinity is Au($^2S_{1/2}$) + Au($^2D_{5/2}$), at 9161.3 cm^{-1}.[3] Accordingly, the A 0_u^+ state is assigned as the 0_u^+ state correlating to this separated atom limit.

A similar analysis[18] shows the B 0_u^+ state extrapolating to an asymptote 19 011 cm^{-1} above ground-state

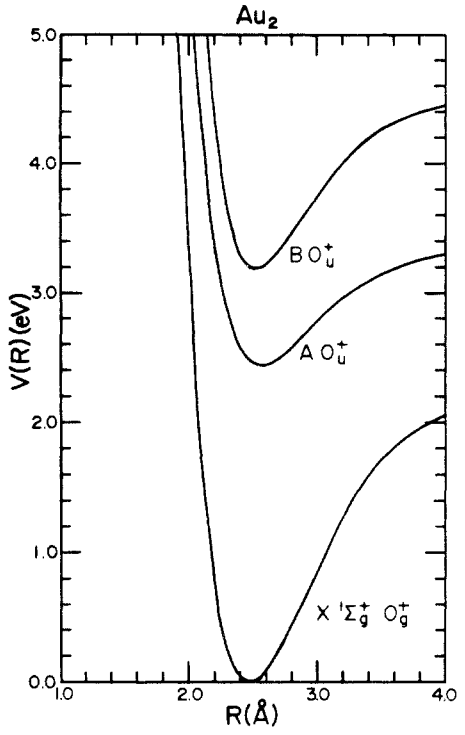

Figure 13. Potential energy curves for Au_2, calculated from the experimental data of Table 12.

atoms. Two asymptotes exist in this vicinity: $Au(^2S_{1/2})$ + $Au(^2D_{3/2})$, at 21 435.3 cm^{-1} and $Au(^2D_{5/2})$ + $Au(^2D_{5/2})$, at 18 322.6 cm^{-1}.[3] Although both asymptotes are energetically possible, only $Au(^2S_{1/2})$ + $Au(^2D_{3/2})$ gives rise to a 0_u^+ state. Accordingly, B 0_u^+ is assigned as the 0_u^+ state correlating to this separated atom limit.

Klotzbücher and Ozin have reported absorption spectra of digold isolated in a low-temperature argon matrix.[228] Broad absorptions attributed to Au_2 occur at 365 (27 400) and 317 nm (31 500 cm^{-1}); more narrow and intense absorption features occur at 208 (48 000) and 198 nm (50 500 cm^{-1}).[228] The first of these is attributed to the B $0_u^+ \leftarrow$ X 0_g^+ $^1\Sigma_g^+$ system, while the remaining systems are currently unassigned.

Relativistic Hartree–Fock–Slater[208] and effective core potential[153,297,319-321] calculations have been reported for diatomic gold. Relativistic effects are quite important for the proper description of Au_2. Lee et al., for example, find that on the SCF level the digold bond contracts 0.3 Å, is strengthened by 1 eV, and increases in vibrational frequency by about 50% when relativistic effects are included.[319] The primary source of these effects is the relativistic contraction of the 6s orbital due to its penetration into the near-nucleus region.[319] This contraction has the additional effect of shielding the high-l orbitals more effectively, causing a relativistic expansion of d and f orbitals.[322] The expansion of the 5d orbitals probably contributes substantially to the increased binding energy of the open 5d-shell transition-metal clusters by making these orbitals more accessible for chemical bonding.

The relativistic effective core potential MCSCF-CI procedure has been carefully applied to the ground and excited electronic states of Au_2 by Ermler, Lee, and Pitzer.[320] The resulting X, A, and B states are in almost quantitative agreement with experiment. In addition, predictions of higher lying states are made. For high-lying states of 0_u^+ or 0_g^+ symmetry substantial ionic contributions from Au^+Au^- are possible.[321] The 0_u^+ states possessing large Au^+Au^- contributions are expected to lead to intense optical absorptions from the ground 0_g^+ state. These transitions are intense because they correspond to charge-transfer bands and therefore should have a large transition dipole moment. The intense matrix absorptions of Au_2 at 198 and 208 nm may involve significant contributions from the 0_u^+ charge-transfer state.

30. Mercury, Hg_2

Dimercury, Hg_2, was the first of the transition-metal molecules to be investigated, a fact which is particularly ironic because Hg_2 is also among the most weakly bound of the transition-metal dimers. Estimates of the dissociation energy $D_0°(Hg_2)$ were first obtained by Franck and Grotian in 1922 by monitoring the temperature dependence of the absorptions associated with Hg_2.[323] This measurement has been repeated by numerous workers,[302,324-329] and values of $D_0°(Hg_2)$ ranging from 0.055 to 0.07 eV have been obtained. Winans[326,327] has suggested a rotational correction to these values; his procedure appears to be invalid, however. Mrozowski's value $D_0°(Hg_2)$ = 0.74 eV may be dismissed as completely outside the range of possibility.[329]

Measurements of band spectra attached to atomic transitions of Hg permit $D_0°(Hg_2)$ to be independently estimated. With use of this procedure Hamada estimates $D_0°(Hg_2) \geq 0.07$ eV,[215] while Winans obtains $D_0°(Hg_2)$ = 0.15 eV.[330] This method estimates the binding energy of Hg_2 as the difference between the short wavelength limit of Hg_2 molecular absorption and the associated atomic transition, under the assumption that the excited-state potential has not deviated from the atomic excitation energy at the large internuclear separation of ground-state Hg_2. Since van der Waals forces are at work in both excited and ground electronic states, however, there is little reason to expect weaker long-distance interactions between a ground and an excited atom than between two ground state atoms. In as much as this method neglects long-range interactions in the excited state, it suffers from a fundamental flaw.

A number of authors have investigated the interatomic potential in Hg_2 by gas-phase viscosity studies.[219,331-334] All provide D_e in the range of 0.068–0.134 eV. Values of r_e and D_e calculated from viscosity data are highly correlated, with the larger values of D_e corresponding to smaller values of r_e. In view of the interatomic distances in solid mercury, 3.00 and 3.47 Å,[335] a value of r_e = 3.25 ± 0.2 Å is suggested,[331] for which viscosity data provide D_e = 0.07 ± 0.01 eV.

Kuhn has investigated the pressure broadening of mercury atomic lines.[336] A quantitative analysis of the line profiles shows that mercury atoms interact at long distances through the expected r^{-6} potential. Kuhn has also measured the total integrated absorption from the Hg_2 band system at 2540 Å. Assuming the oscillator strength is unchanged from the free atomic transition at 2537 Å, an absolute concentration of Hg molecules may be calculated. Using a third-law expression Kuhn then calculates 0.065 eV $\leq D_0°(Hg_2) \leq$ 0.091 eV.[336] This compares to theoretical estimates of 0.087,[337] 0.084,[338] 0.063,[338] and 0.055 eV[338] for $D_0°(Hg_2)$.

Hilpert has recently used Knudsen effusion mass spectrometry to determine $D_0°(Hg_2)$.[339] Second- and

TABLE 13. Electronic States of Hg_2[a,b]

state	T_e, cm^{-1}	ω_e, cm^{-1}	$\omega_e x_e$, cm^{-1}	separated atom limit	separated atom energy, cm^{-1}	D_0 to this limit, eV	obsd transitns designatn	obsd transitns ν_{00}, cm^{-1}	ref
R $0_u^+(^1\Sigma_u^+)$				$^1S_0 + {}^1S_0$	63928				
Q 0_u^+ $(^3\Sigma_u^-)$		120		$^1S_0 + {}^3S_1$	62350		Q ↔ B	22155	366-368, 381-383
P 1_u $(^3\Sigma_u^-)$	x + 23818	120		$^1S_0 + {}^3S_1$	62350		P ↔ G	15803	366-368
							P → E	19614	381-383
							P ↔ A	23791, 23806	
O 1_u $(^1\Pi_u)$				$^1S_0 + {}^1P_1$	54069		O ← X		216, 330
N 0_g^+ $(^1\Sigma_g^+)$				$^1S_0 + {}^1P_1$	54069				
M 0_u^+ $(^1\Sigma_u^+)$		(200)		$^1S_0 + {}^1P_1$	54069		M → X		215, 379, 380
L 1_g $(^1\Pi_g; {}^3\Sigma_g^+)$				$^1S_0 + {}^1P_1$	54069				
K 2_u $(^3\Pi_u)$				$^1S_0 + {}^3P_2$	44043				
J 0_g^- $(^3\Sigma_g^+)$				$^1S_0 + {}^3P_2$	44043				
I 1_u $(^3\Pi_u)$		(125)		$^1S_0 + {}^3P_2$	44043	(0.25)	I ↔ X	(42640)	215, 326, 343, 377, 378
H 0_u^- $(^3\Pi_u)$				$^1S_0 + {}^3P_2$	44043				
G 1_g $(^3\Sigma_g^+; {}^1\Pi_g)$	x + 7999	152 ± 2	0.9 ± 0.2	$^1S_0 + {}^3P_2$	44043		P → G	15803	382, 383
F 0_u^+ $(^3\Pi_u)$				$^1S_0 + {}^3P_1$	39412		F ← X	(39360)	323-325, 328, 336, 343, 350-352
E 2_g $(^3\Pi_g)$	x + 4192	142 ± 1	0.5 ± 0.1	$^1S_0 + {}^3P_2$	44043		P → E	19614	368, 381-383
D 1_u $(^3\Sigma_u^+)$	~x + 2800	(230)		$^1S_0 + {}^3P_1$	39412	(0.84)	D ↔ X	(33000)	215, 325, 328, 340, 341, 343, 344, 348, 350, 352-365, 372, 373
C 0_u^- $(^3\Sigma_u^+)$				$^1S_0 + {}^3P_0$	37645				
B 1_g $(^3\Pi_g)$	~x + 1700	143		$^1S_0 + {}^3P_1$	39412		Q ↔ B	22155	368, 382
A 0_g^- $(^3\Pi_g)$	x + 15	144 ± 1	0.5 ± 0.1	$^1S_0 + {}^3P_0$	37645		P ↔ A	23791	366-368
A 0_g^+ $(^3\Pi_g)$	x ≈ 29000	144 ± 1	0.5 ± 0.1	$^1S_0 + {}^3P_1$	39412		P ↔ A	23806	381-383
X 0_g^+ $^1\Sigma_g^+$	0	(49)		$^1S_0 + {}^1S_0$	0	0.074 ± 0.02			

[a] For details see the text. $D_0°(Hg_2)$ = 0.074 ± 0.020 eV. IP(Hg_2) = 9.103 ± 0.010 eV. $D_0°(Hg_2^+)$ = 1.40 ± 0.03 eV. [b] Uncertain values are given in parentheses.

third-law values are in agreement and place $D_0°(Hg_2)$ = 0.074 ± 0.020 eV. This value is in agreement with the results of previous workers and is adopted as the selected value in Table 2.

The low dissociation energy of Hg_2 results from the filled shell configuration $5d^{10}6s^2$ of atomic mercury, which permits only van der Waals interactions between atoms. Excited-state mercury atoms, however, are capable of interacting through strong chemical forces, which lead to strongly bound excited states of dimercury. As a result of the disparity between ground- and excited-state binding energies, the absorption and emission spectra of Hg_2 are characterized by broad continua and diffuse bands. These have been the subject of much investigation since the turn of the century.[215-217,221,302,323-325,328-330,336,340-383]

To describe the observed bands and explain their origins, we must first understand the isolated mercury atom. The ground state is $5d^{10}6s^2$, $^1S_0$. The lowest excited states are $5d^{10}6s^16p^1$, $^3P_0$ (at 37645.08 cm^{-1}), $^3P_1$ (at 39412.30 cm^{-1}), $^3P_2$ (at 44042.98 cm^{-1}), and $^1P_0$ (at 54068.78 cm^{-1}).[3] Molecular states correlating to two separated excited-state atoms must have an asymptote above 75000 cm^{-1} and are not expected to be bound by more than 10000 cm^{-1}, so absorption to these states will occur at wavelengths below 1500 Å. The absorptions and emissions which have been observed in the near- and mid-ultraviolet therefore involve molecular states derived from one ground ($^1S_0$) and one excited ($5d^{10}6s^16p^1$) mercury atom. Potential energy curves calculated for these molecular states are given in Figure 14.

Winans has observed a continuous absorption band extending from the atomic $^1P_1 \leftarrow {}^1S_0$ transition at 1849–1808 Å.[216,330] Presumably this absorption is due to Hg_2 molecules (ground state X 0_g^+ $^1\Sigma_g^+$) being excited to either the M 0_u^+ ($^1\Sigma_u^+$) or O 1_u ($^1\Pi_u$) molecular states correlating to the $^1P_1 + {}^1S_0$ separated atom limit. On the basis of the calculations of Mies et al.[309] the upper state is probably O 1_u (see Figure 14). In a discharge Hamada has observed a banded emission system in the

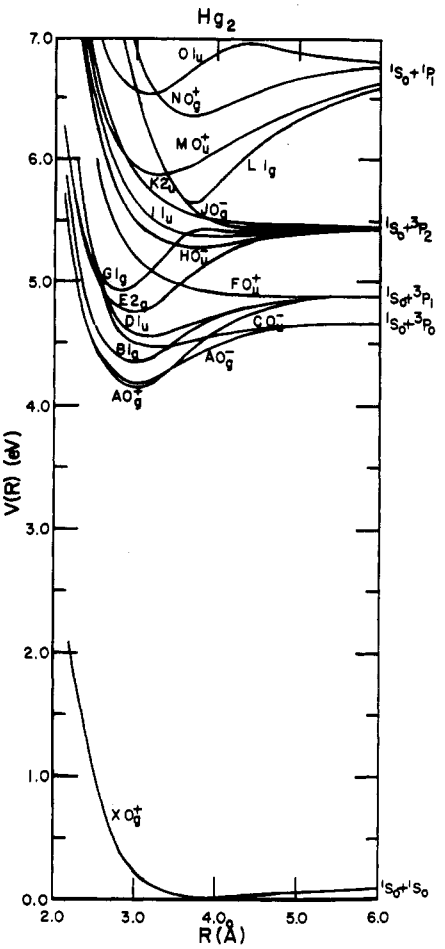

Figure 14. Potential energy curves for Hg_2, including spin–orbit coupling as calculated by Mies, Stevens, and Krauss[309] and modified according to new experimental data. Reprinted with permission from ref 309. Copyright 1978 Academic Press.

region 2170–2040 Å, with vibrational intervals converging to the 1849 atomic transition.[215] At the longest wavelengths the vibrational interval is approximately 200 cm^{-1}, indicating substantial bonding in the excited state.[215] Recent work by Ehrlich and Osgood casts doubt on this interpetation; they have observed a well-resolved Condon diffraction pattern characteristic of a bound-free transition when mercury vapor is excited with radiation from an ArF excimer laser at 193 nm.[379,380] Nevertheless, the upper state is presumably the M 0_u^+ ($^1\Sigma_u^+$) state, in accord with the calculations of Mies et al.[309] Other vacuum ultraviolet bands at 169[216,330,375] and 175 nm[376] are less confidently assigned.

The next lower lying separated atom asymptote is $^1S_0$ + $^3P_2$ at 44 042.98 cm^{-1}, from which the K 2_u ($^3\Pi_u$), I 1_u ($^3\Pi_u$), H 0_u^- ($^3\Pi_u$), E 2_g ($^3\Pi_g$), G 1_g ($^3\Sigma_g^+$; $^1\Pi_g$), and J 0_g^- ($^3\Sigma_g^+$) molecular states arise.[309] In this designation the rigorous Hund's case (c) symbol is given, followed by the parent case (a) states in parentheses.[309] In Hg_2 an avoided crossing has been calculated for the 1_g states arising from $^3P_2$ + $^1S_0$ ($^3\Sigma_g^+$) and $^1P_1$ + $^1S_0$ ($^1\Pi_g$); hence the G 1_g state is of mixed parentage.[309] Of these states, only I 1_u ($^3\Pi_u$) is optically coupled to the ground (X 0_g^+ $^1\Sigma_g^+$) state. Narrow bands (2345–2309 Å) converging to the forbidden $^3P_2 \rightarrow {}^1S_0$ transition at 2270 Å have been observed in emission,[215,326,343,377,378] though only a band at 2345 Å is visible in absorption.[343] These results suggest the I 1_u excited state is bound by approximately 0.25 eV relative to the Hg($^1S_0$) + Hg($^3P_2$) atomic limit, assuming $D_0°(Hg_2)$ = 0.07 eV for dissociation of the ground electronic state. The largest vibrational interval observed is approximately 125 cm^{-1}, and this interval drops rapidly with increasing excitation within the I 1_u ($^3\Pi_u$) state.[215] The observation of only the 2345-Å (0–0) band in absorption indicates that the equilibrium bond lengths of the I 1_u ($^3\Pi_u$) and X 0_g^+ ($^1\Sigma_g^+$) states are nearly the same; otherwise Franck–Condon factors would favor an extended progression in absorption. These general conclusions are upheld by detailed theoretical calculations.[222,309]

The next lower separated atom limit, Hg($^1S_0$) + Hg($^3P_1$), gives rise to D 1_u ($^3\Sigma_u^+$), F 0_u^+ ($^3\Pi_u$), B 1_g ($^3\Pi_g$), and A 0_g^+ ($^3\Pi_g$) molecular states.[309] Of these, both the D 1_u ($^3\Sigma_u^+$) and F 0_u^+ ($^3\Pi_u$) are optically coupled to the ground state. These states are expected to possess very different potential curves since they derive from different Hund's case (a) parents. The F 0_u^+ ($^3\Pi_u$) state is the one remaining component of the Hund's case (a) $^3\Pi_u$ term which provided the K 2_u ($^3\Pi_u$), I 1_u ($^3\Pi_u$), and H 0_u^- ($^3\Pi_u$) states correlating to Hg($^1S_0$) + Hg($^3P_2$). As such, its potential curve is expected to parallel those of these states. Only a weak, long-range minimum is expected, as observed for the I 1_u ($^3\Pi_u$) component correlating to $^1S_0$ + $^3P_2$ atoms. Transitions to this component are expected to occur near the $^3P_1 \leftarrow {}^1S_0$ atomic transition at 2537 Å.[3] A complex of discrete bands with absorption maximum at 2540.34 Å therefore corresponds to the F 0_u^+ ($^3\Pi_u$) ← X 0_g^+ $^1\Sigma_g^+$ transition of Hg_2. This narrow, intense band system has been observed by numerous investigators.[323–325,328,336,343,350–352] No detailed assignment is available, despite Mrozowski's high-resolution (0.15 cm^{-1}) attempt.[352]

The D 1_u ($^3\Sigma_u^+$) state correlating to the Hg($^1S_0$) + Hg($^3P_1$) separated atoms is calculated to be much more strongly bound than any of the components of the $^3\Pi_u$ term.[222,309,384] The remaining component of the $^3\Sigma_u^+$ term is C 0_u^- ($^3\Sigma_u^+$), which along with the A 0_g^- ($^3\Pi_g$) state correlates to the Hg($^1S_0$) + Hg($^3P_0$) separated atom limit. Absorption to these states from the X 0_g^+ $^1\Sigma_g^+$ ground state is forbidden under Hund's case (c) selection rules. The absorption and emission features observed by numerous investigators between 260 and 360 nm are therefore assigned to the D 1_u ($^3\Sigma_u^+$) ↔ X 0_g^+ $^1\Sigma_g^+$ transition.[340,341,343,344,348,350,352–365,372,373] In absorption this transition is most intense near 260 nm, dropping in intensity as one moves to the red.[328,344] Vibrational structure is observed from 300.9 to 265 nm, with a convergence limit slightly shorter than 253.7 nm.[328,344] In emission vibrational structure may be discerned from approximately 280 to 334 nm.[215,328] Vibrational frequencies of approximately 49 cm^{-1} for the ground X 0_g^+ $^1\Sigma_g^+$ state and 230 cm^{-1} for the excited D 1_u ($^3\Sigma_u^+$) state have been suggested.[215,344] Although interpretation is difficult owing to emissions to the dissociative continuum of the ground state, Kuhn and Freudenberg estimate a binding energy of the D 1_u ($^3\Sigma_u^+$) state of about 0.84 eV.[325]

Although all states lying below 50 000 cm^{-1} which are optically coupled to the ground state by case (c) dipole selection rules have been accounted for, a major emission system is as yet unexplained in this review. Following excitation of the 2537-Å $^3P_1 \leftarrow {}^1S_0$ atomic resonance line a long-lived broad continuum emission centered at 485 nm is observed.[341,345,349,350,352,357,358,361–363] It is also observed as a long-lived emission in a mercury discharge[215,343,355,360,364] and in mercury vapors excited at 256,[373] 257.2,[328] and 266 nm.[365] From these observations it is clear that the upper state of the emission possesses no more than 40 000 cm^{-1} of energy, since multiple excitations are not expected to contribute under the various experimental conditions in these investigations. The nature of the 485-nm transition has been the subject of considerable controversy and extreme activity, especially since Houtermans' 1960 suggestion of using Hg_2 as an excimer laser medium.[354]

Following Mrozowski's original suggestion,[347] a number of workers have considered the long-lived 485 nm emission to arise from the Hg_2 C 0_u^- ($^3\Sigma_u^+$) → X 0_g^+ $^1\Sigma_g^+$ transition.[221,347,352,357,358,361–364] Although this transition is forbidden under case (c) selection rules, the long lifetimes observed for it and the observed dependence on total pressure led some investigators to postulate its occurrence as a collision-induced emission process.[352,358] As a result of some beautiful, careful work by Drullinger, Hessel, and Smith[328,372,373] and Callear and coworkers[366–371] the 485-nm emission is now known to arise from electronically excited mercury *trimer* emitting to dissociated levels of the ground state. By studying the pressure and temperature dependence of the 335- and 485-nm emission intensities Drullinger, Hessel, and Smith established that the 485-nm radiator is a triatomic complex lying 6500 cm^{-1} below the diatomic D 1_u ($^3\Sigma_u^+$) state which radiates at 335 nm.[328]

A more detailed kinetic analysis by Stock et al. leads to a model in which the lowest-lying excited states of Hg_2 are the energy reservoir for the system.[372] These are the A $0_g^\pm$ ($^3\Pi_g$) metastable states, correlating to $^3P_0$ + $^1S_0$ and $^3P_1$ + $^1S_0$ separated atoms.[309] The temperature dependence of the kinetic data places A $0_g^\pm$ ($^3\Pi_g$) 2800 cm^{-1} below the optically active D 1_u ($^3\Sigma_u^+$) mo-

lecular state.[372] It also establishes the dissociation energy $Hg_3^* \rightarrow Hg_2(A\ 0_g^{\pm}\ ^3\Pi_g) + Hg(^1S_0)$ as 3800 cm^{-1},[372] in close agreement with the previous result that Hg_3^* lies 6500 cm^{-1} below $Hg_2(D\ 1_u\ ^3\Sigma_u^+) + Hg(^1S_0)$.[328] The energetics determined experimentally for these various Hg_2 molecular states are in reasonable agreement with the results of ab initio calculations.[222,309,384]

More recently Callear and Lai[366-368] have investigated the transient absorption spectra of mercury vapors following flash photolysis. Several diffuse absorption bands were observed which followed the same concentration dependence as the intensity of the 485-nm emission. They were accordingly assigned to absorptions of the electronically excited Hg_3^* complex. In addition, numerous banded absorption spectra were obtained with lower state vibrational frequencies of 144 ± 1 cm^{-1}. Many had been previously observed in emission by Takeyama,[381] although analysis of the spectra was impaired by the uncertain experimental conditions inherent to emission spectroscopy. Most of the discrete transient absorption features observed by Callear and Lai[366-368] may be assigned as absorptions from the metastable $A\ 0_g^{\pm}\ (^3\Pi_g)$ states of Hg_2, although some weak absorptions which become relatively more intense at higher temperatures have been assigned as absorptions from the $B\ 1_g\ (^3\Pi_g)$ state. On the basis of the temperature dependence of the relative intensities, the zero-point level of the $B\ 1_g\ (^3\Pi_g)$ state is calculated to lie 1700 ± 150 cm^{-1} above the $A\ 0_g^{\pm}\ (^3\Pi_g)$ vibrationless level.[368]

The upper states of the transitions observed in transient absorption by Callear and Lai[366-368] are all at least 20 000 cm^{-1} above $A\ 0_g^{\pm}\ (^3\Pi_g)$, and all possess vibrational frequencies of 121 ± 4 cm^{-1}. These high-energy states are Rydberg states, correlating to one ground-state $6s^2\ ^1S_0$ atom and one excited $6s^1ns^1$ or $6s^1np^1$ atom ($n \geq 7$) at the separated atom limit. Accordingly, it is not surprising that the vibrational frequency is nearly the same for all of these highly excited states; this is presumably the vibrational frequency of the Hg_2^+ ground state as well. Owing to the difficulties in assigning the dissociation limits and symmetry species of these Rydberg states, most are omitted from Table 13. The interested reader will find the relevant details in ref 368.

Niefer et al.[382,383] have recently investigated the *gerade* electronic states of Hg_2 (which are *not* optically coupled to either the ground $X\ 0_g^+\ (^1\Sigma_g^+)$ or the $A\ 0_g^{\pm}\ (^3\Pi_g)$ states) by a clever study employing two tunable lasers. The first excites the mercury vapor system to provide a population of Hg_2 molecules in the $A\ 0_g^{\pm}\ (^3\Pi_g)$ states, while the second excites these metastable states to the $P\ 1_u\ (^3\Sigma_u^-)$ Rydberg state, presumed to correlate with the $6s^2\ ^1S_0 + 6s7s\ ^3S_1$ separated atom limit. Fluorescence from this level is then dispersed, revealing much about the lower lying *gerade* states to which it is coupled. These elegant experiments have provided the vibrational parameters ω_e and $\omega_e x_e$ and the electronic origins of the $A\ 0_g^{\pm}\ (^3\Pi_g)$, $E\ 2_g\ (^3\Pi_g)$, and $G\ 1_g\ (^3\Sigma_g; {}^1\Pi_g)$ states and have unambiguously identified the P state as one of 1_u symmetry.[383] Some unexplained phenomena are observed, however, suggesting that the $P\ 1_u\ (^3\Sigma_u^-)$ state is weakly coupled to the $B\ 1_g\ (^3\Pi_g)$ state but that another highly excited state close to $P\ 1_u\ (^3\Sigma_u^-)$ in energy is strongly coupled to $B\ 1_g\ (^3\Pi_g)$. The $Q\ 0_u^+\ (^3\Sigma_u^-)$ state, which is another component of the $^3\Sigma_u^-$ state arising from $6s^2\ ^1S_0 + 6s7s\ ^3S_1$ separated atoms is suggested to play this role. There is also evidence that $Q\ 0_u^+\ (^3\Sigma_u^-)$ is in turn weakly coupled to the $E\ 2_g\ (^3\Pi_g)$ and $A\ 0_g^{\pm}\ (^3\Pi_g)$ states.[383] Although the $Q\ 0_u^+\ (^3\Sigma_u^-) \rightarrow E\ 2_g\ (^3\Pi_g)$ transition is forbidden, it remains a puzzle why both the $Q\ 0_u^+\ (^3\Sigma_u^-) \leftrightarrow A\ 0_g^+\ (^3\Pi_g)$ and the $P\ 1_u\ (^3\Sigma_u^-) \leftrightarrow B\ 1_g\ (^3\Pi_g)$ transitions are weak or absent in this system.

Finally, Callear and Kendall have observed a new continuous emission system at 3950 Å in mercury vapors excited to create a population of metastable $A\ 0_g^{\pm}\ (^3\Pi_g)$ Hg_2 molecules.[369,370] This system requires collisions with an inert gas and is best observed with nearly an atmosphere of nitrogen added to the system. Its intensity follows the dependence on mercury density expected for a diatomic molecule; it has been assigned as the collisionally induced emission $A\ 0_g^{\pm}\ (^3\Pi_g) \rightarrow X\ 0_g^+\ (^1\Sigma_g^+)$.[369]

Matrix-isolation studies of dimercury have been generally inconclusive.[305,306,385] Continuous absorption bands near 2260, 2474, and 2499 Å are observed in argon which correlate well with the gas-phase absorptions at 2345 ($C\ 1_u\ (^3\Pi_u) \leftarrow X\ 0_g^+\ ^1\Sigma_g^+$), 2540 ($B\ 0_u^+\ (^3\Pi_u) \leftarrow X\ 0_g^+\ ^1\Sigma_g^+$), and 2600 Å ($A\ 1_u\ (^3\Sigma_u) \leftarrow X\ 0_g^+\ ^1\Sigma_g^+$).[385] This assignment, particularly of the 2260-Å band, has not always been accepted however.[306] A matrix-isolation fluorescence study has also been reported.[386]

Arnot has investigated the formation of Hg_2^+ ions by recombination of electronically excited Hg* atoms with ground-state atoms and concomitant electron ejection.[387] The lowest electronic state of atomic mercury capable of associative ionization is $6s8p\ ^1P_1$, with 9.722 eV of electronic energy.[387] This places an upper limit on the adiabatic ionization potential of Hg_2. More recently Linn et al. have measured the photoionization efficiency of Hg_2 in the vacuum ultraviolet.[388] A steplike onset of ionization at 1362 ± 1.5 Å was identified, from which the adiabatic ionization potential of Hg_2 is set as 9.103 ± 0.010 eV. Given the atomic ionization potential of 10.43 eV[3] and the binding energy of the neutral dimer $D_0°(Hg_2)$ = 0.074 ± 0.020 eV,[339] this measurement provides $D_0°(Hg_2^+)$ = 1.40 ± 0.03 eV. Linn et al. also observed many autoionizing states in their vacuum ultraviolet study.[388] The deviation of the energies of these states from the analogous transitions in atomic mercury reach a limiting value at high Rydberg levels of −0.285 eV. This has been analyzed in terms of the charge-induced dipole interaction of Hg^+ interacting with Hg at the equilibrium ground-state separation, r_e, yielding the value r_e = 3.35 Å,[388] which is close to the values obtained by measurement of transport coefficients.[331-334]

Finally, several band spectra have been observed in electric discharges through mercury vapors which may not be assigned to the low-lying electronic states of Hg_2. Several of these have been postulated to arise from the Hg_2^+ molecular ion, although little confirmation for this assignment is available.[342,346,351]

B. Heteronuclear Transition-Metal Diatomics

Although little is known about many of the homonuclear transition-metal dimers, our knowledge of the heteronuclear transition-metal dimers is even more severely limited. Of the 435 mixed transition-metal

dimers which might be formed, only 59 have been studied at all, and most of these investigations are fragmentary. In this subsection the current knowledge of the mixed transition-metal diatomic molecules is reviewed.

1. Group IIB (12) Mixed Dimers: ZnCd, ZnHg, and CdHg

The mixed group IIB (12) dimers, like their homonuclear counterparts, are bound only by van der Waals forces in the ground electronic state. Excited states may be strongly bound, however, leading to diffuse and continuous band spectra in both emission and absorption. The possibility of using these molecules as the active medium in an excimer laser has encouraged considerable recent activity investigating their spectroscopy, photophysics, and photochemistry.

ZnCd has, to our knowledge, only been observed in absorption as matrix-isolated molecules.[305,306] A broad band with hints of vibrational structure at the long-wavelength end, occurring at 261 nm (38 300 cm^{-1}) for a deposit of zinc and cadmium in solid argon has been assigned to ZnCd.[305,306] This band falls roughly midway between the Zn_2 band at 252 nm and the Cd_2 band at 273 nm. In the homonuclear dimers these are $A\ ^1\Sigma_u^+ \leftarrow X\ ^1\Sigma_g^+$ transitions with the excited state correlating to $^1S_0 + {}^1P_1$ separated atoms. For ZnCd a mixture of excitations on the zinc and cadmium atoms presumably occurs, leading to a band positioned between the two homonuclear transitions. In addition, a second $^1\Sigma^+ \leftarrow X\ ^1\Sigma^+$ transition should occur nearby, corresponding to the forbidden $^1\Sigma_g^+ \leftarrow X\ ^1\Sigma_g^+$ transition in the homonuclear dimers. This becomes allowed when inversion symmetry is removed, as in the heteronuclear dimers. This second band system, possibly of low intensity or overlapping Zn_2 or Cd_2 absorptions, has not yet been observed.

ZnHg has been investigated by matrix-isolation methods as well.[305,306] A vibronically structured absorption band with a possible 0–0 transition at 262.1 nm (38 153 cm^{-1}) and $\Delta G' = 85\ cm^{-1}$ was observed for ZnHg isolated in argon.[305,306] It has been suggested that the observed transition is $^1\Sigma^+ \leftarrow X\ ^1\Sigma^+$, with the upper state correlating to $Zn(^1P_1) + Hg(^1S_0)$.[306] A far-ultraviolet absorption study of gas-phase ZnHg has been reported,[389] and an emission continuum at 455 nm has also been investigated.[390] The 455-nm emission continuum is thought to arise from the $1\ (^3\Sigma^+) \rightarrow X\ 0^+\ ^1\Sigma^+$ transition, in analogy to the $1_u\ (^3\Sigma_u^+) \rightarrow X\ 0^+\ ^1\Sigma_g^+$ transition of Hg_2.[390] In this case the $1\ (^3\Sigma^+)$ state correlates with $Zn(^3P_1) + Hg(^1S_0)$ separated atoms.[390]

CdHg has been more thoroughly investigated than any of the mixed group IIB (12) transition-metal dimers. In studies of absorption spectra of CdHg isolated in argon matrices, a band system was observed with a possible 0–0 transition at 272.1 nm (36 751 cm^{-1}) and $\Delta G' = 81\ cm^{-1}$.[305,306] Winans has observed banded absorption in CdHg to the red of the cadmium 2288-Å resonance line ($^1P_1 \leftarrow {}^1S_0$), in the 240–249-nm region.[391] Winans' bands show a strongly bound excited state, presumably correlating with $Cd(^1P_1) + Hg(^1S_0)$ separated atoms. At the long-wavelength limit, a vibrational interval of 140 cm^{-1} is observed, but this is strongly anharmonic and rapidly decreases below 100 cm^{-1} as vibrational excitation is added to the upper state.[391]

TABLE 14. Contributions to the Half-Filled σ^* Orbital in Group IB–IIB 11–12 Mixed Dimers[d]

molecule	Cu(4s),[b] %	Zn(4s),[c] %	remainder[d]
CuZn	68.2	?	?
CuCd	68.5	(18.7)	(12.8)
CuHg	80.9	(7.1)	(12.0)
AgZn	73.2	?	?
AgCd	73.4	(16.4)	(10.2)
AgHg	86.3	(6.6)	(7.1)
AuZn	44.6	?	?
AuCd	46.0	(37.8)	(16.2)
AuHg	68.2	(16.1)	(15.7)

[a] References 398–400; see text for details. [b] Contribution from Cu(4s), Ag(5s), or Au(6s) atomic orbital to σ^*. [c] Contribution from Zn(4s), Cd(5s), or Hg(6s) atomic orbital to σ^*. In the case of Zn this is not measurable because $I = 0$ for the abundant isotopes of zinc. [d] Remaining contribution is thought to be primarily Zn(4p), Cd(5p), and Hg(6p).

Finally, a fluorescence continuum peaking near 470 nm has been observed and investigated in several reports.[392–397] The net conclusion is that although CdHg offers an excellent medium for energy storage, prospects for an efficient CdHg excimer laser are poor, owing to strong excited state absorption at the lasing wavelength.[395,397]

2. Group IB–IIB (11–12) Mixed Dimers: CuZn, CuCd, CuHg, AgZn, AgCd, AgHg, AuZn, AuCd, and AuHg

Kasai and McLeod have investigated all of the group IB–IIB (11–12) mixed dimers by ESR spectroscopy in argon matrices.[398–400] These diatomic species lack one electron of having filled-shell configurations and are expected to possess the dominant electronic configuration of $\sigma^2\sigma^{*1}$, $^2\Sigma^+$. By monitoring the hyperfine coupling of the unpaired spin to both nuclei, Kasai and McLeod have been able to deduce the spin densities in the valence s orbitals of both atoms. This is a direct monitor of the makeup of the half-filled σ^* antibonding orbital. The results of their investigations are given in Table 14. As expected, the contributions from Zn(4s) and Cd(5s) are considerably larger than those from the less easily ionized Hg(6s) orbital. Also as expected, the contribution of the Au(6s) orbital is much less than that of the Cu(4s) or Ag(5s) orbitals. The high electron affinity of gold dictates that its 6s orbital contributes strongly to the filled σ-bonding orbital. As a result, gold cannot contribute so much 6s character to the half-filled σ^* antibonding orbital.

3. Group IB (11) Mixed Dimers: CuAg, CuAu, and AgAu

The mixed dimers of the coinage metals have been investigated by their thermal emissions from high-temperature King furnaces.[19–21] No rotational analyses are presently available, but vibrational analyses have been reported for CuAg and CuAu.

Ruamps has observed two emissions systems in CuAg.[19] One of these has also been reported by Joshi and Majumdar.[20] Spectroscopic constants are listed in Table 15 and potential energy curves based on the data of Table 15 are given in Figure 15. The ground-state vibrational frequency of CuAg, 231.8 cm^{-1}, compares well with the arithmetic average of Cu_2 and Ag_2, which is 228.8 cm^{-1}.

TABLE 15. Electronic States of CuAg[a]

state	T_e, cm^{-1}	ω_e, cm^{-1}	$\omega_e x_e$, cm^{-1}	obsd transitns designatn	obsd transitns ν_{00}	ref
B	25851.6	178.5	0.50	B → X	25825.0	19, 20
A	20836	171.5	<0.50	A → X	20807	19
X	0	231.8	0.80			19, 20

[a] See text for details.

TABLE 16. Electronic States of $^{63}Cu^{197}Au$[a]

state	T_e, cm^{-1}	ω_e, cm^{-1}	$\omega_e x_e$, cm^{-1}	obsd transitns designatn	obsd transitns ν_{00}	ref
D	23699	182		D → X	23665	21
C	22176	231		C → X	22167	21
B	20652.3	257	2.2	B → X[b]	20655.4	21
A	20241	$\Delta G_{1/2}$ = 195.7		A → X[c]	20214	21
X	0	250	0.7			21

[a] See text for details. [b] Perturbations are present, probably induced by A state. [c] Perturbations are present, probably induced by B state.

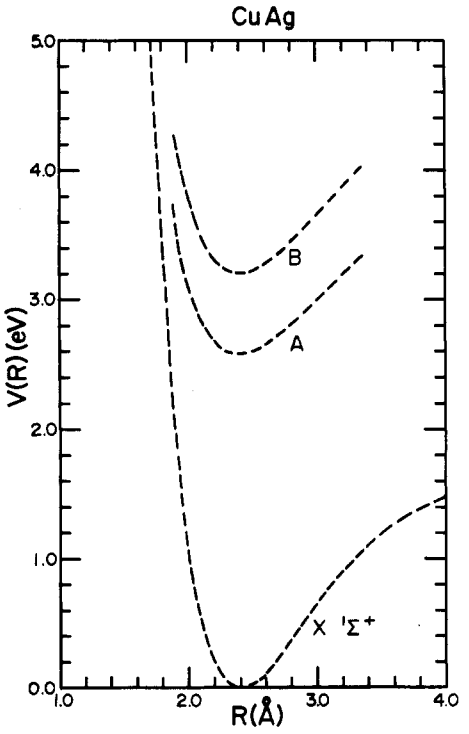

Figure 15. Potential energy curves for CuAg, based on the data of Table 15. Curves are shown as dashed lines to indicate that the equilibrium internuclear separation is unknown, and therefore a horizontal shift of unknown magnitude is required to correctly position these curves.

Ruamps has also reported four thermal emission systems of CuAu observed in a King furnace.[21] Spectroscopic constants are reported in Table 16, and potential energy curves based on experimental data are shown in Figure 16. The A and B states show vibrational perturbations, probably induced by each other. In addition to the transitions listed in Table 16, Ruamps also observes numerous other bands in the 3900–4800 Å region. Bands near 5200, 5570, and 5700 Å are also observed, which Ruamps suggests may be due to a polyatomic $AuCu_n$ molecule.[21]

4. Mixed Open d-Shell Transition-Metal Dimers Observed by Optical Spectroscopy

The first mixed open d-shell transition-metal dimer

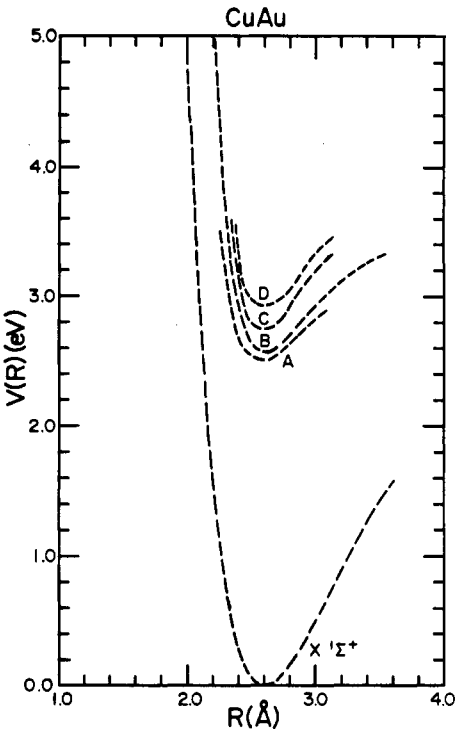

Figure 16. Potential energy curves for CuAu, based on the data of Table 16. Curves are shown as dashed lines to indicate that the equilibrium internuclear separation is unknown, and therefore a horizontal shift of unknown magnitude is required to correctly position these curves.

observed was CrMo, observed in 1976 by Efremov, Samoilova, and Gurvich in a transient absorption study following flash photolysis of $Cr(CO)_6$ and $Mo(CO)_6$ vapors.[38] Bands observed at 4860–4880 Å were positioned very close to the arithmetic mean of the Cr_2 (4590 Å) and Mo_2 (5180 Å) absorptions and were assigned to the congeneric CrMo molecule.[38] Klotzbücher and Ozin find strong absorptions at 487 nm and weaker, broader absorptions at 248 nm in argon-isolated CrMo.[80,94,245] Vibronic structure is observed in one study, with an average spacing of 147 cm^{-1}.[94] Rotationally resolved gas-phase spectra are not presently available for CrMo, but chemical intuition and Xα calculations[94] identify the 487-nm band system as the $^1\Sigma^+ \leftarrow X\ ^1\Sigma^+$ analogue of the $A\ ^1\Sigma_u^+ \leftarrow X\ ^1\Sigma_g^+$ systems of Cr_2 and Mo_2.

In other work on presumably multiple-bonded heteronuclear transition-metal dimers, Klotzbücher and Ozin report absorption spectra of NbMo isolated in solid argon.[401] Transitions are observed at 590 (16949), 568 (17605), 558 (17921), and 551 nm (18148 cm^{-1}), along with a shoulder attributed to an unstable matrix site at 575 nm (17391 cm^{-1}). Klotzbücher and Ozin also present an extended Hückel calculation for NbMo.[401]

Finally, Klotzbücher and Ozin have investigated the heteronuclear diatomics AgCr, AgMn, AgCu, and AgMo.[110,290] The matrix studies are complicated by numerous bands associated with the atomic and homonuclear diatomic absorption spectra; nevertheless, bands have been assigned to the mixed dimers. For AgCr isolated in argon these occur at 283 and 220 nm.[290] Bands are assigned to AgMn/Ar at 362, 263, 266, 240, 244, and 248 nm.[110] AgMo is assigned bands at 440 and 431 nm, while AgCu is assigned features at 382 and 271 nm.[110] Extended Hückel calculations are also presented

TABLE 17. Mössbauer Spectroscopic Constants for Iron-Containing Transition-Metal Dimers[a]

molecule	conditns	IS,[b] mm/s	QS,[c] mm/s	ref
FeCr	Ar 4.2 K	0.12 ± 0.05	±2.94 ± 0.05[d]	408
	Ar 15 K	0.15 ± 0.10	±3.10 ± 0.10[d]	408
	Kr 15 K	0.17 ± 0.06	±2.90 ± 0.06[d]	408
FeMn	Ar 4.2 K	0.24 ± 0.03	±1.93 ± 0.03[d]	126, 402
Fe_2	Ar 4.2 K	−0.12 ± 0.06	−4.08 ± 0.08	124–126, 404, 408
	Kr 15 K	0.06 ± 0.06	−3.78 ± 0.06	408
FeCo	Ar 4.2 K	0.55 ± 0.05	−3.60 ± 0.05	126, 405
FeNi	Ar 4.2 K	−0.54 ± 0.05	±1.95 ± 0.05[d]	126, 404
FeCu	Ar 4.2 K	0.46 ± 0.07	±1.63 ± 0.07[d]	126
		0.47 ± 0.10	±1.55 ± 0.10[d]	406

[a] See text for details. [b] Isomer shift. [c] Quadrupole splitting. [d] Sign is undetermined.

for these mixed dimers.[110,290]

5. Iron-Containing Heteronuclear Dimers: FeCr, FeMn, FeCo, FeNi, and FeCu

The iron-containing transition-metal dimers differ from the other transition-metal molecules by the fact that they may be readily studied by Mössbauer spectroscopy. Investigations of the Mössbauer spectra of matrix-isolated FeCr, FeMn, Fe_2, FeCo, FeNi, and FeCu have been extensively pursued by Montano and coworkers.[124–126,402–408] In this technique two important spectroscopic parameters are measured: the isomer shift (IS) and the quadrupole splitting (QS). The former is an indicator of the electron density at the nucleus and is approximately −0.75 mm/s for $Fe^0(3d^64s^2)$, +0.25 mm/s for $Fe^+(3d^64s^1)$, and +1.8 mm/s for $Fe^+(3d^7)$, with respect to metallic iron as the zero of velocity.[126] The quadrupole splitting (QS) arises by coupling of the nuclear electric quadrupole moment to the gradient of the electric field at the nucleus and thereby provides information about the electronic structure near the nucleus.[126]

Measured values of isomer shifts (IS) and quadrupole splitting (QS) for FeCr, FeMn, Fe_2, FeCo, FeNi, and FeCu are given in Table 17. Montano has interpreted the isomer shift (IS) to be correlated with the strength of chemical bonding: the more positive the value of IS, the stronger the chemical bond which is formed.[126] In addition, Montano has used the observed quadrupole splittings to suggest ground electronic state assignments for the iron-containing transition-metal dimers.[126]

The iron–nickel diatomic molecule has also been investigated by resonance Raman spectroscopy in solid argon and krypton matrices.[121,122] Vibrational constants of $\omega_e'' = 320.0$ cm^{-1} and $\omega_e''x_e'' = 1.32$ cm^{-1} were obtained. This indicates strong chemical bonding in FeNi, contrary to Montano's conclusion the FeNi is a very weakly bound molecule.[126]

6. Mixed Open d-Shell Transition-Metal Dimers Observed by ESR Spectroscopy

In this subsection results of ESR investigations of matrix-isolated heteronuclear dimers are presented, grouped according to the number of valence electrons. For this purpose both the nd and $(n + 1)$s electrons are considered to belong to the valence space.

a. 9-Electron Systems: TiV. Van Zee and Weltner have observed the ESR spectrum of TiV isolated in an argon matrix at 4 K.[409] The molecule was assigned as a $^4\Sigma$ state, although the $^4\Sigma_{3/2}$ component was not observed. This indicates a zero-field splitting, D, between the $^4\Sigma_{1/2}$ component and the $^4\Sigma_{3/2}$ component of more than 1 cm^{-1}.[409] Such a splitting is not surprising in view of the $^3\Sigma_{0+g}^- - {}^3\Sigma_{1g}^-$ splitting in V_2 of 69.5 cm^{-1}.[43] Hyperfine coupling of the unpaired spins to ^{51}V ($I = {}^7/_2$) and ^{47}Ti ($I = {}^5/_2$) nuclei were observed and analyzed to find the percentage of unpaired spin s character on each atom.[409] The results, about 7% s character on the Ti atom, about 8% s character on the V atom indicate that the unpaired spins are mainly located in dσ, dπ, and dδ orbitals.[409]

Walch and Bauschlicher have investigated TiV at the CASSCF level,[2] and their results compare favorably with experiment. TiV may be considered by removing one electron from the V_2 molecule, which has the ground-state configuration $(4s\sigma_g)^2(3d\sigma_g)^2(3d\pi_u)^4(3d\delta_g)^2$, $^3\Sigma_g^-$. The electron may be removed from the 3dσ, 3dπ, or 3dδ orbitals, leading to $^4\Sigma^-$, $^4\Pi$, or $^2\Delta$ states, respectively. Considerations of orbital overlap would favor an energy ordering of $^2\Delta < {}^4\Sigma^- < {}^4\Pi$.[2] The $^2\Delta$ state, however, dissociates to an admixture of Ti (^{5}F, 20%) and Ti (^{5}P, 80%) atoms. This destabilizes $^2\Delta$, leading to a ground state of $(4s\sigma)^2(3d\sigma)^1(3d\pi)^4(3d\delta)^2$, $^4\Sigma^-$.[2] Calculated spectroscopic constants are $r_e = 1.86$ Å, $\omega_e = 495$ cm^{-1}, and $D_e = 0.80$ eV, relative to Ti ($4s^13d^3$) + V ($4s^13d^4$).[2] The $^2\Delta$ and $^4\Pi$ states are calculated to have similar values of r_e (1.89 and 1.95 Å, respectively) and ω_e (472 and 410 cm^{-1}, respectively) but lie 0.37 and 0.65 eV above $^4\Sigma^-$, respectively.[2]

b. 13-Electron Systems: ScNi, TiCo, and YPd. Van Zee and Weltner have also investigated ScNi and TiCo in argon matrices at 4 K by ESR spectroscopy.[410] Both 13-electron systems exhibit $^2\Sigma$ ground states. Hyperfine splittings due to ^{45}Sc ($I = {}^7/_2$) have been observed in ScNi; hyperfine splittings due to both ^{47}Ti ($I = {}^5/_2$) and ^{59}Co ($I = {}^7/_2$) have been observed in TiCo.[410]

An analysis of the hyperfine constants in these molecules places most of the spin density on the more electropositive elements Sc and Ti.[410] In ScNi, 85% (0.35 $s\sigma_{Sc}$ + 0.50 $d\sigma_{Sc}$) of the unpaired spin is on the scandium atom. In TiCo, 66% (0.33 $s\sigma_{Ti}$ + 0.33 $d\sigma_{Ti}$) is on titanium and 25% exhibits s character localized on Co. In both cases the unpaired electron is in a hybridized sσ–dσ orbital which is more localized on the lighter element.[410] Van Zee and Weltner point out that charge transfer is likely to be important in these species, with the more electropositive element donating to the heavier one.[410] Presumably this is occurring in the filled molecular orbitals, forcing the singly occupied molecular orbital onto the more electropositive element by orthogonality.[410]

Shim and Gingerich have explored these possibilities by an all-electron Hartree–Fock investigation of YPd, which is another 13-valence-electron system, congeneric with ScNi.[411] In this study chemical bonding based on the ground-state atomic configurations $4d^15s^2$, ^{2}D (Y) and $4d^{10}$, ^{1}S (Pd) was considered. From this separated atom limit three electronic states arise: $^2\Delta$, $^2\Pi$, and $^2\Sigma^+$. These correspond to the placement of the 4d electron of yttrium in a 4dδ, 4dπ, or 4dσ orbital, respectively. Because the 4d orbitals of palladium lie much lower in energy than those of yttrium, the 4d orbitals on the two

atoms do not mix to a large extent. Thus the $4d^1$ electron of yttrium is expected to remain primarily localized on yttrium.

Chemical bonding in YPd occurs by donation from the filled 5s shell of yttrium into the empty 5s shell of palladium, compensated by a back-donation of charge from the filled $4d\sigma$ and $4d\pi$ orbitals of Pd into the corresponding $4d\sigma$ and $4d\pi$ orbitals of Y.[411] According to the calculations of Shim and Gingerich, this produces an overall slight negative charge on the *yttrium* atom and predicted dipole moments of 0.37, 0.61, and 0.51 D for the $^2\Sigma^+$, $^2\Pi$, and $^2\Delta$ states, respectively. Of these, the $^2\Delta$ state is calculated as the ground state with r_e = 2.69 Å, ω_e = 144 cm^{-1}, and D_e = 1.87 eV.[411] The low-lying $^2\Pi$ and $^2\Sigma^+$ are calculated to possess r_e = 2.77 Å, ω_e = 127 cm^{-1}, and D_e = 1.67 eV and r_e = 2.78 Å, ω_e = 128 cm^{-1}, and D_e = 1.69 eV, respectively. These values are modified slightly when spin–orbit coupling is considered.[412]

The calculation on YPd provides a framework from which to view the experimental data on ScNi and TiCo. In the case of ScNi, an entirely analogous chemical bond may be produced by the interaction of ground-state scandium atoms ($3d^14s^2$) and excited-state nickel atoms ($3d^{10}$). This excitation in nickel requires 1.71 eV of promotion energy (see Table 1). The experimental results show that in the case of ScNi, the 3d electron of scandium is preferentially placed in a $3d\sigma$ orbital, which hybridizes with the Sc $4s\sigma$ orbital to some degree. The magnitude and direction of the dipole moment would provide very interesting data for comparison with theoretical calculations in this system.

c. 15-Electron Systems: VNi. The ESR spectrum of VNi, isolated in an argon matrix at 4K, has recently been obtained by Van Zee and Weltner.[409] The lowest Kramers doublet transition ($m_s = {}^1/_2 \leftrightarrow m_s = -{}^1/_2$) was observed, with an effective g value of approximately 4, indicating a $^4\Sigma$ ground state. Hyperfine coupling of the ^{51}V ($I = {}^7/_2$) nucleus to the electron spin was observed. Analysis of the hyperfine constants demonstrates that the unpaired spin has approximately 10% 4s character on the vanadium atom. The dipolar contribution to the hyperfine coupling is small and negative, implying that the vanadium 3d contribution to the unpaired spins is predominantly due to $3d\delta$ electrons. The $^4\Sigma_{3/2}$ component is not observed, placing the zero-field splitting parameter, D, greater than 1 cm^{-1}. On the basis of these results, Van Zee and Weltner suggest a ground electronic state based on the $(4s\sigma)^2(3d\sigma)^2(3d\pi)^4(3d\delta)^4(4s\sigma^*)^1(3d\delta^*)^2$, $^4\Sigma^-$ electronic configuration, with the $4s\sigma^*$ orbital hybridized with orbitals of $3d\sigma$ type.[409]

d. 17-Electron Systems: CrCu, CrAg, and CrAu. Atomic chromium has the ground electronic configuration $3d^54s^1$, $^7S_3$ while the coinage metals have ground configurations of $nd^{10}(n+1)s^1$. One may easily imagine bringing two such atoms together, spin pairing the s electrons to form a single σ bond, and leaving the $3d^5$ core of atomic chromium high-spin coupled to give a $^6\Sigma^+$ molecular ground state. This is precisely what Baumann, Van Zee, and Weltner observe for CrAg and CrAu.[413]

Chromium–silver and chromium–gold were demonstrated to exist as ground-state sextets by the measurement of effective g values of 5.846 and 5.999, respectively, for the argon-isolated molecules.[413] Hyperfine structure was observed for ^{107}Ag and ^{109}Ag nuclei (both $I = {}^1/_2$) in CrAg, but the splitting due to ^{53}Cr ($I = {}^3/_2$) nuclei was too small to be resolved.[413] The very small hyperfine splitting observed ($|A(^{107,109}Ag)| = 17 \pm 3$ MHz), compared to that of the free atom (−1831 MHz for ^{107}Ag)[414] indicates very little Ag(5s) character associated with unpaired spin. The unobservably small ^{53}Cr hyperfine splitting ($|A(^{53}Cr)| \leq 1.4$ MHz) compares with a free atom value, A_{iso}, of −748.2 MHz,[414] again indicating essentially zero Cr(4s) character associated with the unpaired spin. This confirms the expected model of a CrAg molecule with all five unpaired spins localized on the chromium 3d orbitals. The zero-field splitting constant, D, was determined to be 0.44 ± 0.01 cm^{-1}.[413]

Similar spectra were obtained for CrAu, although no attempt was made to observe hyperfine structure due to ^{53}Cr.[413] Hyperfine constants for ^{197}Au were determined to be $A_{iso} = 39 \pm 30$ MHz and $A_{dip} = 0 \pm 30$ MHz.[413] This compares with a free atom value of A_{iso} of 2876 MHz,[414] indicating an Au(6s) contribution to the unpaired spin which is only about 7%. Only the lowest energy $m_s = -{}^1/_2 \leftrightarrow m_s = +{}^1/_2$ Kramers doublet was observed, determining the zero-field splitting constant, D, to be greater than 2 cm^{-1}.[413]

The ESR spectra of CrCu require a different interpretation. Although initially interpreted as a $^6\Sigma$ molecule,[415] the high value obtained for the amount of Cu(4s) character associated with the unpaired spins (65%) was difficult to accept.[416] A revised interpretation based on an $^8\Sigma$ ground state was then suggested, based on chemical bonding between a $3d^54s$ Cr atom and a $3d^94s^2$ Cu atom.[416] With a high-spin $3d^5$ (^6S) core on chromium, an $s = {}^1/_2$ hole in the copper 3d shell, and an unpaired outer 4s electron, an $^8\Sigma$ state is conceivable. To resolve the question, further studies using isotopically enriched ^{53}Cr ($I = {}^3/_2$, 96.98% pure) were undertaken.[413] Hyperfine parameters for $^{53}Cr^{63}Cu$ isolated in solid krypton unequivocally rule out $^8\Sigma$ and $^6\Sigma$ as possible ground states of CrCu. A $^2\Sigma$ ground state is eliminated by the observation of $m_s = {}^3/_2 \leftrightarrow m_s = {}^1/_2$ transitions. A fit of the observed transitions to the spin Hamiltonian of a $^4\Sigma$ gound state, however, yields excellent agreement with experiment.[413] Baumann et al. suggest some possibilities for the electronic configuration of CrCu, but further work is required before the chemical bonding is understood in this molecule.

e. 18-Electron Systems: CrZn and MnAg. The ESR spectrum of the intermetallic MnAg molecule isolated in solid neon, argon, and krypton has been observed by Baumann et al.[129] The expected interactions between ground-state Mn($3d^54s^2$, $^6S_{5/2}$) and Ag($4d^{10}5s^1$, $^2S_{1/2}$) atoms involve placing the three s electrons in an $(s\sigma)^2(s\sigma^*)^1$ configuration and leaving the five d electrons spin-paired on manganese. Thus one might expect the molecule to be described by the interaction of a $^6\Sigma^+$ system of d electrons with a $^2\Sigma^+$ system derived from the s-electrons. This results in $^7\Sigma^+$ and $^5\Sigma^+$ states, of which $^7\Sigma^+$ is expected to be the ground state. In molecular orbital terms this derives from an $(s\sigma)^2(d\sigma)^2(d\pi)^4(d\delta)^4(d\delta^*)^2(d\pi^*)^2(d\sigma^*)^1(s\sigma^*)^1$ electronic configuration. In essence, the highly contracted 4d shell of silver is expected to interact only mildly with the other orbitals (except for $s\sigma$–$d\sigma$ hybridization, which may be considerable). In this regard MnAg may be

TABLE 18. Measured Dissociation Energies of Heteronuclear Transition-Metal Dimers (eV)

molecule	no. of valence electrons	second law	third law	selected value	atomic cell model	Pauling model	empirical valence bond model	ref
AgAu	22 ($d^{10}s^1$–$d^{10}s^1$)		2.06 ± 0.10	2.06 ± 0.10	1.99[a]	2.12[a]		158
AgCu	22 ($d^{10}s^1$–$d^{10}s^1$)		1.76 ± 0.10	1.76 ± 0.10	1.44	1.83[d]		158
AgMn	18 ($d^{10}s^1$–d^5s^2)			0.99 ± 0.22	0.70[b]	1.10[d]		28
AuCo	20 ($d^{10}s^1$–d^7s^2)	2.19 ± 0.13	2.29 ± 0.26	2.22 ± 0.17	1.49[b]	2.73[a]		418
AuCr	17 ($d^{10}s^1$–d^5s^1)	2.28 ± 0.30	2.27 ± 0.22	2.28 ± 0.30	1.65[b]	2.56[a]		77, 418
AuCu	22 ($d^{10}s^1$–$d^{10}s^1$)	2.31 ± 0.08	2.36 ± 0.10	2.34 ± 0.10	1.81[a]	2.29[a]		158, 433
AuFe	19 ($d^{10}s^1$–d^6s^2)	1.90 ± 0.17	2.29 ± 0.30	1.90 ± 0.20	1.20[b]	2.03[a]		418
AuLa	14 ($d^{10}s^1$–d^1s^2)	3.39 ± 0.44	3.44 ± 0.03	3.44 ± 0.10	4.36[b]	3.61[a]		419–421
AuMn	18 ($d^{10}s^1$–d^5s^2)		2.01 ± 0.22	2.01 ± 0.22	1.33[b]	2.18[a]		317, 418
AuNi	21 ($d^{10}s^1$–d^9s^1)	2.52 ± 0.30	2.60 ± 0.22	2.55 ± 0.30	1.81[b]	2.59[a]		418
AuPd	21 ($d^{10}s^1$–d^{10})		1.44 ± 0.22	1.44 ± 0.22	1.44[b]	1.73[a]		77
AuRh	20 ($d^{10}s^1$–d^8s^1)		2.37 ± 0.30	2.37 ± 0.30	2.24[b]	2.55[a]		422
AuSc	14 ($d^{10}s^1$–d^1s^2)			2.87 ± 0.18	4.20[a]	2.96[a]		423
AuV	16 ($d^{10}s^1$–d^3s^2)	2.51 ± 0.09	2.52 ± 0.01	2.51 ± 0.09	2.67[a]	3.02[a]		424
AuY	14 ($d^{10}s^1$–d^1s^2)	3.19 ± 0.11	3.18 ± 0.02	3.19 ± 0.11	4.07[b]	3.16[a]		425
CoCu	20 (d^7s^2–$d^{10}s^1$)	1.63 ± 0.17	1.65 ± 0.22	1.63 ± 0.17	1.72[b]	1.73[d]		426
CrCu	17 (d^5s^1–$d^{10}s^1$)	1.61 ± 0.13	1.56 ± 0.26	1.60 ± 0.15	1.50[b]	1.73[d]		426
CuNi	21 ($d^{10}s^1$–d^9s^1)	2.06 ± 0.22	2.14 ± 0.22	2.08 ± 0.25	2.12[b]	2.05[d]		426
IrLa	12 (d^7s^2–d^1s^2)	6.03 ± 0.18	5.91 ± 0.05	5.94 ± 0.12	5.57[a]	(4.18)[d]	5.86[a]	421
IrNb	14 (d^7s^2–d^4s^1)			4.78 ± 0.26	5.33[c]	(4.01)[d]		427
IrY	12 (d^7s^2–d^1s^2)	4.75 ± 0.20	4.66 ± 0.03	4.75 ± 0.20	5.41[a]	(3.53)[d]	4.67[a]	425
LaPt	13 (d^1s^2–d^9s^1)	5.07 ± 0.31	5.16 ± 0.07	5.14 ± 0.22	5.94[a]	(3.89)[d]	4.38[a]	428
LaRh	12 (d^1s^2–d^8s^1)	5.44 ± 0.15	5.61 ± 0.03	5.44 ± 0.17	4.87[b]	(3.91)[d]	5.60[a]	429
LaY	6 (d^1s^2–d^1s^2)		2.05 ± 0.22	2.05 ± 0.22	1.93[c]	2.07[d]		53
MoNb	11 (d^5s^1–d^4s^1)		4.64 ± 0.26	4.64 ± 0.26	3.73[c]	(3.65)[d]		235
PdY	13 (d^{10}–d^1s^2)	2.58 ± 0.15	2.39 ± 0.03	2.46 ± 0.16	3.51[c]	(2.34)[d]	2.28[e]	412
PtTi	14 (d^9s^1–d^2s^2)	4.07 ± 0.21	4.09 ± 0.06	4.08 ± 0.11	5.12[a]	(2.58)[d]	3.73[a]	430
PtY	13 (d^9s^1–d^1s^2)	4.92 ± 0.13	4.83 ± 0.04	4.87 ± 0.12	5.75[b]	(3.24)[d]	3.27[a]	314
RhSc	12 (d^8s^1–d^1s^2)	4.64 ± 0.06	4.48 ± 0.03	4.56 ± 0.11	4.84[a]	(3.08)[d]	4.01[a]	431
RhTi	13 (d^8s^1–d^2s^2)	4.04 ± 0.22	3.93 ± 0.04	4.01 ± 0.15	4.11[b]	(2.59)[d]	4.43[a]	263, 264
RhV	14 (d^8s^1–d^3s^2)			3.73 ± 0.30	3.75[b]	(3.05)[d]	4.77[a]	432
RhY	12 (d^8s^1–d^1s^2)	4.54 ± 0.07	4.62 ± 0.03	4.58 ± 0.11	4.68[b]	(3.26)[d]	4.39[a]	431
RuV	13 (d^7s^1–d^3s^2)			4.25 ± 0.30	3.96[b]	(3.29)[d]	5.90[a]	432

[a] Reference 27. [b] Reference 434. [c] Reference 260. [d] Calculated by using $D_0°$ of homonuclear dimers given in ref 434 and electronegativities of ref 435. [e] Reference 431.

compared to MnH, which is known to possess a ground state of $^7\Sigma$ symmetry.[417]

Baumann et al. have used the spin Hamiltonian appropriate to a $^7\Sigma$ species to fit the observed data for MnAg.[129] Calculated transitions match the observed values very well. Hyperfine splittings due to both ^{55}Mn and ^{107,109}Ag nuclei are observed as well (although the isotopes of silver are not resolved). The magnitudes of the measured hyperfine constants indicate an s spin density of 0.28 on manganese and 0.48 on silver. Presumably most of this spin density is from the sσ* orbital, although some may derive from the dσ* orbital through sσ–dσ hydridization. The remaining components of the sσ* orbital are from pσ and dσ orbitals on each metal center. The comparable s spin densities on manganese and silver in the sσ* orbital are indicative of covalent bonding in this intermetallic molecule.

Baumann et al. have also observed the 18-electron CrZn molecule by ESR spectroscopy.[129] Again, all observed lines were explained by a $^7\Sigma$ ground state, although studies with isotopically enriched samples were not performed, and hyperfine structure was therefore not resolved. On the basis of the excellent fit to the observed fine structure, however, $^7\Sigma$ is now established as the ground state of CrZn, with a zero-field splitting parameter, D, of 0.084 cm^{-1}.[129] Here, as in MnAg, the molecule may be considered as a $^6\Sigma^+$ group of electrons (derived from the $3d^5$, ^6S configuration of the chromium 3d shell) interacting with an $(s\sigma)^2(s\sigma^*)^1$ σ framework. The difference relative to MnAg is that now two of the three sσ electrons come from the larger, more electronegative element, Zn, instead of the more electropositive element (Mn in the case of MnAg).

Despite these results which confirm our expectations, ESR investigations of the related MnCu, MnAu, and CrCd molecules were unsuccessful.[129] In the case of MnAu and CrCd the failure to observe a $^7\Sigma$ ground state is attributed to a large zero-field splitting, D, due to the large spin–orbit coupling constants in these molecules.[129] The MnCu molecule, however, should have a value of D less than that of MnAg and should have been observed. This suggests an orbitally degenerate ground state, such as $^5\Pi$ or $^5\Delta$, may be present in this system.[129]

f. Diatomics Believed Prepared But Not Observed by ESR Techniques. The failure to observe an ESR spectrum of a molecule present in the matrix will occur if (1) $S = 0$, (2) the molecule is in an orbitally degenerate state, or (3) S is integral and the zero-field splitting, D, places the $m_s = 0 \leftrightarrow |m_s| = 1$ transition outside the range of the ESR spectrometer. For some combination of these reasons the following molecules are unobserved in ESR:[129] CrFe (14 electrons); MnFe (15 electrons); Fe_2, MnCo, and CrNi (16 electrons); FeCo and MnNi (17 electrons); Co_2, FeNi, MnCu, MnAu, and CrCd (18 electrons); FeCu, FeAg, and CoNi (19 electrons); Ni_2, CoCu, and CoAg (20 electrons); NiCu and NiAg (21 electrons); and NiZn (22 electrons).

7. Thermochemical Investigations by High-Temperature Mass Spectrometry

A number of intermetallic transition-metal molecules have been investigated by high-temperature Knudsen

effusion mass spectrometry.[28,53,77,158,233,263,264,314,317,412,418-433] The resulting values of $D_0°$ for heteronuclear diatomic transition metals are listed in Table 18. In cases where both second- and third-law values have been obtained, both are listed, along with the selected, recommended value.

Table 18 also lists the predicted dissociation energies obtained by using the atomic cell model of Miedema and Gingerich.[27,260,434] The atomic cell model is an extension of a previous theory of the heat of mixing of liquid alloys of arbitrary combinations of two metals.[230-233] It is an empirical model which correlates the bonding energy of the mixed diatomic molecule, $D_0°$(AB), with the dissociation energies of the homonuclear dimers, $D_0°(A_2)$ and $D_0°(B_2)$, the molar volumes V_A and V_B, the parameters representing the electron density at the boundary of a Wigner–Seitz atomic cell in the pure solid metal, n_{ws}^A and n_{ws}^B, and the difference in contact potential between the two metals, $\Delta\phi^*$. Details of the model are given by Miedema and Gingerich.[434]

Table 18 also lists values predicted from the Pauling model of a polar single bond.[435] According to this model the single bond energy $D_0°$(AB) is given by

$$D_0°(AB) = \tfrac{1}{2}[D_0°(A_2) + D_0°(B_2)] + 96\,(\chi_A - \chi_B)^2 \text{ kJ/mol}$$

where $D_0°(A_2)$ and $D_0°(B_2)$ are single-bond energies of the homonuclear dimers and χ_A and χ_B are the Pauling electronegativities of the respective elements. As discussed by Gingerich,[27] the parameters required for this model are not uniquely defined, and some uncertainty in the predicted values results. This is particularly true of $D_0°(A_2)$ and $D_0°(B_2)$, since the dissociation energies of singly bonded dimers are not directly measured. In compiling Table 18 Pauling's electronegativity scale[435] has been used along with the bond dissociation energies $D_0°(A_2)$ given by Miedema and Gingerich.[434]

Finally, Gingerich has developed an empirical valence bond model for multiply bonded transition-metal dimers.[27,436,437] The method explicitly includes atomic promotion energies to form the atomic states necessary for multiple bonding and calculates the bond energy per electron pair using curves developed by Brewer.[438] The results, for selected dimers which are thought to be multiply bonded, are also given in Table 18.

Table 18 demonstrates that the bond energy predicted by the Pauling model is quite accurate for molecules which are not expected to be multiply bonded. For LaY and all the diatomics containing Cu, Ag, or Au the root-mean-square error of the Pauling model is only 0.18 eV. Binding energies of multiply bonded molecules are calculated in the Pauling model to be considerably too low, as expected. These are indicated in Table 18 by Pauling values enclosed in parentheses. The atomic cell model provides some improvement over the Pauling model for the multiply bonded dimers but is considerably worse for singly bonded molecules. The rms error of this method is 0.61 eV. Finally, the empirical valence bond model provides some improvement over the simple Pauling model for the multiply bonded dimers but is not as accurate as the atomic cell model. Nevertheless, it provides a useful empirical method of estimating bond strengths in intermetallic dimers.

TABLE 19. Atomization Energies of Polyatomic Metals[a]

molecular type	molecule	$D_0°$, eV	ref
open d-shell trimer	Rh_2Ti	10.32 ± 0.43	27, 264
coinage metal trimers	Cu_3	3.05 ± 0.13	273
	Ag_3	2.62 ± 0.13	273
	Au_3	3.80 ± 0.13	273
electropositive diaurides	$AlAu_2$	5.25 ± 0.26	27, 440
	$BaAu_2$	5.72 ± 0.22	27, 444
	$EuAu_2$	5.85 ± 0.11	27, 422
	$HoAu_2$	5.69 ± 0.35	27, 441
	$LuAu_2$	6.24 ± 0.35	27, 441
	$TbAu_2$	6.21 ± 0.35	27, 441
group IV (14) diaurides	$GeAu_2$	5.58 ± 0.12	27, 433
	$SnAu_2$	5.62 ± 0.19	27, 443
group IV (14) dicupride	$SnCu_2$	4.68 ± 0.26	27, 446
triatomic monoaurides	Al_2Au	4.77 ± 0.22	27, 440
	Ge_2Au	5.54 ± 0.10	27, 433
	Sn_2Au	5.04 ± 0.19	27, 443
triatomic monocuprides	Ge_2Cu	5.24 ± 0.26	27, 445
	Sn_2Cu	4.05 ± 0.26	27, 446
tetratomic monoaurides	Ge_3Au	9.36 ± 0.21	27, 433
	Sn_3Au	8.15 ± 0.26	27, 443
tetratomic diaurides	Ge_2Au_2	9.68 ± 0.15	27, 433
	Sn_2Au_2	9.03 ± 0.26	27, 443
pentatomic monoauride	Ge_4Au	13.55 ± 0.31	27, 433
other triatomic	Al_2Pd	5.10 ± 0.25	27, 442

[a] Based primarily on third-law values.

C. Polyatomic Transition-Metal Molecules

Data on polyatomic transition-metal molecules is very limited indeed. The current knowledge of these species is summarized in this subsection.

1. Knudsen Effusion Mass Spectrometric Studies

Only a few polyatomic molecules composed solely of the transition metals have been investigated by Knudsen effusion mass spectrometry: Cu_3, Ag_3, Au_3, and Ti_2Rh.[264,272] Other polyatomics involving rare earths ($EuAu_2$, $TbAu_2$, $HoAu_2$, $LuAu_2$) and main-group metals ($AlAu_2$, Al_2Au, Al_2Pd, $BaAu_2$, Ge_2Au, Ge_3Au, Ge_4Au, $GeAu_2$, Ge_2Au_2, Sn_2Au, Sn_3Au, $SnAu_2$, Sn_2Au_2, Ge_2Cu, Sn_2Cu, and $SnCu_2$) have been more extensively investigated by these methods.[27,318,422,433,440-446] In most cases second-law evaluations of the various reaction enthalpies have not been reported. As discussed above, the third-law method requires assumptions about the structure of the molecule which limit its usefulness. Nevertheless, atomization energies of polyatomic metals have been derived.[27] These are given in Table 19 for the known polyatomic metals containing at least one transition-metal atom.

A comparison of Table 19 with Table 2 reveals that the dissociation energy of the coinage metal trimers (Cu_3, Ag_3, Au_3) into dimeric and atomic species, given by $D_0°(Cu_2–Cu) = 1.08 \pm 0.19$ eV, $D_0°(Ag_2–Ag) = 0.97 \pm 0.16$ eV, and $D_0°(Au_2–Au) = 1.51 \pm 0.15$ eV, is less than the binding energy of the corresponding dimers: $D_0°(Cu_2) = 2.01 \pm 0.08$ eV, $D_0°(Ag_2) = 1.65 \pm 0.03$ eV, $D_0°(Au_2) = 2.29 \pm 0.02$ eV. That the binding energy of a coinage metal atom to a preexisting dimer is lower than that of two isolated coinage metal atoms is not surprising. In simple molecular orbital theory the unpaired electron in these trimers is in a nonbonding or weakly antibonding orbital, thereby decreasing the net bonding relative to the dimer.

The situation is quite different in the one known open d-shell trimer: Rh_2Ti. The large atomization energy of this molecule, 10.32 ± 0.43 eV, demonstrates that

TABLE 20. UV-Visible Absorptions of Matrix-Isolated Transition-Metal Polyatomic Molecules

molecule	transitions obsd, nm	matrix	ref
Cr_3	477	Ar	80, 290
	479	Kr	80
Mn_x	253, 312, 400	Ar	110
	254, 317, 410	Kr	110
Mn_y	329, 345	Ar	110
	332, 336, 349	Kr	110
Co_3	287, 316	Ar	144
Ni_3	420, 480 (ν_{00} = 20 820 cm^{-1}; $\Delta\bar{G}$ = 202 cm^{-1})	Ar	148
Cu_3	221, 230, 234, 262, 376, 500	Ar	169
	227, 260, 280, 335, 404, 533	CH_4	169
Cu_4	402	Ar	169
	272, 424	CH_4	169
Mo_3	534	Ar	80
	538	Kr	80
Rh_3	490	Ar	144
Ag_3	245, 440	Ar	273, 274, 290
	226, 235/240, 400	Ar	276
Ag_3[a]	244, 260, 440	Ar	276
Ag_3	222, 232, 246, 422	Kr	110, 278
	233, 247, 420	Kr	276
Ag_3[a]	445	Kr	276
Ag_3	242, 260, 422/440	Xe	276
Ag_3[a]	474	Xe	276
Ag_4	213/217, 340/345	Ar	276
	273, 283, 347, 363, 426, 490	Ar	274
	222, 348	Kr	276
	286, 524	Kr	110, 278
	229, 360	Xe	276
Ag_5	333, 370, 396, 505	Ar	274
	349, 476	Kr	110, 278
Ag_6	340, 520	Ar	274
	366, 509	Kr	110, 278
Ag_7	536	Ar	274
Au_3	292, 471	Ar	228
Cr_2Mo	494	Ar	80
	496	Kr	80
$CrMo_2$	498	Ar	80
	496	Kr	80
$CrAg_2$	276	Ar	290
Ag_xMn_y	492, 502, 550, 592, 604	Kr	110

[a] Absorption assigned to an isomeric form of Ag_3, stabilized by matrix interactions.

contributions from d-electron bonding are quite significant for trimers as well as dimers. It will be fascinating to learn the detailed structure of this and other polyatomic transition-metal molecules.

2. Matrix-Isolation Optical Spectra

Ultraviolet and visible absorption spectra of matrix-isolated polyatomic transition-metal clusters have been studied by numerous investigators. The observed spectral transitions are given in Table 20. Caution is demanded in using this table, however, because it is difficult to unambiguously determine the cluster size which is responsible for a given absorption. This problem is particularly acute for larger clusters. Nevertheless, the one polyatomic transition metal which has been observed in the gas phase (Cu_3) exhibits a strong absorption at 5397 Å,[52] quite close to the reported matrix values of 500 (Cu_3/Ar) and 533 nm (Cu_3/CH_4).[169] This demonstrates that with sufficient care, correct assignments may be made for matrix-isolated species. Even with proper assignments, however, detailed interpretation is difficult. Generally, vibrational structure is unresolved, and theoretical calculations are usually incapable of accurate descriptions of polyatomic transition metals. Nevertheless, matrix-isolation spectra provide valuable starting points for gas-phase spectral searches and for resonance Raman investigations.

3. Raman and Resonance Raman Investigations: Sc_3, Cr_3, Ni_3, Cu_3, and Ag_3

The five species listed above are the only polyatomic transition-metal molecules yet investigated by Raman spectroscopy. These are discussed individually below. The reader is cautioned that unambiguous assignment of Raman transitions to specific metal clusters is difficult, however, and the assignments given below are open to some question.

Moskovits, DiLella, and Limm have obtained resonance Raman spectra of argon matrices containing scandium.[63] Features assigned to Sc_2 have been discussed above; in addition, Raman transitions at 246, 151, and 145 cm^{-1} are attributed to Sc_3. These are assigned as the symmetric stretch, antisymmetric stretch, and bending vibration, respectively, of an Sc_3 molecule of close to D_{3h} geometry. Upon warming the matrix, the two lower frequencies coalesce, suggesting that the departure from D_{3h} symmetry is induced by matrix interactions. The assignment of Sc_3 to D_{3h} symmetry is in agreement with matrix ESR studies, which show Sc_3 to contain three symmetrically equivalent atoms (see below).[227] The observed Raman-active frequencies, however, are much smaller than those found in CASSCF-CCI calculations, which obtain 513 cm^{-1} for the totally symmetric breathing vibration of D_{3h} Sc_3 (see below).[447] Moskovits et al. also observe a resonance Raman progression beginning at 395 cm^{-1} with an interval of 248 cm^{-1}.[63] This is interpreted as an electronic resonance Raman process in which an electronically excited state lying 395 cm^{-1} above the ground state is populated along with simultaneous excitation of a progression in the totally symmetric mode, with a vibrational frequency of 248 cm^{-1}.[63] An alternative assignment which would be in agreement with the CASSCF-CCI results would be to assign these features to a larger molecule, with a totally symmetric vibration of 248 cm^{-1} which builds progressions on other Raman-active modes, including one with a frequency of 395 cm^{-1}.

The resonance Raman spectrum of trichromium has also been observed.[82] A progression with ω_e'' = 313 cm^{-1} and $\omega_e''x_e''$ = 2 cm^{-1} has been assigned to Cr_3 isolated in argon. When not in resonance two other Raman transitions are observed at 226 and 123 cm^{-1}. These frequencies are assigned as the symmetric stretch (313 cm^{-1}), antisymmetric stretch (226 cm^{-1}), and bending mode (123 cm^{-1}) of a Cr_3 molecule of C_{2v} symmetry.[82]

Trinickel has been observed by resonance Raman spectroscopy with 476.5-, 488.0-, 496.5-, and 501.7-nm excitation.[448] Resonance Raman spectra were not obtained with 514.5-nm radiation, and 457.9-nm excitation produced an intense fluorescence. These observations are in approximate agreement with expectations based on the absorption systems assigned to Ni_3 (see above).[148] The dominant feature observed was a progression with ω_e'' = 232.3 cm^{-1} and $\omega_e''x_e''$ = 1.0 cm^{-1}.[448] A fit of the isotopic fine structure of the spectrum suggests that Ni_3 is a C_{2v} molecule with an apex angle between 90° and 100°, based on simulations using reasonable values of the valence force field constants.

Triatomic copper has been the center of considerable controversy. It is discussed in detail below. For the

present one should note that a resonance Raman spectrum attributed to Cu_3 was obtained in 1983 by DiLella et al.[449] and was subsequently reinterpreted by Moskovits in 1985.[450] The resonance Raman spectrum was dominated by a progression consisting of lines at 355, 710, 1063, and 1430 cm^{-1}; a second, weaker progression was observed at 404, 760, and 1115 cm^{-1}.[449]

Finally, Schulze et al. have observed a Raman band at 120.5 cm^{-1} for silver isolated in a krypton matrix.[284] At higher silver concentrations other bands at 203, 170, 151, 112, 107, 90, and 73 cm^{-1} grow in and at still higher concentrations, decay. None of these, however, grow with the same concentration dependence of the 120.5 cm^{-1} band. Because this band is the first to appear as concentration is increased (after the dimer band at 194 cm^{-1}), it is assigned to Ag_3.[284] Schulze et al. consider the presence of only one strong Raman active band as a strong indication that Ag_3 is linear.[284] This result is in conflict with a matrix-isolation ESR study which suggests that Ag_3 is bent, with a $^2B_2$ (C_{2v}) ground state (see below).[451] Kettler et al. report resonance Raman spectra of Ag_3 in Kr and Xe matrices, with a vibrational fundamental of 111 ± 2 cm^{-1} and overtones at 221 and 332 cm^{-1}.[452]

4. ESR Studies of Open d-Shell Transition-Metal Polyatomics: Sc_3, Y_3, Cr_4, Mn_5, and Sc_{13}

The molecules listed above represent the only open d-shell polyatomic transition metals yet detected by ESR spectroscopy. The first of these, Sc_3, was studied by Knight et al. in 1983.[227] The triscandium molecule, isolated in solid argon, exhibits an ESR spectrum consistent with one unpaired electron interacting with three equivalent ^{45}Sc ($I = {}^7/_2$) nuclei: 22 equally spaced hyperfine lines are observed. The equivalency of the three ^{45}Sc nuclei implies a D_{3h} geometry, with the single unpaired electron in a nondegenerate orbital. An orbital degeneracy would lead to Jahn–Teller distortion, thereby lifting the equivalency of the three scandium atoms. On this basis Sc_3 may be assigned a ground-state symmetry of $^2A_1'$, $^2A_2'$, $^2A_1''$, or $^2A_2''$ in D_{3h} symmetry. The observed hyperfine splitting, $A_{iso}(^{45}Sc)$ = 24 ± 4 MHz, is quite small compared to the hyperfine splitting expected for a 4s electron on an isolated scandium atom (2823 MHz),[414] indicating that only about 3% of the unpaired spin density is due to s-electron character.

These results are supported by CASSCF-CCI calculations by Walch and Bauschlicher.[447] These authors calculate the ground state of Sc_3 to be $^2A_2''$, $(4sa_1')^2(4se')^4(3da_1')^2(3da_2'')^1$, derived from the interaction of three ground-state ($4s^23d^1$, ^2D) scandium atoms. This ground state is orbitally nondegenerate and will therefore not undergo a Jahn–Teller distortion. In addition, the singly occupied orbital is antisymmetric with respect to reflection in the plane of the molecule and therefore cannot possess any 4s character. The small amount of 4s character observed in ESR studies can only arise when excited configurations are allowed to contribute, via configuration interaction. Walch and Bauschlicher calculate an interatomic distance of 3.04 Å and a symmetric stretch vibrational frequency of 513 cm^{-1} for the $^2A_2''$ ground state of Sc_3.[447]

A $^2E'$, $(4sa_1')^2(4se')^3(3da_1')^2(3da_2'')^2$ excited state of Sc_3, derived from two ground-state ($4s^23d^1$, ^2D) and one-excited ($4s^13d^2$) scandium atom is calculated about 0.1 eV above the $^2A_2''$ ground state. This state, however, is susceptible to Jahn–Teller distortion and places most of the unpaired spin in an orbital of 4s parentage. This is contrary to the matrix ESR results,[227] indicating that it cannot be the state observed in those experiments. For an equilateral, D_{3h} geometry, this state exhibits a potential energy minimum at a Sc–Sc separation of approximately 2.96 Å, with a symmetric stretching frequency of 204 cm^{-1}.[447] A possible resolution of the discrepancy between the resonance Raman, ESR, and CASSCF-CCI results is the possibility that both the $^2A_2''$ and $^2E'$ states are thermally populated in low-temperature matrices.[447] If this explanation is discarded, as seems likely, either the resonance Raman study involves a molecule other than Sc_3 or the CASSCF-CCI calculation is in error.

Triyttrium, Y_3, is congeneric with Sc_3, but displays a very different ESR spectrum.[227] The hyperfine structure due to ^{89}Y ($I = {}^1/_2$) unequivocally shows the molecule to possess two equivalent yttrium atoms and one unique one. Although the spectrum is consistent with a linear structure, since only parallel and perpendicular components of the **g** and **A** tensors are required for its simulation, the g components are more reasonably explained by a structure of C_{2v} symmetry. The observed hyperfine constants imply that only about 5% of the unpaired spin derives from yttrium 5s orbitals. The inequivalency of the three yttrium atoms is consistent with a structure derived from the yttrium analogue of the Sc_3 $^2E'$ state, which would undergo a Jahn–Teller distortion to C_{2v} symmetry. The small amount of s character in the singly occupied orbital, however, removes this assignment from consideration. Presumably d bonding is more important in Y_3 than in Sc_3, thereby lowering the energy of states correlating to excited ($5s^14d^2$) yttrium atoms. The ground state of Y_3 may therefore derive from atomic asymptotes which were not considered in Walch and Bauschlicher's calculation of Sc_3.[447] These asymptotes would involve two, or even three, electronically excited ($4s^14d^2$) yttrium atoms.

Van Zee et al. have recently observed ESR spectra of chromium clusters in neon, argon, and krypton matrices.[453] A chromium cluster was found with $S = 3$ and with axial symmetry. Furthermore, the observed ^{53}Cr ($I = {}^3/_2$) hyperfine structure indicated a molecule in which the s component of the unpaired spin is largely localized on one unique, axial chromium atom. The hyperfine tensor possessed little or no anisotropy, despite the definite axial symmetry of the **g** tensor. Analysis of the quadrupole coupling of the unique, axial chromium atom indicated that this atom exists in a significant electric field gradient. The zero-field splitting parameter, D, was found to be 0.110 cm^{-1}. These results are consistent with a trigonally distorted Cr_4 tetrahedron (C_{3v} symmetry), a square-pyramidal Cr_5 molecule (C_{4v} symmetry), or a chromium atom in an unusually strong axially symmetric crystal field, such as in a $Cr{\cdot}Cr_3$ complex.[453] Further work is required before these alternatives may be reduced to a single possibility. In addition to this spectrum, Van Zee et al. observed another spectrum which may be due to a D_{3h} trichromium molecule. At this time, however, the carrier of this second spectrum is quite uncertain.[453]

TABLE 21. ESR Spectroscopic Constants of Coinage Metal Trimers[a]

molecule	g_{iso}	$A(2)$,[b] MHz	$A(1)$,[c] MHz	$\rho_s(2)^{b,d}$	$\rho_s(1)^{c,d}$	ref
$^{63}Cu_3$	1.9925	1744	155	0.29	0.026	457
$^{107}Ag_3$	1.9622	810.2 ± 0.8	105.7 ± 0.8	0.44	0.058	451
$^{197}Au_3$	1.865	999.3	151.4	0.35	0.053	458
$^{63}Cu^{107}Ag^{63}Cu$	1.9623	2418	97.5	0.40	0.053	459

[a] See text for details. [b] Refers to the two equivalent (end) nuclei. [c] Refers to the unique (central) nucleus. [d] Contribution of s electrons on this nucleus to the unpaired spin.

TABLE 22. ESR Spectroscopic Constants of Coinage Metal Pentamers[a]

	g		$A(2)$,[b] MHz							
molecule	$g_\parallel$	$g_\perp$	$A_\parallel(2)^b$	$A_\perp(2)^b$	$A(2)$,[c] MHz	$A(1)$,[d] MHz	$\rho_s(2)^{b,e}$	$\rho_s(2)^{c,e}$	$\rho_s(1)^{d,e}$	ref
$^{63}Cu_5$	2.055		1749		43.1	86.3	0.292	0.007	0.014	460
$^{107}Ag_5$	2.002	2.085	-594.5	-587.5	15.8	31.7	0.322	0.009	0.017	461
$^{63}Cu^{107}Ag_4$	1.994	2.060	1613[f]	1614[f]	...	...	0.269 (Cu)			462
			-653[g]	-654[g]			0.357 (Ag)			
$^{63}Cu_2{}^{107}Ag_3$	1.994	2.050	1777[f]	1772[f]	...	...	0.296			462

[a] See text for details. [b] For high-spin equatorial positions. [c] For axial positions. [d] For low-spin equatorial position. [e] Contribution of s character from this position to the singly occupied molecular orbital. [f] Hyperfine parameter for ^{63}Cu. [g] Hyperfine parameter for ^{107}Ag.

Van Zee et al. have also reported an ESR spectrum attributed to the manganese pentamer, Mn_5.[113,114] The spectrum was observed for manganese deposited in argon, krypton, and xenon matrices on a sapphire rod and was found to exhibit a strong orientational dependence. Thus the carrier of the spectrum is preferentially oriented with respect to the surface of the sapphire rod. With the magnetic field oriented parallel to the surface of the sapphire rod a 25-line spectrum is observed which is assigned to the perpendicular transitions of an axially symmetric $S = 25/2$ molecule. The parallel transitions are observed when the sapphire face is perpendicular to the magnetic field, indicating that the unique molecular axis is normal to the sapphire surface. No hyperfine splittings due to the ^{55}Mn ($I = {}^5/_2$) nucleus were observed, indicating that the unpaired spins exhibit little s character. The total spin value of $S = 25/2$, the negligible s character of the unpaired spins, and the difficulty in promoting manganese atoms from $3d^54s^2$ to $3d^64s^1$ (see Table 1) all argue in favor of a pentatomic species with five ferromagnetically coupled $3d^5$ ^6S cores. On the basis of the high degree of orientation observed, Baumann et al. suggest a plane pentagonal Mn_5 cluster as the carrier of the spectrum.[113] The lack of measurable hyperfine splitting leaves this possibility unverified, however, and a square-pyramidal form is equally consistent with the current ESR data.

Finally, Knight et al. report an ESR spectrum of a large scandium cluster in neon matrices.[227] Over sixty equally spaced hyperfine lines are observed, indicating that at least nine equivalent ^{45}Sc ($I = {}^7/_2$) atoms are present. The spectrum is centered at $g = 1.9914 \pm 0.0004$ and shows no evidence of zero-field splitting, indicating $S = {}^1/_2$. Knight et al. discuss possible structures based on Sc_{13}, including (1) a 3–7–3 (ABA) array of 13 atoms, forming a truncated hexagonal bipyramid of D_{3h} symmetry, (2) a cuboctahedron, with 3–7–3 (ABC) structure of O_h symmetry, and (3) an icosahedron with one interior scandium atom. All of these structures possess 12 equivalent surface atoms and could be responsible for the observed spectrum. Knight et al. suggest an icosahedral structure, Sc_{13}, for the carrier of this remarkable spectrum, based primarily on the calculated stability of such structures for transition-metal clusters.[139,287,454–456] At this time, however, the other possibilities cannot be rigorously excluded.

5. ESR Studies of Coinage Metal Polyatomic Molecules: Cu_3, Ag_3, Au_3, Cu_2Ag, Cu_5, Ag_5, $CuAg_4$, and Cu_2Ag_3

ESR spectra of triatomic and pentatomic coinage metal molecules have been extensively invest[illegible] by Howard, Sutcliffe, Mile, and co-workers.[451,457] [illegible]eir work has recently been reviewed.[464] The [illegible]ic species Cu_3, Ag_3, Au_3, and CuAgCu have all been formed in inert matrices of adamantane (Cu_3)[457] and perdeuteriobenzene (Ag_3, Au_3, and CuAgCu).[451,458,459] In all four cases a spectrum with $S = {}^1/_2$ is obtained. Analysis of the hyperfine structure shows all molecules to contain two equivalent nuclei with large hyperfine constants and a third nucleus, with a small hyperfine constant. All trimers exhibit an isotropic (or nearly isotropic)[451] **g** tensor which is substantially reduced from the free electron value of 2.0023. This implies that the coinage metal trimers are bent, rather than linear or equilateral triangular. Hyperfine parameters may be used to identify the amount of s character from each atomic center contributing to the singly occupied molecular orbital. As shown in Table 21, most of the spin density is derived from the s orbitals of the outer atoms, with only a very small contribution from the central atom. These results may be rationalized by assuming that the singly occupied molecular orbital has a node on the central atom in the predominant electronic configuration.[464] This requires all four coinage metal trimers to possess a ground electronic state of $^2B_2$ symmetry in the C_{2v} symmetry group. In the case of Cu_3, Ag_3, and Au_3 this is one of the states resulting from Jahn–Teller distortion of a $^2E'$ state in D_{3h} symmetry.

Howard et al. have also reported ESR spectra for the matrix-isolated coinage metal pentamers Cu_5,[460] Ag_5,[461] $CuAg_4$,[462] and Cu_2Ag_3.[462] Spectroscopic constants for the ESR spectra are given in Table 22. All molecules have been synthesized by using isotopically pure ^{63}Cu ($I = {}^3/_2$) and ^{107}Ag ($I = {}^1/_2$). The observed spectra show one unpaired spin ($S = {}^1/_2$) along with hyperfine splittings induced by these nuclei. The homonuclear molecules Cu_5 and Ag_5 show two equivalent nuclei with large hyperfine splitting constants, two equivalent nuclei with a very small hyperfine splitting, and a unique nucleus, again with a small hyperfine splitting. In the case of Ag_5 the magnetogyric tensor, **g**, and the

TABLE 23. Vibronic Levels of the Ã State of Cu_3

obsd level,[a] cm^{-1}	Ã $^2A_1'$ assignt[b]			Ã $^2E''$ assignt[c]		
	(v_1, v_2)	vibronic symmetry	calcd energy[d]	(n_z, n_e, j)	vibronic symmetry	calcd energy
0.0	(0, 0)	A_1'	0.00	(0, 0, $^1/_2$)	E″	0.0
146.4 ± 0.7	(1, 0)	E′	146.43	(0, 1, $^1/_2$)	E″	146.6
242.9 ± 1.1	(0, 1)	A_1'	242.32	(0, 2, $^5/_2$)	E″	244.4
291.7 ± 1.1	(2, 0)	A_1' + E′	290.70	(0, 2, $^1/_2$)	E″	292.4
377.9 ± 1.9	(1, 1)	E′	378.02	(0, 3, $^7/_2$)	E″	376.3
432.0 ± 5.0	(3, 0)	A_1' + A_2' + E′	432.81	(0, 3, $^1/_2$)	E″	430.8
				(0, 3, $^5/_2$)	E″	440.0
476.6 ± 1.1	(0, 2)	A_1'	476.94	(1, 0, $^1/_2$)	E″	476.6
511.6 ± 4.0	(2, 1)	A_1' + E′	511.56	(0, 4, $^5/_2$)	E″	511.1
572.8 ± 15.0	(4, 0)	A_1' + 2E′	572.76	(0, 4, $^1/_2$)	E″	571.9

[a] Reference 52. [b] This work. [c] Reference 472. [d] Calculated by using $G(v_1, v_2) = (v_1 + 1)\omega_1 + (v_2 + {}^1/_2)\omega_2 + x_{11}(v_1 + 1)^2 + x_{12}(v_1 + 1)(v_2 + {}^1/_2) + x_{22}(v_2 + {}^1/_2)^2$ and $\omega_1 = 155.03\ cm^{-1}$, $\omega_2 = 260.75\ cm^{-1}$, $x_{11} = -1.08\ cm^{-1}$, $x_{12} = -10.73\ cm^{-1}$, and $x_{22} = -3.85\ cm^{-1}$.

major hyperfine splittings are anisotropic. Howard et al.[460-464] demonstrate that these spectra are consistent with a distorted trigonal-bipyramidal structure, in which the two nuclei with high-spin density are in the equatorial plane, and the remaining three nuclei (occupying two axial and one equatorial position) contribute very little s character to the singly occupied molecular orbital. The unpaired electron occupies an orbital of e′ symmetry in D_{3h}, resulting in a Jahn–Teller distortion to C_{2v} symmetry. The pentatomic molecule which results is precisely that obtained by placing additional atoms above and below the plane of the Jahn–Teller distorted trimers discussed above.

Mixed copper–silver pentamers $CuAg_4$ and Cu_2Ag_3 have also been identified by Howard et al.[462] The $CuAg_4$ species exhibits large hyperfine splittings due to one copper and one silver atom. Hyperfine structure due to the remaining silver nuclei is not resolved. The Cu_2Ag_3 species exhibits large hyperfine splittings due to both copper atoms, while silver hyperfine splittings are unresolved. In the absence of resolved hyperfine splittings for all five nuclei no unambiguous assignment is possible. Nevertheless, the similarity of the observed hyperfine constants for ^{63}Cu in Cu_5, $CuAg_4$, and Cu_2Ag_3 and for ^{107}Ag in Ag_5, $CuAg_4$, and Cu_2Ag_3 suggests structures based upon distorted trigonal bipyramids for all four species. This is the predicted stable structure of Cu_5 calculated by ab initio LCAO-MO-SCF methods.[197]

A review of results obtained for transition-metal molecules by ESR techniques, comparable to that given here, has been recently presented by Weltner and Van Zee.[465]

Note Added In Proof: *Weltner has recently reported an ESR spectrum of Ag_7, which is identical to the spectrum previously assigned to Ag_5,[461] except additional lines have not been resolved. This new observation opens the other coinage metal pentamer ESR spectra to question.*

6. Copper Trimer, Cu_3: Reinvestigation of All Available Data[466]

Without a doubt tricopper is the best-studied of the polyatomic transition-metal molecules. As alluded to above, it is also the center of some controversy. For these reasons Cu_3 deserves special mention in this review.

Moskovits and Hulse first identified Cu_3 by visible and ultraviolet absorption spectroscopy in inert matrices in 1977.[169] Bands attributed by them to triatomic copper are listed in Table 20. In subsequent work, mentioned briefly above, a resonance Raman spectrum was observed by DiLella et al. and assigned to copper trimer.[449] At about the same time as this work Howard et al. reported the ESR spectrum discussed above, which firmly established Cu_3 as a distorted Jahn–Teller system under matrix-isolation conditions, with an electronic symmetry of $^2B_2$ in the C_{2v} symmetry group.[457] Morse et al. then provided a spectroscopic study of jet-cooled copper trimer by resonant two-photon ionization and depletion methods,[52] and this was followed by laser-induced fluorescence work by Gole and co-workers[467] and by dispersed fluorescence studies by Rohlfing and Valentini.[468]

Much of the current controversy centers on the optical spectroscopy of Cu_3, which was first investigated in the gas phase by Morse et al. in 1983.[52] Twelve vibronic bands were observed in the spectrum of jet-cooled Cu_3, with an origin band at 5397 Å. Three of these were vibrational hot bands, two of which originated from a level 99.6 cm^{-1} above the zero-point level.[52] The remaining nine vibronic bands correspond to excitations from the ground vibronic state of Cu_3 to vibronic levels of an excited electronic state. The vibronic levels of the excited electronic state, listed in Table 23, could be explained by a set of vibrational constants given by $\omega_1' = 155.03\ cm^{-1}$, $\omega_2' = 260.75\ cm^{-1}$, $x_{11}' = -1.08\ cm^{-1}$, $x_{12}' = -10.73\ cm^{-1}$, and $x_{22}' = -3.85\ cm^{-1}$ (recalculated by least-squares fit to the vibronic levels of Table 23). The large values of the anharmonicities led Morse et al. to reject this fit in favor of an explanation involving an excited state of $^2E''$ symmetry, which undergoes a Jahn–Teller distortion.[52]

Assuming a $^2E''$ excited state, Morse et al. were able to fit the observed spectra by appropriate choice of the Jahn–Teller parameters.[52] The theory which was used closely followed the work of Longuet-Higgins[470] and Gerber and Schumacher[471] but erred in the parameterization of the Hamiltonian. As discussed by Thompson et al., a term proportional to $r \cos 3\phi$ was erroneously included in the Hamiltonian.[472,473] Thompson et al. were able to fit the observed spectrum quite accurately by removing this term from the Hamiltonian, still assuming a transition of $^2E'' \leftarrow {}^2E'$ electronic symmetry.[472] The fitted energy levels and symmetry species are given in Table 23, from which it is evident that the upper state is equally well-described by either the normal mode or Jahn–Teller models. To distinguish between these possibilities additional information is required.

Ab initio calculations on copper trimer offer a potential source of the additional information which is needed. Although numerous calculations have been reported for Cu_3,[179,189,197,201,202,469,474] most reports only provide estimates of ground-state parameters. Extended Hückel calculations[179] and one SCF calculation[197] predict Cu_3 to have a linear, $^2\Sigma_u^+$ ground state, contrary to the ESR results.[457] Another SCF calculation[202] and the semiempirical diatomics-in-molecules method[474] predict Cu_3 to possess a ground state of $^2E'$ symmetry in the D_{3h} equilateral configuration, with Jahn–Teller distortion to either $^2A_1$ or $^2B_2$ forms. These studies obtain $^2A_1$ and $^2B_2$ forms of equal energy.[202,474] Finally, pseudopotential calculations[189] and SCF/SDCI[469] both predict the $^2B_2$ form to be preferentially stabilized by 400 and 200 cm^{-1}, respectively. This is in agreement with the ESR data.[457]

Excited states of Cu_3 have been calculated in the SCF approximation by Miyoshi et al.[202] and in the SCF/SDCI approximation by Walch and Laskowski.[469] Given the importance of correlation found in all studies of transition-metal molecules, the SCF/SDCI method probably provides a more accurate description of the excited states of Cu_3. With this method Walch and Laskowski calculate a $^2A_2''$ state 1.25 eV above the ground state.[469] This is not accessible from the $^2E'$ ground state under electric dipole selection rules, although the transition can be vibronically induced from the $^2A_1$ (in C_{2v}) component of the Jahn–Teller distorted $^2E'$ ground state. The intensity of the observed Cu_3 absorption system (which exhibits a radiative lifetime for the origin band of 28 ns[468]) and the location of its origin at 2.30 eV[52] argue against this assignment, however. The next higher state is $^2A_1'$ (in D_{3h}), calculated 2.14 eV above the ground state.[469] This energy is close to the experimental value, and the $^2A_1' \leftarrow {}^2E'$ transition is fully allowed and is expected to be intense, since it corresponds to a (3s ← 2p)-like Rydberg transition of the united atom.[469] Other possibilities for the upper state include a $^2E''$ Rydberg-like state calculated at 3.32 eV, a $^2E'$ Rydberg-like state calculated with valence CI (not SDCI) at 2.14 eV, and a $^2E''$ state produced by excitation of a 3d electron to the 4se′ level, located 2.14 eV above the ground state.[469]

The possibility of a $^2E'$ upper state in the 5397-Å system is readily dismissed, since a $^2E' \leftarrow {}^2E'$ transition would be induced by the E′ component of the electric dipole operator, and *all* vibronic components of the lower $^2E'$ state (whether of A_1', A_2', or E′ vibronic symmetry) would be radiatively coupled to the vibrationless level of the $^2E'$ upper state (of E′ vibronic symmetry). The presence of vibronic components of the lower state *not* coupled to the zero-point level of the upper state was demonstrated first by Morse et al.[52] and subsequently verified by Rohlfing and Valentini.[468] Assuming that the 5397-Å system is a fully allowed electric dipole transition (as is evident from the intensity of the system) and that the ground state of Cu_3 is $^2E'$ in D_{3h} symmetry, the only transitions consistent with this result are $^2E'' \leftarrow {}^2E'$ (induced by the A_2'' component of the electric dipole operator) and $^2A_1' \leftarrow {}^2E'$ and $^2A_2' \leftarrow {}^2E'$ (both induced by the E′ component of the electric dipole operator). On this basis only the $^2A_1'$ and $^2E''$ states calculated by Walch and Laskowski[469] need be considered as candidates for the upper state. The former ($^2A_1'$) requires that the vibronic levels of the upper state not exhibit a Jahn–Teller effect and therefore corresponds to the normal mode description given in Table 23. The latter ($^2E''$) requires the Jahn–Teller description initially proposed by Morse et al.[52] and corrected by Thompson, Truhlar, and Mead.[472] Calculated vibronic levels along with vibronic symmetry species are provided in Table 23 for both of these possible assignments.

The dispersed fluorescence study by Rohlfing and Valentini provides a means of determining which assignment is correct.[468] In this investigation fluorescence from the vibrationless level of the upper state was dispersed, revealing numerous vibronic levels of the ground state. The experiment was repeated, dispersing the fluorescence from the upper state vibronic level 146 cm^{-1} above the zero-point level, and new bands were observed which were notably absent in the former experiment. Consider first the assignment of the transition as $^2E'' \leftarrow {}^2E'$. In this assignment both the vibrationless level of the upper state and the level at 146 cm^{-1} are of E″ vibronic symmetry, and should possess the same selection rules in fluorescence: $E'' \rightarrow E'$; $E'' \not\rightarrow A_1', A_2'$. *If the upper state were $^2E''$, no new levels should have been observed in the dispersed fluorescence originating from the 146-cm^{-1} band.* This is contrary to the observations of Rohlfing and Valentini.[468] Now consider the assignment of the 5397-Å band system as $^2A_1' \leftarrow {}^2E'$. In this assignment the vibrationless level of the upper state is of A_1' vibronic symmetry, and electric dipole transitions (induced by the $^2E'$ component of the electric dipole operator) limit fluorescence to vibronic states of E′ vibronic symmetry. The 146-cm^{-1} vibronic level of the upper state, however, corresponds to excitation of the doubly degenerate bending mode and is of E′ vibronic symmetry. Electric dipole transitions from this level are allowed for fluorescence to states of A_1', A_2', or E′ vibronic symmetry. All vibronic levels of the lower state are accessible by allowed electric dipole transitions when this state fluoresces. Rohlfing and Valentini observe many new vibronic levels of the ground electronic state with substantial intensity in the fluorescence from the 146-cm^{-1} level, confirming the transition as $\tilde{A}\ ^2A_1' \leftrightarrow \tilde{X}\ ^2E'$.[468]

This assignment is consistent with the high intensity of the $^2A_1' \leftarrow \tilde{X}\ ^2E'$ transition predicted by Walch and Laskowski.[469] In hindsight it also explains the anomalously large vibronic bandwidths observed by Morse et al.[52] for selected vibronic levels of the upper electronic state. The widths of the transitions observed by Morse et al. are reflected in the uncertainties given in Table 23 for the vibronic level positions of the upper state. The observed bandwidths are *not* correlated with vibrational energy in the upper state, since the level at 476.6 cm^{-1} has a narrow bandwidth, while levels at 432.0, 511.6, and 572.8 cm^{-1} are noticeably broad. The broadening *is* correlated with the number of quanta excited in the doubly degenerate bending mode, however. When this vibration is multiply excited the degeneracy is lifted by anharmonicities of the molecule, since a D_{3h} molecule cannot have a symmetry-required degeneracy greater than 2.[475] The various vibronic species obtained under these conditions are listed in Table 23. The anomalous widths of the transitions

observed by Morse et al. correspond to unresolved splittings of this multiply excited doubly-degenerate vibration. For the particular case of a $^2A_1' \leftarrow {}^2E'$ electronic transition, transitions from the E′ vibrationless level of the $^2E'$ ground electronic state are electric dipole-allowed to all vibronic levels of the upper state, resulting in the observation of all of the (unresolved) vibronic components of a given (v_1, v_2) vibronic level. This would not occur if the ground state were not an orbitally degenerate electronic state, subject to the Jahn–Teller effect. This analysis therefore supports the assignment of the ground state as $\tilde{X}\ ^2E'$ as well.

The preceding analysis establishes the symmetric stretch vibrational frequency as 261 cm^{-1}, and the bending vibrational frequency as 155 cm^{-1} for the excited $\tilde{A}\ ^2A_1'$ state of Cu_3. This state results from promotion of the nonbonding or weakly antibonding 4se′ electron to a Rydberg-like orbital of 4p parentage.[469] On this basis one would expect the ground electronic state to possess vibrations of comparable or lower frequency in the corresponding normal modes, although these would be complicated by the Jahn–Teller effect. With these ideas in mind, let us turn our attention to the ground electronic state of Cu_3, now universally accepted as a Jahn–Teller distorted $^2E'$ state.

Rohlfing and Valentini have unambiguously provided vibronic energy levels of the $\tilde{X}\ ^2E'$ state of Cu_3 by dispersing the fluorescence induced by excitation of the $\tilde{A}\ ^2A_1' \leftarrow \tilde{X}\ ^2E'$ transition in a supersonic jet.[468] According to the analysis presented above, excitation of the origin band leads to fluorescence to ground-state levels of E′ vibronic symmetry only. Excitation of the 146 cm^{-1} vibronic level of $\tilde{A}\ ^2A_1'$, however, permits fluorescence to all levels of A_1', A_2', or E′ vibronic symmetry within the $\tilde{X}\ ^2E'$ ground state. This experiment therefore allows one to measure and classify the vibronic levels of the $\tilde{X}\ ^2E'$ state, although A_1' and A_2' levels cannot be distinguished without further experiments. The observed levels, classified as A′ or E′, are given in Table 24.

Although this procedure for classifying levels as A′ or E′ is correct in theory, there are difficulties in practice. For example, not all levels reported observed in fluorescence from the origin band excitation are observed when the 146 cm^{-1} band is excited. No selection rules prevent their observation, so one must conclude that they are of weak intensity due to poor Franck–Condon factors. This prospect opens the possibility that some levels observed when the 146 cm^{-1} band is excited, but not observed with excitation of the origin, may fail to appear because of poor Franck–Condon factors rather than due to selection rules. Thus some of the states assigned a symmetry of A′ in Table 24 may possibly be of E′ symmetry. Other problems arise because the bands observed in fluorescence are broad and overlapping and are quite weak, especially at high excitations of $\tilde{X}\ ^2E'$ Cu_3.[468]

With these caveats in mind, some conclusions may be drawn concerning the ground state of copper trimer. The lowest observed vibronic level of A′ symmetry lies only 16 cm^{-1} above the degenerate E′ ground vibronic level. In the limit of strong Jahn–Teller stabilization of a distorted C_{2v} copper trimer, this energy difference measures the tunneling splitting between the three equivalent C_{2v} species. The value of this splitting, 16 cm^{-1}, demonstrates that the barrier to pseudorotation is small, since the tunneling splitting goes to zero as the barrier increases. Truhlar, Thompson, and Mead have recently used this tunneling splitting and the positions of other levels of E′ vibronic symmetry to fit the observed spectrum using a quadratic coupling model of the Cu_3 vibronic problem.[476] Zwanziger, Whetten, and Grant have recently published a similar analysis employing a quadratic coupling Jahn–Teller model.[477] In addition, however, they have calculated intensities of the observed transitions for comparison to experiment, based on an assignment of the transition as $^2E'' \leftrightarrow {}^2E'$. It will be interesting to see if a recalculation based upon an upper state of $^2A_1'$ electronic symmetry improves the agreement between experimental and theoretical intensities. The energy levels calculated by both Truhlar, Thompson, and Mead[476] and Zwanziger, Whetten and Grant[477] are compared to experiment in Table 24.

The ground-state potential energy surfaces obtained by Truhlar, Thompson, and Mead[476] and Zwanziger, Whetten, and Grant[477] are comparable. The former group of investigators find a Jahn–Teller stabilization energy of 221 cm^{-1} and a barrier to pseudorotation of 95 cm^{-1}.[476] Zwanziger et al. find corresponding values of 305 cm^{-1} and 111 cm^{-1}, respectively.[477] Both groups assign a band at 270 cm^{-1} as the fundamental of the symmetric stretching vibration, rather close to the value of ω_2 = 260.75 cm^{-1} obtained for the $\tilde{A}\ ^2A_1'$ state. Recent unpublished ab initio calculations by the coupled pair functional method, which should provide the most accurate calculations to date, provide support for both fits, finding a Jahn–Teller stabilization energy below 300 cm^{-1} and a pseudorotation barrier below 100 cm^{-1}.[478] With this combination of theoretical and experimental results, triatomic copper now appears to be the best-understood of the transition-metal trimers.

TABLE 24. Vibronic Levels of the $\tilde{X}\ ^2E'$ State of Cu_3

obsd level,[a] cm^{-1}	obsd state symmetry[a]	calcd fit[e] level	calcd fit[e] symmetry	calcd fit[h] level	calcd fit[h] symmetry
0.0	E′ [b,c]	0	E′	0	E′
16.0 ± 1.0	A′ [c]	16	A′	12	A′
99.3 ± 1.5	E′ [b,c]	100	E′	101	E′
144.5 ± 1.5	A′ [c]	105, 150	A′	148	A′
153.0 ± 2.0	E′ [b,c]	154	E′	143	E′
219.8 ± 2.0	E′ [b,c]	229	E′	223	E′
230.4 ± 1.0	E′ [b]			234	E′
237.7 ± 1.0	E′ [b,c]	241	E′		
269.5 ± 2.0[d]	E′ [b]	270[f]	E′ [f]	269.5[f]	E′ [f]
274.3 ± 2.0[d]	A′ [c]			281	A′
304.0 ± 3.0	E′ [b]	307	E′	296	E′
323.9 ± 2.0	A′ [c]			300	A′
345.2 ± 1.5					
352.5 ± 1.5	E′ [b]	360	E′	361	E′
357.7 ± 1.5					
375.9 ± 2.0	A′ [c]			382	E′
399.0 ± 3.0	E′ [b,c]	392	E′	404	E′
407.0 ± 2.0	E′ [b,c]	421	E′		
458.5 ± 2.0	E′ [b]	474	E′		
465.7 ± 2.0	E′ [b]			462	E′
484.0 ± 3.0	E′ [b,c]	486	E′	481	E′
520.0 ± 4.0	E′ [b,c]	521	E′	514	E′
543.0 ± 4.0	E′ [b,c]	540[g]	E′ [g]	539[g]	E′ [g]
556.0 ± 2.0	E′ [b]	561	E′	553	E′

[a] Reference 468. [b] Observed in fluorescence when the origin band is pumped. [c] Observed in fluorescence when the 146 cm^{-1} band is pumped. [d] Possibly a single band. [e] Reference 476. [f] Assigned as the fundamental of the symmetric stretching vibration. [g] Assigned as the first overtone of the symmetric stretch vibration. [h] Reference 477.

7. Theory and Expected Trends for Homonuclear Transition-Metal Trimers

The determinants of homonuclear transition-metal trimer structure have been recently discussed by Walch and Bauschlicher.[447] The major properties which are pertinent involve the relative size of the s and d orbitals, the $(n + 1)s^2nd^m \rightarrow (n + 1)snd^{m+1}$ promotion energy, and the number of valence electrons, just as in the diatomic molecules.

Walch and Bauschlicher consider the molecular orbitals which derive from 3d orbitals localized on three atoms at the vertices of an equilateral triangle (D_{3h} geometry).[447] With the σ direction given by the axis connecting a given atom with the center of the molecule, the five 3d functions may be classified as $3d\sigma$, $3d\pi'$, $3d\pi''$, $3d\delta'$, and $3d\delta''$, where the primes denote symmetry with respect to the molecular plane and double primes denote antisymmetry with respect to this plane. Under D_{3h} symmetry $3d\sigma$ and $3d\delta'$ transform as a_1' and e', $3d\pi'$ transforms as a_2' and e', $3d\pi''$ transforms as a_2'' and e'', and $3d\delta''$ transforms as a_1'' and e''. As in the homonuclear dimers, $3d\sigma$, $3d\pi'$, and $3d\pi''$ have moderate overlaps in the molecule and form the bonding orbitals, while $3d\delta'$ and $3d\delta''$ are essentially nonbonding.[447] According to Walch and Bauschlicher the best bond orbitals are $3d\sigma$ (a_1') and $3d\pi''$ (a_2'') because these combinations have no nodal planes between pairs of atoms.[447] Both are symmetric under $\hat{C}_3$ operations; they are symmetric and antisymmetric, respectively, under reflection in the molecular plane. Not surprisingly, the calculated ground state of triscandium, Sc_3, involves occupation of these strongly bonding 3d-orbitals: Sc_3, $(4sa_1')^2(4se')^4(3d\sigma a_1')^2(3d\pi''a_2'')^1$, $^2A_2''$.[447]

Lying above the bonding orbitals $3d\sigma a_2'$ and $3d\pi''a_2''$, Walch and Bauschlicher find the $3d\pi'e'$ orbital, which possesses some bonding character, the $3d\sigma e'$ and $3d\pi''e''$ orbitals, which are not favorable to bonding, and the $3d\pi'a_2'$ orbital, which places nodal planes between all pairs of atoms and is outright antibonding in character.[447] In addition to these orbitals, the $3d\delta'a_1'$, $3d\delta'e'$, $3d\delta''a_1''$, and $3d\delta''e''$ orbitals are essentially nonbonding due to weak overlaps between δ orbitals. On the basis of these results, the energetic ordering of the 3d orbitals expected is $3d\sigma a_1' < 3d\pi''a_2'' < 3d\pi'e' < (3d\sigma e', 3d\pi''e'', 3d\delta'a_1', 3d\delta'e', 3d\delta''a_1'', 3d\delta''e'') < 3d\pi'a_2'$, with the orbitals listed in parentheses essentially nonbonding in character.

On the basis of these ideas one might expect the Ti_3^+ ion to exist as $(3sa_1')^2(4se')^4(3d\sigma a_1')^2(3d\pi''a_2'')^2(3d\pi'e')^1$, $^2E'$. Walch and Bauschlicher, however, find that the low promotion energy for titanium favors $s \rightarrow d$ promotions. Thus configurations with six or seven 3d electrons appear to be more favored for Ti_3^+.[447] For V_3^+ and Cr_3^+ stronger net bonding is expected, as the $3d\pi'e'$ orbital, with some degree of bonding character, is filled.[447]

Trimanganese is expected to exist as a weakly bonded molecule due to the high promotion energy required to open the 4s shell of atomic manganese.[447] For the trimers Fe_3, Co_3, and Ni_3 bonding is mainly expected from the 4s electrons since the 3d orbitals have contracted substantially in these molecules.[447] The d electrons are expected to be high-spin-coupled, as might be expected from the ferromagnetic behavior of these elements in their bulk crystalline forms. Thus, for example, Basch et al. find the ground state of Ni_3 to arise from three $3d^94s^1$ atoms, giving a $3d_A^9 3d_B^9 3d_C^9 (4sa_1')^2(4se')^1$ ground configuration in D_{3h} symmetry.[154] The 3d cores are weakly interacting, and Ni_3 is expected to distort according to the Jahn–Teller theorem in much the same manner as does Cu_3. Basch et al. find that at the SCF level the distortion in Ni_3 is so severe that the ground state is linear.

Basch has also investigated Ag_3, Ag_3^+, and Ag_3^- by ab initio relativistic effective core potential methods within the framework of the self-consistent field and configuration interaction methods.[296] As found for Cu_3, trisilver is calculated to exist as a $^2B_2$ (C_{2v}) molecule based upon a Jahn–Teller distorted $^2E'$ state in D_{3h} symmetry. When an electron is removed to form Ag_3^+, the ion favors a ground state which is $^1A_1'$ and of D_{3h} symmetry. This is expected, since the e' electron has been removed, and Jahn–Teller distortion is no longer required. In the anion a linear configuration of $^1\Sigma_g^+$ symmetry is obtained. This is expected because two electrons now occupy an orbital which puts antibonding character between two adjacent nuclei.

III. Properties of Transition-Metal Clusters as Functions of Size: The Approach to the Bulk

The previous section of this review has concentrated on the detailed chemical bonding and electronic architecture of small transition-metal molecules of definite size. In this section the broader question of how many atoms are required before the bulk metallic state is reached is considered. Of course, such a question has no precise answer, since the bulk metallic state is only approached, never truly reached. In addition, the properties of a bulk solid metal depend considerably on the crystalline face under consideration. Also, different properties may approach the bulk values at different rates. The real question is: how quickly are bulk properties approached, and in what manner does this occur? In this section an outline is provided of what is presently known about the approach of various properties of transition-metal clusters to the limiting bulk values.

A. Ionization Potentials, Electron Affinities, and the Development of Band Structure

Few physical properties, if any, are as directly relevant to chemistry as are ionization potentials. Ionization potentials provide direct measures of the amount of energy required to remove an electron from a compound and therefore are a measure of the compound's ability to donate electrons in a chemical reaction. For metals, this property varies dramatically with cluster size, typically falling by 3 eV (or more) as one proceeds from atom to bulk. This is illustrated in Table 25 which displays the atomic ionization potentials, bulk work functions, and atomic electron affinities for the transition metals.

A careful study of the approach of the ionization potential to the bulk work function has been provided by Schumacher and co-workers for the alkali metals;[134,135] similar studies now exist for V_n,[485] Fe_n,[130,131] Ni_n,[486] Cu_n,[50] and Nb_n[486,487] clusters. In the case of Ni_n and Cu_n clusters, the fluence dependence of the photoionization yield using various fixed-frequency lasers

TABLE 25. Atomic Ionization Potentials, Bulk Work Functions, and Atomic Electron Affinities of the Transition Metals (eV)[j]

element	Sc	Ti	V	Cr	Mn	Fe	Co	Ni	Cu	Zn
IP	6.56[a]	6.83[a]	6.74[a]	6.763[a]	7.432[a]	7.90[a]	7.86[a]	7.633[a]	7.724[a]	9.391[a]
work function	3.3[i]	3.95[i]	4.12[i]	4.58[i]	3.83[i]	4.31[i]	4.41[i]	4.50[i]	4.4[i]	4.24[i]
electron affinity	0.189[h]	0.080[c]	0.526[c]	0.667[c]	<0[g]	0.151[b]	0.662[b]	1.157[d]	1.226[e]	0[g]
element	Y	Zr	Nb	Mo	Tc	Ru	Rh	Pd	Ag	Cd
IP	6.5[a]	6.95[a]	6.77[a]	7.10[a]	7.28[a]	7.364[a]	7.46[a]	8.33[a]	7.574[a]	8.991[a]
work function	3.3[i]	3.9[i]	3.99[i]	4.3[i]	(4.4)[i]	4.60[i]	4.75[i]	4.8[i]	4.3[i]	4.1[i]
electron affinity	0.308[h]	0.427[c]	0.894[c]	0.747[c]	0.7[g]	(1.1)[g]	1.138[c]	0.558[c]	1.303[e]	0[g]
element	La	Hf	Ta	W	Re	Os	Ir	Pt	Au	Hg
IP	5.61 ± 0.03[a]	7[a]	7.88[a]	7.98[a]	7.87[a]	8.7[a]	9[a]	9.0[a]	9.22[a]	10.43[a]
work function	3.3[i]	3.53[i]	4.12[i]	4.5[i]	5.0[i]	4.7[i]	5.3[i]	5.32[i]	4.3[i]	4.52[i]
electron affinity	(0.5)[g]		0.323[c]	0.816[c]	(0.15)[g]	(1.1)[g]	1.566[c]	2.128[f]	2.309[f]	<0[g]

[a] Reference 3. [b] Reference 41. [c] Reference 479. [d] Reference 480. [e] Reference 481. [f] Reference 482. [g] Reference 439. [h] Reference 483. [i] Reference 484. [j] Estimated or uncertain values are given in parentheses.

TABLE 26. Ionization Thresholds of Transition-Metal Clusters (eV)

n	V_n[a]	Fe_n[b]	Ni_n[c]	Cu_n[d]	Nb_n[a,e]
1	6.74[f]	7.90[f]	7.633[f]	7.724[f]	6.77[f]
2	6.10 ± 0.05	6.30 ± 0.01	7.1 ± 0.7[g]	7.894 ± 0.015	...
3	5.49 ± 0.05	6.45 ± 0.05	6.0 ± 0.4	5.78 ± 0.20[h]	...
4	5.63 ± 0.05	6.40 ± 0.10	6.0 ± 0.4	7.15 ± 0.75	5.58 ± 0.05
5	5.47 ± 0.05	5.95 ± 0.05	6.0 ± 0.4	5.99 ± 0.41	5.43 ± 0.05
6	5.37 ± 0.05	5.90 ± 0.10	7.15 ± 0.75	7.15 ± 0.75	5.34 ± 0.05
7	5.24 ± 0.05	5.75 ± 0.05	6.0 ± 0.4	5.99 ± 0.41	5.32 ± 0.05
8	5.36 ± 0.05	5.65 ± 0.05	6.0 ± 0.4	5.99 ± 0.41	5.46 ± 0.05
9	5.20 ± 0.05	5.45 ± 0.05	6.0 ± 0.4	5.28 ± 0.30	4.93 ± 0.05
10	5.17 ± 0.05	5.37 ± 0.10	6.0 ± 0.4	5.28 ± 0.30	5.33 ± 0.05
11	4.99 ± 0.05	5.35 ± 0.05	6.0 ± 0.4	5.28 ± 0.30	4.72 ± 0.05
12	4.95 ± 0.05	5.45 ± 0.05	6.0 ± 0.4	5.28 ± 0.30	4.91 ± 0.05
13	4.93 ± 0.05	5.50 ± 0.05	6.0 ± 0.4	5.28 ± 0.30	4.84 ± 0.05
14	4.96 ± 0.05	5.65 ± 0.05	6.0 ± 0.4	5.28 ± 0.30	4.65 ± 0.05
15	≤4.70	5.60 ± 0.10	6.0 ± 0.4	5.28 ± 0.30	≤4.60
16	4.99 ± 0.05	5.55 ± 0.05	6.0 ± 0.4	5.28 ± 0.30	4.76 ± 0.05
17	5.00 ± 0.05	5.50 ± 0.05	6.0 ± 0.4	5.28 ± 0.30	≤4.60
18	4.91 ± 0.05	5.55 ± 0.10	6.0 ± 0.4	5.28 ± 0.30	4.60 ± 0.05
19	≤4.70	5.25 ± 0.05	6.0 ± 0.4	5.28 ± 0.30	≤4.60
20	≤4.70	5.25 ± 0.05	6.0 ± 0.4	5.28 ± 0.30	≤4.60
21	≤4.70	5.25 ± 0.05	6.0 ± 0.4	5.28 ± 0.30	≤4.60
22	≤4.70	5.25 ± 0.05	6.0 ± 0.4	5.28 ± 0.30	≤4.60
23	...	5.15 ± 0.15	6.0 ± 0.4	5.28 ± 0.30	4.67 ± 0.05
24	...	5.15 ± 0.15	6.0 ± 0.4	5.28 ± 0.30	4.73 ± 0.05
25	...	5.15 ± 0.15	6.0 ± 0.4	5.28 ± 0.30	4.68 ± 0.05
26	...	...	...	...	4.77 ± 0.05
27	...	...	...	...	4.67 ± 0.05
28	...	...	...	...	4.60 ± 0.05
...					
...					
∞	4.12[i]	4.31[i]	4.50[i]	4.4[i]	3.99[i]

[a] Reference 485. [b] Reference 131. [c] Reference 486. [d] Reference 50. [e] Reference 487. [f] Reference 3. [g] Reference 47. [h] Reference 52. [i] Reference 484.

was used to roughly bracket the ionization potential as a function of cluster size.[50,486] This method provides only a crude measure of the approach to the bulk work function but is useful nevertheless. In the case of V_n, Fe_n, and Nb_n, tunable lasers have been used and the ionization thresholds are more precisely known.[131,485,487]

Table 26 summarizes our knowledge of the ionization thresholds of V_n, Fe_n, Ni_n, Cu_n, and Nb_n clusters. Although the data are limited and in the cases of Ni_n and Cu_n are not very precise, it is apparent that the approach to the bulk work function is not monotonic in any of these cases. It is also clear that the limiting bulk work function has not yet been reached, even for 25-atom clusters.

Among the smaller copper clusters we see a pronounced even–odd alternation, with odd clusters having lower ionization thresholds than their neighboring even clusters. This has been observed in the alkalis as well[134,135] and is readily explained in terms of simple molecular orbital theory. Treating copper as possessing a single valence electron, in the even clusters all the valence electrons occupy bonding orbitals; in the odd clusters, however, one electron is unpaired and occupies a nonbonding or weakly antibonding orbital. This nonbonding electron is easily removed, leading to a lower ionization potential for the odd clusters.

In the open d-shell transition metals, vanadium, iron, nickel, and niobium, the approach of the ionization potential to the bulk work function is also nonmonotonic, but less amenable to simple explanation. Local maxima in ionization potential occur for V_4, V_8, V_{14}, and V_{17}, for Fe_3, Fe_{14}, and Fe_{18}, for Ni_6, and for Nb_8, Nb_{10}, Nb_{12}, Nb_{16}, Nb_{24}, and Nb_{26}. At present there is no reliable explanation for these trends in ionization potentials. The nonmonotonic pattern of ionization thresholds as functions of cluster size, however, does

TABLE 27. Electron Affinities of Copper Clusters (eV)[a]

n	Cu_n electron affinity	n	Cu_n electron affinity
1	1.226[b]	19	2.70 ± 0.27
...	...	20	<2.97
...	...	21	<2.97
...	...	22	<2.97
7	1.87 ± 0.08	23	<2.97
8	<1.44	24	<2.97
9	2.27 ± 0.06	25	<2.97
10	2.01 ± 0.06	26	<2.97
11	2.38 ± 0.07	27	<2.97
12	2.14 ± 0.07	28	<2.97
13	2.60 ± 0.17	29	>2.97
14	2.08 ± 0.02	30	<2.97
15	2.58 ± 0.14	...	...
16	2.32 ± 0.12	...	...
17	<2.72	...	...
18	2.57 ± 0.13	∞	4.4[c]

[a] Reference 489. [b] Reference 481. [c] Reference 484.

suggest that small clusters of transition-metal atoms have distinct electronic properties and may possess distinctive chemical properties which vary with cluster size as well. This important point has been verified in chemical reactivity experiments, which are discussed below.

Recent work has demonstrated that intense beams of jet-cooled transition-metal cluster *anions* can be produced by using a laser-vaporization source.[488] This achievement is quite significant because it enables the measurement of photodetachment thresholds and thereby electron affinities as functions of cluster size. Such an experiment has now been carried out by Zheng and co-workers for copper clusters.[489] Using a pulsed dye laser, Zheng et al. measured the photodetachment fluence dependence for particular jet-cooled, mass-selected copper clusters and found the wavelengths at which a transition from two-photon to one-photon detachment occurred.[489] The result was identified as the cluster adiabatic electron affinity and is given in Table 27.

Immediately apparent from Table 27 is the lower electron affinity of even copper clusters compared to their odd neighbors. Zheng et al. have explained this observation within the simple molecular orbital model mentioned above.[489] Among the even clusters, molecular orbitals are either strongly bonding or strongly antibonding, with the bonding orbitals filled in the neutral clusters. Hence the additional electron of the anion occupies a molecular orbital of antibonding character and is readily detached. In the odd clusters a nonbonding or weakly antibonding orbital is half-filled, and an electron added to the cluster to form the anion is more strongly bound than would be the case if it occupied a purely antibonding orbital. In both ionization potential and electron affinity, the odd clusters are analogous to the odd-numbered conjugated polyenyl radicals (allyl, pentadienyl, ...) which possess a singly occupied molecular orbital which is nonbonding in character, while the even clusters are analogous to the even polyenes (ethylene, butadiene, ...), which have a large gap between the filled bonding orbitals and the empty antibonding orbitals. This observation is not meant to suggest that the copper clusters are linear, with a delocalized $4s\sigma$ framework; rather, an interesting analogy is observed, which may serve to guide our thinking concerning these interesting species. This general pattern of increased stability of odd-numbered cluster cations and anions of the coinage metals has also been observed by secondary ion mass spectrometry (SIMS)[490-492] and in studies using the liquid metal ion source (LMIS) as well.[492,493]

It is useful to examine whether the overall trends in ionization potential and electron affinity of metal clusters as functions of size conform qualitatively to the formulae

$$\mathrm{IP}(R) = W + \tfrac{3}{8}\, e^2/R \tag{3.1}$$

$$\mathrm{EA}(R) = W - \tfrac{5}{8}\, e^2/R \tag{3.2}$$

which were given in section II.A.6. These formulae were derived by assuming metal clusters which behave as uniform conducting spheres of radius R, with a bulk work function given by W.[132-135] Assuming an atomic volume V, a spherical cluster volume NV for the N-atom cluster, and expressing W, IP, and EA in electron volts, the formulae become

$$\mathrm{IP}(N) = W + 8.705N^{-1/3}V^{-1/3} \tag{3.3}$$

$$\mathrm{EA}(N) = W - 14.508N^{-1/3}V^{-1/3} \tag{3.4}$$

where V is the atomic volume in cubic angstroms. Fitting the observed cluster ionization thresholds (excluding the atomic ionization potentials and bulk work functions) to this functional form allows one to verify if reasonable bulk work functions, W, and atomic volumes are obtained. With this procedure and the values given in Table 26 fitted values of (W, V) of (3.89 eV, 35.5 Å^3), (4.21 eV, 25.2 Å^3), and (3.49 eV, 17.5 Å^3) are obtained for vanadium, iron, and niobium clusters, respectively. These compare to accepted bulk values of (4.12 eV, 14.19 Å^3), (4.31 eV, 11.80 Å^3), and (3.99 eV, 18.00 Å^3), respectively. For copper cluster electron affinity data fitted values are obtained of (W, V) = (4.30 eV, 31.6 Å^3), as compared to accepted values of (4.4 eV, 11.83 Å^3). It appears that the functional dependence of ionization potential and electron affinity is on average a linear function of $N^{-1/3}$, extrapolating rather well to the bulk work function. Interpretation of the slope in terms of an average atomic volume appears erroneous, however, in contrast to Schumacher's results for the simpler alkali-metal clusters.[134,135]

Finally, a very intriguing study of autoionizing inner-shell transitions in mercury clusters has been reported by Brêchignac et al.[494] In this work the autoionizing transitions corresponding to the atomic Hg ($5d^{10}6s^2\ ^1S_0$) → Hg ($5d^96s^2(D_{5/2,3/2})6p$) transitions were observed for mercury clusters of up to eight atoms. Synchrotron radiation was used to provide tunable radiation in the 9–12-eV range, and photoionization was detected by using a quadrupole mass spectrometer to follow the autoionizing transitions as functions of cluster size. To my knowledge this is the first direct measurement of the development of electronic band structure in metal clusters of definite size. Brêchignac et al. find that the energies of the two autoionizing transitions indicated above drop as cluster size increases, occurring at energies given by the functional form $h\nu = \epsilon_0 + C/n$, where n is the number of atoms in the cluster. Despite this functional dependence, however, the value of ϵ_0 which fits the data differs greatly from the bulk value as derived from ESCA measurements. This demonstrates that mercury clusters of up to eight atoms still differ strongly from bulk mercury in the energetic positioning of the electronic

bands. Moreover, smooth extrapolation of the band positions does not lead to the bulk values. This leaves open the tantalizing question: Over what size range is the bulk electronic structure attained? Does the mercury system undergo a phase transition to metallic behavior over a narrow cluster size range, or does the electronic structure evolve smoothly, leading eventually to the bulk metallic state? Further experiments are needed to resolve this and related questions.

B. Response of Clusters to External Fields: Magnetic Moments and Electric Polarizabilities

Another set of fundamental properties of metal clusters involve their response to external electric and magnetic fields. The questions one would like to resolve include: At what point does an iron cluster (for example) become paramagnetic, and at what point does ferromagnetism set in? To what extent is the electron density in a cluster free to move in response to an externally applied electric field?

Very few experimental studies have yet addressed these points. Only three studies of metal cluster magnetic moments have as yet been reported.[495-497] In these studies the investigators have used a Stern–Gerlach magnet in conjunction with a supersonic cluster beam and have directly measured the magnetic deflection of the metal clusters. This deflection is proportional to $\mu_n (dB/dZ)/M_n v_n^2$ where μ_n is the magnetic moment of the n-atom cluster, dB/dZ is the gradient of the magnetic field, M_n is the mass of the n-atom cluster, and v_n is its velocity. In the first measurement of the magnetic moments of metal clusters, Knight et al. determined that small potassium clusters with even numbers of atoms have no magnetic moment and hence possess no net spin.[495] Evidence was also provided that K_5 possesses a magnetic moment equal to that of atomic potassium, corresponding to the expected total spin $S = {}^1/_2$.

A study of the magnetic behavior of Fe_n, Fe_nO, and Fe_nO_2 clusters using similar methods has recently been presented by Cox et al.[496] In this work clusters were formed by laser vaporization of an iron target in the throat of a pulsed supersonic nozzle. The resulting cluster beam was collimated, passed through a Stern–Gerlach magnet, and detected by photoionization in a limited spatial region. Photoions were analyzed by using a time-of-flight mass spectrometer. The instrument was calibrated by using the magnetic deflection of the atomic iron ($^5D_4$) ground state, and magnetic moments of 6.5 ± 1, 8.1 ± 1, and 6.5 ± 1 μ_B were observed for Fe_2, Fe_3, and Fe_2O, respectively.[496] These values are consistent with the theoretically predicted $^7\Delta_u$ ground state of Fe_2,[56,118,138] for which $S = 3$ and a magnetic moment of 6 μ_B is expected, provided electronic orbital angular momentum is neglected. On the basis of these measurements the iron trimer is thought to possess an $S = 4$ ground state.

Investigations of the magnetic behavior of larger iron clusters have proceeded by measuring the depletion of the on-axis signal at high magnetic field gradients.[496] Over the range of clusters from Fe_2 to Fe_{17} the amount of depletion observed is roughly constant, implying that the magnetic moment grows linearly with cluster size. The magnetic moments observed are roughly ≥2.2 μ_B/atom, comparable to or larger than the magnetic moment of bulk iron. These values are consistent with theoretical predictions of 2.7–3.0 μ_B/atom for iron clusters in this size range[131,498-501] and indicate that iron clusters are clearly precursors to bulk ferromagnetic iron.

Cox et al. have also investigated the magnetic properties of aluminum clusters using the depletion method described in the preceding paragraph.[497] Aluminum dimer is strongly depleted, implying a ground state with $S = 1$. Likewise, significant depletion is also observed in Al_6 and Al_8, implying unpaired electrons in these species and most probably a ground electronic state with $S = 1$. On the other hand, Al_{10} and all larger even-numbered clusters show no depletion and probably exist as ground-state singlets. All odd clusters are consistent with $S = {}^1/_2$. The pattern of magnetic moments observed for aluminum clusters is thus completely consistent with that of a system approaching a diamagnetic solid phase.

Of equal interest is the behavior of metal clusters in an external electric field. Using an apparatus similar to the magnetic apparatus mentioned above, Knight et al. have determined the static electric polarizability of alkali clusters.[502] The technique measures the deflection of an alkali cluster beam in an inhomogeneous electric field. The measured electric polarizability per atom decreases from the atomic value with increasing cluster size yet remains 50% above the bulk limit for clusters as large as Na_{40}. More interestingly, a common pattern is observed in sodium and potassium clusters, showing an abrupt drop in polarizability per atom at Na_7 and Na_8, followed by a second drop at Na_{17} and Na_{18}.[502] Knight and co-workers have also observed strongly varying abundances of sodium and potassium clusters in a supersonic expansion using argon carrier gas and have explained these results by the closing of electronic shells in a spherically symmetric jellium model.[503,504] The drops in electric polarizability mentioned above seem to be associated with electronic shell closings for clusters of 8 and 20 atoms. These clusters, along with Na_{40}, Na_{58}, and Na_{92}, are particularly abundant compared to clusters of 9, 21, 41, 59, and 93 atoms, respectively, indicating increased stability of filled electronic shells in the jellium model.[503,504] Thus far no measurements of electric polarizability are available for transition-metal clusters.

C. Metal Cluster Structure and Interatomic Distances

Without a doubt the most vexing question concerning metal clusters is that of structure. This is unfortunately also one of the most difficult aspects to probe. Essentially the only techniques currently available are electron diffraction studies of gas-phase[505-509] and supported[510-514] clusters and EXAFS studies of supported clusters.[128,515-517]

Prior to his untimely death, Gil Stein pioneered the use of electron diffraction techniques to investigate the structure of gas-phase clusters.[505-509] Although many experiments concentrated on clusters of rare gases or of SF_6,[505-507] Stein also succeeded in investigating the structures of Bi_n,[508] Pb_n,[508] In_n,[508] and Ag_n,[509] using an oven to vaporize metal in combination with a supersonic expansion in an inert carrier gas to promote cluster formation. Stein's experiments succeeded in demon-

strating interesting size dependences in metal cluster structure and interatomic distances. Deviations from the bulk fcc structure were observed for silver clusters, particularly for clusters smaller than 80 Å in diameter.[509] A partially liquid or amorphous model was suggested but was not unambiguously demonstrated.[509] More interesting is the case of indium clusters, which appear to undergo a phase transition for clusters smaller than 60 Å in diameter.[508] Below this size indium clusters approach a face-centered cubic arrangement with the lattice parameter ratio c/a approaching 1 for 40 Å diameter clusters (containing approximately 2000 atoms). Clusters above 65 Å in diameter (approximately 6000 atoms), however, take on a face-centered tetragonal arrangement (c/a = 1.06) approaching that of bulk indium (c/a = 1.075).[508]

Wasserman and Vermaak have investigated the interatomic spacing in silver,[510] copper,[511] and platinum[511] particles supported on thin carbon films by electron diffraction methods. These authors present a detailed analysis of the potential errors in the method[510] and criticize previous workers who have based their analysis on overlapping diffraction rings.[512,513] Wasserman and Vermaak report contractions in the lattice parameters of small silver and platinum particles (measured by electron microscopy to have diameters of 20–180 Å) due to surface stress and deduce surface stresses of 1415 ± 300 dyn/cm and 2574 ± 400 dyn/cm for silver and platinum particles, respectively.[510,511] Corresponding measurements for copper particles indicate no observable lattice contraction for clusters as small as 23.7 Å in diameter, placing the surface stress at 0 ± 450 dyn/cm.[511] Measurements on gold particles are well-described by a surface stress of 1175 ± 93 dyn/cm.[514]

Extended X-ray absorption fine-structure (EXAFS) techniques have also been used to investigate nearest-neighbor distances in small copper,[515,516] nickel,[516] iron,[128] and silver[517] particles. EXAFS studies of copper particles deposited on carbon films disagree with the electron diffraction work of Wasserman and Vermaak,[511] indicating a Cu–Cu interatomic distance of 2.33 ± 0.04 Å for the smallest particles.[515,516] Nickel particles deposited on thin carbon films exhibited a stronger contraction, yielding an interatomic distance of 2.24 ± 0.04 Å for the smallest particles.[516] These compare with the known bond lengths of the gas-phase copper and nickel dimers of 2.22[7] and 2.20 Å,[47] respectively. Purdum et al. have investigated small iron particles supported in solid neon and also find a considerable contraction in nearest-neighbor distances compared to bulk iron, but this occurs for clusters of unspecified size.[128] Finally, Montano et al. report on EXAFS study of argon-isolated silver clusters of known size and find a contraction in near-neighbor distances which is consistent with a surface stress of 2286 ± 200 dyne/cm,[517] in reasonable agreement with the measurements of Wasserman and Vermaak.[510] The coordination number obtained for the smallest silver particles was N = 11 ± 2, showing little if any departure from a face-centered cubic structure (N = 12), even for clusters as small as 25 Å in diameter.[517]

D. Dissociation of Multiply Charged Clusters: Coulomb Explosions

Small clusters which are multiply charged have been demonstrated to be unstable with respect to dissociation for sufficiently small clusters and sufficiently high charges.[518–521] This instability is due to the Coulomb repulsion of the charges, which counteracts the normal bonding forces in the cluster, leading to a "Coulomb explosion". The minimum number of atoms necessary for a cluster to stabilize a charge q+, N_q, is thus characteristic for each material and is determined by the bonding forces and cluster geometry. The number of atoms or molecules required to stabilize a cluster of charge q+ are given in Table 28 as experimentally determined by various researchers.[520–531] From this table it is evident that small metal clusters are in general far more readily capable of stabilizing multiple charges than are van der Waals or ionic clusters.

TABLE 28. Smallest Observed Multiply Charged Clusters

material	smallest observed clusters: doubly charged	triply charged	quadruply charged	ref
Kr	Kr_{73}^{2+}			519
Xe	Xe_{52}^{2+}	Xe_{114}^{3+}	Xe_{208}^{4+}	518, 528
CO_2	$(CO_2)_{44}^{2+}$	$(CO_2)_{108}^{3+}$	$(CO_2)_{216}^{4+}$	529
c-C_4H_8	$(c\text{-}C_4H_8)_{30}^{2+}$			530
NaCl	$(NaCl)_{20}^{2+}$			530
NaI	$(NaI)_{20}^{2+}$			518
PbO	$(PbO)_3^{2+}$			531
$PbCl_2$	$Pb_{11}Cl_{21}^{2+}$			531
Si	Si_3^{2+}			527
Ni	Ni_3^{2+}			527
Sn	Sn_3^{2+}			523
Sb	Sb_3^{2+}			525
W	W_3^{2+}			527
Au	Au_3^{2+}			492, 522, 527
Hg	Hg_5^{2+}			526
Pb	Pb_7^{2+}			520
Bi	Bi_3^{2+}			524

Several investigators have presented theoretical models to calculate the stability of multiply charged clusters.[521,532] All models are based on a comparison of the estimated binding energy (relative to the lowest energy fragmentation channel) with the repulsive energy due to Coulomb forces. Using this procedure and assuming fragmentation of van der Waals clusters into symmetric fragments (fission), Tomânek et al. predict critical sizes for doubly, triply, and quadruply charged clusters in the proportion $N_{crit}^{(2)}:N_{crit}^{(3)}:N_{crit}^{(4)}$ = 1:2.3:3.7.[512] This compares well with the proportions 1:2.19:4.00 and 1:2.45:4.91 found for xenon[518,528] and CO_2[529] clusters, respectively. Using Lennard–Jones parameters from the literature, Kreisle et al.[521] have been extremely successful in predicting the limits of stability of multiply charged clusters of Kr, Xe, and CO_2 by using a model with no adjustable parameters.

In the case of metallic clusters, however, greater difficulties arise. This is particularly evident for mercury clusters, which interact by van der Waals forces in the neutral cluster. Application of simple theories predicts the smallest stable doubly charged mercury cluster to contain 300–400 atoms, in marked contrast to the experimental observation of Hg_5^{2+}.[526] Bréchignac et al. have rationalized this discrepancy by considering the polarization energy of an Hg^{2+} ion surrounded by four Hg atoms.[526] The calculated polarization energy stabilizes the Hg_5^{2+} cluster at an energy below the dissociation limit into two ions. Although this model of the electronic structure of Hg_5^{2+} is undoubtedly oversimplified, it suggests that the high polarizability of

metals contributes substantially toward their ability to stabilize multiple charges on small clusters.

E. Chemical Reactions of Neutral Clusters

As alluded to above (section III.A), one of the more intriguing possibilities is that transition-metal clusters of differing sizes may exhibit different chemistries. This possibility has led to an enormous research effort regarding the reactivity of various unsupported metal particles in matrices and in solvents. This fast-growing field was reviewed in 1982[533] and lies beyond the scope of the current review. In this subsection only investigations of the gas-phase chemical reactions of neutral transition-metal clusters of definite size are reviewed.

Investigations of chemical reactions of gas-phase, neutral transition-metal clusters have only been possible since 1984, when the laser-vaporization, supersonic expansion source was first mated onto a flow-tube reactor. Several groups are now providing interesting results using these methods.[534-545] In some of the earliest work reported, Geusic et al. demonstrated that metal clusters of different sizes indeed possess significantly different chemistries.[534] In this preliminary study it was found that clusters of cobalt and niobium vary in their reactivity with deuterium by orders of magnitude over the 3–20-atom size range.[534] Moreover, the variation in reactivity is far from monotonic, with certain clusters being particularly stable and unreactive (e.g., Nb_8, Nb_{10}, and Nb_{16}).[534] In subsequent work this pattern of reactivity was fully confirmed and was demonstrated for the reactions of cobalt and niobium clusters with N_2 as well.[536] Iron clusters also show a strong size dependence in their reactivity with hydrogen,[536,538] but nickel clusters display only a monotonic dependence.[536]

In contrast to these results involving reactions between transition-metal clusters and H_2, D_2, or N_2, reactions with CO, O_2, H_2S, and NH_3 show little cluster size specificity.[536,541,543] This seems to be true for transition-metal cluster reactions with benzene, naphthalene, pyridine, and pyrimidine as well.[546] It thus appears that it is possible to divide metal cluster reactions into two categories: (1) those which occur with high rates and little size specificity, i.e., *facile* reactions, and (2) those which exhibit rates which are strongly dependent on cluster size and may be characterized as *demanding* reactions. In the instances thus far investigated, reactions which are found to be demanding on clusters are known to exhibit widely varying reaction probabilities on differing surface planes of the corresponding bulk metallic crystals. This suggests one possible interpretation: that clusters of varying sizes occur with differing surface geometries, with the result that certain clusters have the correct interatomic distances, surface defects, or surface sites to permit reaction readily, while others do not. This opens the intriguing possibility that clusters of particular sizes may correspond to reaction sites of the bulk metallic surface, isolated in small molecule form.

An alternate explanation has been emphasized by the Exxon group.[485,487,544] These investigators have noted a strong correlation between cluster reactivity with hydrogen and ionization potential: clusters with high ionization potentials relative to clusters of a few more or a few less atoms exhibit a lower rate of reaction with hydrogen than their neighboring clusters. This is definitely true for niobium clusters, in which the local ionization potential maxima at Nb_8, Nb_{10}, Nb_{16}, Nb_{24}, and Nb_{26} correspond to particularly unreactive clusters.[485,487,536] Likewise, the local ionization potential maximum for Fe_{13}–Fe_{16} correlates rather closely with a reactivity minimum for Fe_{15}–Fe_{19}.[536,538,544] Whetten et al. have proposed that the mechanism of hydrogen reaction on a metal cluster involves donation of metal d electrons into the H_2 σ^* orbital.[544] Presumably this is accompanied by back-donation from the H_2 σ orbital into the metal s orbitals, thereby breaking the H_2 bond and forming two new metal–hydrogen bonds. While this picture is very appealing and doubtless contains an element of truth, it remains true that the ionization potential of the metal cluster is not the sole determinant of chemical reactivity. Nb_4, for example, has an ionization potential 0.82 eV higher than Nb_{16} and would be expected to be much less reactive than Nb_{16} under this reasoning.[485] Quite to the contrary, Nb_4 is about a factor of 6 more reactive than Nb_{16}.[485] At this point it remains an open question why certain clusters are particularly reactive or unreactive, and why the ionization potential as a function of cluster size fluctuates in the observed manner.

The most careful and definitive work on transition-metal cluster reactivity has been provided by the Argonne group in their beautiful studies of the Fe_n + H_2/D_2 reaction.[538-540] These investigators use a continuous-flow system which permits the measurement of absolute reaction rate constants, for species as large as Fe_{68}.[538] In addition, reaction rates have been measured for different temperatures of the reactants, shedding new light on the reactive process. Clusters which are unreactive under cool conditions become more reactive when warmed, consistent with an activated process.[538] Clusters which are reactive under cool conditions, however, become less reactive when warmed.[538] In these cases desorption of H_2 prior to deactivation of the reaction complex competes with product stabilization.[538] For clusters larger than Fe_{23}, the reaction rate constants measured by Richtsmeier et al.[538] are consistent with bulk values of the sticking probability measured in surface experiments, indicating a rather abrupt onset of bulk behavior in this regard.

In the second paper of the Argonne series, the composition of fully hydrogenated iron clusters was examined.[539] Below about Fe_{30} hydrogenated clusters were formed with a 1:1 ratio of H:Fe. Above this cluster size, the ratio of H:Fe decreases, consistent with a model in which one surface site capable of chemically bonding a hydrogen atom is associated with each surface iron atom. Within this model the data are equally consistent with icosahedral, face-centered cubic, or body-centered cubic packings.[539]

Finally, Liu et al. report multiphoton dissociation measurements for the fully hydrogenated iron clusters.[540] In this study, it is found that absorption of ultraviolet light below the ionization limit leads to rapid conversion of electronic to vibrational energy, with a resulting loss of H_2 molecules from the cluster. The pattern of H_2 molecular losses observed could be interpreted with the aid of an RRKM model to provide the critical desorption energies for hydrogen on various hydrogenated iron clusters. For Fe_{10}–Fe_{32}, values in the range 1.21–1.34 eV were obtained,[540] somewhat higher

than those reported for bulk iron (0.8–1.1 eV).[547,548]

In more recent work the Argonne group has investigated reactions of iron clusters with ammonia.[541] Compositions of the fully ammoniated products indicate binding of one ammonia for every three surface atoms. Ammonia desorption occurs with multiphoton excitation; an RRKM investigation similar to that outlined above gives a binding energy of approximately 1.3 eV. More interesting, however, is the observation that ammoniated iron clusters react with H_2. Despite the fact that the fully ammoniated clusters have ionization potentials as much as 2.0 eV lower than the bare clusters, the rate with which these species react with H_2 is about an order of magnitude less than the bare clusters. Nevertheless, a strong dependence of reaction rate on cluster size is still apparent but is shifted relative to the bare iron clusters. For ammoniated clusters it is the Fe_{13} species which is unreactive, as opposed to the Fe_{17} species which is unreactive for the bare clusters.[541]

In addition to these investigations Gole et al. have been able to observe chemiluminescent oxidation of silver clusters with ozone.[549] These studies employ a hot oven source and demonstrate the possibilities inherent to this technique very well. One should also note that the Exxon group has recently demonstrated the ability to desorb methanol from iron clusters by infrared multiphoton absorption.[545] This experiment opens the very important prospect of establishing a viable infrared spectroscopy of molecules chemisorbed on clusters, using desorption as a means of determining that the infrared laser is tuned to an absorption feature. From these preliminary results it is clear that tremendous strides will be made in this field as it matures further.

F. Chemical Reactions of Ionized Clusters

Investigations of the chemical reactions of transition-metal cluster ions have also benefitted from recent technological advances and show great promise for the future. Many additional experimental techniques are available for the study of ions than are available for neutrals; as a result a much more detailed knowledge of certain aspects of their chemistry is possible than is the case for the neutral clusters. Thus, for example, it is relatively simple to study reactivity as a function of kinetic energy, to determine reaction product composition directly by mass spectrometry, and to investigate bond energies by measuring the thresholds for chemical reaction. Chemical reactions of atomic transition metal ions have been extensively studied by using these techniques,[550–558] though much remains to be learned.

Chemical reactions of transition-metal *cluster* ions have been far less extensively studied. Armentrout et al. have investigated the reaction between Mn_2^+ and O_2 as a function of relative energy using an ion beam guide technique.[559] The results are typical of an exothermic reaction, showing a reaction rate about half the collision rate at low kinetic energies. However, the products observed include Mn_2O^+, Mn^+, and MnO^+, so several reactive channels are apparently open at low energy. Armentrout et al. have carefully investigated these possibilities and have provided a list of reaction energies which are consistent with their data. This makes the $Mn_2^+ + O_2$ system one of the best-understood of the metal cluster–reactant systems studied to date.

Hanley and Anderson have used a similar radio-frequency ion guide to investigate reactions of metal clusters produced by sputtering.[560,561] Although the sputtering technique produces hot clusters, these authors demonstrate that with proper care clusters may be collisionally cooled prior to entering the chemical reaction zone. Although the current results with this technique are rather preliminary, it is clear that sputtering provides a convenient means of producing metal cluster ions and that this technique holds some promise, provided the internal motions of the ions can be cooled to acceptable levels.

An alternative to ion beam studies is provided by ion cyclotron resonance (ICR) methods. Although collision energies are generally less accurately known than in guided ion–beam studies, ion cyclotron methods compensate for this deficiency by permitting highly accurate mass measurements and by allowing one to follow several reaction steps in a single experiment. In addition, the long trapping times possible in ICR experiments (on the order of seconds) permit chemical equilibrium to be reached in many reactions, thereby providing direct measurements of equilibrium constants. These methods have been extensively used to investigate relative ligand binding energies to various transition-metal atomic ions.[562–566]

Transition-metal cluster ions have been produced by electron impact on volatile transition-metal carbonyls,[567–570] by multiphoton dissociation/ionization of the volatile carbonyls,[571] and by reaction of transition-metal atomic ions generated by laser vaporization with transition-metal carbonyls, followed by removal of CO ligands by collision-induced dissociation.[572–574] More recently metal cluster ions have been produced by laser vaporization in the throat of a pulsed supersonic expansion, followed by laser photoionization and injection into an ICR cell.[575] All of these methods show great promise as techniques for metal cluster ion production for ICR studies of reactivity.

Among the results reported to date using the ion cyclotron resonance method is the observation that Mn_2^+ and Co_2^+ are unreactive with alkanes,[567] as is Mn^+.[567] The observation that both Co^+[576] and Co_2CO^+[568] are highly reactive with alkanes has led to the suggestion that a concentrated positive charge on Co, as occurs in Co^+ and is postulated on one end of Co_2CO^+, is necessary for insertion into the alkane C–H bond.[568] In other work from Ridge's laboratory, Mn_2^+ has been reacted with a series of Lewis bases to form $MnB^+ + Mn$.[569] This work, in combination with the measured[562] equilibria for base exchange $MnA^+ + B \rightleftarrows MnB^+ + A$ and the measured bond energy of Mn_2^+[115] has permitted the construction of an absolute scale of Mn^+ affinities of various Lewis bases.[569]

In other recent studies using the ICR technique, Jacobson and Freiser have investigated the chemistry of mixed iron–cobalt cluster ions.[572–574] These authors produce the mixed cluster ions by first laser desorbing metal atomic cations from a solid metal sample. These atomic ions then collide with a volatile transition-metal carbonyl to form a polynuclear metal carbonyl ion, through reactions such as $Fe^+ + Co_2(CO)_8 \rightarrow FeCo_2(CO)_5^+ + 3CO$. The resulting polynuclear ion is accelerated and collided with inert gas to strip the remaining carbonyls, leaving the bare transition-metal cluster ion. At high inert gas pressures excess energy

may be thermalized prior to the final phase of the sequence, chemical reaction with an added gas. With this method $CoFe^+$ has been produced, and the Co^+–Fe bond strength has been found to lie between those of Co^+–benzene and Co^+–CH_3CN, thereby providing $D_0(Co^+–Fe) = 2.86 \pm 0.30$ eV.[572] $CoFe^+$, like Mn_2^+ and Co_2^+,[567] is unreactive with alkanes but is quite reactive toward alkenes, leading primarily to dehydrogenation products.[574] Collisional activation of these products leads in some cases to facile dehydrocyclizations.[574] For a detailed look at the chemistry of $CoFe^+$ the interested reader is referred to the paper by Jacobson and Freiser,[574] which demonstrates quite convincingly the power of the ICR technique, as applied to the chemistry of metal clusters. Recent extensions of this work to $FeCo_2^+$ shows that the method is not limited to simple diatomic species.[573]

Finally, a promising study of Alford, Williams, and Smalley[575] demonstrates that the laser vaporization–supersonic expansion source can be coupled to an ICR instrument. With this method bare niobium clusters of up to six atoms have been successfully injected into the ICR cell, with a net trapping efficiency of roughly 60%. It thus appears likely that the chemistry of quite large metal clusters will be accessible for experimental study in the immediate future.

IV. Summary and Outlook

In the preceding sections the current state of our knowledge of the bare transition-metal clusters has been summarized. Clearly much of this knowledge has been obtained through recent breakthroughs in experimental techniques, new theoretical methods, and the recent availability of supercomputers. Despite the considerable advances which these have enabled, our understanding of transition-metal clusters and their chemistry is negligible compared to our current knowledge of other fields of chemistry, such as the chemistry of carbon compounds.

It is reasonable to expect that the continued interplay between theory and experiment will lead to a vastly improved understanding of the transition-metal clusters in the next decade. Within this time frame questions of chemical bonding in the diatomic transition-metal molecules will certainly be addressed, and the chemical reactivity of the transition-metal clusters will undoubtedly be thoroughly investigated. Physical properties (ionization potential, electron affinity, magnetic moment, electric polarizability, etc.) will be studied, and it is likely that a photoelectron spectroscopy of size-selected metal clusters will be developed. The single most difficult aspect to determine, however, is the geometrical structure of small polyatomic clusters. It is by no means certain that general experimental progress will be made toward this end in the foreseeable future. For this reason, among others, it is important that theoretical methods be developed of general validity for the description of transition-metal cluster structure. The increasing sophistication of computers and theoretical methods and the difficulty of the experimental problem for larger than triatomic clusters leads one to believe that our best hope in this regard lies with the theoreticians. One can expect, however, that experimentalists will continue to provide tests and challenges for theory in this field for some time to come.

V. Acknowledgment

The author gratefully acknowledges helpful discussions with Dr. Richard E. Smalley, especially in the early stages of preparation of this review. I also thank Drs. D. M. Cox, J. L. Gole, S. R. Langhoff, W. C. Lineberger, G. A. Ozin, E. A. Rohlfing, S. J. Riley, D. R. Salahub, R. E. Smalley, D. G. Truhlar, J. J. Valentini, S. P. Walch, W. Weltner, Jr., and R. L. Whetten for communicating their results prior to publication and for helpful discussions and Ms. Cheryl Gabbott for her dedicated efforts in preparing this manuscript. Research on transition-metal clusters in my laboratory at the University of Utah is currently supported by the Research Corp., the National Science Foundation under Grant No. CHE-85-21050, and a Faculty Research Grant from the University of Utah. Acknowledgment is also made to the donors of the Petroleum Research Fund, administered by the American Chemical Society, for support of research related to transition-metal clusters in my laboratory.

VI. References

(1) Weltner, W., Jr.; Van Zee, R. J. *Annu. Rev. Phys. Chem.* **1984**, *35*, 291.
(2) Walch, S. P.; Bauschlicher, C. W., Jr. In *Comparison of Ab Initio Quantum Chemistry with Experiment*; Bartlett, R. J., Ed.; D. Reidel: Dordrecht, 1985, p 17.
(3) Moore, C. E. *Natl. Bur. Stand. Circ. (U.S.)* **1949**, 467.
(4) Kleman, B.; Lindqvist, S. *Ark. Fys.* **1954**, *8*, 333.
(5) Ruamps, J. *C. R. Hebd. Seances Acad. Sci.* **1954**, *238*, 1489.
(6) Ruamps, J. *Ann. Phys. (Paris)* **1959**, *4*, 1111.
(7) Åslund, N.; Barrow, R. F.; Richards, W. G.; Travis, D. N. *Ark. Fys.* **1965**, *30*, 171.
(8) Pesič, D. S.; Weniger, S. *C. R. Hebd. Seances Acad. Sci., Ser. B* **1971**, *272*, 46.
(9) Pesič, D. S.; Weniger, S. *C. R. Hebd. Seances Acad. Sci., Ser. B* **1971**, *273*, 602.
(10) Rao, T. V. R.; Lakshman, S. V. J. *J. Quant. Spectrosc. Radiat.* Transfer. **1971**, *11*, 1157.
(11) Lochet, J. *J. Phys. B* **1978**, *11*, L55.
(12) Kleman, B.; Lindqvist, S. *Ark. Fys.* **1955**, *9*, 385.
(13) Maheshwari, R. C. *Indian J. Phys.* **1963**, *37*, 368.
(14) Choong, S.-P.; Wang, L.-S.; Lim, Y.-S. *Nature (London)* **1966**, *209*, 1300.
(15) Brown, C. M.; Ginter, M. L. *J. Mol. Spectrosc.* **1978**, *69*, 25.
(16) Srdanov, V. I.; Pesič, D. S. *J. Mol. Spectrosc.* **1981**, *90*, 27.
(17) Kleman, B.; Lindqvist, S.; Selin, L. E. *Ark. Fys.* **1954**, *8*, 505.
(18) Ames, L. L.; Barrow, R. F. *Trans. Faraday Soc.* **1967**, *63*, 39.
(19) Ruamps, J. *Spectrochim. Acta, Suppl.* **1957**, *11*, 329.
(20) Joshi, K. C.; Majumdar, K. *Proc. Phys. Soc., London* **1961**, *78*, 197.
(21) Ruamps, J. *C. R. Hebd. Seances Acad. Sci.* **1954**, *239*, 1200.
(22) Drowart, J.; Honig, R. E. *J. Phys. Chem.* **1957**, *61*, 980.
(23) Drowart, J.; Goldfinger, P. *Angew. Chem., Int. Ed. Engl.* **1967**, *6*, 581.
(24) Drowart, J. In *Phase Stability in Metals and Alloys*; Rudman, P. S., Stringer, J., Jaffee, R. I., Eds.; McGraw-Hill: New York, 1967; p 307.
(25) Gingerich, K. A. *J. Cryst. Growth* **1971**, *9*, 31.
(26) Gingerich, K. A. *Chimia* **1972**, *26*, 619.
(27) Gingerich, K. A. *Faraday Symp. Chem. Soc.* **1980**, *14*, 109.
(28) Gurvich, L. V.; Karachevstev, G. V.; Kondrat'yev, V. N.; Lebedev, Y. A.; Mendredev, V. A.; Potapov, V. K.; Khodeev, Y. S. *Bond Energies, Ionization Potentials, and Electron Affinities*; Nauka: Moscow, 1974, in Russian.
(29) Kant, A.; Strauss, B. *J. Chem. Phys.* **1964**, *41*, 3806.
(30) Shim, I.; Gingerich, K. A. *J. Chem. Phys.* **1983**, *78*, 5693.
(31) Jacox, M. E. *J. Mol. Spectrosc.* **1985**, *113*, 286.
(32) Givan, A.; Loewenschuss, A. *Chem. Phys. Lett.* **1979**, *62*, 592.
(33) Kowalski, A.; Czajkowski, M.; Breckenridge, W. H. *Chem. Phys. Lett.* **1985**, *119*, 368.
(34) Jacobi, K.; Scheisser, D.; Kolb, D. K. *Chem. Phys. Lett.* **1980**, *69*, 113.
(35) Grinter, R.; Stern, D. R. *J. Chem. Soc., Faraday Trans. 2* **1983**, *79*, 1011.
(36) Breithaupt, B.; Hulse, J. E.; Kolb, D. M.; Rotermund, H. H.; Schroeder, W.; Schrittenlacher, W. *Chem. Phys. Lett.* **1983**, *95*, 513.
(37) Efremov, Y. M.; Samoilova, A. N.; Gurvich, L. V. *Opt. Spectrosc.* **1974**, *36*, 381.

(38) Efremov, Y. M.; Samoilova, A. N.; Gurvich, L. V. *Chem. Phys. Lett.* **1976**, *44*, 108.
(39) Efremov, Y. M.; Samoilova, A. N.; Kozhukhovsky, V. B.; Gurvich, L. V. *J. Mol. Spectrosc.* **1978**, *73*, 430.
(40) Leopold, D. G.; Miller, T. M.; Lineberger, W. C. *J. Am. Chem. Soc.* **1986**, *108*, 178.
(41) Leopold, D. G.; Lineberger, W. C. *J. Chem. Phys.* **1986**, *85*, 51.
(42) Dietz, T. G.; Duncan, M. A.; Powers, D. E.; Smalley, R. E. *J. Chem. Phys.* **1981**, *74*, 6511.
(43) Langridge-Smith, P. R. R.; Morse, M. D.; Hansen, G. P.; Smalley, R. E. *J. Chem. Phys.* **1984**, *80*, 593.
(44) Michalopoulos, D. L.; Geusic, M. E.; Hansen, S. G.; Powers, D. E.; Smalley, R. E. *J. Phys. Chem.* **1982**, *86*, 3914.
(45) Bondybey, V. E.; English, J. H. *Chem. Phys. Lett.* **1983**, *94*, 443.
(46) Riley, S. J.; Parks, E. K.; Pobo, L. G.; Wexler, S. *J. Chem. Phys.* **1983**, *79*, 2577.
(47) Morse, M. D.; Hansen, G. P.; Langridge-Smith, P. R. R.; Zheng, L.-S.; Geusic, M. E.; Michalopoulos, D. L.; Smalley, R. E. *J. Chem. Phys.* **1984**, *80*, 5400.
(48) Powers, D. E.; Hansen, S. G.; Geusic, M. E.; Puiu, A. C.; Hopkins, J. B.; Dietz, T. G.; Duncan, M. A.; Langridge-Smith, P. R. R.; Smalley, R. E. *J. Phys. Chem.* **1982**, *86*, 2556.
(49) Gole, J. L.; English, J. H.; Bondybey, V. E. *J. Phys. Chem.* **1982**, *86*, 2560.
(50) Powers, D. E.; Hansen, S. G.; Geusic, M. E.; Michalopoulos, D. L.; Smalley, R. E. *J. Chem. Phys.* **1983**, *78*, 2866.
(51) Hopkins, J. B.; Langridge-Smith, P. R. R.; Morse, M. D.; Smalley, R. E. *J. Chem. Phys.* **1983**, *78*, 1627.
(52) Morse, M. D.; Hopkins, J. B.; Langridge-Smith, P. R. R.; Smalley, R. E. *J. Chem. Phys.* **1983**, *79*, 5316.
(53) Verhaegen, G.; Smoes, S.; Drowart, J. *J. Chem. Phys.* **1964**, *40*, 239.
(54) Busby, R.; Klotzbücher, W.; Ozin, G. A. *J. Am. Chem. Soc.* **1976**, *98*, 4013.
(55) Knight, L. B., Jr.; Van Zee, R. J.; Weltner, W., Jr. *Chem. Phys. Lett.* **1983**, *94*, 296.
(56) Harris, J.; Jones, R. O. *J. Chem. Phys.* **1979**, *70*, 830.
(57) Wood, C.; Doran, M.; Hillier, I. H.; Guest, M. F. *Faraday Symp. Chem. Soc.* **1980**, *14*, 159.
(58) Walch, S. P.; Bauschlicher, C. W., Jr. *J. Chem. Phys.* **1983**, *79*, 3590.
(59) Wolf, A.; Schmidtke, H.-H. *Int. J. Quantum Chem.* **1980**, *18*, 1187.
(60) Cooper, W. F.; Clarke, G. A.; Hare, C. R. *J. Phys. Chem.* **1972**, *76*, 2268.
(61) Das, G. *Chem. Phys. Lett.* **1982**, *86*, 482.
(62) Walch, S. P.; Bauschlicher, C. W., Jr. *Chem. Phys. Lett.* **1983**, *94*, 290.
(63) Moskovits, M.; DiLella, D. P.; Limm, W. *J. Chem. Phys.* **1984**, *80*, 626.
(64) Kant, A.; Lin, S.-S. *J. Chem. Phys.* **1969**, *51*, 1644.
(65) Cosse, C.; Fouassier, M.; Mejean, T.; Tranquille, M.; DiLella, D. P.; Moskovits, M. *J. Chem. Phys.* **1980**, *73*, 6076.
(66) Anderson, A. B. *J. Chem. Phys.* **1976**, *64*, 4046.
(67) Klotzbücher, W. E.; Mitchell, S. A.; Ozin, G. A. *Inorg. Chem.* **1977**, *16*, 3063.
(68) Ford, T. A.; Huber, H.; Klotzbücher, W.; Kündig, E. P.; Moskovits, M.; Ozin, G. A. *J. Chem. Phys.* **1977**, *66*, 524.
(69) Andrews, M. P.; Ozin, G. A. *J. Phys. Chem.* **1986**, *90*, 2852.
(70) Barrow, R. F.; DuParcq, R. P.; Ricks, J. M. *J. Phys. B* **1969**, *2*, 413.
(71) Greenwood, D. J.; Barrow, R. F. *J. Phys. B* **1976**, *9*, 2123.
(72) Geusic, M. E.; Morse, M. D.; Smalley, R. E., unpublished results.
(73) Walch, S. P.; Bauschlicher, C. W., Jr.; Roos, B. O.; Nelin, C. J. *Chem. Phys. Lett.* **1983**, *103*, 175.
(74) Salahub, D. R.; Baykara, N. A. *Surf. Sci.* **1985**, *156*, 605.
(75) Salahub, D. R. In *Proceedings of Applied Quantum Chemistry Symposium*; Morokuma, K., Schaefer III, H. F., Smith, V. H., Jr., Eds.; D. Reidel: Dordrecht, in press.
(76) Salahub, D. R. In *Contributions of Cluster Physics to Materials Science and Technology*; Davenas, J., Rabette, P., Eds.; M. Nijhoff: Amsterdam, 1986.
(77) Ackerman, M.; Stafford, F. E.; Verhaegen, G. *J. Chem. Phys.* **1962**, *36*, 1560.
(78) Kant, A.; Strauss, B. *J. Chem. Phys.* **1966**, *45*, 3161.
(79) Kündig, E. P.; Moskovits, M.; Ozin, G. A. *Nature (London)* **1975**, *254*, 503.
(80) Klotzbücher, W. E.; Ozin, G. A. *J. Am. Chem. Soc.* **1978**, *100*, 2262.
(81) Pellin, M. J.; Gruen, D. M. *J. Chem. Phys.* **1983**, *79*, 5887.
(82) DiLella, D. P.; Limm, W.; Lipson, R. H.; Moskovits, M.; Taylor, K. V. *J. Chem. Phys.* **1982**, *77*, 5263.
(83) Moskovits, M.; Limm, W.; Mejean, T. *J. Phys. Chem.* **1985**, *89*, 3886.
(84) Moskovits, M.; Limm, W.; Mejean, T. *J. Chem. Phys.* **1985**, *82*, 4875.
(85) Goodgame, M. M.; Goddard, W. A., III *Phys. Rev. Lett.* **1982**, *48*, 135.
(86) Geusic, M. E.; Michalopoulos, D. L.; Smalley, R. E., unpublished results.
(87) Montano, P. A.; Purdum, H.; Shenoy, G. K.; Morrison, T. I.; Schulze, W. *Surf. Sci.* **1985**, *156*, 228.
(88) Cotton, F. A. *Acc. Chem. Res.* **1978**, *11*, 225.
(89) Trogler, W. C.; Gray, H. B. *Acc. Chem. Res.* **1978**, *11*, 232.
(90) Bursten, B. E.; Cotton, F. A. *Faraday Symp. Chem. Soc.* **1980**, *14*, 180.
(91) Cotton, F. A.; Walton, R. A. *Multiple Bonds Between Metal Atoms*; Wiley: New York, 1982.
(92) Kok, R. A.; Hall, M. B. *Inorg. Chem.* **1983**, *22*, 728.
(93) Klotzbücher, W.; Ozin, G. A. *Inorg. Chem.* **1977**, *16*, 984.
(94) Klotzbücher, W.; Ozin, G. A.; Norman, J. G., Jr.; Kolari, H. J. *Inorg. Chem.* **1977**, *16*, 2871.
(95) Atha, P. M.; Hillier, I. H. *Mol. Phys.* **1982**, *45*, 282.
(96) Goodgame, M. M.; Goddard, W. A., III *J. Phys. Chem.* **1981**, *85*, 215.
(97) McLean, A. D.; Liu, B. *Chem. Phys. Lett.* **1983**, *101*, 144.
(98) Das, G. P.; Jaffe, R. L. *Chem. Phys. Lett.* **1984**, *109*, 206.
(99) Kok, R. A.; Hall, M. B. *J. Phys. Chem.* **1983**, *87*, 715.
(100) Dunlap, B. I. *Phys. Rev. A* **1983**, *27*, 2217.
(101) Von Barth, U.; Hedin, L. *J. Phys. C* **1972**, *5*, 1629.
(102) Janak, J. F.; Moruzzi, V. L.; Williams, A. R. *Phys. Rev. B: Solid State* **1975**, *12*, 1257.
(103) Gunnarsson, O.; Lundqvist, B. I. *Phys. Rev. B: Solid State* **1976**, *13*, 4274.
(104) Vosko, S. H.; Wilk, L.; Nusair, M. *Can. J. Phys.* **1980**, *58*, 1200.
(105) Delley, B.; Freeman, A. J.; Ellis, D. E. *Phys. Rev. Lett.* **1983**, *50*, 488.
(106) Bernholc, J.; Holzwarth, N. A. W. *Phys. Rev. Lett.* **1983**, *50*, 1451.
(107) Baykara, N. A.; McMaster, B. N.; Salahub, D. R. *Mol. Phys.* **1984**, *52*, 891.
(108) Kant, A.; Lin, S.-S.; Strauss, B. *J. Chem. Phys.* **1968**, *49*, 1983.
(109) DeVore, T. C.; Ewing, A.; Franzen, H. F.; Calder, V. *Chem. Phys. Lett.* **1975**, *35*, 78.
(110) Klotzbücher, W. E.; Ozin, G. A. *Inorg. Chem.* **1980**, *19*, 3776.
(111) Rivoal, J.-C.; Shakhs-Emampour, J.; Zeringue, K. J.; Vala, M. *Chem. Phys. Lett.* **1982**, *92*, 313.
(112) Van Zee, R. J.; Baumann, C. A.; Weltner, W., Jr. *J. Chem. Phys.* **1981**, *74*, 6977.
(113) Baumann, C. A.; Van Zee, R. J.; Weltner, W., Jr. *J. Chem. Phys.* **1983**, *78*, 190.
(114) Van Zee, R. J.; Baumann, C. A.; Bhat, S. V.; Weltner, W., Jr. *J. Chem. Phys.* **1982**, *76*, 5636.
(115) Ervin, K.; Loh, S. K.; Aristov, N.; Armentrout, P. B. *J. Phys. Chem.* **1983**, *87*, 3593.
(116) Nesbet, R. K. *Phys. Rev. A* **1964**, *135*, 460.
(117) Lin, S.-S.; Kant, A. *J. Phys. Chem.* **1969**, *73*, 2450.
(118) Shim, I.; Gingerich, K. A. *J. Chem. Phys.* **1982**, *77*, 2490.
(119) Moskovits, M. *Acc. Chem. Res.* **1979**, *12*, 229.
(120) Hulse, J. E. Ph.D. Thesis, University Microfilms, Ann Arbor, MI, 1979.
(121) Moskovits, M.; DiLella, D. P. *J. Chem. Phys.* **1980**, *73*, 4917.
(122) Moskovits, M.; DiLella, D. P. In *Metal Bonding and Interactions in High Temperature Systems*; Gole, J. L., Stwalley, W. C., Eds.; *ACS Symposium Series 179*; American Chemical Society: Washington, DC, 1982; p 153.
(123) LeRoy, R. J.; Bernstein, R. B. *J. Chem. Phys.* **1970**, *52*, 3869.
(124) McNab, T. K.; Micklitz, H.; Barrett, P. H. *Phys. Rev. B: Solid State* **1971**, *4*, 3787.
(125) Montano, P. A.; Barrett, P. H.; Shanfield, Z. *J. Chem. Phys.* **1976**, *64*, 2896.
(126) Montano, P. A. *Faraday Symp. Chem. Soc.* **1980**, *14*, 79.
(127) Montano, P. A. *Solid State Commun.* **1980**, *35*, 53.
(128) Purdum, H.; Montano, P. A.; Shenoy, G. K.; Morrison, T. *Phys. Rev. B: Condens. Matter* **1982**, *25*, 4412.
(129) Baumann, C. A.; Van Zee, R. J.; Weltner, W., Jr. *J. Phys. Chem.* **1984**, *88*, 1815.
(130) Rohlfing, E. A.; Cox, D. M.; Kaldor, A. *Chem. Phys. Lett.* **1983**, *99*, 161.
(131) Rohlfing, E. A.; Cox, D. M.; Kaldor, A.; Johnson, K. H. *J. Chem. Phys.* **1984**, *81*, 3846.
(132) Smith, J. M. *AIAA J.* **1965**, *3*, 648.
(133) Wood, D. M. *Phys. Rev. Lett.* **1981**, *46*, 749.
(134) Schumacher, E.; Kappes, M.; Marti, K.; Radi, P.; Schär, M.; Schmidhalter, B. *Ber. Bunsenges. Phys. Chem.* **1984**, *88*, 220.
(135) Kappes, M. M.; Schär, M.; Radi, P.; Schumacher, E. *J. Chem. Phys.* **1986**, *84*, 1863.
(136) Plieth, W. J. *Surf. Sci.* **1985**, *156*, 530.
(137) Brucat, P. J.; Zheng, L.-S.; Pettiette, C. L.; Yang, S.; Smalley, R. E. *J. Chem. Phys.* **1986**, *84*, 3078.
(138) Anzelm, J.; Radzio, E.; Salahub, D. R., unpublished results.
(139) Upton, T. H.; Goddard, W. A., III *J. Am. Chem. Soc.* **1978**, *100*, 5659.
(140) Shim, I.; Dahl, J. P.; Johansen, H. *Int. J. Quantum. Chem.* **1979**, *15*, 311.

(141) Noell, J. O.; Newton, M. D.; Hay, P. J.; Martin, R. L.; Bobrowicz, F. W. *J. Chem. Phys.* **1980**, *73*, 2360.
(142) Shim, I. *Theor. Chim. Acta* **1981**, *59*, 413.
(143) Shim, I. *Theor. Chim. Acta* **1980**, *54*, 113.
(144) Ozin, G. A.; Hanlan, A. J. L. *Inorg. Chem.* **1979**, *18*, 1781.
(145) DiLella, D. P.; Loewenschuss, A.; Moskovits, M., unpublished data.
(146) Kant, A. *J. Chem. Phys.* **1964**, *41*, 1872.
(147) Huber, H.; Ozin, G. A.; Power, W. J. *J. Am. Chem. Soc.* **1976**, *98*, 6508.
(148) Moskovits, M.; Hulse, J. E. *J. Chem. Phys.* **1977**, *66*, 3988.
(149) Ozin, G. A.; Power, W. J.; Upton, T. H.; Goddard, W. A., III *J. Am. Chem. Soc.* **1978**, *100*, 4750.
(150) Ahmed, F.; Nixon, E. R. *J. Chem. Phys.* **1979**, *71*, 3547.
(151) Anderson, A. B. *J. Chem. Phys.* **1977**, *66*, 5108.
(152) Melius, C. F.; Moskowitz, J. W.; Mortola, A. P.; Baillie, M. B.; Ratner, M. A. *Surf. Sci.* **1976**, *59*, 279.
(153) Basch, H. *Faraday Symp. Chem. Soc.* **1980**, *14*, 149.
(154) Basch, H.; Newton, M. D.; Moskowitz, J. W. *J. Chem. Phys.* **1980**, *73*, 4492.
(155) Shim, I. *Mol. Phys.* **1980**, *39*, 185.
(156) Drowart, J.; Honig, R. E. *J. Chem. Phys.* **1956**, *25*, 581.
(157) Schissel, P. *J. Chem. Phys.* **1957**, *26*, 1276.
(158) Ackerman, M.; Stafford, F. E.; Drowart, J. *J. Chem. Phys.* **1960**, *33*, 1784.
(159) Hilpert, K. *Ber. Bunsenges. Phys. Chem.* **1979**, *83*, 161.
(160) Gingerich, K. A.; Shim, I.; Gupta, S. K.; Kingcade, J. E., Jr. *Surf. Sci.* **1985**, *156*, 495.
(161) Rohlfing, E. A.; Valentini, J. J. *J. Chem. Phys.* **1986**, *84*, 6560.
(162) Steele, R. E. *J. Mol. Spectrosc.* **1976**, *61*, 477.
(163) Smirnov, A. D.; Kuzmenko, N. E.; Kuzyakov, Y. Y. *Opt. Spectrosc. (Engl. Transl.)* **1980**, *48*, 111.
(164) Smirnov, A. D.; Kuzmenko, N. E.; Kuzyakov, Y. Y. *Opt. Spectrosc. (Engl. Transl.)* **1979**, *47*, 149.
(165) Bondybey, V. E.; Schwartz, G. P.; English, J. H. *J. Chem. Phys.* **1983**, *78*, 11.
(166) Singh, N. L. *Phys. Rev.* **1955**, *99*, 1624.
(167) Rao, S. S. S.; Rao, S. V. K. *Indian J. Pure Appl. Phys.* **1978**, *16*, 923.
(168) Ozin, G. A. *Appl. Spectrosc.* **1976**, *30*, 573.
(169) Moskovits, M.; Hulse, J. E. *J. Chem. Phys.* **1977**, *67*, 4271.
(170) Ozin, G. A.; Huber, H.; McIntosh, D.; Mitchell, S.; Norman, J. G., Jr.; Noodleman, L. *J. Am. Chem. Soc.* **1979**, *101*, 3504.
(171) Ozin, G. A.; Mitchell, S. A.; Garcia-Prieto, J. *J. Phys. Chem.* **1982**, *86*, 473.
(172) Ozin, G. A.; Mitchell, S. A.; Mattar, S. M.; Garcia-Prieto, J. *J. Phys. Chem.* **1983**, *87*, 4666.
(173) Grinter, R.; Armstrong, S.; Jayasooriya, U. A.; McCombie, J.; Norris, D.; Springall, J. P. *Faraday Symp. Chem. Soc.* **1980**, *14*, 94.
(174) Zeringue, K.; Shaks-Emampour, J.; Vala, M., in "Metal Bonding and Interactions in High-Temperature Systems"; eds. J. L. Gole; W. C. Stwalley *ACS Symp. Ser.* **1982**, *179*, 229.
(175) Bondybey, V. E. *J. Chem. Phys.* **1982**, *77*, 3771.
(176) Bondybey, V. E.; English, J. H. *J. Phys. Chem.* **1983**, *87*, 4647.
(177) Preuss, D. R.; Pace, S. A.; Gole, J. L. *J. Chem. Phys.* **1979**, *71*, 3553.
(178) Hare, C. R.; Sleight, T. P.; Cooper, W.; Clarke, G. A. *Inorg. Chem.* **1968**, *7*, 669.
(179) Anderson, A. B. *J. Chem. Phys.* **1978**, *68*, 1744.
(180) Baetzold, R. C. *J. Chem. Phys.* **1971**, *55*, 4355.
(181) Boeyens, J. C. A.; Lemmer, R. H. *J. Chem. Soc., Faraday Trans. 2* **1977**, *73*, 321.
(182) Dixon, R. N.; Robertson, I. L. *Mol. Phys.* **1978**, *36*, 1099.
(183) Pelissier, M. *J. Chem. Phys.* **1981**, *75*, 775.
(184) Jeung, G. H.; Barthelat, J. C.; Pelissier, M. *Chem. Phys. Lett.* **1982**, *91*, 81.
(185) Jeung, G. H.; Barthelat, J. C. *J. Chem. Phys.* **1983**, *78*, 2097.
(186) Stoll, H.; Fuentealba, P.; Dolg, M.; Flad, J.; Szentpaly, L. v.; Preuss, H. *J. Chem. Phys.* **1983**, *79*, 5532.
(187) Stoll, H.; Fuentealba, P.; Schwerdtfeger, P.; Flad, J.; Szentpaly, L. v.; Preuss, H. *J. Chem. Phys.* **1984**, *81*, 2732.
(188) Flad, J.; Igel, G.; Preuss, H.; Stoll, H. *Ber. Bunsenges. Phys. Chem.* **1984**, *88*, 241.
(189) Flad, J.; Igel-Mann, G.; Preuss, H.; Stoll, H. *Chem. Phys.* **1984**, *90*, 254.
(190) Flad, J.; Igel-Mann, G.; Preuss, H.; Stoll, H. *Surf. Sci.* **1985**, *156*, 379.
(191) Post, D.; Baerends, E. J. *Chem. Phys. Lett.* **1982**, *86*, 176.
(192) Guenzburger, D. *Chem. Phys. Lett.* **1982**, *86*, 316.
(193) Averill, F. W.; Painter, G. S. *Phys. Rev. B: Condens. Matter* **1985**, *32*, 2141.
(194) Delley, B.; Ellis, D. E.; Freeman, A. J.; Baerends, E. J.; Post, D. *Phys. Rev. B: Condens. Matter* **1983**, *27*, 2132.
(195) Painter, G. S.; Averill, F. W. *Phys. Rev. B: Condens. Matter* **1983**, *28*, 5536.
(196) Joyes, P.; Leleyter, M. *J. Phys. B* **1973**, *6*, 150.
(197) Bachmann, C.; Demuynck, J.; Veillard, A. *Faraday Symp. Chem. Soc.* **1980**, *14*, 170.
(198) Tatewaki, H.; Huzinaga, S. *J. Chem. Phys.* **1980**, *72*, 399.
(199) Tatewaki, H.; Sakai, Y.; Huzinaga, S. *J. Comput. Chem.* **1981**, *2*, 96.
(200) Tatewaki, H.; Sakai, Y.; Huzinaga, S. *J. Comput. Chem.* **1981**, *2*, 278.
(201) Tatewaki, H.; Miyoshi, E.; Nakamura, T. *J. Chem. Phys.* **1982**, *76*, 5073.
(202) Miyoshi, E.; Tatewaki, H.; Nakamura, T. *J. Chem. Phys.* **1983**, *78*, 815.
(203) Witko, M.; Beckmann, H.-O. *Mol. Phys.* **1982**, *47*, 945.
(204) Bauschlicher, C. W., Jr.; Walch, S. P.; Siegbahn, P. E. M. *J. Chem. Phys.* **1982**, *76*, 6015.
(205) Bauschlicher, C. W., Jr. *Chem. Phys. Lett.* **1983**, *97*, 204.
(206) Shim, I.; Gingerich, K. A. *J. Chem. Phys.* **1983**, *79*, 2903.
(207) Raghavachari, K.; Sunil, K. K.; Jordan, K. D. *J. Chem. Phys.* **1985**, *83*, 4633.
(208) Ziegler, T.; Snijders, J. G.; Baerends, E. J. *J. Chem. Phys.* **1981**, *74*, 1271.
(209) Martin, R. L. *J. Chem. Phys.* **1983**, *78*, 5840.
(210) Pelissier, M. *J. Chem. Phys.* **1983**, *79*, 2099.
(211) Werner, H.-J.; Martin, R. L. *Chem. Phys. Lett.* **1985**, *113*, 451.
(212) Pauling, L. *J. Chem. Phys.* **1983**, *78*, 3346.
(213) Bauschlicher, C. W., Jr.; Walch, S. P.; Siegbahn, P. E. M. *J. Chem. Phys.* **1983**, *78*, 3347.
(214) Fischer, C. F. *The Hartree-Fock Method for Atoms*; Wiley: New York, 1977; pp 28–88.
(215) Hamada, H. *Philos. Mag.* **1931**, *12*, 50.
(216) Winans, J. G. *Phys. Rev.* **1931**, *37*, 902.
(217) Mohler, F. L.; Moore, H. R. *J. Opt. Soc. Am.* **1927**, *15*, 74.
(218) Winans, J. G. *Philos. Mag.* **1929**, *7*, 555.
(219) Carlson, K. D.; Kuschnir, K. R. *J. Phys. Chem.* **1964**, *68*, 1566.
(220) Ault, B. S.; Andrews, L. *J. Mol. Spectrosc.* **1977**, *65*, 102.
(221) Finkelnburg, W. *Kontiniuerliche Spektren*; Springer-Verlag: Berlin, 1938.
(222) Hay, P. J.; Dunning, T. H., Jr.; Raffenetti, R. C. *J. Chem. Phys.* **1976**, *65*, 2679.
(223) Schmidtke, H.-H.; Wolf, A. *Chem. Phys. Lett.* **1977**, *50*, 451.
(224) Bender, C. F.; Rescigno, T. N.; Schaefer, H. F., III; Orel, A. E. *J. Chem. Phys.* **1979**, *71*, 1122.
(225) Tomonari, M.; Tatewaki, H.; Nakamura, T. *J. Chem. Phys.* **1984**, *80*, 344.
(226) Tatewaki, H.; Tomonari, M.; Nakamura, T. *J. Chem. Phys.* **1985**, *82*, 5608.
(227) Knight, L. B., Jr.; Woodward, R. W.; Van Zee, R. J.; Weltner, W., Jr. *J. Chem. Phys.* **1983**, *79*, 5820.
(228) Klotzbücher, W. E.; Ozin, G. A. *Inorg. Chem.* **1980**, *19*, 3767.
(229) Miedema, A. R.; Gingerich, K. A. *J. Phys. B* **1979**, *12*, 2081.
(230) Miedema, A. R.; Boom, R.; de Boer, F. R. *J. Less-Common Met.* **1975**, *41*, 283.
(231) Miedema, A. R. *J. Less-Common Met.* **1976**, *46*, 67.
(232) Boom, R.; de Boer, F. R.; Miedema, A. R. *J. Less-Common Met.* **1976**, *45*, 237.
(233) Boom, R.; de Boer, F. R.; Miedema, A. R. *J. Less-Common Met.* **1976**, *46*, 271.
(234) Gupta, S. K.; Gingerich, K. A. *J. Chem. Phys.* **1979**, *70*, 5350.
(235) Gupta, S. K.; Gingerich, K. A. *J. Chem. Phys.* **1978**, *69*, 4318.
(236) Krasnov, K. S. *Teplofiz. Vys. Temp.* **1975**, *13*, 441.
(237) Green, D. W.; Gruen, D. M. *J. Chem. Phys.* **1972**, *57*, 4462.
(238) Müller, H.; Optiz, C.; Seifert, G. *Z. Phys. Chem. (Leipzig)* **1982**, *263*, 1005.
(239) Seifert, G.; Mrosan, E.; Müller, H.; Ziesche, P. *Phys. Status Solidi B* **1978**, *89*, K175.
(240) Cotton, F. A.; Shim, I. *J. Phys. Chem.* **1985**, *89*, 952.
(241) Gupta, S. K.; Atkins, R. M.; Gingerich, K. A. *Inorg. Chem.* **1978**, *17*, 3211.
(242) Schoch, F.; Kay, E. *J. Chem. Phys.* **1973**, *59*, 718.
(243) Green, D. W.; Gruen, D. M. *J. Chem. Phys.* **1974**, *60*, 1797.
(244) Hewett, W. D., Jr.; Newton, J. H.; Weltner, W., Jr. *J. Phys. Chem.* **1975**, *79*, 2640.
(245) Ozin, G. A.; Klotzbücher, W. *J. Mol. Catal.* **1977/78**, *3*, 195.
(246) Bates, J. K.; Gruen, D. M. *J. Mol. Spectrosc.* **1979**, *78*, 284.
(247) Pellin, M. J.; Foosnaes, T.; Gruen, D. M. *J. Chem. Phys.* **1981**, *74*, 5547.
(248) Pellin, J. J.; Foosnaes, T.; Gruen, D. M. In *Metal Bonding and Interactions in High-Temperature Systems*; Gole, J. L., Stwalley, W. C., Eds.; ACS Symposium Series 179; American Chemical Society: Washington, DC, 1982; p 219.
(249) Becker, K. H.; Schürgers, M. *Z. Naturforsch., A* **1971**, *26A*, 2072.
(250) Samoilova, A. N.; Efremov, Y. M.; Zhuravlev, D. A.; Gurvich, L. V. *Khim. Vys. Energ.* **1974**, *8*, 229.
(251) Norman, J. G., Jr.; Kolari, H. J. *J. Chem. Soc., Chem. Commun.* **1975**, 649.
(252) Norman, J. G., Jr.; Kolari, H. J.; Gray, H. B.; Trogler, W. C. *Inorg. Chem.* **1977**, *16*, 987.

(253) Atha, P. M.; Hillier, I. H.; Guest, M. F. *Chem. Phys. Lett.* **1980**, *75*, 84.
(254) Bursten, B. E.; Cotton, F. A.; Hall, M. B. *J. Am. Chem. Soc.* **1980**, *102*, 6348.
(255) Castro, M.; Keller, J.; Mareca, P. *Int. J. Quantum Chem.* **1981**, *15*, 429.
(256) Andzelm, J.; Radzio, E.; Salahub, D. R. *J. Chem. Phys.* **1985**, *83*, 4573.
(257) Cotton, F. A.; Shive, L. W. *Inorg. Chem.* **1975**, *14*, 2032.
(258) Cotton, F. A.; Gage, L. D. *Nouv. J. Chim.* **1977**, *1*, 441.
(259) Cotton, F. A.; Fanwick, P. E.; Gage, L. D. *J. Am. Chem. Soc.* **1980**, *102*, 1570.
(260) Miedema, A. R. *Faraday Symp. Chem. Soc.* **1980**, *14*, 136.
(261) Brewer, L.; Winn, J. S. *Faraday Symp. Chem. Soc.* **1980**, *14*, 126.
(262) Cotton, F. A.; Shim, I. *J. Am. Chem. Soc.* **1982**, *104*, 7025.
(263) Gingerich, K. A.; Cocke, D. L. *J. Chem. Soc., Chem. Commun.* **1972**, 536.
(264) Cocke, D. L.; Gingerich, K. A. *J. Chem. Phys.* **1974**, *60*, 1958.
(265) Hanlan, A. J. L.; Ozin, G. A. *Inorg. Chem.* **1977**, *16*, 2848.
(266) Brom, J. M., Jr.; Graham, W. R. M.; Weltner, W., Jr. *J. Chem. Phys.* **1972**, *57*, 4116.
(267) Norman, J. G., Jr.; Kolari, H. J. *J. Am. Chem. Soc.* **1978**, *100*, 791.
(268) Shim, I. *Mat.-Fys. Medd—K. Dan. Vidensk. Selsk.* **1985**, *41*, 147 (in English).
(269) Lin, S.-S.; Strauss, B.; Kant, A. *J. Chem. Phys.* **1969**, *51*, 2282.
(270) Shim, I.; Gingerich, K. A. *J. Chem. Phys.* **1984**, *80*, 5107.
(271) Basch, H.; Cohen, D.; Topiol, S. *Isr. J. Chem.* **1980**, *19*, 233.
(272) Hilpert, K.; Gingerich, K. A. *Ber. Bunsenges. Phys. Chem.* **1980**, *84*, 739.
(273) Mitchell, S. A.; Ozin, G. A. *J. Am. Chem. Soc.* **1978**, *100*, 6776.
(274) Ozin, G. A.; Huber, H. *Inorg. Chem.* **1978**, *17*, 155.
(275) Mitchell, S. A.; Kenney-Wallace, G. A.; Ozin, G. A. *J. Am. Chem. Soc.* **1981**, *103*, 6030.
(276) Mitchell, S. A.; Ozin, G. A. *J. Phys. Chem.* **1984**, *88*, 1425.
(277) Welker, T.; Martin, T. P. *J. Chem. Phys.* **1979**, *70*, 5683.
(278) Schulze, W.; Becker, H. U.; Abe, H. *Chem. Phys.* **1978**, *35*, 177.
(279) Schulze, W.; Abe, H. *Faraday Symp. Chem. Soc.* **1980**, *14*, 87.
(280) Schrittenlacher, W.; Rotermund, H. H.; Schroeder, W.; Kolb, D. M. *Surf. Sci.* **1985**, *156*, 777.
(281) Gruen, D. M.; Bates, J. K. *Inorg. Chem.* **1977**, *16*, 2450.
(282) Bechthold, P. S.; Kettler, U.; Krasser, W. *Solid State Commun.* **1984**, *52*, 347.
(283) Bechthold, P. S.; Kettler, U.; Krasser, W. *Surf. Sci.* **1985**, *156*, 875.
(284) Schulze, W.; Becker, H. U.; Minkwitz, R.; Manzel, K. *Chem. Phys. Lett.* **1978**, *55*, 59.
(285) Hopkins, J. B.; Langridge-Smith, P. R. R.; Morse, M. D.; Smalley, R. E., unpublished results.
(286) Baetzold, R. C. *J. Chem. Phys.* **1971**, *55*, 4363.
(287) Baetzold, R. C.; Mack, R. E. *J. Chem. Phys.* **1975**, *62*, 1513.
(288) Baetzold, R. C. *J. Chem. Phys.* **1978**, *68*, 555.
(289) Sahyun, M. R. V. *Photogr. Sci. Eng.* **1978**, *22*, 317.
(290) Ozin, G. A.; Klotzbücher, W. E. *Inorg. Chem.* **1979**, *18*, 2101.
(291) Sahyun, M. R. V. *J. Chem. Educ.* **1980**, *57*, 239.
(292) Mitchell, J. W. *Photogr. Sci. Eng.* **1978**, *22*, 1.
(293) Klobukowski, M. *J. Comput. Chem.* **1983**, *4*, 350.
(294) McLean, A. D. *J. Chem. Phys.* **1983**, *79*, 3392.
(295) Hay, P. J.; Martin, R. L. *J. Chem. Phys.* **1985**, *83*, 5174.
(296) Basch, H. *J. Am. Chem. Soc.* **1981**, *103*, 4657.
(297) Ross, R. B.; Ermler, W. C. *J. Phys. Chem.* **1985**, *89*, 5202.
(298) Martins, J. L.; Andreoni, W. *Phys. Rev. A* **1983**, *28*, 3637.
(299) Grinter, R. *Chem. Phys.* **1986**, *102*, 187.
(300) Benard, M. *Chem. Phys. Lett.* **1983**, *96*, 183.
(301) Jablonski, A. *Z. Phys.* **1927**, *45*, 878.
(302) Su, C.-H.; Liao, P.-K.; Huang, Y.; Liou, S.-S.; Brebrick, R. F. *J. Chem. Phys.* **1984**, *81*, 11.
(303) Duley, W. W. *Proc. Phys. Soc.* **1967**, *91*, 976.
(304) Freedhoff, H. S. *Proc. Phys. Soc.* **1967**, *92*, 505.
(305) Miller, J. C.; Andrews, L. *Appl. Spectrosc. Rev.* **1980**, *16*, 1.
(306) Miller, J. C.; Andrews, L. *J. Chem. Phys.* **1978**, *69*, 3034.
(307) Vreede, H. J.; Claridge, R. F. C.; Phillips, L. F. *Chem. Phys. Lett.* **1974**, *27*, 3.
(308) Drullinger, R. E.; Stock, M. *J. Chem. Phys.* **1978**, *68*, 5299.
(309) Mies, F. H.; Stevens, W. J.; Krauss, M. *J. Mol. Spectrosc.* **1978**, *72*, 303.
(310) Cram, S. W. *Phys. Rev.* **1934**, *46*, 205.
(311) Ashcroft, N. W.; Mermin, N. D. *Solid State Physics*; Saunders College: Philadelphia, 1976.
(312) Cotton, F. A.; Curtis, N. F.; Harris, C. B.; Johnson, B. F. G.; Lippard, S. J.; Mague, J. T.; Robinson, W. R.; Wood, J. S. *Science (Washington, D.C.)* **1964**, *145*, 1305.
(313) Norman, J. H.; Staley, H. G.; Bell, W. E. *J. Phys. Chem.* **1967**, *71*, 3686.
(314) Gupta, S. K.; Nappi, B. M.; Gingerich, K. A. *Inorg. Chem.* **1981**, *20*, 966.
(315) Appelblad, O.; Nilsson, C.; Scullman, R. *Phys. Scr.* **1973**, *7*, 65.
(316) Jansson, K.; Scullman, R. *J. Mol. Spectrosc.* **1976**, *61*, 299.
(317) Smoes, S.; Drowart, J. *Chem. Commun.* **1968**, 534.
(318) Kordis, J.; Gingerich, K. A.; Seyse, R. J. *J. Chem. Phys.* **1974**, *61*, 5114.
(319) Lee, Y. S.; Ermler, W. C.; Pitzer, K. S.; McLean, A. D. *J. Chem. Phys.* **1979**, *70*, 288.
(320) Ermler, W. C.; Lee, Y. S.; Pitzer, K. S. *J. Chem. Phys.* **1979**, *70*, 293.
(321) Pitzer, K. S. *Int. J. Quantum Chem.* **1984**, *25*, 131.
(322) Hay, P. J., personal communication.
(323) Franck, J.; Grotian, W. *Z. Techn. Phys.* **1922**, *3*, 194.
(324) Koernicke, E. *Z. Phys.* **1925**, *33*, 219.
(325) Kuhn, H.; Freudenberg, K. *Z. Phys.* **1932**, *76*, 38.
(326) Winans, J. G.; Heitz, M. P. *Z. Phys.* **1952**, *133*, 291.
(327) Winans, J. G.; Heitz, M. P. *Z. Phys.* **1953**, *135*, 406.
(328) Drullinger, R. E.; Hessel, M. M.; Smith, E. W. *J. Chem. Phys.* **1977**, *66*, 5656.
(329) Mrozowski, S. *Z. Phys.* **1929**, *55*, 338.
(330) Winans, J. G. *Phys. Rev.* **1931**, *37*, 897.
(331) Epstein, L. F.; Powers, M. D. *J. Phys. Chem.* **1964**, *68*, 336.
(332) Hildebrand, J. H.; Wakeham, H. R. R.; Boyd, R. N. *J. Chem. Phys.* **1939**, *7*, 1094.
(333) Kerr, R. H.; Lund, L. H. *J. Chem. Phys.* **1951**, *19*, 50.
(334) Moelwyn-Hughes, E. A. *J. Phys. Chem.* **1951**, *55*, 1246.
(335) Neuberger, M. C. *Z. Anorg. Allg. Chem.* **1933**, *212*, 40.
(336) Kuhn, H. *Proc. R. Soc. London* **1937**, *A158*, 230.
(337) London, F. *Z. Phys. Chem., Abt. A* **1930**, *11*, 222.
(338) Ekstein, H.; Magat, M. *C. R. Hebd. Seances Acad. Sci.* **1934**, *199*, 264.
(339) Hilpert, K. *J. Chem. Phys.* **1982**, *77*, 1425.
(340) Wood, R. W. *Astrophys. J.* **1907**, *26*, 41.
(341) Phillips, F. S. *Proc. R. Soc. London* **1913**, *A89*, 39.
(342) Stark, J.; Wendt, G. *Phys. Z.* **1913**, *14*, 562.
(343) Lord Rayleigh *Proc. R. Soc. London* **1927**, *A114*, 620.
(344) Lord Rayleigh *Proc. R. Soc. London* **1927**, *A116*, 702.
(345) Lord Rayleigh *Proc. R. Soc. London* **1932**, *A137*, 101.
(346) Winans, J. G. *Phys. Rev.* **1932**, *42*, 800.
(347) Mrozowski, S. *Z. Phys.* **1937**, *104*, 228; **1937**, *106*, 458.
(348) Mrozowska, I. *Acta Phys. Pol.* **1933**, *2*, 81.
(349) Lennuier, R. *C. R. Hebd. Seances Acad. Sci.* **1941**, *213*, 169.
(350) Lennuier, R.; Crenn, Y. *C. R. Hebd. Seances Acad. Sci.* **1943**, *216*, 486.
(351) Mrozowski, S. *Phys. Rev.* **1949**, *76*, 1714.
(352) McCoubrey, A. O. *Phys. Rev.* **1954**, *93*, 1249.
(353) Berberet, J. A.; Clark, K. C. *Phys. Rev.* **1955**, *100*, 506.
(354) Houtermans, F. G. *Helv. Phys. Acta* **1960**, *33*, 933.
(355) Carbone, R. J.; Litvak, M. M. *J. Appl. Phys.* **1968**, *39*, 2413.
(356) Penzes, S.; Gunning, H. E.; Strausz, O. P. *J. Chem. Phys.* **1967**, *47*, 4869.
(357) McAlduff, J. E.; Drysdale, D. D.; LeRoy, D. J. *Can. J. Chem.* **1968**, *46*, 199.
(358) Ladd, A. G.; Freeman, C. G.; McEwan, M. J.; Claridge, R. F. C.; Phillips, L. F. *J. Chem. Soc., Faraday Trans. 2* **1973**, *69*, 849.
(359) Penzes, S.; Sandhu, H. S.; Strausz, O. P. *Int. J. Chem. Kinet.* **1972**, *4*, 449.
(360) Eckstrom, D. J.; Hill, R. M.; Lorents, D. C.; Nakano, H. H. *Chem. Phys. Lett.* **1973**, *23*, 112.
(361) Phaneuf, R. A.; Skonieczny, J.; Krause, L. *Phys. Rev.* **1973**, *A8*, 2980.
(362) Skonieczny, J.; Krause, L. *Phys. Rev.* **1974**, *A9*, 1612.
(363) Siara, I. N.; Krause, L. *Phys. Rev.* **1975**, *A11*, 1810.
(364) Schlie, L. A.; Guenther, B. D.; Drummond, D. L. *Chem. Phys. Lett.* **1975**, *34*, 258.
(365) Komine, H.; Byer, R. L. *J. Chem. Phys.* **1977**, *67*, 2536.
(366) Callear, A. B.; Lai, K.-L. *Chem. Phys. Lett.* **1979**, *64*, 100.
(367) Callear, A. B.; Lai, K.-L. *Chem. Phys. Lett.* **1980**, *75*, 234.
(368) Callear, A. B.; Lai, K.-L. *Chem. Phys.* **1982**, *69*, 1.
(369) Callear, A. B.; Kendall, D. R. *Chem. Phys. Lett.* **1979**, *64*, 401.
(370) Callear, A. B.; Kendall, D. R. *Chem. Phys.* **1981**, *57*, 65.
(371) Callear, A. B.; Devonport, C. P.; Kendall, D. R. *Chem. Phys.* **1981**, *61*, 65.
(372) Stock, M.; Smith, E. W.; Drullinger, R. E.; Hessel, M. M.; Pourein, J. *J. Chem. Phys.* **1978**, *68*, 1785.
(373) Smith, E. W.; Drullinger, R. E.; Hessel, M. M.; Cooper, J. *J. Chem. Phys.* **1977**, *66*, 5667.
(374) Nagaoka, H. *Jpn. J. Phys.* **1922**, *1*, 1.
(375) Finkelnburg, W. *Z. Phys.* **1935**, *96*, 714.
(376) Kremenewsky, N. *Dokl. Akad. Nauk SSSR* **1934**, *3*, 237.
(377) Mrozowski, S. *Z. Phys.* **1930**, *62*, 314.
(378) Takamine, T. *Z. Phys.* **1926**, *37*, 76.
(379) Ehrlich, D. J.; Osgood, R. M., Jr. *Phys. Rev. Lett.* **1978**, *41*, 547.
(380) Ehrlich, D. J.; Osgood, R. M., Jr. *Chem. Phys. Lett.* **1979**, *61*, 150.
(381) Takeyama, H. *J. Sci. Hiroshima Univ., Ser. A: Math. Phys. Chem.* **1952**, *15*, 235.

(382) Niefer, R.; Atkinson, J. B.; Krause, L. *J. Phys. B* **1983**, *16*, 3531.
(383) Niefer, R.; Atkinson, J. B.; Krause, L. *J. Phys. B* **1983**, *16*, 3767.
(384) Celestino, K. C.; Ermler, W. C. *J. Chem. Phys.* **1984**, *81*, 1872.
(385) Brewer, L.; Meyer, B.; Brabson, G. D. *J. Chem. Phys.* **1965**, *43*, 3973.
(386) Butchard, J. A.; Claridge, R. F. C.; Phillips, L. F. *Chem. Phys. Lett.* **1971**, *8*, 139.
(387) Arnot, F. L.; M'Ewen, M. B. *Proc. R. Soc. London* **1938**, *A165*, 133.
(388) Linn, S. H.; Liao, C. L.; Liao, C. X.; Brom, J. M., Jr.; Ng, C. Y. *Chem. Phys. Lett.* **1984**, *105*, 645.
(389) Winans, J. G. *Phys. Rev.* **1928**, *32*, 427.
(390) Eden, J. G. *Opt. Commun.* **1978**, *25*, 201.
(391) Winans, J. G. *Philos. Mag.* **1929**, *7*, 565.
(392) McGeoch, M. W.; Fournier, G. R.; Ewart, P. *J. Phys. B* **1976**, *9*, L121.
(393) Fournier, G. R.; McGeoch, M. W. *J. Appl. Phys.* **1978**, *49*, 2651.
(394) McGeoch, M. W.; Fournier, G. R. *J. Appl. Phys.* **1978**, *49*, 2659.
(395) West, J. B.; Komine, H.; Stappaerts, E. A. *J. Appl. Phys.* **1979**, *50*, 7929.
(396) McGeoch, M. W. *J. Chem. Phys.* **1980**, *72*, 140.
(397) McGeoch, M. W. *J. Chem. Phys.* **1980**, *73*, 2534.
(398) Kasai, P. H.; McLeod, D., Jr. *J. Phys. Chem.* **1975**, *79*, 2324.
(399) Kasai, P. H.; McLeod, D., Jr. *J. Phys. Chem.* **1978**, *82*, 1554.
(400) Kasai, P. H.; McLeod, D. *Faraday Symp. Chem. Soc.* **1980**, *14*, 65.
(401) Klotzbücher, W. E.; Ozin, G. A. *Inorg. Chem.* **1980**, *19*, 2848.
(402) Dyson, W.; Montano, P. A. *J. Am. Chem. Soc.* **1978**, *100*, 7439.
(403) Montano, P. A. *J. Appl. Phys.* **1978**, *49*, 1561.
(404) Montano, P. A. *J. Appl. Phys.* **1978**, *49*, 4612.
(405) Dyson, W.; Montano, P. A. *Phys. Rev. B: Condens. Matter* **1979**, *20*, 3619.
(406) Montano, P. A.; Talarico, M. A. *J. Appl. Phys.* **1979**, *50*, 2405.
(407) Dyson, W.; Montano, P. A. *Solid State Commun.* **1980**, *33*, 191.
(408) Nagarathna, H. M.; Montano, P. A.; Naik, V. M. *J. Am. Chem. Soc.* **1983**, *105*, 2938.
(409) Van Zee, R. J.; Weltner, W., Jr. *Chem. Phys. Lett.* **1984**, *107*, 173.
(410) Van Zee, R. J.; Weltner, W., Jr. *High Temp. Sci.* **1984**, *17*, 181.
(411) Shim, I.; Gingerich, K. A. *Chem. Phys. Lett.* **1983**, *101*, 528.
(412) Ramakrishnan, E. S.; Shim, I.; Gingerich, K. A. *J. Chem. Soc., Faraday Trans. 2* **1984**, *80*, 395.
(413) Baumann, C. A.; Van Zee, R. J.; Weltner, W., Jr. *J. Chem. Phys.* **1983**, *79*, 5272.
(414) Weltner, W., Jr. *Magnetic Atoms and Molecules*; Van Nostrand Reinhold: New York, 1983.
(415) Van Zee, R. J.; Weltner, W., Jr. *J. Chem. Phys.* **1981**, *74*, 4330.
(416) Van Zee, R. J.; Weltner, W., Jr. *J. Chem. Phys.* **1981**, *75*, 2484.
(417) Huber, K. P.; Herzberg, G. *Molecular Spectra and Molecular Structure IV. Constants of Diatomic Molecules*; Van Nostrand Reinhold: New York, 1979.
(418) Kant, A. *J. Chem. Phys.* **1968**, *49*, 5144.
(419) Gingerich, K. A.; Finkbeiner, H. C. *J. Chem. Phys.* **1970**, *52*, 2956.
(420) Gingerich, K. A.; Finkbeiner, H. C. *J. Chem. Phys.* **1971**, *54*, 2621.
(421) Haque, R.; Pelino, M.; Gingerich, K. A. *J. Chem. Phys.* **1979**, *71*, 2929.
(422) Cocke, D. L.; Gingerich, K. A.; Kordis, J. *High Temp. Sci.* **1975**, *7*, 61.
(423) Gingerich, K. A.; Finkbeiner, H. C. In *Proc. 9th Rare Earth Conf.*, Oct 10–14, 1971, Blacksburg, VA, Field, P. E., Ed. (CONF-711001 Chemistry [TID-4500], National Information Service, U.S. Dept. Commerce, Springfield, VA 22151), Vol. 2, pp 795–803.
(424) Gupta, S. K.; Pelino, M.; Gingerich, K. A. *J. Chem. Phys.* **1979**, *70*, 2044.
(425) Haque, R.; Pelino, M.; Gingerich, K. A. *J. Chem. Phys.* **1980**, *73*, 4045.
(426) Kant, A.; Strauss, B.; Lin, S.-S. *J. Chem. Phys.* **1970**, *52*, 2384.
(427) Gingerich, K. A.; Gupta, S. K.; Finkbeiner, H. C., to be submitted for publication.
(428) Nappi, B. M.; Gingerich, K. A. *Inorg. Chem.* **1981**, *20*, 522.
(429) Cocke, D. L.; Gingerich, K. A.; Kordis, J. *High Temp. Sci.* **1973**, *5*, 474.
(430) Gupta, S. K.; Pelino, M.; Gingerich, K. A. *J. Phys. Chem.* **1979**, *83*, 2335.
(431) Haque, R.; Gingerich, K. A. *J. Chem. Thermodyn.* **1980**, *12*, 439.
(432) Gingerich, K. A.; Choudary, U. V., unpublished data.
(433) Kingcade, J. E.; Choudary, U. V.; Gingerich, K. A. *Inorg. Chem.* **1979**, *18*, 3094.
(434) Miedema, A. R.; Gingerich, K. A. *J. Phys. B* **1979**, *12*, 2255.
(435) Pauling, L. *The Nature of the Chemical Bond*, 3rd ed.; Cornell University Press: Ithaca, NY, 1960.
(436) Gingerich, K. A. *Chem. Phys. Lett.* **1973**, *23*, 270.
(437) Gingerich, K. A. *J. Chem. Soc., Faraday Trans. 2* **1974**, *70*, 471.
(438) Brewer, L. In *Phase Stability of Metals and Alloys*; Rudman, P. S., Stringer, J., Jaffee, R. I., Eds.; McGraw-Hill: New York, 1967.
(439) Hotop, H.; Lineberger, W. C. *J. Phys. Chem. Ref. Data* **1975**, *4*, 539.
(440) Gingerich, K. A.; Cocke, D. L.; Finkbeiner, H. C.; Chang, C. A. *Chem. Phys. Lett.* **1973**, *18*, 102.
(441) Gingerich, K. A. *Chem. Phys. Lett.* **1972**, *13*, 262.
(442) Cocke, D. L.; Gingerich, K. A.; Chang, C. *J. Chem. Soc., Faraday Trans. 1* **1976**, *72*, 268.
(443) Gingerich, K. A.; Cocke, D. L.; Choudary, U. V. *Inorg. Chim. Acta* **1975**, *14*, L47.
(444) Choudary, U. V.; Krishnan, K.; Gingerich, K. A., unpublished data.
(445) Kingcade, J. E.; Gingerich, K. A.; Choudary, U. V. *J. Phys. Chem.* **1978**, *82*, 49.
(446) Kingcade, J. E.; Dufner, D. C.; Gupta, S. K.; Gingerich, K. A. *High Temp. Sci.* **1978**, *10*, 213.
(447) Walch, S. P.; Bauschlicher, C. W., Jr. *J. Chem. Phys.* **1985**, *83*, 5735.
(448) Moskovits, M.; DiLella, D. P. *J. Chem. Phys.* **1980**, *72*, 2267.
(449) DiLella, D. P.; Taylor, K. V.; Moskovits, M. *J. Phys. Chem.* **1983**, *87*, 524.
(450) Moskovits, M. *Chem. Phys. Lett.* **1985**, *118*, 111.
(451) Howard, J. A.; Preston, K. F.; Mile, B. *J. Am. Chem. Soc.* **1981**, *103*, 6226.
(452) Kettler, U.; Bechthold, P. S.; Krasser, W. *Surf. Sci.* **1985**, *156*, 867.
(453) Van Zee, R. J.; Baumann, C. A.; Weltner, W., Jr. *J. Chem. Phys.* **1985**, *82*, 3912.
(454) Demuynck, J.; Rohmer, M.-M.; Strich, A.; Veillard, A. *J. Chem. Phys.* **1981**, *75*, 3443.
(455) Blyholder, G. *Surf. Sci.* **1974**, *42*, 249.
(456) Messmer, R. P.; Knudson, S. K.; Johnson, K. H.; Diamond, J. B.; Yang, C. Y. *Phys. Rev. B: Solid State* **1976**, *13*, 1396.
(457) Howard, J. A.; Preston, K. F.; Sutcliffe, R.; Mile, B. *J. Phys. Chem.* **1983**, *87*, 536.
(458) Howard, J. A.; Sutcliffe, R.; Mile, B. *J. Chem. Soc., Chem. Commun.* **1983**, 1449.
(459) Howard, J. A.; Sutcliffe, R.; Mile, B. *J. Am. Chem. Soc.* **1983**, *105*, 1394.
(460) Howard, J. A.; Sutcliffe, R.; Tse, J. S.; Mile, B. *Chem. Phys. Lett.* **1983**, *94*, 561.
(461) Howard, J. A.; Sutcliffe, R.; Mile, B. *J. Phys. Chem.* **1983**, *87*, 2268.
(462) Howard, J. A.; Sutcliffe, R.; Mile, B. *J. Phys. Chem.* **1984**, *88*, 2183.
(463) Howard, J. A.; Sutcliffe, R.; Mile, B. *J. Catal.* **1984**, *90*, 156.
(464) Howard, J. A.; Sutcliffe, R.; Mile, B. *Surf. Sci.* **1985**, *156*, 214.
(465) Weltner, W., Jr.; Van Zee, R. J., In *Comparison of Ab Initio Quantum Chemistry with Experiment*; Bartlett, R. J., Ed.; D. Reidel: Dordrecht, 1985.
(466) Morse, M. D. *Chem. Phys. Lett.*, in press.
(467) Crumley, W. H.; Hayden, J. S.; Gole, J. L. *J. Chem. Phys.* **1986**, *84*, 5250.
(468) Rohlfing, E. A.; Valentini, J. J. *Chem. Phys. Lett.* **1986**, *126*, 113.
(469) Walch, S. P.; Laskowski, B. C. *J. Chem. Phys.* **1986**, *84*, 2734.
(470) Longuet-Higgins, H. C. *Adv. Spectrosc.* **1961**, *2*, 461.
(471) Gerber, W. H.; Schumacher, E. *J. Chem. Phys.* **1978**, *69*, 1692.
(472) Thompson, T. C.; Truhlar, D. G.; Mead, C. A. *J. Chem. Phys.* **1985**, *82*, 2392.
(473) Thompson, T. C.; Mead, C. A. *J. Chem. Phys.* **1985**, *82*, 2408.
(474) Richtsmeier, S. C.; Eades, R. A.; Dixon, D. A.; Gole, J. L. In *Metal Bonding and Interactions in High Temperature Systems*; Gole, J. L., Stwalley, W. C., Eds.; *ACS* Symposium Series 179; American Chemical Society: Washington, DC, 1982; p 153.
(475) Herzberg, G. *Molecular Spectra and Molecular Structure II. Infrared and Raman Spectra of Polyatomic Molecules*; Van Nostrand Reinhold: New York, 1945, p 125.
(476) Truhlar, D. G.; Thompson, T. C.; Mead, C. A. *Chem. Phys. Lett.* **1986**, *127*, 287.
(477) Zwanziger, J. F.; Whetten, R. L.; Grant, E. R. *J. Phys. Chem.* **1986**, *90*, 3298.
(478) Laskowski, B. C.; Langhoff, S. R.; Bauschlicher, C. W.; Walch, S. P., unpublished work.

(479) Feigerle, C. S.; Corderman, R. R.; Bobashev, S. V.; Lineberger, W. C. *J. Chem. Phys.* **1981**, *74*, 1580.
(480) Corderman, R. R.; Engelking, P. C.; Lineberger, W. C. *J. Chem. Phys.* **1979**, *70*, 4474.
(481) Hotop, H.; Bennett, R. A.; Lineberger, W. C. *J. Chem. Phys.* **1973**, *58*, 2373.
(482) Hotop, H.; Lineberger, W. C. *J. Chem. Phys.* **1973**, *58*, 2379.
(483) Feigerle, C. S.; Herman, Z.; Lineberger, W. C. *J. Electron Spectrosc. Relat. Phenom.* **1981**, *23*, 441.
(484) Fomenko, V. S. In *Handbook of Thermionic Properties*; Samsanov, G. V., Ed.; Plenum: New York, 1966.
(485) Cox, D. M.; Whetten, R. L.; Zakin, M. R.; Trevor, D. J.; Reichmann, K. C.; Kaldor, A. *Proc. Int. Laser Sci. Conf.*, in press.
(486) Rohlfing, E. A.; Cox, D. M.; Kaldor, A. *J. Phys. Chem.* **1984**, *88*, 4497.
(487) Whetten, R. L.; Zakin, M. R.; Cox, D. M.; Trevor, D. J.; Kaldor, A. *J. Chem. Phys.* **1986**, *85*, 1697.
(488) Zheng, L.-S.; Brucat, P. J.; Pettiette, C. L.; Yang, S.; Smalley, R. E. *J. Chem. Phys.* **1985**, *83*, 4273.
(489) Zheng, L.-S.; Karner, C. M.; Brucat, P. J.; Yang, S. H.; Pettiette, C. L.; Craycraft, M. J.; Smalley, R. E. *J. Chem. Phys.* **1986**, *85*, 1681.
(490) Rodriguez-Murcia, H.; Beske, H. E. Dissertation, Kernforschungsanlage, Jülich, 1976.
(491) Devienne, F. M.; Roustan, J. C. *Org. Mass Spectrosc.* **1982**, *17*, 173.
(492) Sudraud, P.; Colliex, C.; Van de Walle, J. *J. Phys. (Orsay, Fr.)* **1979**, *40*, L107.
(493) Joyes, P.; Sudraud, P. *Surf. Sci.* **1985**, *156*, 451.
(494) Brêchignac, C.; Broyer, M.; Cahuzac, Ph.; Delacretaz, G.; Labastie, P.; Wöste, L. *Chem. Phys. Lett.* **1985**, *120*, 559.
(495) Knight, W. D.; Monot, R.; Dietz, E. R.; George, A. R. *Phys. Rev. Lett.* **1978**, *40*, 1324.
(496) Cox, D. M.; Trevor, D. J.; Whetten, R. L.; Rohlfing, E. A.; Kaldor, A. *Phys. Rev. B: Condens. Matter* **1985**, *32*, 7290.
(497) Cox, D. M.; Trevor, D. J.; Whetten, R. L.; Rohlfing, E. A.; Kaldor, A. *J. Chem. Phys.* **1986**, *84*, 4651.
(498) Yang, C. Y.; Johnson, K. H.; Salahub, D. R.; Kaspar, J.; Messmer, R. P. *Phys. Rev. B: Condens. Matter* **1981**, *24*, 5673.
(499) Salahub, D. R.; Messmer, R. P. *Surf. Sci.* **1981**, *106*, 15.
(500) Lee, K.; Callaway, J.; Dhar, S. *Phys. Rev. B: Condens. Matter* **1984**, *30*, 1724.
(501) Lee, K.; Callaway, J.; Kwong, K.; Tang, R.; Ziegler, A. *Phys. Rev. B: Condens. Matter* **1985**, *31*, 1796.
(502) Knight, W. D.; Clemenger, K.; de Heer, W. A.; Saunders, W. A. *Phys. Rev. B: Condens. Matter* **1985**, *31*, 2539.
(503) Knight, W. D.; Clemenger, K.; de Heer, W. A.; Saunders, W. A.; Chou, M. Y.; Cohen, M. L. *Phys. Rev. Lett.* **1984**, *52*, 2141.
(504) Knight, W. D.; de Heer, W. A.; Clemenger, K.; Saunders, W. A. *Solid State Commun.* **1985**, *53*, 445.
(505) Kim, S. S.; Stein, G. D. *Rev. Sci. Instrum.* **1982**, *53*, 838.
(506) Kim, S. S.; Stein, G. D. *Heterogeneous Atmospheric Chem. Geophys. Monograph Ser.* **1982**, *26*, 33.
(507) Lee, J. W.; Stein, G. D. *Surf. Sci.* **1985**, *156*, 112.
(508) Yokozeki, A.; Stein, G. D. *J. Appl. Phys.* **1978**, *49*, 2224.
(509) De Boer, B. G.; Stein, G. D. *Surf. Sci.* **1981**, *106*, 84.
(510) Wasserman, H. J.; Vermaak, J. S. *Surf. Sci.* **1970**, *22*, 164.
(511) Wasserman, H. J.; Vermaak, J. S. *Surf. Sci.* **1972**, *32*, 168.
(512) de Planta, T.; Ghez, R.; Piuz, F. *Helv. Acta* **1964**, *37*, 74.
(513) Berry, C. R. *Phys. Rev.* **1952**, *88*, 596.
(514) Mays, C. W.; Vermaak, J. S.; Kuhlmann-Wilsdorf, D. *Surf. Sci.* **1968**, *12*, 134.
(515) Hamilton, J. F.; Apai, G.; Lee, S. T.; Mason, M. G. In *Growth and Properties of Metal Clusters*; Bourdon, J., Ed.; Elsevier: The Netherlands, 1980; p 387.
(516) Apai, G.; Hamilton, J. F.; Stohr, J.; Thompson, A. *Phys. Rev. Lett.* **1979**, *43*, 165.
(517) Montano, P. A.; Schulze, W.; Tesche, B.; Shenoy, G. K.; Morrison, T. I. *Phys. Rev. B: Condens. Matter* **1984**, *30*, 672.
(518) Sattler, K.; Mühlbach, J.; Echt, O.; Pfau, P.; Rechnagel, E. *Phys. Rev. Lett.* **1981**, *47*, 160.
(519) Ding, A.; Hesslich, J. *Chem. Phys. Lett.* **1983**, *94*, 54.
(520) Pfau, P.; Sattler, K.; Pflaum, R.; Recknagel, E. *Phys. Lett. A* **1984**, *104*, 262.
(521) Kreisle, D.; Echt, O.; Knapp, M.; Recknagel, E.; Leiter, K.; Märk, T. D.; Sáenz, J. J.; Soler, J. M. *Phys. Rev. Lett.* **1986**, *56*, 1551.
(522) Waugh, A. R. *J. Phys. D* **1980**, *13*, L203.
(523) Dixon, A.; Colliex, C.; Sudraud, P.; van de Walle, J. *Phys. Rev. Lett.* **1981**, *46*, 865.
(524) Swanson, L. W.; Bell, A. E.; Schwind, G. A.; Larson, D. In *Proc. 27th Intern. Field Emission Symp.*, Yashiro, Y., Ugata, N., Eds., Tokyo, 1980, p 418.
(525) Gamo, K.; Ochiai, Y.; Inomoto, Y.; Namba, S. In *Proc. 28th Intern. Field Emission Symp.*, Swanson, L. W., Bell, A. E., Eds.; Portland, OR, 1981, p 83.
(526) Brêchignac, C.; Broyer, M.; Cahuzac, Ph.; Delacrêtaz, G.; Labastie, P.; Wöste, L. *Chem. Phys. Lett.* **1985**, *118*, 174.
(527) Drachsel, W.; Jentsch, Th.; Gingerich, K. A.; Block, J. H. *Surf. Sci.* **1985**, *156*, 173.
(528) Echt, O. In *Annual Report Universität Konstanz, Nucleare Festkörperphysik*, 1981 (unpublished), p 92.
(529) Echt, O.; Sattler, K.; Recknagel, E. *Phys. Lett. A* **1982**, *90*, 185.
(530) Recknagel, E. *Ber. Bungenges. Phys. Chem.* **1984**, *88*, 201.
(531) Novinsky, H. J.; Pflaum, R.; Pfau, P.; Sattler, K.; Recknagel, E. *Surf. Sci.* **1985**, *156*, 126.
(532) Tománek, D.; Mukherjee, S.; Bennemann, K. H. *Phys. Rev. B: Condens. Matter* **1983**, *28*, 665.
(533) Davis, S. C.; Klabunde, K. J. *Chem. Rev.* **1982**, *82*, 153.
(534) Geusic, M. E.; Morse, M. D.; Smalley, R. E. *J. Chem. Phys.* **1985**, *82*, 590.
(535) Geusic, M. E.; Morse, M. D.; O'Brien, S. C.; Smalley, R. E. *Rev. Sci. Instrum.* **1985**, *56*, 2123.
(536) Morse, M. D.; Geusic, M. E.; Health, J. R.; Smalley, R. E. *J. Chem. Phys.* **1985**, *83*, 2293.
(537) Riley, S. J.; Parks, E. K.; Pobo, L. G.; Wexler, S. *Ber. Bunsenges. Phys. Chem.* **1984**, *88*, 287.
(538) Richtsmeier, S. C.; Parks, E. K.; Lin, K.; Pobo, L. G.; Riley, S. J. *J. Chem. Phys.* **1985**, *82*, 3659.
(539) Parks, E. K.; Liu, K.; Richtsmeier, S. C.; Pobo, L. G.; Riley, S. J. *J. Chem. Phys.* **1985**, *82*, 5470.
(540) Liu, K.; Parks, E. K.; Richtsmeier, S. C.; Pobo, L. G.; Riley, S. J. *J. Chem. Phys.* **1985**, *83*, 2882, 5353.
(541) Riley, S. K.; Parks, E. K.; Liu, K. *Int. Symp. Optical and Optoelectronic Appl. Sci. Eng.* Québec, 1986.
(542) Trevor, D. J.; Whetten, R. L.; Cox, D. M.; Kaldor, A. *J. Am. Chem. Soc.* **1985**, *107*, 518.
(543) Whetten, R. L.; Cox, D. M.; Trevor, D. J.; Kaldor, A. *J. Phys. Chem.* **1985**, *89*, 566.
(544) Whetten, R. L.; Cox, D. M.; Trevor, D. J.; Kaldor, A. *Phys. Rev. Lett.* **1985**, *54*, 1494.
(545) Zakin, M. R.; Brickman, R. O.; Cox, D. M.; Reichmann, K. C.; Trevor, D. J.; Kaldor, A. *J. Chem. Phys.* **1986**, *85*, 1198.
(546) Morse, M. D.; Geusic, M. E.; O'Brien, S. C.; Smalley, R. E., unpublished results.
(547) Wedler, G.; Geuss, K. P.; Colb, K. G.; McElhiney, G. *Appl. Surf. Sci.* **1978**, *1*, 471.
(548) Bozso, F.; Ertl, G.; Grunze, M.; Weiss, M. *Appl. Surf. Sci.* **1977**, *1*, 103.
(549) Gole, J. L.; Woodward, R.; Hayden, J. S.; Dixon, D. A. *J. Phys. Chem.* **1985**, *89*, 4905.
(550) Halle, L. F.; Crowe, W. E.; Armentrout, P. B.; Beauchamp, J. L. *Organometallics* **1984**, *3*, 1694.
(551) Tolbert, M. A.; Beauchamp, J. L. *J. Am. Chem. Soc.* **1984**, *106*, 8117.
(552) Mandich, M. L.; Halle, L. F.; Beauchamp, J. L. *J. Am. Chem. Soc.* **1984**, *106*, 4403.
(553) Houriet, R.; Halle, L. F.; Beauchamp, J. L. *Organometallics* **1983**, *2*, 1818.
(554) Peake, D. A.; Gross, M. L.; Ridge, D. P. *J. Am. Chem. Soc.* **1984**, *106*, 4307.
(555) Larsen, B. S.; Ridge, D. P. *J. Am. Chem. Soc.* **1984**, *106*, 1912.
(556) Cassady, C. J.; Freiser, B. S.; McElvany, S. W.; Allison, J. *J. Am. Chem. Soc.* **1984**, *106*, 6125.
(557) Jacobson, D. B.; Byrd, G. D.; Freiser, B. S. *Inorg. Chem.* **1984**, *23*, 553.
(558) Jacobson, D. B.; Freiser, B. S. *J. Am. Chem. Soc.* **1983**, *105*, 7492.
(559) Armentrout, P. B.; Loh, S. K.; Ervin, K. M. *J. Am. Chem. Soc.* **1984**, *106*, 1161.
(560) Hanley, L.; Anderson, S. L. *Chem. Phys. Lett.* **1985**, *122*, 410.
(561) Anderson, S. L.; Hanley, L. *Int. Symp. Optical and Optoelectronic Appl. Sci. Eng.* Québec, 1986.
(562) Uppal, J. S.; Staley, R. H. *J. Am. Chem. Soc.* **1982**, *104*, 1238.
(563) Kappes, M. M.; Staley, R. H. *J. Am. Chem. Soc.* **1982**, *104*, 1813.
(564) Kappes, M. M.; Staley, R. H. *J. Am. Chem. Soc.* **1982**, *104*, 1819.
(565) Jones, R. W.; Staley, R. H. *J. Phys. Chem.* **1982**, *86*, 1387.
(566) Jones, R. W.; Staley, R. H. *J. Am. Chem. Soc.* **1982**, *104*, 2296.
(567) Freas, R. B.; Ridge, D. P. *J. Am. Chem. Soc.* **1980**, *102*, 7129.
(568) Freas, R. B.; Ridge, D. P. *J. Am. Chem. Soc.* **1984**, *106*, 825.
(569) Larsen, B. S.; Freas, R. B.; Ridge, D. P. *J. Phys. Chem.* **1984**, *88*, 6014.
(570) Ridge, D. P. *Lecture Notes in Chemistry*; Hartmann, H., Wanczek, K. P., Eds.; Springer-Verlag: West Berlin, 1982; Vol. 31, p 140.
(571) Leopold, D. G.; Vaida, V. *J. Am. Chem. Soc.* **1983**, *105*, 6809.
(572) Jacobson, D. B.; Freiser, B. S. *J. Am. Chem. Soc.* **1984**, *106*, 4623.
(573) Jacobson, D. B.; Freiser, B. S. *J. Am. Chem. Soc.* **1984**, *106*, 5351.
(574) Jacobson, D. B.; Freiser, B. S. *J. Am. Chem. Soc.* **1985**, *107*, 1581.

(575) Alford, J. M.; Williams, P. E.; Trevor, D. J.; Smalley, R. E. *Int. J. Mass Spectrom. Ion Phys.*, in press.
(576) Armentrout, P. B.; Beauchamp, J. L. *J. Am. Chem. Soc.* **1980**, *102*, 1736.
(577) In this paper the periodic group notation in parentheses is in accord with recent actions by IUPAC and ACS nomenclature committees. A and B notation is eliminated because of wide confusion. Groups IA and IIA become groups 1 and 2. The d-transition elements comprise groups 3 through 12 and the p-block elements comprise groups 13 through 18. (Note that the former Roman number designation is presented in the last digit of the new numbering: e.g., III → 3 and 13.)